GEOTECHNICAL AND GROUND IMPROVEMENT ASPECTS OF MOTORWAY EMBANKMENTS IN SOFT CLAY, SOUTHEAST QUEENSLAND

A thesis submitted in fulfilment of the requirements
for the award of the degree

Doctor of Philosophy

by

YAN-NAM ERWIN OH
BSc Eng., MSc Eng, MIEAust

from

Griffith School of Engineering
Faculty of Engineering & Information Technology

GRIFFITH UNIVERSITY
GOLD COAST CAMPUS

August 2006

ABSTRACT

This dissertation is the first Geotechnical Engineering doctoral thesis in Griffith University, and a detail study of the soft clay as encountered in Southeast Queensland is carried out. In the study process, due to the insufficient laboratory equipments and access to Geotechnical softwares, the dissertation has to be presented in a practical format. In addition, laboratory tests were conducted to investigate the application of chemical (cement and lime) treatments.

Three case histories (Sunshine Motorway, Port of Brisbane Motorway, and Gold Coast Highway) are presented in this thesis. The main focuses are on the following aspects: i) soil parameters needed in engineering design from laboratory tests and field measurement, ii) the behaviour of constructed embankment on soft ground with and without ground improvement, iii) the performance of ground improvement techniques. The methods which have been employed to achieve the main aims were conventional methods.

Laboratory test data and field measurement data, which were utilised for back-analyses and prediction of constructed embankment of soft ground behaviours, were obtained from QDMR. Thick layer of soft sensitive marine clay were found in the studied areas with up to 13m depth. The performance behaviour of constructed embankment on Southeast Queensland soft clay deposit has been evaluated based on the interpretation of test data, the theoretical analyses and conventional methods for settlement, lateral displacement, and excess pore pressure dissipation.

Detail study of the estuarine soft clay as encountered in the Sunshine Motorway is carried out. 33 borehole data were examined to delineate the soft clay profile, which is about 10.5m thickness and varies substantially along the longitudinal section of the motorway. The laboratory value of the coefficient of volume decrease ranged from 1 to 5 MN/m^2 and the laboratory values of the coefficient of consolidation are in the range of 0.25 to 0.5 m^2/year.

The Port of Brisbane Motorway embankments are installed with vertical drains and consist of three sections. Embankment A had drains at 3 meter spacing, and Embankments B and C had drains at 1.5 meter spacings. The maximum settlement obtained after 226 days of monitoring is shown. It can be seen that vertical drain

treatment significantly increased final settlement. This increase varied from 70 to 80%. It can be concluded from the settlement results that vertical drains would have increased rate of consolidation.

A trial embankment was constructed along the Gold Coast Highway. This embankment was divided into three sections, one section contained no ground improvement, and the other two sections had stone columns at 2m spacing and 3m spacing. For embankment with 3m spacing, the maximum settlement was 490 mm. For embankment with 2m spacing, the maximum settlement was 386 mm. For embankment without stone column, the maximum settlement was 522 mm.

Based on the laboratory tests, for cement treated samples with 5 percent to 15 percent cement content, the maximum unconfined compressive strength increased from 132 kPa to 370 kPa for 7 days curing period; these values for 28days curing increased from 170 kPa to 405 kPa. For lime treated samples with lime contents from 2 percent to 15 percent, the maximum unconfined compressive strength increases from 47 kPa to 199 kPa (for 7 days curing period). Results indicated that, 2 percent lime has little effect on peak unconfined compressive strength.

This thesis summarises some ground improvement techniques used in Southeast Queensland, and demonstrated the applicable of chemical stabilisation. Overall it was concluded that the addition of cement and lime has favourable effects on the strength characteristics of Southeast Queensland soft clays.

Keywords: Embankments, soft clay, settlement, excess pore pressure, lateral displacement.

DECLARATION

This work has not been previously submitted for a degree or diploma in any university. To the best of my knowledge and belief, the thesis contains no material previously published or written by another person except where due reference is made in the thesis itself.

_____

Yan-Nam Erwin Oh

August 2006

AKNOWLEDGEMENTS

I thank God for giving me the guidance, patience, perseverance and strength to complete this thesis.

The completion of this PhD would not have been possible without the encouragement and support of many individuals to whom I would like to express my deepest gratitude.

I am extremely grateful to my supervisors, Professor A. S. Balasubramaniam and Professor Yew-Chaye Loo. I would like to thank Professor Balasubramaniam for his enthusiastic guidance, invaluable help and encouragement in all aspects of this research project. His numerous comments, criticisms and suggestions during the preparation of this thesis are gratefully acknowledged. His patience and availability for any help whenever needed is appreciated. I would like to acknowledge Professor Loo for his continuing supports, encouragement and inspiration.

Financial supports provided by the Griffith University Postgraduate Research Scholarship (GUPRS) and International Postgraduate Research Scholarship (IPRS) are gratefully acknowledged.

I would like to thank Mr. Vasantha Wijeyakulasuriya (Queensland Department of Main Roads) for his invaluable comments and suggestions during the course of this research. Also, I would like to express my appreciation to Geotechnical Branch of the Queensland Department of Main Roads, for their support in providing the soil samples and their permission to use the data presented in this thesis.

Special thanks are due to all the academic, technical and administrative staff at the Griffith School of Engineering. I would like to thank fellow postgraduate students in Griffith School of Engineering for their support and social interaction during my study.

Heartfelt acknowledgements are expressed to my parents and brother, for their encouragement, understanding and support. Very special and sincere gratitude is offered to my wife, Carol, for her constant love, patience and support, during my PhD programme.

LIST OF PUBLICATIONS

The following publications were produced to disseminate the results of the work undertaken by the author during the course of this PhD study.

Journal Publications

1. Balasubramanuam, A. S., **Oh, E. Y. N**., Bolton, M., Bergado, D. T., and Phienwej, N., and (2005). "Deep well pumping in the Bangkok plain and its influence on the ground improvement development with surcharge and vertical drains Ground Improvement (ISSN: 1365-781X), 9(4):149 – 162.
2. Balasubramaniam, A. S., **Oh, E. Y. N**., and Bolton, M., (2005). "The application of normality rule and energy balance equations for normally consolidated clays". *Lowland Technology International*, Journal of the International Association of Lowland Technology (ISSN 1344-9656), 7(1):1-12.
3. Jeng, D. S., Lee, T. L., Chien, L. K., Rahman, M. S., **Oh Y. N.**, (2004). "Analytical Assessment of Non-Linear Wave-Induced Seabed Response". *Geotechnical Engineering* (Journal of the Southeast Asian Geotechnical Society), 35(2): 87-94.
4. Balasubramaniam, A. S., Kim, S. R., and **Oh, Y. N.** (2004). "Discussion on "Numerical Interpretation of a Shape of Yield Surface Obtained From Stress Probe Tests", By Kobayashi *et al*., Volume 43, Number 3, 95-104". *Soils and Foundations*, 44(6):129-132.
5. Balasubramaniam, A. S., and **Oh, Y. N.** (2004). "Discussion on "Applicability Of Shansep Method To Six Different Natural Clays, Using Triaxial And Direct Shear Tests", By Tanaka *et al*., Volume 43, Number 3, 43-56". *Soils and Foundations*, 44(6):129-129.
6. Balasubramaniam, A. S., Phienwej, N., Bergado, D. T., and **Oh, Y-N.**, (2004). "Discussion on Geotechnical Hazards in Bangkok - Present & Future", *Lowland Technology International* (Journal of the International Association of Lowland Technology), 6(1):63-66.
7. Balasubramaniam, A. S., Bergado, D. T., Lorenzo, G. A., and **Oh, Y-N.**, (2003). "Discussion on Lime treated clay: salient engineering properties and a conceptual model", *Soils and Foundations*, 43(6):189-190.
8. Balasubramaniam, A. S., Lee, Y. H. and **Oh, Y-N.** (2002). "Modified Soil

Mechanics from Practice to Theory", *Journal of Institution of Engineers Malaysia* (ISSN 0125-513X), 63(4):1-13.

Conference Publications

1. **Oh, E. Y. N.**, and Chai, G. W. K. (2006). "Characterization of Marine Clay for Road Embankment Design in Coastal Area". *Proceedings of Sixteenth (2006) International Offshore and Polar Engineering Conference* (ISBN 1-880653-66-4), San Francisco, USA, Vol. 2, 560-563.
2. Chai, G. W. K and **Oh, E. Y. N**. (2005). "Development of A Predictive Model for Cement Stabilised Road-base*". Proceedings of The 5th International Conference on Road and Airfield Pavement Technology* (ISBN 89-956678-0-X), Seoul, Korea, Vol. 1, 137-141.
3. Chai, G. W. K, **Oh, E. Y. N**., and Balasubramaniam, A. S. (2005). "In-Situ Stabilization of Road Base Using Cement - A Case Study in Malaysia". *Proceedings of Fifteenth (2005) International Offshore and Polar Engineering Conference* (ISBN 1-880653-64−8), Seoul, Korea, Vol. 2, 400-403.
4. Buessucesco, B., Balasubramaniam, A. S., **Oh, E. Y-N.**, Bolton, M., Bergado, D. T., Lorenzo, G. A. (2005). "Strength degradation and critical state seeking behaviour of lime treated soft clay". *Proceeding of International Conference on Deep Mixing - Best Practice and Recent Advances* (ISBN 1402-2036), Vol. 1, 35-40.
5. Kwan, P. S., Bouazza, A., Fletcher, P., Ranjith, P. G., **Oh, E. Y. N.**, Shuttlewood, K., and Balasubramaniam, A. S. (2005). "Behaviour of cement treated Melbourne and Southeast Queensland soft clays in deep stabilization works". *Proceeding of International Conference on Deep Mixing - Best Practice and Recent Advances* (ISBN 1402-2036), Vol. 1, 101-110.
6. Kim, S., R., Khan, M., R. A., Pornpong, A., **Oh, E. Y. N.**, Balasubramaniam A. S. (2004). "Failure States For Normally and Overconsolidated Soft Bangkok Clay". *Proceedings of 15th Southeast Asian Geotechnical Engineering Conference*, Bangkok, Thailand, Vol. 1, 37-42.
7. Lee, C., J., Handali, S., Kim, S. R., Lee, Y. H., **Oh, E. Y. N.**, Bolton, M., Balasubramaniam, A. S. (2004). "New Method to Predict Pore Pressures For Settlement Calculations and Stability Analysis". *Proceedings of 15th Southeast Asian Geotechnical Engineering Conference*, Bangkok, Thailand, Vol. 1, 803-808.

8. **Oh, E. Y. N.**, Balasubramaniam, A. S., Bolton, M., Chai, G. W. K., Braund, M, Wijeyakulasuriya, V., Nithiraj, R., Bergado, D. T. (2004). "Soft Clay Properties and Their Influence in Preloading with PVD and Sur-charge". *Proceedings of 15th Southeast Asian Geotechnical Engineering Conference*, Bangkok, Thailand, Vol. 1, 79-84.
9. **Oh, E. Y. N**. (2004). "Selection of suitable ground improvement techniques for southeast Queensland soft clay". *Proceedings of 6th ANZ Young Geotechnical Professionals Conference*, Gold Coast, Australia, Vol. 1, 188-193.
10. Chai, G. W. K., **Oh, Y-N.**, Smith, W., Asnan, A. (2004). "Sustainability in Road Construction through Cement Stabilization". *Proceedings of International Conference of Advanced Technologies in Transportation Engineering (AATT)*, Beijing, China (Paper 304 in CDROM).
11. Balasubramaniam, A. S., Phienwej, N., C. H. Gan, and **Oh, Y-N**, (2004). "Piled foundation and basement excavation for Tall Buildings in Bangkok sub-soils". *Proceedings of the 2004 Malaysian Geotechnical Conference*, Kuala Lumpur, Malaysia, Vol. 1, 89-108.
12. Balasubramaniam, A. S., Bergado, D.T., Wijekulasuriya , V., and **Oh, Y-N.** (2004). "The influence of piezometric draw down on the test embankment with vertical drains and surcharge in the Bangkok sub-soils". *Proceedings of the 9th Australia New Zealand Conference on Geomechanics*, Auckland, New Zealand, Vol. 1, 446-452.
13. Balasubramaniam, A. S., Phienwej, N., **Oh, Y-N,** Sanmugarasa, K (2004). "Back analysis and interpretation of driven and bored pile tests data in Bangkok sub-soils". *Proceedings of the 9th Australia New Zealand Conference on Geomechanics*, Auckland, New Zealand, Vol. 1, 81-87
14. Chai, G., Faisal, H. A., Balasubramaniam, A. S., and **Oh, Y-N**., (2004). "Prediction of the undrained shear strength of pavement subgrade using falling weight Deflectometer". *Proceedings of the 9th Australia New Zealand Conference on Geomechanics*, Auckland, New Zealand, Vol. 2, 846-852.
15. Chu, J., Kim, S. R., **Oh**, **Y-N.**, Balasubramaniam, A. S., and Bergado, D. T. (2004). "An experimental and theoretical study on the dilatancy of sand and clays". *Proceedings of the 9th Australia New Zealand Conference on Geomechanics*, Auckland, New Zealand, Vol. 2, 654-660.

16. Phienwej, N., Photayanuvat, C., Sanmugarasa, K., **Oh, Y-N.**, and Balasubramaniam, A. S, (2004). "Deformation of diaphragm walled deep excavation in Bangkok sub-soils". *Proceedings of the 9th Australia New Zealand Conference on Geomechanics*, Auckland, New Zealand, Vol. 2, 888-894.
17. **Oh, Y. N.**, Sivaneswaran , N., Balasubramaniam, A. S., Wijeyakulasuriya, V., and Sanmugarasa, K. (2003). "Case histories of ground improvement schemes relevant to railroad embankments". *Proceedings of AusRAIL (Australasian Railway) PLUS 2003 conference*, Sydney, Australia, Paper No. RTAA 16 (in CD-ROM).
18. Balasubramaniam, A. S., Uddin, K., Sanmugarasa, K., Lee, Y.H., **Oh, Y-N.**, Gurung, N., and Bergado, D. T. (2003). "Effects of Additives on Soft Clay Behaviour". *Proc. of the 21st ARRB and 11th Road Engineering Association of Asia and Australia (REAAA) Conference,* Cairns, Queensland, Australia, Paper No. 56 (CD-ROM).
19. **Oh, Y-N**., Jeng, D. S., Chen, S. and Chien, L. K. (2002). "A parametric study using discontinuous deformation analysis to model wave-induced seabed response", *The fifth International Conference on Analysis of Discontinuous Deformation* (Editor: Hatzor, Y. H.). Beer Sheva, Isreal, Vol. 1, 113-120.
20. Jeng, D. S., **Oh, Y-N.**, Chen, S. and Chien, L. K. (2002). "Analysis of displacement and stress around a tunnel", *The fifth International Conference on Analysis of Discontinuous Deformation* (Editor: Hatzor, Y. H.), Beer Sheva, Isreal, Vol. 1, 107-112.
21. Jeng, D. S., **Oh, Y-N.**, Chen, S. (2002). "Discontinuous deformation analysis for wave-induced settlement of a seawall". *The 3rd International Conference on Engineering Computation Technology* (ECT2002), Czech of Republic, September 2002 (CD ROM).
22. Jeng, D. S., **Oh, Y-N**. and Chen, S. (2002). "Wave-induced pore pressure and effective stresses in a saturated porous seabed". *The Second International Conference on Advances in Structural Engineering and Mechanics* (ASEM02), Korea, August 2002 (CD ROM).
23. **Oh, Y-N.**, Jeng, D-S. and Chen, S. (2002). "Discontinuous deformation analysis for wave-induced pore pressure in the vicinity of a breakwater". *Proceedings of The 17th Australasian Conference on The Mechanics of Structures And Material*, Vol. 1, 733-738.

24. Jeng, D. S., Cha, F. D. H., Rahman, M. S., Sekiguchi, H., **Oh, Y-N**. and Teo, L. (2002). "Quasi-static solution, *u-p* approximation and dynamic solution for the wave-induced seabed response". *Proceedings of The 12th (2002) International Offshore and Polar Engineering Conference (ISOPE02)*, Vol. II, 731-737.
25. **Oh, Y-N**., Jeng, D. S., Teo, H-T. and Cha, D-H. (2002)."Effects of wave non-linearity on the wave-induced seabed response". *Proceedings of The 12th (2002) International Offshore and Polar Engineering Conference (ISOPE02)* , Vol. II, 738-744.
26. Teo, H. T., Jeng, D. S., **Oh, Y-N**. and D-H Cha (2002). "Wave kinematics of short-crested waves: fifth-order approximation". *Proceedings of The 12th (2002) International Offshore and Polar Engineering Conference (ISOPE02)* , Vol. III, 26-30.

TABLE OF CONTENTS

LIST OF TABLES

LIST OF FIGURES

LIST OF NOTATIONS

a_v - Coefficient of compressibility (m^2/MN)

$c', \bar{c}$ - Cohesion in term of effective stress (kN/m^2)

C_C - Compression index (dimensionless)

c_h - Coefficient of horizontal consolidation (m^2/year)

c_v - Coefficient of vertical consolidation (m^2/year)

C_α - Secondary compression parameter

d_m - Diameter of the circle with an equal area to the cross-sectional area of the mandrel (m)

d_s - Diameter of the smeared zone around the drain (m)

d_w - Equivalent diameter of drain (m)

D - Constrained modulus (MN/m^2)

D_e - Diameter of the equivalent cylinder for PVD (m)

e - Voids ratio (dimension less)

$E', \bar{E}$ - Young's modulus (kN/m^2)

F - Total factor due to drains spacing, well resistance and smear effect for PVD (dimensionless)

FS - Factor of safety (dimensionless)

F(n) - Factor for PVD spacing (dimensionless)

F_r - Factor for well resistance of PVD (dimensionless)

F_s - Factor for smear effect of PVD (dimensionless)

H - Drainage length (m)

k_h - Coefficient of horizontal permeability (m/day)

k_v - Coefficient of vertical permeability (m/day)

L - Twice the drain length (m)

m_v - Coefficient of volume decrease (m^2/MN)

n - Spacing ratio (dimensionless)

OCR - Over consolidation ratio (dimensionless)

q - Surcharge pressure (kN/m^2)

q_w - Discharge capacity of the drain at a hydraulic gradient of one

R - Radial distance (of considered point) from centre of the drained soil cylinder

s - Centre to centre spacing of the drains (m)

S_{100} - Final Settlement (mm, m)

S'_{100} - Final settlement resulting from initial fill (mm, m)

u - Average excess pore pressure (kN/m^2)

U - Degree of consolidation (%)

U_h - Horizontal degree of consolidation (%)

U_v - Vertical degree of consolidation (%)

z - Distance from drainage end of the drain in well resistance consideration (m)

Δu_o - Excess pore pressure at reference time, t - 0 (kN/m^2)

Δu_t - Excess pore pressure at reference time t (kN/m^2)

Δt - Equivalent time increments (day)

$\varphi', \overline{\varphi}$ - Friction angle (degree)

κ - Swelling index (dimensionless)

κ^* - Modified swelling index (dimensionless)

λ - Compression index (dimensionless)

λ^* - Modified compression index (dimensionless)

$\nu', \overline{\nu}$ - Poison's ratio (dimensionless)

σ_w - Total pore water pressure (kN/m^2)

σ'_w - Excess pore water pressure (kN/m^2)

σ_n - Total normal stress (kN/m^2)

σ'_n - Effective normal stress (kN/m^2)

σ_{xx} - Total horizontal stress in x direction (kN/m^2)

σ_{yy} - Total vertical stress (kN/m^2)

σ_{zz} - Total horizontal stress in z direction (kN/m^2)

σ'_{xx}, - Effective horizontal stress in x direction (kN/m^2)

σ'_v, σ'_{yy} - Effective vertical stress (kN/m^2)

σ'_{zz} - Effective horizontal stress in z direction (kN/m^2)

τ - Shear stress (kN/m^2)

ψ - Dilatancy angle (degree)

CHAPTER 1

INTRODUCTION

1.1 General

This dissertation is the first Geotechnical Engineering doctoral thesis in Griffith University, and is focussed on the laboratory and field behaviour of alluvial soft clay as found in Southeast Queensland. Soft clays are wide spread in Australia along the coastlines and pose difficult problems in design and construction of roads, expressways and motorways. In Southeast Queensland, soft clays were encountered by Queensland Department of Main Roads (QDMR) in the Gold Coast Highway, Sunshine Motorway and Port of Brisbane Motorway.

In the study process, due to the insufficient laboratory equipments and access to Geotechnical Engineering softwares, the dissertation has to be presented in a practical form, where three case histories are discussed and the analyses are based on practical methods. Further, laboratory tests were conducted to investigate the application of chemical (cement and lime) treatments.

In this study, the author concentrated fully on the available data in various QDMR reports as related to the soft clay behaviour at three sites (Gold Coast Highway, Sunshine Motorway, and Port of Brisbane Motorway). All the laboratory and field test data were re-analysed and assembled in a suitable form for further analysis using PLAXIS (Brinkgreve, 2002). In carrying out this task most of the time was spent in trying to assemble this information from raw data scattered in many places. Especially, the test embankment data need to be interpreted in great detail for their accuracy. The soft clay behaviour can vary from deposit to deposit depending on the mode of deposition, organic content, water content, presence or absence of weathered zone, presence or absence of sand and silt seems which cause the field permeability to be

substantially different from those of the laboratory tests. Then, there are also phenomena such as anisotropy, undrained and drained creep, 3-D effects which often makes the modelling features very complicated. In this study, well known and classical formulations on interpreting the field data from the test embankment are first made. Available borehole data close to the trial embankment were used to delineate the soft clay and other soil deposits in a longitudinal section close to the test embankment location. Finally, the PLAXIS Version 8 was used to do a coupled consolidation analysis of the test sections with and without the PVD, and with and without stone columns.

1.2 Background

Due to the rapid increase in population and associated development activities taking place in Southeast Queensland during the past few years, construction activities are now mainly concentrated on low-lying marshy areas, which comprise of highly compressible weak organic soils of varying thickness. These soft clay deposits have low bearing capacity as well as excessive settlement characteristics. Therefore, in order to prevent differential settlements, it is essential to stabilise the existing soft soils before commencing the construction activities.

The School of Engineering at Griffith University has a collaborative research with QDMR on a detailed study of the engineering behaviour of soft soils deposits. The QDMR is posed with abundant engineering challenges as these soft clays are very difficult to sample and test in the laboratory. Thus, it has been necessary to carry out large-scale test embankments to investigate the field behaviour very similar to the actual embankments built along the expressways and motorways. These test embankments were fully instrumented to measure the settlements, lateral movements and the development of excess pore pressures under the embankment load and their dissipation

with time. Also, ground improvement techniques such as the use of vertical drains and stone column were also evaluated for their potential applications.

Preloading is the most successful ground improvement technique that can be used in low- lying areas. It involves loading of the ground surface to induce a greater part of the ultimate settlement that the ground is expected to experience after construction. Since most compressible soils are characterized by very low permeability and considerable thickness, the time needed for the required consolidation can be long, and also the surcharge load required may be significantly high. In this study, the effectiveness of vertical drains and stone columns subjected to combined surcharge was evaluated by in large-scale field tests and laboratory tests.

This dissertation is concerned with the geotechnical problems encountered with the design and construction of Motorways and Highways in the soft estuarine clays of Southeast Queensland. Three Motorways are selected and these are the Gold Coast Highway, Sunshine Coast Motorway and Port of Brisbane Motorway. The soft clay deposits are encountered in these projects at locations where the land is low-lying, and the deposits are sediments from river tributaries in the recent past. The engineering properties of soft clays and very soft clays are most difficult to obtain from laboratory tests due to serious errors in sampling and testing. Therefore more reliance is often made on field tests.

The Gold Coast Highway is the major route through the Gold Coast of Queensland. Due to the increased traffic, it has become necessary to upgrade the existing two-lane road to a four-lane facility. There is an important wetland reserve adjacent to this section of highway, which has environmental significance. The section of highway traverses a swamp of soft clay up to 13.5 m deep. The soils and rocks along the highway belong to the Neranleigh-Fernvale Group of the Silurian Age. The rocks are mainly greywacke

with some inter-bedded argillite. Quaternary alluvium is present in valleys between the ridges. This alluvium consists of clays and silty clay overlain by soft organic clays. The boreholes indicated a subsurface profile of consolidated alluvium or argillite below soft to very soft estuarine clays. The soft clay deposit is a maximum 13.5m deep towards the centre of the plain, thinning to a minimum of 3m at the outer edges. Field and laboratory tests were performed to investigate the geotechnical properties of the subsurface profile. The field-testing was to investigate the general subsurface profile and to perform the field vane shear test. The laboratory testing included the standard classification and the tests involved in determining the engineering properties of the soils.

The Sunshine Motorway is the main connection between the Sunshine Coast and Brisbane. Test data from a number of soft soil and swampy areas along the alignment were collected. Included were the consolidation parameters, Atterberg limits and shear strengths. This area extends through cane farm lowlands, a minor swamp section adjacent to the Maroochy River, then higher terrain south of West Coolum Road, before another swamp area and more cane farm lowlands. This alignment of the Motorway predominantly traverses low lying unconsolidated sediments including: estuarine swamp and lagoonal deposits; Pleistocene to Holocene deposits consisting of soft organic clay, mud, sand-clay mixtures and fine sand; coastal mangrove and tidal deposits; and, Holocene deposits consisting of very soft fine grained clay/silt mixtures which contain minor sand. These sediments are from the Quaternary Age.

The Port Brisbane Motorway connects the Gateway Motorway to the Port of Brisbane. The Gateway Motorway is the western end of the road and the Port of Brisbane is the eastern end. The route generally traverses flat low-lying estuarine terrain. However, at the western end it traverses sloping residual terrain. The estuarine deposits encountered

were generally dark grey to dark brown, very soft to firm, moist to wet, compressible silty clays of medium to high plasticity. It was found that the creek bed comprised of extremely soft, recently deposited, estuarine silty clay, which overlies young deposits of soft to firm estuarine silty clay and silty sand. This very soft soil thickness varies up to 5m depth. These deposits overlie old beds of residual and alluvial soils and bedrock belonging to the Tingalpa Formation. The layer thicknesses vary across the site with a maximum depth of 26.5m. The upper silty clay alluvial layer was found continuously along the alignment except the western end. This alluvial silty clay has low plasticity compared to the estuarine silty clay. The residual soils exhibit the engineering properties of a moist, stiff to hard sandy clay/sandy silty clay.

Ground improvement techniques have now become popular with construction activities on soft clay deposits and these include the use of vertical drains, stone columns, lime and cement columns at the base of the embankments. The best way to evaluate the suitability of a particular type of ground improvement is often verified in the field by carrying out large scaled field tests. The use of vertical drains with surcharge, and the use of stone columns are investigated in this thesis work. Also, the use of lime and cement columns is further investigated on laboratory tests.

1.3 Objectives and Scope of Study

The objectives of this study are to:

i. Analyse the extensive laboratory and field data of soft clay in the Gold Coast Highway, Sunshine Motorway, and Port of Brisbane Motorway.

ii. Evaluate the performance of vertical drains in accelerating consolidation settlement below the test embankment.

iii. Evaluate the performance of stone columns in reducing settlement below the test embankment.

iv. Compare the field measurements with preliminary predictions as made by settlement and stability analysis and the use of PLAXIS finite element program.

v. Investigate the usefulness of lime and cement treatments on Southeast Queensland soft clay, by evaluating the increase in strengths based on Unconfined Compression Tests.

The scope of the study is in line with the objectives and initially, the laboratory test data are analysed in detail. From the available borehole data, initially the soil profile below the test embankment will be delineated. This is then followed by a complete description of the index properties and shear strength. Then a detailed analysis is made on the consolidation and triaxial tests data. The field data were then interpreted on the settlement, lateral movement and excess pore pressures. From the settlement measurements, field values of the compressibility parameter and the coefficient of consolidation were evaluated. Also, these values were computed from pore pressure dissipation. The limit equilibrium method was used to evaluate the factor of safety of the embankment. Barron (1948) and Hansbo (1979, 1981, 2001, 2003) contributions were used to evaluate the performance of the vertical drain in accelerating the consolidation. Finally, the PLAXIS finite element program was used to predict the performance of the embankment.

1.4 Organisation of the Thesis

In Chapter 1, a brief introduction was presented where the aim and scope of the present research were highlighted. The following Chapter 2 presents a comprehensive survey of the literature associated with the present work. History of vertical drains, present theories related to vertical drains, the analyses of embankments stabilized with vertical drains and related numerical and experimental investigations are reviewed in detail.

Further, related work on stone columns and chemical treatment are also presented. Chapter 3 gives the analysis methods adopted in this research.

Chapter 4 presents the laboratory and field tests of a case study, and discussion of findings for Sunshine Motorway trial embankments. The details of the large-scale trial embankment and the instrumentation to monitor the settlement and pore water pressure are explained. Chapter 5 presents the findings from Port of Brisbane Motorway embankment.

Chapter 6 presents the application of stone column in soft estuarine clay with a case study in Gold Coast. Settlement, pore pressures and lateral displacements are investigated with the field measurements. Chapter 7 discusses the application of chemical additives to stabilise soft estuarine clay. Chapter 8 presents the conclusions of present research and recommendations for further research followed by the bibliography.

CHAPTER 2

LITERATURE REVIEW

2.1 Introduction

In this chapter, a literature review is conducted on the clays deposits in Southeast Queensland, ground improvement techniques used in road embankments and their analysis methods. Relevant literatures on vertical drains, stone columns, and chemical treatment are presented.

This chapter consists of four main sections. Following the introduction, the first section (as in Section 2.2) focuses on the soft clays in Southeast Queensland. Second section (From Section 2.3 to 2.11) gives a review on vertical drains. The third section (Section 2.12) presents the relevant stone column information. The fourth and final section (Section 2.13) shows the application of cement and lime additives in soft clay.

2.2 Southeast Queensland Soft Estuarine Clay

2.2.1 Geological Description

The estuarine deposits normally encountered in Southeast Queensland are classified geologically as originating in the Holocene age. Generally they are grey to dark brown, very soft to firm, moist to wet, compressible organic silty clays of medium to high plasticity. Discontinuous interbeds of sandy silt and sandy silty clay are also common. This material has a strong odour resembling a material deposited in anaerobic and low energy environments. In most instances, a thin surface crust is evident on top of this layer, possibly due to aerial oxidation, desiccation and hardening. This infers that the top surface of this layer may have been the original surface of the estuarine environment prior to reclamation or land filling.

As mentioned above, areas of soft estuarine clay deposits are usually covered with a layer of engineered or non-engineered fill. Engineered fills are a controlled blend of

clay, silt sand, gravel and crushed rock allowing its properties to be safely estimated and maintained for road and railway construction. Non-engineered fill consists of clay, silt sand, gravel, and coal ash and construction material with variable composition. It is mostly uncontrolled and poor quality; placed for the purpose of tidal control, flood mitigation, land reclamation, and embankments (Transport Technology, 2000).

2.2.2 Typical Geotechnical Characteristics

Southeast Queensland Clays have widely varying engineering properties, depending largely on the deposit's depth below the ground surface and the proximity to the water table. For this reason, only approximate ranges of its physical properties and strength characteristics and other properties can be provided. Studies on the general characteristics of soft clays found in the Southeast Queensland have been carried out by various authors.

The compressibility characteristics of the soft clays in Southeast Queensland were compiled by Pyke (2003) and the ground improvement techniques adopted in these area by Eddie (2003). These works were preliminary in nature and were mainly intended as the data compilation from various QDMR reports. Subsequently, Braund (2004) concentrated on the trial embankment study made at the Gold Coast Highway near the Coombabah Creek Bridge in a marine environment. Scott (2004) had concentrated on piled foundations as used in the various structures of the Port of Brisbane Motorway.

Following the work on soft clays in Southeast Queensland, Surarak (2005) concentrated fully on the available data in various QDMR reports as related to the soft clay behaviour at the Sunshine Coast. All the laboratory and field test data were re-analysed and assembled in a suitable form. Thus, in the study of Surarak (2005), well known and classical formulations on interpreting the field data from Sunshine Coast were first made. Additional works on soft clays and ground improvement techniques in Southeast

Queensland were also undertaken by Shuttlewood (2003), Baker (2005), Eke (2005), Scarr (2005), Botha (2005) and Sathawara (2006).

Based on the field shear vane, the undrained shear strength of soft/very soft clays is around 10-15 kPa. Natural moisture contents commonly vary between 60 and 120%. The liquidity indices are generally in the range of 1.5 - 2.5, displaying high sensitivity. Compressibilities as high as $C_c/(1 + e_o) = 0.4 - 0.5$ have been observed in the laboratory. At these high compressibilities, strain rate effects can be significant (Wijeyakulasuriya et al, 1999).

Macro fabric features (sand lenses, etc) have been variable and in the worst cases C_v = 0.1 - 0.3 m^2/yr and $C_v/C_h = 1.0$ have been typical based on laboratory testing. Organic contents up to 10% have been observed, with high creep rates ($C_{\alpha\varepsilon} > 1\%$). Given the sensitivity of soft clays, the compressibility parameters are likely to be underestimated in the normally consolidated range. Piezocone dissipation tests are also masked by the remoulding of the clay caused by insertion of the cone (Wijeyakulasuriya et al, 1999).

2.2.3 Distribution of Soft Clay Deposits

Soft estuarine clay deposits can be found in low lying areas close to the coastline, in layer depths varying from 1 to 30 metres. The distribution of these soft clays is dependant on geological formations, with deposits from the Holocene age being the primary source (Transport Technology, 2000). A series of extracts from this map are also shown in Figures 2.1(a) to 2.1(d) (Whitaker and Green, 1980).

While these maps do not show exact deposits of soft estuarine clays, they do show sites of Holocene deposits where soft estuarine clays are likely to be encountered. It can then be inferred that such soft clay deposits are commonly found in the coastal areas of south-east Queensland, often outlying the estuaries of creeks and rivers. The proximity of such deposits to the major population centres of Queensland is evident, with large

areas of Holocene age material located throughout the Sunshine Coast, Brisbane and Gold Coast regions. As urban sprawl continues, more engineering projects will be required to be conducted upon such a soft estuarine clay foundation.

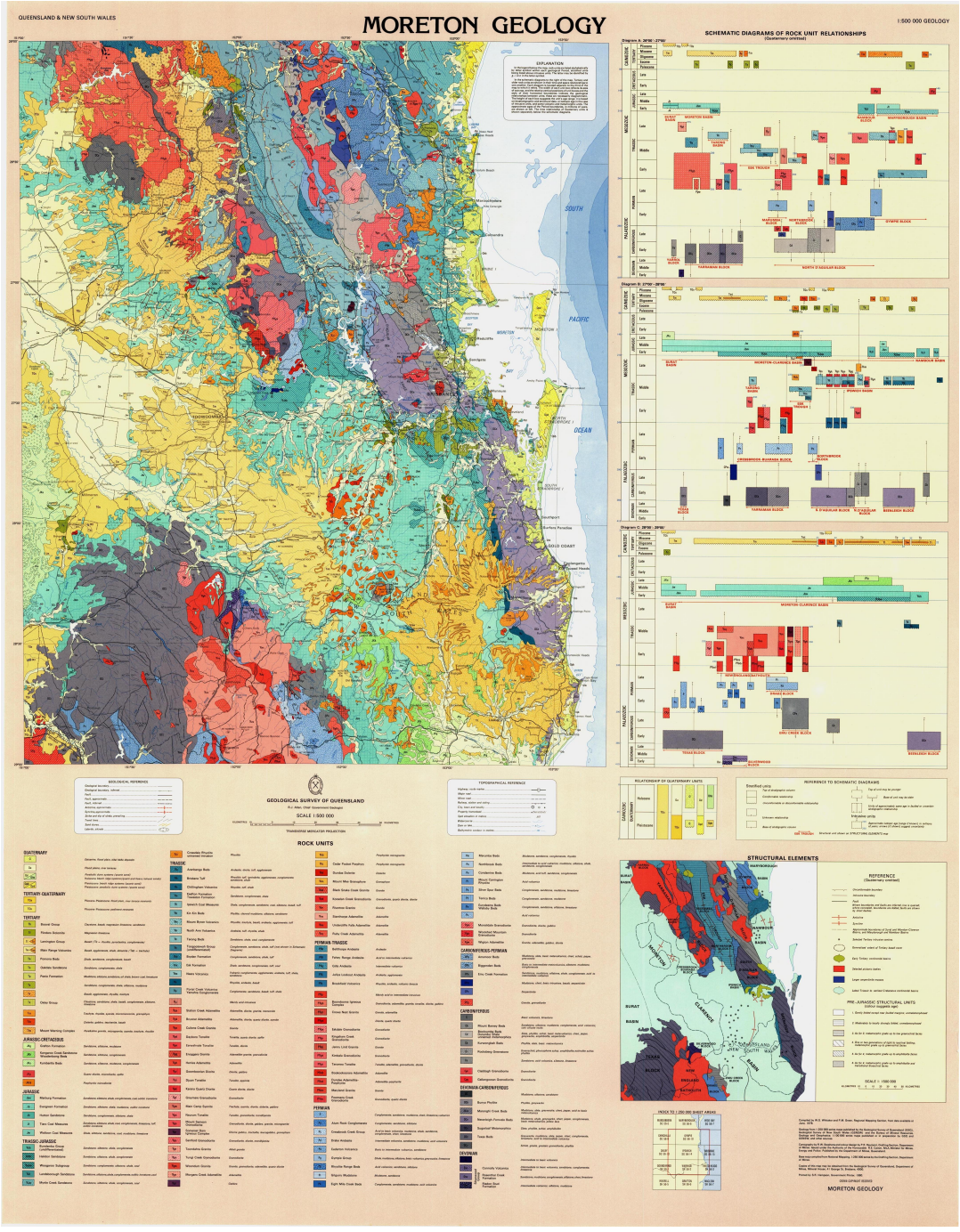

Figure 2.1(a) Geology of South East Queensland (Moreton geology)

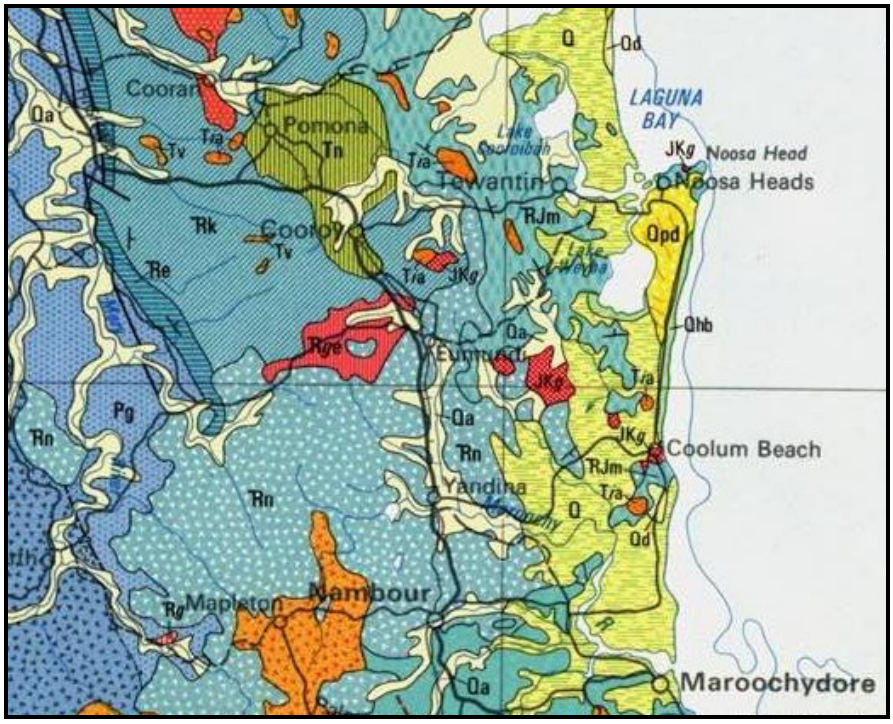

Figure 2.1(b) Distribution of Holocene Deposits (Q), Noosa-Maroochydore

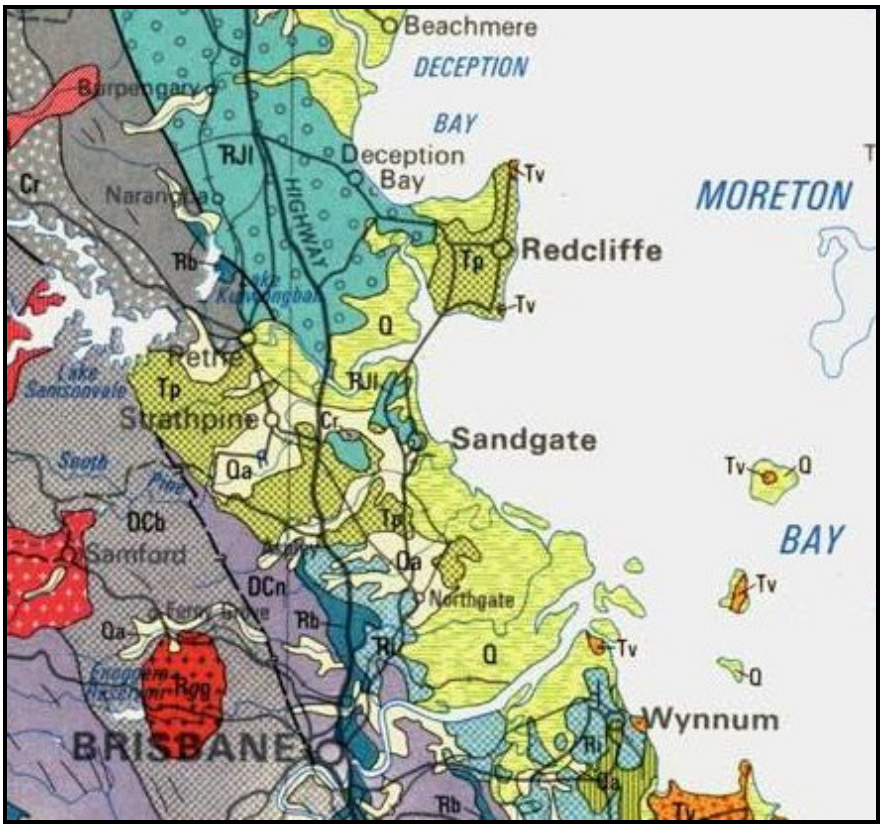

Figure 2.1(c) Distribution of Holocene Deposits in Brisbane

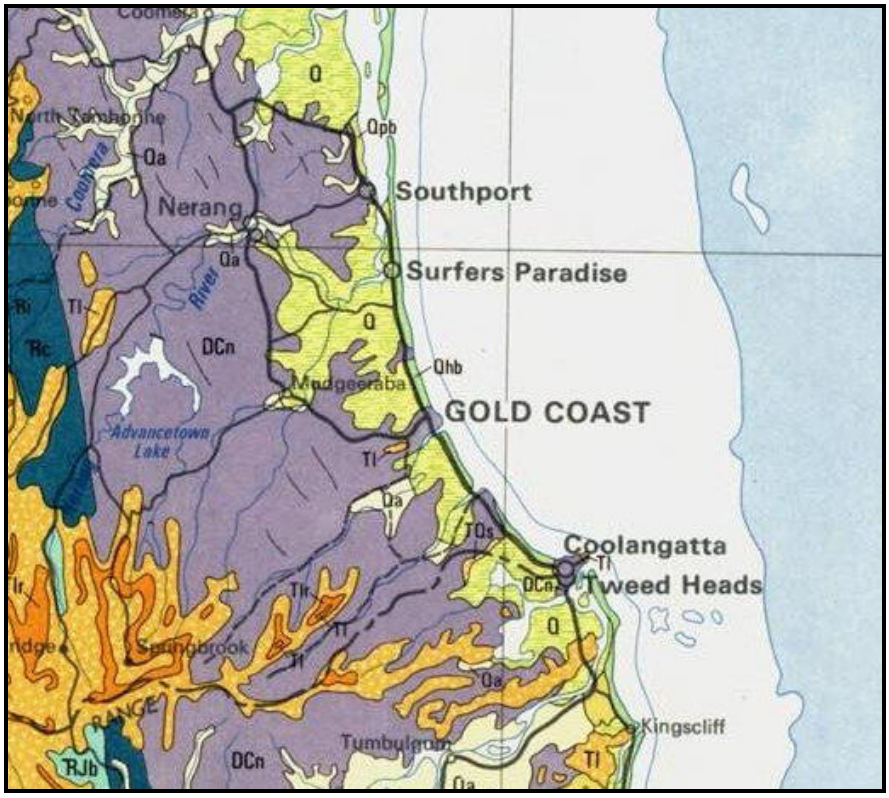

Figure 2.1(d) Distribution of Holocene Deposits in Gold Coast

2.2.4 Construction Implications of Soft Clay

The very nature of soft clay deposits is that they are arguably the most interesting soil to work with from the viewpoint of geotechnical engineering. Soft clays are fairly widespread and the majority of these are of marine origin. Several extensive deltaic deposits exist in Southeast Queensland, some of which are of considerable importance because of their occurrence at the sites of major cities. Soft clays present severe but interesting geotechnical engineering problems (Brand et al., 1989). By their nature, soft clays are of low strength and high compressibility, often with water contents at or close to their liquid limits (Skempton, 1969). Although they are commonly normally consolidated, they nearly always exhibit light over-consolidation caused by self weight consolidation, dessication and the rise and fall of sea levels in the geological past.

There are two main problems encountered when undertaking civil construction on soft clay deposits, excessive settlement and low shear strength. Due to the large void ratio

and inherent compressibility of such clays, consolidation and vertical settlement can be noticeable under construction loads and may continue long after implementation of the structure. Low shear strength is particularly hazardous when constructing large embankments on a soft clay base, facilitating potential circular or sliding failure planes that create slope stability concerns. These issues lead to the need to design structural foundations and/or ground improvement schemes.

Foundation design alternatives can be categorised into two broad types, structural methods and soil treatments. Two different approaches can be used in selecting a foundation design: isolating the superstructure from the soil movements; or, designing a foundation stiff enough to resist differential movements without causing distress to the superstructure.

2.2.5 Benefits of Ground Improvement

While the fore-mentioned structural foundation techniques are likely to be effective, they can become uneconomical where projects of scale are concerned. Therefore the field of ground improvement is of great interest to the transportation engineering sector, where highways and railways may traverse many kilometres of soft soils. These applications also require the formation of sizable embankments, which can exhibit slope stability issues during and after construction due to soft sub-grades. It follows then, that in-situ soil improvement techniques present an economic alternative to traditional structural foundations.

Ground improvement is generally conducted with the following goals in mind:

i. to increase the bearing capacity;

ii. to increase the resistance to shear movement;

iii. to decrease the foundation settlements; and/or,

iv. to increase the resistance against liquefaction.

2.3 Development of Vertical Drains

There are various ground improvement methods that provide soil strength improvement, shorten construction time, mitigation of total and differential settlement, economical construction costs and other characteristics which may impact on their utilisation to specific projects. Factors such as the significance of the structure, applied loading, site conditions, period of construction have to be considered in the selection of the ground treatment method (Bergado et al., 1996).

Various ground improvement methods currently available for soft ground projects include ground improvement by vertical drains, vibro-replacement with stone columns, and lime/cement columns. With special regard for the ground treatment of soft clays, vertical drain with preloading technique remains the most widely used and economical method.

The performance of vertical drains with preloading can be evaluated by various analytical means inclusive of design predictions, field instrumentation monitoring and in-situ testing was investigated in this research study. Firstly, the one-dimensional consolidation settlement behaviour of clays is described by Terzaghi (1925). This method when used in conjunction with Barron (1947) and Carrillo (1942) methods can be used for the design of vertical drains. lmai (1995) had described on the time rate of settlement effect of clays. Many researchers (Hansbo, 1979; Choa et al., 1981; Bo et al., 1997; Bergado et al., 2002; Chu et al., 2002; lndraratna and Bamunawita, 2002) had reported consolidation behaviour of clays by using prefabricated vertical drains. Holtz et al. (1988, 1991) had given an in-depth coverage of the study of vertical drains, which included the method of installation of vertical drains, static penetration or vibratory driving, types of mandrels and type of shoes. These publications have coverage on the theories and mechanisms of vertical drains. The various types of vertical drains and

their characteristics are also covered in these publications as well as design methodology and consolidation processes. In addition, Van Impe (1989) and Hausmann (1990) had also described the theories and mechanisms of vertical drains. Onoue (1988) have suggested a simplified formula for the average degree of consolidation with respect to radial flow.

The performances of the vertical drains were also predicted by the finite element modelling method, and the results are being compared to that of the field instrumentation (Indraratna et al., 1992, 2005a, 2005b). Modelling of untreated control sub-areas was carried out by the full-scale analysis method (Balasubramaniam et al., 1988; Bergado et al., 1993).

Various theories, considerations, design methodologies and predictions for the ground treatment of soft clay with prefabricated vertical drains and preloading will be discussed in the following sections.

2.3.1 History of Vertical Drains

In the past twenty years, sand compaction piles, chemical stabilisation, and prefabricated vertical drains have been used extensively for the purpose of soft ground improvement. Sand drains were first used in practice in and around 1920's (Bo et al., 2003). The California Division of Highways has conducted the first comprehensive laboratory and field tests in 1933. In Japan, during 1940's, the behaviour of vertical sand drains was not well understood, because the bearing capacity of foundations after installation of sand drains was considered to provide sufficient reinforcement, hence, the full load was placed on the foundation too quickly resulting in frequent foundation failure (Aboshi, 1992). In 1956, the method of sand compaction piles was developed in which the vertical sand drains were compacted during installation (Aboshi, 1992). After sand was poured into the pipe (casing), it was withdrawn partway and again driven

down to compact the sand column and enlarge its diameter. Although no effect of densification was expected in clayey soils, these sand columns behaved as granular piles in soft ground, thereby carrying a greater load. At the same time, they also worked as vertical drains to accelerate consolidation of clayey ground, by rapid pore pressure dissipation.

Since 1940, prefabricated band shaped drains and Kjellman cardboard wick drains have been introduced in ground improvement. Subsequently, several types of prefabricated band drains were developed such as: Geodrain (Sweden), Alidrain (England), Mebradrain (Netherlands) etc. Basically, the prefabricated band drains compose of a plastic core with a longitudinal channel wick functioning as a drain, and a sleeve of paper or fibrous material as a filter protecting the core (Bergado et al., 1996; Bo et al., 2003).

2.3.2 Installation and Monitoring of Vertical Drains

Figure 2.2(a) illustrates a typical scheme of vertical drains installation and monitoring instruments required to monitor the performance of the soil foundation beneath an embankment. Prior to vertical drain installation, it is necessary to conduct general site preparation. This work may include the removal of vegetation and surficial debris, establishing site grading and constructing a sand blanket. The purpose of the sand blanket is to conduct the expelled water away from the drains and to provide a sound-working mat.

In the case of vacuum preloading (Cognon et al., 1996), the next step is to install horizontal drains in transverse and longitudinal directions. These drains are linked through transverse connecters and are subsequently linked to the edge of the peripheral trench. The trenches are excavated around the preloaded area to a depth of 0.5m below the ground water level and filled with impervious Bentonite Polyacrolyte slurry for

sealing of the impermeable membrane along the perimeter. Impermeable membrane is installed on the ground surface and sealed along the peripheral trenches. The trenches are backfilled with water to improve the sealing between the membrane and Bentonite slurry. Finally the vacuum pumps are connected to the prefabricated discharge module extending from the trenches. Figure 2.2(b) shows a typical embankment subjected to vacuum preloading.

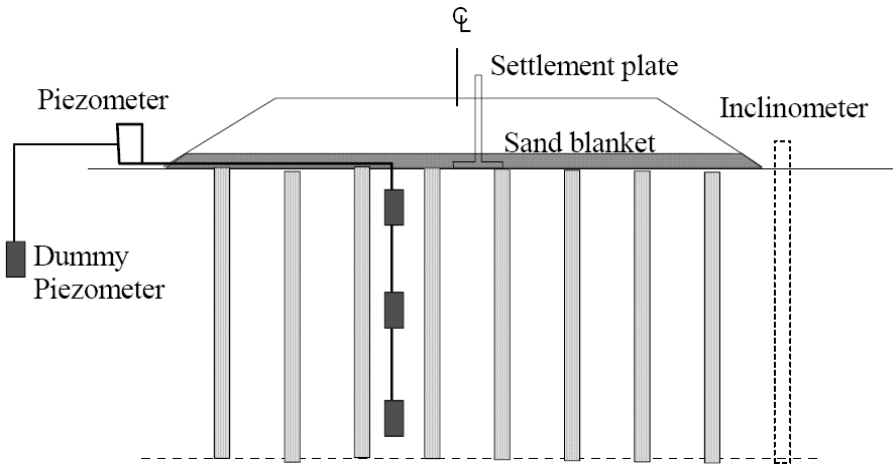

Figure 2.2(a) Basic instrumentation of road embankment

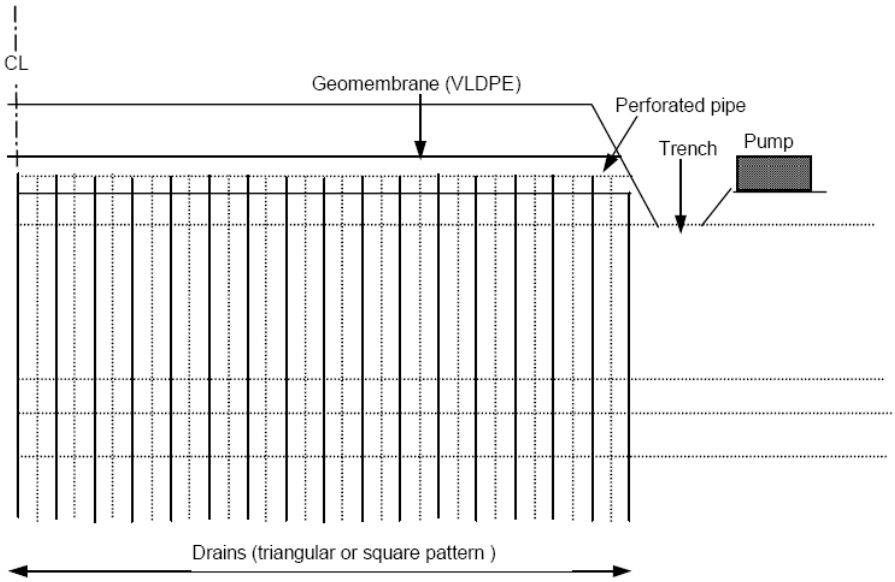

Figure 2.2(b) Schematic diagram of embankment subjected to vacuum loading

Several types of geotechnical instrumentation are required to install before and after construction, in order to monitor the performance of the embankment. Monitoring is essential to prevent sudden failures, to record changes in the rate of settlement and to verify the design parameters (Bo and Choa, 2002). Performance evaluation is also important to improve settlement predictions and to provide sound guidelines for the future projects.

Settlement gauges (e.g. of hydraulic type) are used to measure the long-term settlements at the original ground surface and should be placed immediately after the installation of vertical drains. Settlement plates are suitable for initial reading and should be installed at the bottom of sand blanket, at intermediate depths, and at the bottom of the compressible layer to monitor its settlement. A benchmark is usually set up on a stable ground at a reasonable distance from the fill. Piezometers are used to monitor the complete pore pressure profiles and should be installed at the bottom of sand blanket, at intermediate depths and at the bottom of the compressible layer (Bo and Choa, 2004; Dunnicliff, 1993). A dummy or remote piezometer should also be installed at an adequate distance from the embankment to record the original or natural ground water level, and in general, the pore water pressure at a particular depth. Alignment stakes can be installed parallel to the embankment slope prior to the placement of the fill. The alignment stake is a simple means of measuring the lateral displacement of the foundation during construction of the embankment. In fact, they could provide an early warning of bearing capacity failure. A more sophisticated equipment to measure lateral displacement is an inclinometer, which is usually placed set around the toe of the embankment (Chu and Choa, 1995; Dunnicliff, 1993)

2.3.3 Drain Properties

2.3.3.1 Equivalent Drain Diameter for Band Shaped Drain

The conventional theory of consolidation with vertical drains assumes that the vertical drains are circular in cross-section. Therefore, a band-shaped drain needs to be converted to an equivalent circular diameter, which implies that the equivalent diameter of a circular drain has the same theoretical radial drainage capacity as the band-shaped drain. Kjellman (1948) stated, —the draining effect of a drain depends to a great extent upon the circumference of its cross-section, but very little upon its cross-sectional area“. Based on Kjellman‘s consideration, Hansbo (1981, 2004) introduced the equivalent diameter for a prefabricated band-shaped drain, as given in Equation 2.1.

$$d_w = r_w = 2\frac{a+b}{\pi} \tag{2.1}$$

Another study (Rixner et al., 1986) suggested that the more appropriate d_w is given by the less complex relationship as in Equation 2.2.

$$d = \frac{a+b}{2} \tag{2.2}$$

where, a = the width of the PVD and b = the thickness of the PVD

Pradhan et al. (1993) suggested that the equivalent diameter of band-shaped drains should be estimated by considering the flow net around the soil cylinder of diameter d_e (see Figure 2.3). The mean square distance of their flow net is calculated as:

$$\bar{s}^2 = \frac{1}{4}{d_e}^2 + \frac{1}{12}a^2 - \frac{2a}{\pi^2}d_e \tag{2.3}$$

$$d_w = d_e - 2\sqrt{\bar{s}^2} + b \tag{2.4}$$

Based on finite element studies and by comparing the equivalent band shaped drains

diameter represented by Equations 2.1 and 2.2, it was found that the equivalent diameter given by Equation 2.1 should be reduced by 20 percent. It was suggested by Rixner et al. (1986) that the use of Equation 2.2 is more appropriate than Equation 2.1, based on numerical modelling.

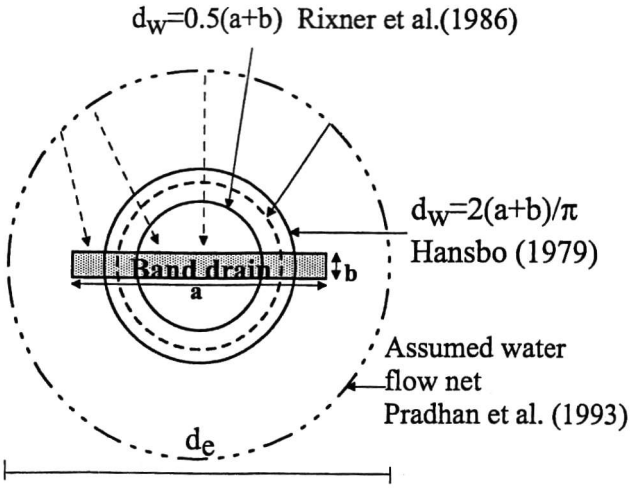

Figure 2.3 Equivalent diameters of band-shaped vertical drains (Pradhan et al., 1993)

2.3.3.2 Filter and Apparent Opening Size (AOS)

The drain material (sand drain) and the filter jacket of PVD have to perform two basic but contrasting requirements, which are retaining the soil particles and at the same time allowing the pore water to pass through. The general guideline of the drain permeability is given by:

$$k_{filter} > 2\, k_{soil} \tag{2.5}$$

An effective filtration can minimise soil particles from moving through the filter. A commonly employed filtration requirement is given by:

$$\frac{O_{95}}{D_{85}} \leq 3 \tag{2.6}$$

where, O_{95} indicates the approximate largest particle that would effectively pass through the filter. Sieving is done using glass beads of successively larger diameter until

5% passes through the filter, and this size in millimetres defines the AOS, O_{95} based on ASTM D 4751 (ASTM, 1993). This apparent opening size (AOS) is usually taken to be less than 90 microns based on Equation 2.6. D_{85} indicates the diameter of clay particles corresponding to 85% passing. The retention ability of the filter is given by:

$$\frac{O_{50}}{D_{50}} \leq 24 \tag{2.7}$$

Filter material can also become clogged if the soil particles become trapped within the filter fabric structure. Clogging is prevented by ensuring that (Christopher and Holtz, 1985; Holtz and Christopher, 1987):

$$\frac{O_{95}}{D_{85}} \geq 3 \tag{2.8}$$

2.3.3.3 Discharge Capacity

The discharge capacity of the prefabricated vertical drain is required to analyse the drain (well) resistance factor. However, well resistance factor is always less significant than the drain spacing and the disturbance (or smear effect). In order to measure the discharge capacity of drains, it is required to simulate as closely as possible the conditions in the field. In this case, the discharge capacity will be a function of the volume of the core or the drain channel, the lateral earth pressure acting on the drains, possible folding, bending and twisting of the drain due to large settlement, infiltration of fine soil particles through the filter, and the biological and chemical degradation. Incorporating the above factors, the actual discharge capacity, q_w, is then given by:

$$q_w = F_t \cdot F_c \cdot F_{fc} \cdot q_{req} \tag{2.9}$$

where F_t, F_c, and F_{fc} are the influence factors due to time, drain deformation and

clogging, respectively. The term q_{req} is the theoretical discharge capacity calculated from Barron's theory of consolidation, which is given by:

$$q_{req} = \frac{\varepsilon_f U_{10} l \pi c_h}{4T_h} \tag{2.10}$$

where, ε_f is the final settlement of the soft soil equivalent to 25% of the length of the drain installed to the soft ground, U_{10} is the 10 percent degree of consolidation, l is the depth of the vertical drain, c_h is horizontal coefficient of consolidation and T_h is the time factor for horizontal (lateral) consolidation.

From laboratory test results, the influence factor of time, F_t, has been estimated to be less than 1.2, and it is usually conservatively taken to be 1.25. The reduction of the discharge capacity under the worst condition of bending, folding and twisting has been suggested to be about 48%, which gives an influence factor of deformation, F_c of about 2. The filtration tests show that the trapped fine soil particles decrease the permeability of the PVD, and in turn decrease the PVD discharge capacity. This deterioration is complicated by the biological and chemical growth in the geo-textile filter. From filtration tests, the value of F_{fc} is suggested to vary between 2.8 and 4.2 with an average of about 3.5. After considering all the worst conditions that may occur in the field, the discharge capacity, q_w of the PVD could be as high as 500-800 m^3/year, but reduced to 100-300 m^3/year where the hydraulic gradient is unity under elevated lateral pressure (Rixner et al., 1986).

The discharge capacity of various types of drains is shown in Figure 2.4, where the discharge capacity is influenced by lateral confining pressure. It is also suggested, in lieu of laboratory test data, that the discharge capacity can be conservatively assumed to

be 100 m^3/year. Hansbo (1981) based on laboratory test results suggested a much smaller discharge capacity of drains, as summarised in Table 2.1.

Table 2.1 Short-term discharge capacity (m^3/year) of eight band drains measured in laboratory (Hansbo, 1981)

Drain Type	Lateral pressure (kPa)			
	40	80	250	500
Geo-drain	26	20	20	16
Other drain types	21	20	18	10
	24	22	14	12
	15	14	14	12
	10	5	1	Clogged
	21	19	17	15
	--	17	13	12
	19	17	9	4

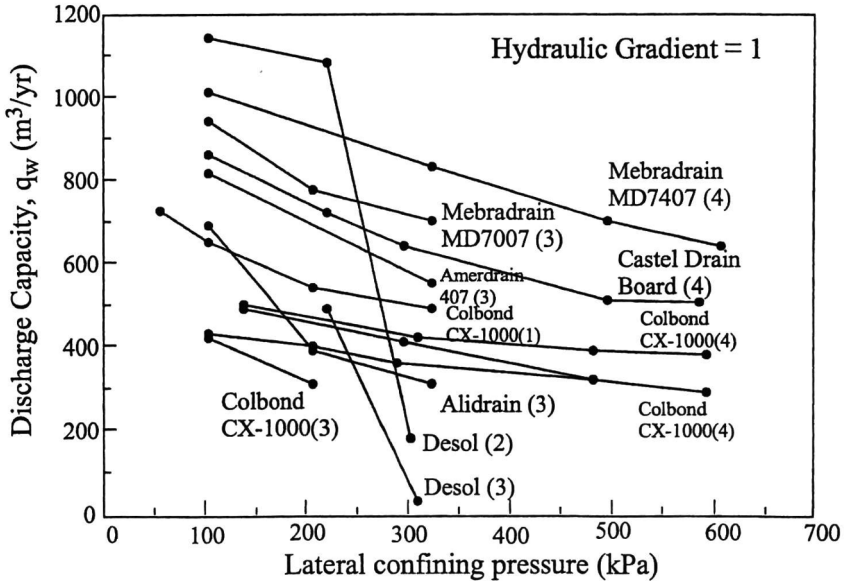

Figure 2.4 Typical values of vertical discharge capacity (Rixner et al., 1986)

Holtz et al. (1991) reported that the discharge capacity of prefabricated vertical drains could vary from 100-800 m^3/year. The discharge capacity of PVD is a function of its filter permeability, core volume or cross section area, lateral confining pressure, drain stiffness controlling its deformation characteristics, among other factors (Hansbo, 1979; Holtz et al. 1991). For long vertical drains that are vulnerable to well resistance, Hansbo (1981) and Holtz et al. (1988, 1991) pointed out that in the field, the actual reduction of the discharge capacity can be attributed to: (a) reduced flow in drain core due to increased lateral earth pressure, (b) folding and crimping of drain due to excessive

settlements, and (c) infiltration of fine silt or clay particles through the filter.

Based on a number of experiments, Holtz et al. (1988) concluded that as long as the initial discharge capacity of PVD exceeds 100-150 m^3/year, some reduction in discharge capacity due to installation should not seriously influence the consolidation rates. However, discharge capacity q_w can fall below this desired minimum value due to the three reasons mentioned earlier. For certain types of PVD, affected by significant vertical compression and high lateral pressure, q_w values may be reduced to 25-100 m^3/year (Holtz et al., 1991). Clearly, the 'clogged' drains are associated with q_w values approaching zero.

2.4 Factors Influencing the Vertical Drain Efficiency

2.4.1 Smear Zone

The installation of vertical drains by means of a mandrel causes significant remoulding of the subsoil especially in the immediate vicinity of the mandrel. Thus, a zone of smear will be developed with reduced permeability and increased compressibility. Barron (1948) stated that if the drain wells are installed by driving cased holes and then back filling as the casing is withdrawn, the driving and pulling of the casing would distort and remould the adjacent soil. In varve soils, the finer and more impervious layers will be dragged down and smeared over the more pervious layers, resulting in a zone of reduced permeability in the soil adjacent to the well periphery. As remoulding retards the consolidation process of the subsoil, it has to be considered in any theoretical solution. Barron (1948) suggested the concept of reduced permeability, which is equivalent to lowering the overall value of the coefficient of consolidation. Hansbo (1979) also introduced a zone of smear in the vicinity of the drain with a reduced value of permeability.

The combined effect of permeability and compressibility within the smear zone brought

a different behaviour from the undisturbed soil, hence, the prediction of the behaviour of the soil stabilised with vertical drains cannot be made accurately if the effect of smear is ignored (Hird and Moseley, 2000). Both Barron (1948) and Hansbo (1981) modelled the smear zone by dividing the soil cylinder dewatered by the central drain into two zones. The smear zone is the region in the immediate vicinity of the drain, which is disturbed, and the other zone is the intact or undisturbed region outside the smear zone (Chai et al., 1997). Onoue et al. (1991) introduced a three zone hypothesis defined by: plastic smear zone in the immediate vicinity of the drain where the soil is highly remolded during the process of installation of the drain, plastic zone where the permeability is reduced moderately, and the undisturbed zone where the soil is not at all affected by the process of drain installation. This three-zone analysis was suggested after extensive laboratory testing by Ting, et al. (1990). However, due to the complex variation of permeability in the radial direction from the drain, the solution of the three-zone approach becomes increasingly difficult. For practical purposes, the two-zone approach is generally sufficient.

Jamiolkowski and Lancellotta (1981) proposed that the diameter of the smear zone (d_s) and the cross sectional area of mandrel can be related as follows:

$$d_s = \frac{(5 \; to \; 6) d_m}{2} \tag{2.11}$$

where d_m is the diameter of the circle with a area is equal to the cross sectional area of the mandrel. Based on the results of Akagi (1977, 1981), Hansbo (1987) proposed another relationship as follows:

$$d_s = 2d_m \tag{2.12}$$

Indraratna and Redana (1998) proposed that the estimated smear zone is about 3-4 times

the cross-sectional area of the mandrel. The proposed relationship was verified using the specially designed large-scale consolidometer (Indraratna and Redana, 1995). The schematic section of the consolidometer and the location of the recovered specimen are shown in Figures 2.5(a) and 2.5(b). Figure 2.6 shows the variation of k_h / k_v ratio along the radial distance from the central distance. According to Hansbo (1987, 1997a), Bergado et al. (1991, 1993), and Cortlever and Hansbo (2004), in the smear zone, the k'_h / k'_v ratio was found to be close to unity, which is in agreement with the results of the study of Indraratna and Redana (1998). The degree of disturbance depends on several factors as described below.

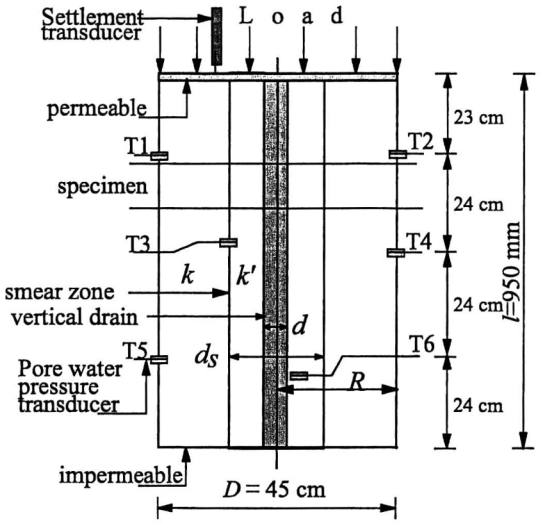

Figure 2.5(a) Schematic section of the test equipment showing the central drain and associated smear (Indraratna and Redana, 1998)

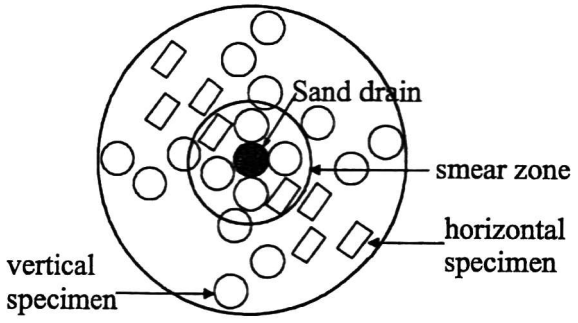

Figure 2.5(b) Locations of small specimens obtained to determine the consolidation and permeability characteristics (Indraratna and Redana, 1998)

2.4.1.1 Mandrel Size and Shape

Generally, disturbance increases with the total mandrel cross sectional area. The mandrel size should be as close as possible to that of the drain to minimise displacement. While working on the effect of mandrel driven drains on soft clays, Akagi (1977, 1981) observed that when a closed-end mandrel is driven into saturated clay, the clay will suffer large excess pore water pressure, associated with ground heave and lateral displacement. The strength and coefficient of consolidation of the surrounding soil can then decrease considerably. However, the excess pore pressure dissipated rapidly followed by the process of consolidation after installation of the mandrel or before the fill is placed. Bergado et al. (1991, 1993) reported from a case study of a Bangkok clay embankment stabilised with vertical drains that a faster rate of settlement took place in the area where the drains were installed using a mandrel with a smaller cross section area rather than a larger mandrel. This verifies that a smaller smear zone was developed in the former.

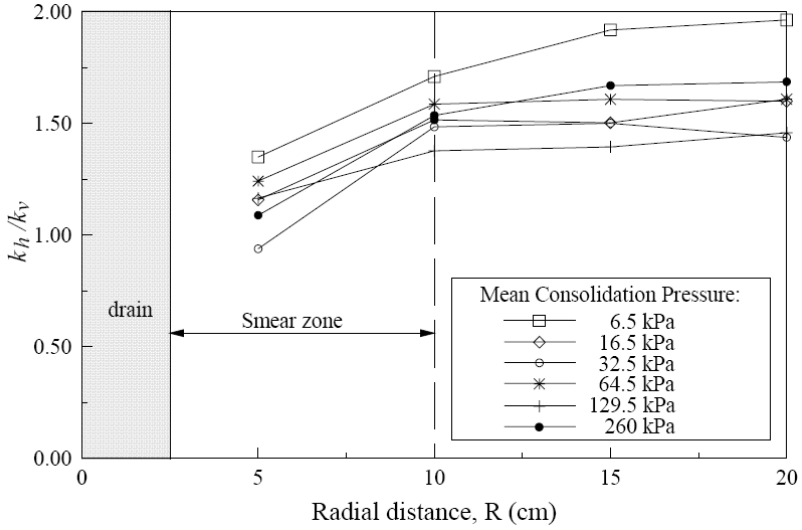

Figure 2.6 Ratio of k_h / k_v along the radial distance from the central drain (Indraratna and Redana, 1998)

2.4.1.2 Soil Macro Fabric

For soil with pronounced macro-fabric, the ratio of horizontal permeability to vertical permeability (k_h / k_v) can be very high, whereas the k_h / k_v ratio becomes unity within

the disturbed (smear) zone (Indraratna and Redana, 1998). The vertical drains are particularly efficient where the clay layers contain many thin horizontal sand or silt lenses (micro-layers). However, if these micro-layers are continuous in the horizontal direction, the installation of vertical drains may not be effective, since rapid drainage of the pore water out of the soil layers may occur irrespective of whether the drains are installed or not.

2.4.1.3 Installation Procedure

Jamiolkowski and Lancellota (1981) suggested that the smear zone is given by

$$d_s = (5 \; to \; 6) r_m \tag{2.13}$$

where r_m is the radius of a circle with an area equal to the mandrel's greatest cross-sectional area, or the cross-sectional area of the anchor or tip, which ever is greater. For design purposes, it is currently assumed that within the disturbed zone, complete soil remoulding occurs.

Evaluation of the effect of installation on the degree of disturbance is a very complex matter in soil mechanics. Equation 2.13 provides only a very simple approach for accounting for disturbance. Baligh (1985) developed a strain path method to estimate the disturbance caused during the installation of piles. The state of strain during undrained axisymmetric penetration of closed end piles have three deviatoric strain components, E_1, E_2 and E_3. E_1 is the shearing strain in a conventional triaxial test, E_2 is the strain from pressuremeter tests (cylindrical cavity expansion tests) and E_3 is the strain from simple shear tests. The second deviatoric strain invariant, the octahedral strain (γ_{oct}) is then given by:

$$\gamma_{oct} = \frac{1}{\sqrt{2}}\left[E_1^2 + E_2^2 + E_3^2\right]^{\frac{1}{2}} \tag{2.14}$$

Figure 2.7 shows the theoretical distribution of octahedral shear strain (γ_{oct}) with radial distance from a circular mandrel. At the distance d_s (smear zone), the estimated theoretical strain is approximately 5%, based on Equation 2.14.

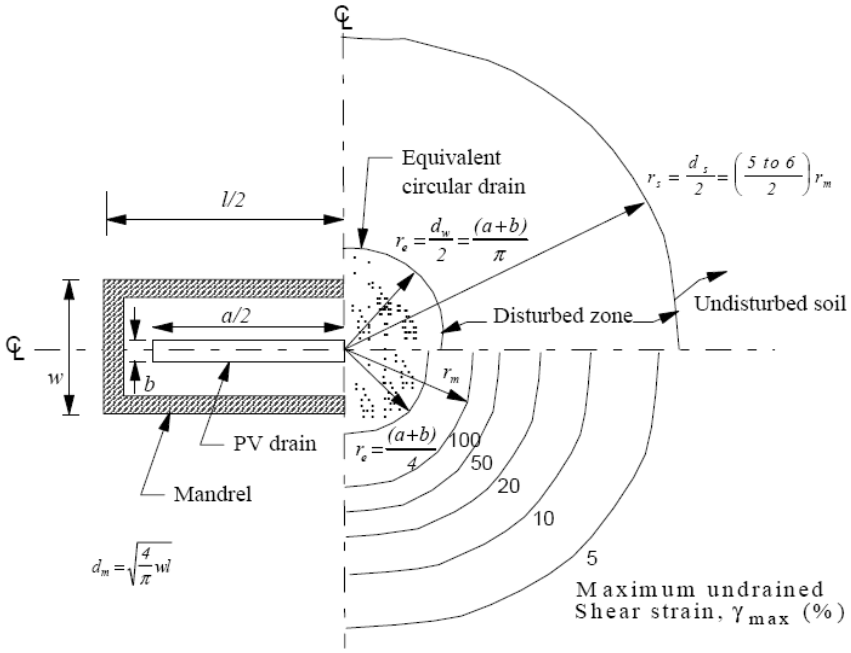

Figure 2.7 Approximation of the smear zone around the mandrel.

2.4.2 Well Resistance

The resistance to the water flowing in the vertical drains is known as the well resistance. The well resistance increases with the increase in the length of the drain and reduces the consolidation rate. Well resistance retards the pore pressure dissipation, hence, retards the settlement. The three main factors, which increase of well resistance, are the deterioration of the drain filter (reduction of drain cross section), passing of fine soil particles through the filter (reduction of drain cross section) and folding of the drain because of large settlement or lateral movement. However, these aspects are still difficult to quantify. Hansbo (1979, 1981) presented a closed form solution, which includes the effect of well resistance on drain performance.

2.5 Influence Zone of Drains

Vertical drains are commonly installed in square or triangular patterns (Figure 2.8). As illustrated in Figure 2.8, the influence zone (R) is a controlled variable, since it is a function of the drain spacing (S) as given by:

$$R = 0.546\ S \text{ for drains installed in a square pattern} \qquad (2.15)$$

$$R = 0.525\ S \text{ for drains installed in a triangular pattern} \qquad (2.15)$$

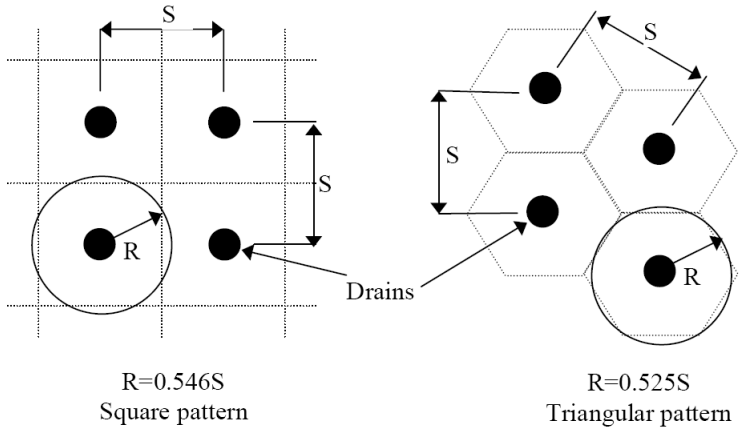

Figure 2.8 Plan of drain well pattern and zone of influence of each well

A square pattern of drains may be easier to lay out and control during installation in the field, however, a triangular pattern is usually preferred since it provides a more uniform consolidation between drains than the square pattern.

2.6 Development of Vertical Drain Theory

The basic theory of radial consolidation around a vertical sand drain system is an extension of Terzaghi's (1925) one-dimensional consolidation theory. Since it is obvious that the coefficient of consolidation in the horizontal direction is much higher than that in the vertical direction, and that the vertical drains reduce the drainage path considerably in the radial direction, the effectiveness of vertical drains in accelerating the rate of consolidation and improving the strength of soft soil is remarkably improved. The theory of vertical drain was probably first solved by Kjellman (1948). His solution based on "*equal vertical strain hypothesis*", was developed on the assumption that

horizontal sections remain horizontal throughout the consolidation process. However, Barron (1948) presented the most comprehensive solution to the problem of radial consolidation by drain wells. He studied the two extreme cases of free strain and equal strain and showed that the average consolidation obtained in these cases is nearly the same. The ‘free strain hypothesis’ assumes that the load is uniform over a circular zone of influence for each vertical drain, and that the differential settlements occurring over this zone have no effect on the redistribution of stresses by arching of the fill load. The ‘equal vertical strain hypothesis’ on the other hand, assumes that arching occurs in the upper layer during the consolidation process without any differential settlement in the clay layer. The arching effect implies a more or less rigid boundary at the surface of the soil layer being consolidated with vertical drains. It means that the vertical strain is uniform in the horizontal section of the soil.

Barron (1948) also considered the influence of well resistance and smear on the consolidation process due to vertical well drains. Takagi (1957) extended Barron‘s solution to incorporate a variable rate of loading, whereas Richart (1959) presented a convenient design chart for the effect of smear, where the influence of variable void ratio was also considered. Hansbo (1960) presented a solution by pointing out that the Darcy's law might not be valid when the hydraulic gradient is in the range of magnitudes prevailing during most consolidation processes in practice. However, in this equal strain solution, the effect of smear and well resistance were not considered. Later, a simplified solution to the problem of smear and well resistance was proposed by Hansbo (1979, 1981), giving results almost identical with those given by Barron (1948), and Yoshikuni and Nakanodo (1974). Onoue (1988) presented a rigorous solution based on the free strain hypothesis.

2.6.1 Equal Vertical Strain Hypothesis

The first conventional procedure for predicting radial consolidation was introduced by Barron (1948). This procedure was based on the extension of the theory of consolidation initially presented by Terzaghi (1925). Barron‘s solution is based on the following assumptions: (a) all vertical loads are initially carried by excess pore water pressure, *u*, which means that the soil is saturated, (b) the applied load is assumed to be uniformly distributed and all compressive strain within the soil occurs in the vertical direction, (c) the zone of influence of the drain is assumed to be circular and axisymmetric, (d) permeability of the drain is infinite in comparison with that of the soil, and (e) Darcy‘s law is valid.

Barron (1948) developed the exact solution of vertical drain based on ‘free strain hypotheses and an approximate solution based on ‘equal strain hypotheses. The difference in the predicted pore water pressures calculated using the free strain and equal strain assumptions are shown to be very small. Therefore, the approximate solution based on the ‘equal strain hypothesis’ gives satisfactory results compared to the rigorous free strain hypothesis.

Figure 2.9 shows the schematic illustration of a soil cylinder with a central vertical drain, where, r_w = the radius of the drain, r_s = the radius of smear zone, R = the radius of soil cylinder and l= the length of the drain installed into the soft ground. The coefficients of permeability in the vertical and horizontal directions are k_v and k_h, respectively, and k'_h is the coefficient permeability in the smear zone. The three dimensional consolidation of radial drainage (Barron, 1948) is given by:

$$\frac{\partial \overline{u}}{\partial t} = c_v\left(\frac{\partial^2 u}{\partial z^2}\right) + c_h\left(\frac{\partial^2 u}{\partial r^2} + \frac{1}{r}\frac{\partial u}{\partial r}\right) \tag{2.17}$$

where t is the time elapsed after the load is applied, u is the excess pore water pressure at radius r and at depth z. For radial flow only, the above equation becomes:

$$\frac{\partial \overline{u}}{\partial t} = c_h \left(\frac{\partial^2 u}{\partial r^2} + \frac{1}{r} \frac{\partial u}{\partial r} \right) \tag{2.18}$$

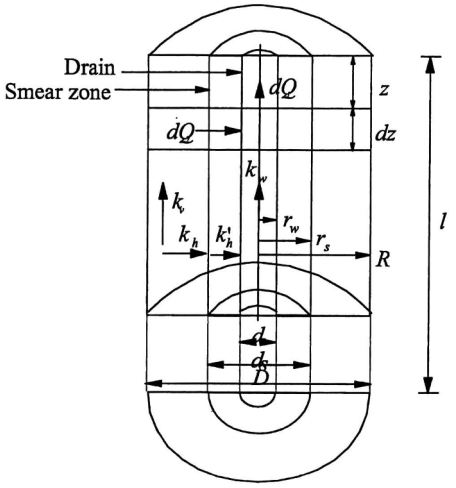

Figure 2.9 Schematic of soil cylinder with vertical drain (Hansbo, 1979)

The solution of the excess pore pressure for radial flow only, u_r of the above equation based on 'equal strain' assumption is given by:

$$u_r = \frac{4\overline{u}}{D^2 F(n)} \left[R^2 \ln\left(\frac{r}{r_w} \right) - \frac{r^2 - r_w^2}{2} \right] \tag{2.19}$$

where, D is the diameter of soil cylinder, the drain spacing factor, $F(n)$ is given by:

$$F(n) = \frac{n^2}{n^2 - 1} \ln(n) - \frac{3n^2 - 1}{4n^2} \tag{2.20}$$

where, $n = R / r_w$ is drain spacing ratio, and the average excess pore water pressure is given by:

$$\overline{u} = u_{av} = u_o \exp\left(\frac{-8T_h}{F(n)} \right) \tag{2.21}$$

The average degree of consolidation, $\overline{U}_h$, in the soil body is given by:

$$\overline{U}_h = 1 - exp\left(\frac{-8T_h}{F(n)}\right) \tag{2.22}$$

where the time factor T_h is defined as:

$$T_h = \frac{c_h\, t}{D^2} \tag{2.23}$$

The coefficient of radial drainage consolidation, c_h, is represented by:

$$c_h = \frac{k_h\,(1+e)}{a_v \gamma_w} \tag{2.24}$$

where γ_w is unit weight of water, and a_v is the coefficient of compressibility of the soil, e is the void ratio, and k_h is the horizontal permeability of the soil. The solution of Equation 2.18 taking account of smear effect is given by:

$$u_r = \overline{u}_r \frac{1}{V}\left[ln\frac{r}{r_s} - \frac{r^2 - r_s^2}{2R^2} + \frac{k_h}{k'_h}\left(\frac{n^2 - s^2}{n^2}\right) ln\, s \right] \tag{2.25}$$

where the smear factor v is given by:

$$v = F(n, s, k_h, k'_h) = \left[\frac{n^2 - s^2}{n^2} ln\frac{n}{s} - \frac{3}{4} + \frac{s^2}{4n^2} + \frac{k_h}{k'_h}\left(\frac{n^2 - s^2}{n^2}\right) ln\, s \right] \tag{2.26}$$

and

$$\overline{u} = u_{av} = u_o\, exp\left(\frac{-8T_h}{v}\right) \tag{2.27}$$

In the above expression, s is the extent factor of the smear zone with respect to the size of the drain and is given by $s = r_s / r_w$.

The average degree of consolidation including smear is now given by:

$$\overline{U}_h = 1 - exp\left(\frac{-8T_h}{v}\right) \tag{2.28}$$

Curves of average radial excess pore water pressure, $\overline{u}_r$, and average degree of consolidation, $\overline{U}_h$ (purely radial flow) versus time factor T_h for various values of n are shown in Figure 2.10. The average degree of consolidation, $\overline{U}_v$ due to vertical flow versus time factor T_v is also indicated.

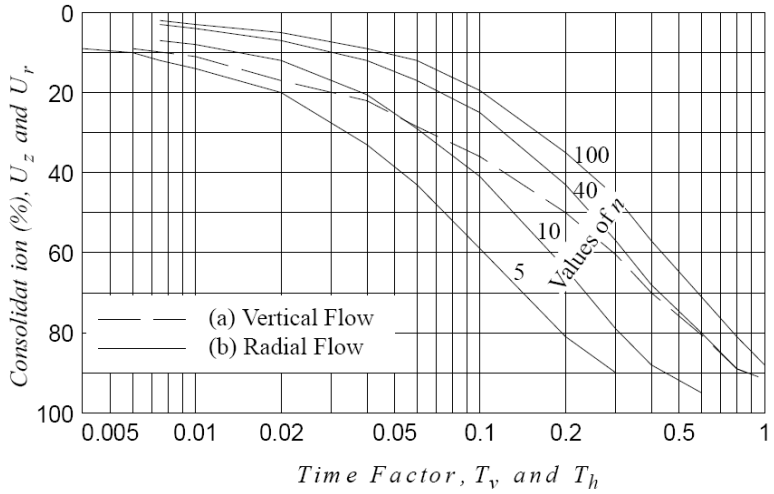

Figure 2.10 Average consolidation rates for (a) vertical flow and (b) for radial flow

2.6.2 Approximate Equal Strain Solution

Hansbo (1981) derived an approximate solution for vertical drain based on the 'equal strain hypotheses' by taking both smear and well resistance into consideration. The general concept of this solution is the same as illustrated previously in Figure 2.9. By applying Darcy's law, the rate of flow of internal pore water in the radial direction can be estimated. The total flow of water from the slice, dz, to the drain, dQ_1, is equal to the change of flow of water from the surrounding soil, dQ_2, which is proportional to the change of volume of the soil mass. The average degree of consolidation, $\overline{U}$, of the soil cylinder with vertical drain is given by:

$$\overline{U}_h = 1 - exp\left(\frac{-8T_h}{\mu}\right) \tag{2.29}$$

$$\mu = ln\left(\frac{n}{s}\right) + \left(\frac{k_h}{k'_h}\right) ln(s) - 0.75 + \pi\ z(2\,l - z)\frac{k_h}{q_w}\left[1 - \frac{\frac{k_h}{k'_h} - 1}{\frac{k_h}{k'_h}\left(\frac{n}{s}\right)^2}\right] \tag{2.30}$$

Or, in a simplified form:

$$\mu = ln\left(\frac{n}{s}\right) + \left(\frac{k_h}{k'_h}\right) ln(s) - 0.75 + \pi\ z(2\,l - z)\frac{k_h}{q_w} \tag{2.31}$$

The effect of smear only is given by:

$$\mu = ln\left(\frac{n}{s}\right) + \left(\frac{k_h}{k'_h}\right) ln(s) - 0.75 \tag{2.32}$$

The effect of well resistance only is given by:

$$\mu \approx ln(n) - 0.75 + \pi\ z(2\,l - z)\frac{k_h}{q_w} \tag{2.33}$$

If both smear and well resistance are ignored, this parameter becomes,

$$\mu = ln(n) - 0.75 \tag{2.34}$$

2.6.3 λ Method

Although the classical theory of consolidation of vertical drains (Barron, 1948) and its later developments are all based on the validity of Darcy‘s law, in the consolidation process, however, the permeability is subjected to gradual reduction. The pore water flow velocity, v caused by a hydraulic gradient, i might be deviated from the original Darcy‘s law $v = ki$, where under a threshold gradient i_0 below which no flow takes

place, the rate of flow is then given by: $v = k(i - i_0)$. The following relations were proposed:

$$v = \kappa i^n \text{ for } i \le i_1 \tag{2.35a}$$

$$v = k(i - i_0) \text{ for } i \ge i_1 \tag{2.35b}$$

where

$$i_1 = \frac{i_0 n}{n-1} \tag{2.35c}$$

and

$$\kappa = n^{-1} \cdot i^{1-n} \cdot k \tag{2.35d}$$

In order to study the effect of the non-Darcian flow, Hansbo (1979, 1997b, 2001) proposed an alternative consolidation equation, which is supported by the full-scale field test at Sweden. The average degree of consolidation is the same as given in Equation 2.22. The time required to reach a certain average degree of consolidation including smear effect is given by:

$$t = \frac{\alpha D^2}{\lambda}\left(\frac{D\gamma_w}{u_0}\right)^{n-1}\left[\frac{1}{(1-\overline{U}_h)^{n-1}} - 1\right] \tag{2.35e}$$

where, the coefficient of consolidation λ is given by $\kappa_h M / \gamma_w$, $M = 1/m_v$ = oedometer modulus; D is the diameter of the influence zone of the drain; d_s is the diameter of smear zone; $n = D/d_w$; d_w is the diameter of the drain; u_0 is the initial average excess pore water pressure; α is $n^{2n}\beta^n / 4(n-1)^{n+1}$ and β is given in Equation 2.35f.

$$\beta = \frac{1}{3n-1} - \frac{n-1}{n(3n-1)(5n-1)} - \frac{(n-1)^2}{2n^2(5n-1)(7n-1)} + \frac{1}{2n}\left[\left(\frac{k_h}{k_s}-1\right)\left(\frac{D}{d_s}\right)^{-\left(1-\frac{1}{n}\right)} - \left(\frac{k_h}{k_s}\right)\left(\frac{D}{d_w}\right)^{-\left(1-\frac{1}{n}\right)}\right] \quad (2.35f)$$

When $n \to 1$, Equation 2.35e yields the same result as the average degree of consolidation given by Equation 2.22, provided that well resistance is ignored, and assuming $\lambda = c_h$ and $\kappa_h / \kappa_s = k_h / k_s$

2.6.4 Plane Strain Consolidation Model

Most finite element analyses on embankments are conducted based on the plane strain assumption. However, this kind of analysis poses a problem, because the consolidation around vertical drains is axisymmetric. Therefore, to employ a realistic 2-D finite element analysis for vertical drains, the equivalence between the plane strain and axisymmetric analysis needs to be established. The matching of axisymmetric and plane strain conditions can be done in three ways:

1. Geometric matching approach œ the spacing of the drains is matched while keeping the permeability the same
2. Permeability matching approach œ permeability coefficient is matched while keeping the spacing of drains to be the same.
3. Combination of permeability and geometric matching approach œ plane strain permeability is calculated for convenient drain spacing.

Indraratna and Redana (1997) converted the vertical drain system (as shown in Figure 2.9) into equivalent parallel drain well by adjusting the coefficient of permeability of the soil and by assuming the plane strain cell to have a width of 2B as shown in Figure 2.11. The half width of drains b_w and half width of smear zone b_s may be taken to be the

same as their axisymmetric radii r_w and r_s respectively, which gives:

$$b_w = r_w \text{ and } b_s = r_s \tag{2.36}$$

The equivalent drain diameter (d_w) or radius (r_w) for band drains can be determined by 'perimeter equivalence' (Hansbo, 1981), and is given in Equation 2.1.

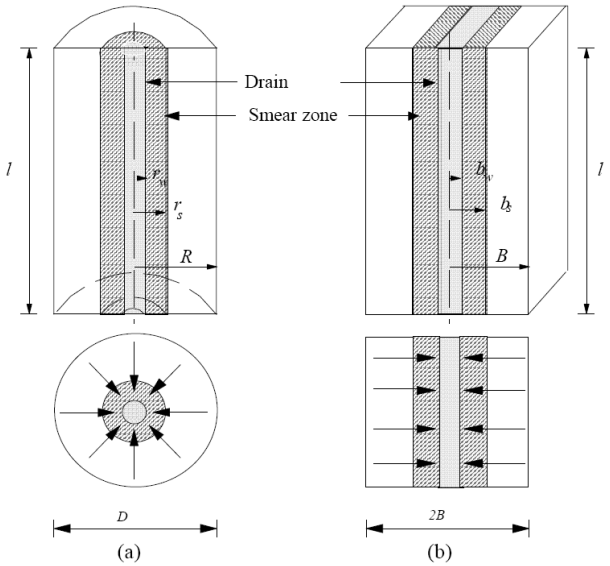

Figure 2.11 Conversion of an axisymmetric unit cell into plane strain condition: a) Axisymmetric Radial Flow b) Plane Strain.

Rixner et al. (1986) presented the equivalent drain diameter d as the average of drain thickness and width by considering the shape of the drain and effective drainage area as given in Equation 2.2. Indraratna and Redana (1997) represented the average degree of consolidation in plane strain condition as:

$$\overline{U}_{hp} = 1 - \frac{\overline{u}}{\overline{u}_0} = 1 - exp\left(\frac{-8T_{hp}}{\mu_p}\right) \tag{2.37}$$

where $\overline{u}_0$ = initial pore pressure; $\overline{u}$ = pore pressure at time t (average values); T_{hp} = time factor in plane strain, and

$$\mu_p = \left[\alpha + \beta\frac{k_{hp}}{k'_{hp}} + \theta\left(2\,l\,z - z^2\right)\right] \tag{2.38a}$$

where, k_{hp} and k'_{hp} are the undisturbed horizontal and corresponding smear zone permeability, respectively. The geometric parameters α, β and the flow term θ are given by:

$$\alpha = \frac{2}{3} - \frac{2b_s}{B}\left(1 - \frac{b_s}{B} + \frac{b_s^2}{3B^2}\right) \tag{2.38b}$$

$$\beta = \frac{1}{B^2}(b_s - b_w)^2 + \frac{b_s}{3B^3}\left(3b_w^2 - b_s^2\right) \tag{2.38c}$$

$$\theta = \frac{2k_{hp}^2}{k'_{hp}\, q_z B}\left(1 - \frac{b_w}{B}\right) \tag{2.38d}$$

where, q_z = the equivalent plane strain discharge capacity.

At a given stress level and at each time step, the average degree of consolidation for both axisymmetric (U_h) and equivalent plane strain (U_{hp}) conditions are made equal, hence:

$$\overline{U}_h = \overline{U}_{hp} \tag{2.39}$$

Combining Equations 2.37 and 2.39 with the original Hansbo (1981) theory, the time factor ratio can be given by following equation:

$$\frac{T_{hp}}{T_h} = \frac{k_{hp}}{k_h}\frac{R^2}{B^2} = \frac{\mu_p}{\mu} \tag{2.40}$$

By assuming the magnitudes of R and B to be the same, Indraratna and Redana (1997) presented the relationship between k_{hp} and k'_{hp} as follows:

$$k_{hp} = \frac{k_h\left[\alpha + \beta\frac{k_{hp}}{k'_{hp}} + \theta\left(2\,l\,z - z^2\right)\right]}{\left[ln\left(\frac{n}{s}\right) + \frac{k_h}{k'_h}ln(s) - 0.75 + \pi\left(2\,l\,z - z^2\right)\frac{k_h}{q_w}\right]} \tag{2.41}$$

If well resistance is ignored in Equation 2.41 by omitting all terms containing *l* and *z*, the influence of smear effect can be represented by the ratio of the smear zone permeability to the undisturbed permeability as follows:

$$\frac{k'_{hp}}{k_{hp}} = \frac{\beta}{\frac{k_{hp}}{k_h}\left[ln\left(\frac{n}{s}\right) + \frac{k_h}{k'_h}ln(s) - 0.75\right] - \alpha} \tag{2.42}$$

If both smear and well resistance effects are ignored in Equation 2.41, then the simplified ratio of plane strain to axisymmetric permeability is readily obtained, as proposed earlier by Hird et al. (1992):

$$\frac{k_{hp}}{k_h} = \frac{0.67}{ln(n) - 0.75} \tag{2.43}$$

The well resistance is derived independently and yields an equivalent plane strain discharge capacity of drains as also proposed earlier by Hird et al. (1992):

$$q_z = \frac{2}{\pi B}q_w \tag{2.44}$$

2.7 Consolidation around Vertical Drains

2.7.1 Rate of Consolidation

The main reason for using pre fabricated vertical drain is to reach the desired degree of consolidation within a specified time period. But in a vertical drain system, both radial and vertical consolidation should be considered in calculating the specified time period (Atkinson and Eldred, 1981). Carillo (1942) gave the combined effect as:

$$1-U=(1-U_r)(1-U_v) \tag{2.45}$$

where, U is the overall degree of consolidation; U_r is the average degree of consolidation due to radial drainage; U_v is the average degree of consolidation due to vertical drainage

2.7.2 Coefficient of Consolidation with Radial Drainage

2.7.2.1 Log U vs. t Approach

Aboshi and Monden (1963) presented a curve fitting method using log U and linear t. This method is developed by taking 'log' on both sides of Barron's solution (Equation 2.22), which results in the following expression:

$$T_h=-\frac{F(n)}{8}ln(1-\overline{U}) \tag{2.46}$$

Equation 2.46 represents the theoretical time factor for radial consolidation of perfect drains without considering the effect of smear. The coefficient of radial consolidation (c_h) is determined by plotting the logarithm of the average degree of consolidation against the linear consolidation time (log U vs. T_h), where a linear slope provides the c_h value (as shown in Figure 2.12). In order to include the effect of smear, 'log' is taken on both sides of Equation 2.28, which yields a new time factor T_h as given by:

$$T_h=-\frac{v}{8}ln(1-\overline{U}) \tag{2.47}$$

By substituting $c_h=T_hH_d^2/t$,

$$c_h=-\frac{D^2v}{8}\frac{H_d\,ln(1-\overline{U})}{dt} \tag{2.48}$$

Using Equation 2.28, the coefficient of radial drainage consolidation c_h can be defined

from the slope of log *U-t* curve with settlement data. The pore water pressure data can also be plotted other than settlement, in this method.

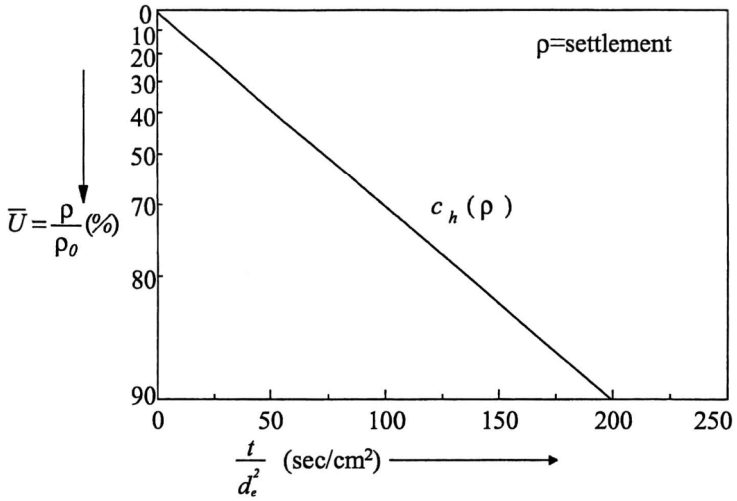

Figure 2.12 Aboshi and Monden (1963) method for determining c_h

2.7.2.2 Plotting Settlement Data

Asaoka (1978) developed a method where a series of settlements (ρ_1, …, ρ_{I-1}, ρ_i, ρ_{i+1} etc.), which are observed at constant time intervals are plotted as shown in Figure 2.13. The coefficient of radial drainage consolidation in this method is derived using Barron's (1948) solution, which is given by:

$$c_h = -\frac{D^2 v}{8}\frac{ln\,\beta}{\Delta t} \tag{2.49}$$

where, v is expressed in Equation 2.26; β is the slope of the line formed by the observed displacement data; and Δt is the time interval between observations. To obtain the average coefficient of consolidation, v (smear factor) is replaced by drain spacing factor, $F(n)$ as expressed in Equation 2.19 which gives:

$$c_h = -\frac{D^2 F(n)}{8}\frac{ln\,\beta}{\Delta t} \tag{2.50}$$

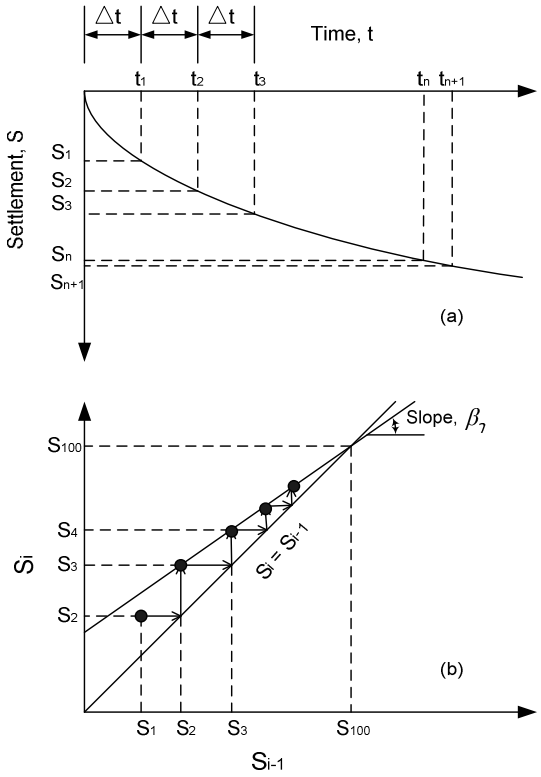

Figure 2.13 Asaoka's Method to determine c_h : (a) partition of settlement record into equal time intervals, (b) plot of settlement values and fitting of straight line (Asaoka, 1978; Magnan and Deroy, 1980)

2.8 Effect of Horizontal to Vertical Permeability Ratio

Generally, the coefficient of permeability can be determined indirectly from conventional oedometer test using Terzaghi's one dimensional consolidation theory. This indirect method of determining coefficient of permeability leads to some error due to the assumption of constant coefficient of permeability (k), constant coefficient of volume change (m_v) and constant coefficient of consolidation (c_v), during the consolidation process. The modified triaxial and oedometer tests equipped with the permeability gauges produce more reliable values of permeability. The falling head permeability test conducted on the modified oedometer appears to be the best (simpler and faster) to determine permeability of natural clays.

The permeability characteristics of a number of intact clays determined using the modified apparatus explained above is reported later by Tavenas et al. (1983). In these

tests, the horizontal permeability was also determined using samples rotated horizontally (90°) and of intermediate inclination, 45°. For marine clays recovered from Champlain sea formation (Canada), the anisotropy ratio ($r_k = k_h / k_v$) estimated using the modified oedometer test was found to vary between 0.91 and 1.42 with an average of 1.1. In triaxial testing, this ratio was found to be in the range of 0.81 to 1.16 with an average of 1.03, which implies that anisotropy was not an influence factor in this soil.

According to the experimental results plotted in Figure 2.6 (Indraratna and Redana, 1995), the value of k'_h / k'_v in the smear zone varies between 0.9 and 1.3 with an average of 1.15. Hansbo (1987) argued that for extensive smearing, the horizontal permeability coefficient in the smear zone (k'_h) should approach that of the vertical permeability coefficient (k'_v), thus suggesting that the ratio k'_h / k'_v could approach 1. The experimental results shown in Figure 2.6 (Indraratna and Redana, 1995) seem to agree with Hansbo (1987). For the applied consolidation pressures, it is observed that the value of k'_h / k'_v varies between 1.4 and 1.9 with an average of 1.63 in the undisturbed zone.

Shogaki et al (1995) reported that the average values of k'_h / k'_v were in the range of 1.36-1.57 for undisturbed isotropic soil samples taken from Hokkaido to Chugoku region in Japan. Tavenas et al. (1983) reported that for the soil tested in conventional oedometer, the k'_h / k'_v ratio was found to vary between 0.91 and 1.42 for intact natural clays, and from 1.2 to 1.3 for Matagami varve clay. Bergado et al. (1991) conducted a thorough laboratory study on the development of smear zone in soft Bangkok clay, and they reported that the horizontal permeability coefficient of undisturbed zone to the smear zone varied between 1.5 and 2 with an average of 1.75. More significantly, the

ratio of k'_h / k'_v was found to be almost unity within the smear zone.

2.9 Soft Clay Characteristics and Modelling

2.9.1 Soft Clay Characteristics

The nature of soft clay deposits is the most interesting soil to work with. Studies on the general characteristics of marine clays found in the coastal regions of various countries have been carried out to date by various authors.

Ohtsubo et al. (2002) had reported the minerals and geotechnical index properties of marine clays in East Asia. Many researchers have reported on the characteristics and mineralogy of soft clay in Japan (Shibuya and Tamrakar, 1999; Tanaka and Tanaka, 1999; Tanaka, 2000). Several other have reported on the microstructure and characteristics of Osaka Bay marine clay in Japan (Tanaka and Locat, 1999; Torrance, 1999; Yashima et al., 1999; Mimura and Jang, 2003). Tsuchida and Mizukami (1991) and Tsuchida (1999) have reported on the natural water content of marine deposits found in Japan. General characteristics of soft marine clay in the Taipei Basin of Taiwan have been reported by Lee et al. (1993) and Feng (1993). Kim et al. (1999) have reported on the general characteristics and distribution of marine clay in South Korea. The characteristics and distribution of Bangkok clay of the Chao Phraya Plain in Thailand has been reported by Bergado at al. (1992), Balasubramaniam et al. (1978, 1993, 1999, 2005) and Shibuya and Tamrakar (1999).

2.9.2 Soft Clay Modelling

In order to predict the behaviour of an engineering structure, it is necessary to use an appropriate constitutive model, which represents the stress-deformation response of the material. Deformation analysis in geotechnical engineering often assumes a linear elastic material at small stresses. This assumption probably holds true for over-consolidated clay, however, most soils exhibit plastic behaviour at increased stresses.

The theories of critical state soil mechanics have been developed based on the application of the theory of plasticity. Utilising the critical state concept based on the theory of plasticity in soil mechanics, a more sophisticated Cam-clay model has been introduced to represent the behaviour of clay (Schofield and Wroth, 1967; Wood, 2004). The Cam-clay model has received wide acceptance due to its simplicity and accuracy to model clay behaviour, especially for normally and lightly overconsolidated clay. In this model, the shear strength of the soil is related to the void ratio. To describe the state of soil during triaxial testing, the following critical state parameters are defined by:

$$p' = \frac{\sigma'_1 + 2\sigma'_3}{3} = \frac{\sigma_1 + 2\sigma_3}{3} - u \tag{2.51}$$

$$q' = \sigma'_1 - \sigma'_3 = \sigma_1 - \sigma_3 \tag{2.52}$$

where, σ'_1 represents the effective axial stress, σ'_3 represents the effective confining stress and u is the pore water pressure.

In critical state theory, the virgin compression, swelling and recompression lines are assumed to be straight lines in ($ln\ p'$–V) plots with slope $-\lambda$ and $-\kappa$, respectively (as shown in Figure 2.14). The isotropic virgin compression line or isotropic normal consolidation line (NCL) is expressed as:

$$V = N - \lambda ln(p') \tag{2.53}$$

where, $N(V_\lambda)$ is the value of V when $ln\ p' = 0$ or $p' = 1$.

The swelling or recompression line is expressed as:

$$V = V_\kappa - \kappa ln(p') \tag{2.54}$$

The relation between C_c (compression index) and λ can be expressed as:

$$\lambda = \frac{C_c}{2.307} \tag{2.55}$$

The slope of the straight line in $q - p'$ plot is called Critical State Line (CSL) as shown in Figure 2.15. The slope of the critical state line, M is expressed as:

$$q = M\ p' \tag{2.56}$$

In the $V - ln\ p'$ plot, if Γ is used to represent the value of V_λ which corresponds to a $ln\ p' = 0$ (i.e. $\Gamma = e_{sc} + 1$), then the equation of the straight line is given by:

$$V = \Gamma - \lambda\, ln\ p' \text{ or } p' = exp\frac{\Gamma - V}{\lambda} \tag{2.57}$$

Hence, the critical state line must satisfy both Equations 2.51 and 2.52.

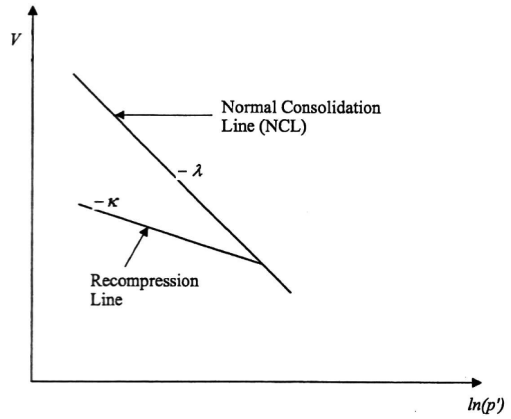

Figure 2.14 Isotropic normal consolidation line (NCL) plot in critical state theory (Schofield and Wroth, 1968; Schofield, 2005)

Combining the CSL equation into the Mohr circle plot, the relationship between drained angle of friction (ϕ') and M may be given by:

$$M = \frac{6\sin\phi'}{3 - \sin\phi'} \tag{2.58}$$

The initial void ratio can be estimated at any given depth below the ground level once p', q and P'_c are known, and the $e - ln\ p'$ plot is shown in Figure 2.16. The parameter e_{cs} is defined as the voids ratio on the critical state line for a value of $p' = 1$.

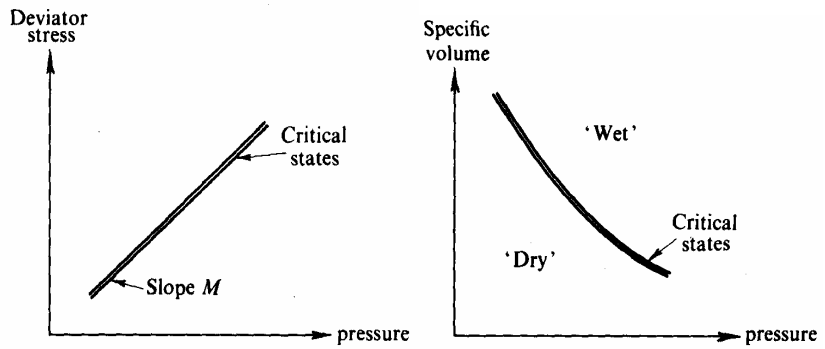

Figure 2.15 Position of the critical state line (Schofield and Wroth, 1968)

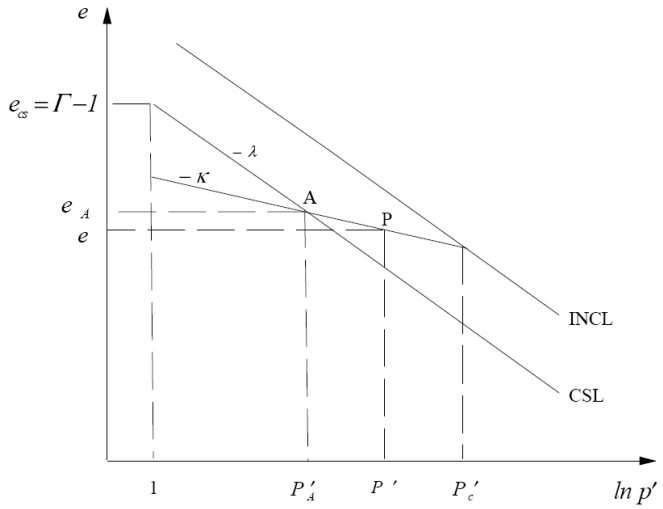

Figure 2.16 Position of the initial void ratio on critical state line

The intersection between the swelling line and the in-situ stress line is assumed to be at point A and given by coordinates e_A and P'_A. Point P represents the intersection between the initial void ratio (e) and the effective mean normal stress (p'). Then, the following relation may be established:

$$e_A = e_{cs} - \lambda \ln P_A^{'} \tag{2.59}$$

where, $P_A^{'} = P_c^{'} / 2$ for Modified Cam-clay, and $P_A^{'} = P_c^{'} / 2.718$ for Cam-clay.

Along the swelling line (κ line) passing through the initial stress state at point P, the following relation can be applied:

$$e - e_A = \kappa\left(\ln p' - \ln P_A^{'}\right) \tag{2.60}$$

Substituting e_A from Equation 2.59 gives:

$$e_{cs} = e + (\lambda + \kappa) ln\, P_A^{'} - \kappa\, ln\, p' \tag{2.61}$$

It was found that the original Cam-clay model was deficient in some aspects of modelling the stress-strain behaviour of soil. Two aspects of dissatisfaction were: the shape of the yield locus at increased $p_c^{'}$ and the predicted value of K_0 (the coefficient of earth pressure at rest). Therefore, the modified Cam-clay was introduced to address those problems (Roscoe and Burland, 1968). The obvious difference between modified Cam-clay and Cam-clay model is the shape of the yield locus, where the yield locus of modified Cam-clay is elliptical as shown in Figure 2.17. The flow rule for modified Cam-clay is given by:

$$\frac{\delta \upsilon^p}{\delta \varepsilon^p} = \frac{M^2 - \eta^2}{2\eta} \tag{2.62}$$

where, $\delta \upsilon^p$ is the volumetric plastic strain increments; $\delta \varepsilon^p$ is the deviatoric plastic strain increments; $\eta = q / p'$ is the stress ratio.

The modified Cam-clay yield locus is given by:

$$q + M^2 p'^2 = M^2 p'\, p'_c \tag{2.63}$$

The equation of the Stable State Boundary Surface (SSBS) is given by:

$$V_\kappa = \Gamma + (\lambda - \kappa)\left\{ ln(2) - ln\left[1 + \left(\frac{\eta}{M^2} \right)^2 \right] \right\} \tag{2.64}$$

2.10 Some Salient Aspects of Numerical Modelling

Currently, pore pressures, settlements, lateral displacements and stresses of the vertical drain installed field site can be analysed as accurately as possible using sophisticated finite element software. Commercial packages such as ABAQUS, FLAC, PLAXIS and

SAGECRISP, are capable of performing fully coupled consolidation analysis. According to past experience, finite element analysis of lateral deformation has been relatively poor in contrast to settlements (Loganathan et al., 1993; Indraratna et al., 1994). The recent finite element models applied to vertical drains are described below.

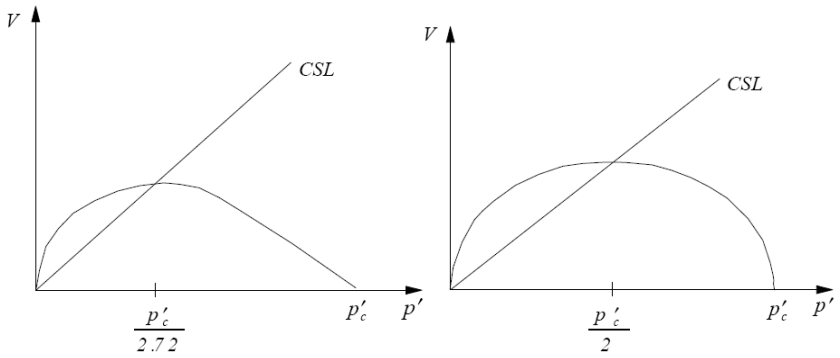

Figure 2.17 Yield locus of Cam-clay and modified Cam-clay

2.10.1 Pore Pressure Dissipation and Drain Efficiency

In this study, the performance of embankment stabilised with vertical drains at Muar clay, Malaysia was analysed using the finite element code, CRISP (Britto and Gunn, 1987). The effectiveness of the prefabricated drains was evaluated according to the rate of excess-pore pressure dissipation at the soil drain interface. Both single and multi-drain (whole embankment) analyses were carried out to predict the settlement and lateral deformation beneath the embankment.

A plane strain analysis was applied to a single drain and to the whole PVD scheme. An axisymmetric horizontal permeability was used in the plane strain model. As explained in detail by Ratnayake (1991), the prediction of settlement using the single drain analysis over-predicts the measured settlement, even though the effect of smear is included. In the case of multi-drain analysis underneath the embankment, the over-prediction of settlement is more significant compared to the single drain analysis. Therefore, to enable better predictions, it was necessary to consider more accurately, the dissipation of the excess pore pressures at the drain boundaries at a given time (Indraratna et al., 1994).

In order to elaborate this technique, the average undissipated excess pore pressures could be estimated by finite element back-analysis of the settlement data at the centreline of the embankment as shown in Figure 2.18. In Figure 2.18, 100% represents zero dissipation when the drains are fully loaded. Accordingly, at the end of the first stage of consolidation (ie., 2.5 m of fill after 105 days), the undissipated pore pressures decrease from 100% to 16%. For the second stage of loading, the corresponding magnitude decreases from 100% to 18% after a period of 284 days, during which the height of the embankment has already attained the maximum of 4.74 m. It can be deduced from Figure 2.18 that perfect drain conditions are approached only after a period of 400 days. Although the general trends between the finite element results and field data are in agreement especially during the initial stages, the marked discrepancy beyond 100 days is too large to be attributed solely to the plane strain assumption. These excess pore-pressures reflect the retarded efficiency of the vertical drains (partial clogging). A better prediction was obtained for settlement, pore pressure and lateral deformation when 'non zero' excess pore pressures at drain interface were input into the finite element model, simulating 'partially clogged' conditions. The 'non zero' excess pore pressures can also represent the smear effect that contributes to decreased efficiency, as discussed later.

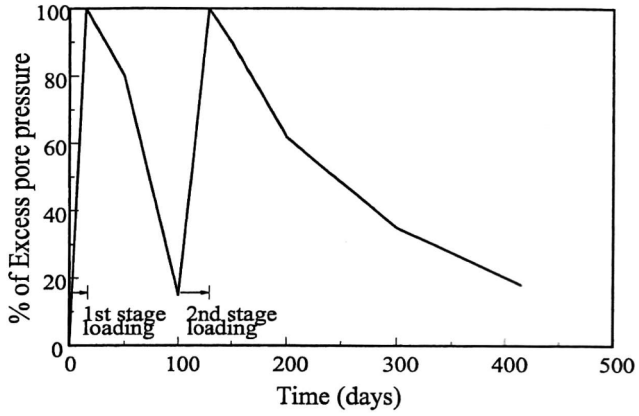

Figure 2.18 Percentage of undissipated excess pore pressures at drain-soil interfaces (Indraratna et al., 1994)

2.10.2 Matching Geometry and Permeability

Hird et al. (1992, 1995) presented a modelling technique of vertical drains in two-dimensional finite element analysis using CRISP (Britto and Gunn, 1987). In this analysis, the permeability and geometry matching were applied to several embankments stabilised with vertical drains in Porto Tolle (Italy), Harlow (UK) and Lok Ma Chau (Hong Kong).

An acceptable prediction of settlements was obtained, although the pore water pressure dissipation was more difficult to predict. However, at Lok Ma Chau, the settlements were significantly over-predicted. This was because, in this case history analysis, the effect of smear was not considered although the plane strain model proposed by Hird et al (1992) allows the smear effect to be modelled.

At Porto Tolle embankment, prefabricated vertical geo-drains were installed on a 3.8 m triangular grid to a depth of 21.5 m below ground level. The equivalent radius of geo-drain was 31 mm, and its discharge capacity was conservatively estimated at about 140 m^3/year. The embankment, which was constructed over a period of 4 months, had a height of 5.5 m, a crest width of 30 m, a length of over 300 m, and a side slope of about 1 in 3. For the purpose of finite element analysis, the clay was modelled using the modified Cam-clay model of Roscoe and Burland (1968). The equivalent plane strain permeability is estimated according to Hird et al. (1992).

In this study, drain analysis at centreline of the embankment was considered. The typical results of finite element analysis are compared in Figure 2.19(a) and 2.19(b). Field settlement data are also plotted in Figure 2.19(a) and these show that both during and after construction, the magnitude of settlement was reasonably well modelled. In Figure 2.19(b) the observed and computed excess pore pressures mid-way between the drains are compared; only the axisymmetric computed results are shown, since in plane

strain analysis, pore pressures are not matched at corresponding points, but merely on average. During construction, the observed and computed pore pressures compared tolerably well. Afterwards, they differed greatly, although the field data may have been unreliable because of the presence of organic gas in the soil (Jamiolkowski and Lancellotta, 1984).

2.10.3 Modelling of Discharge Capacity

Chai et al. (1995, 1996) extended the method proposed by Hird et al. (1992) to include the effect of well resistance and clogging. Four types of analyses were presented considering: (1) no vertical drains, (2) embankment with vertical drains and discharge capacity of the drains increasing with depth, (3) drains with constant discharge capacity and (4) the same as (3) but assuming that the drains were clogged below 9 m depth. The discharge capacity of the drain in plane strain for matching the average degree of horizontal consolidation is given by:

$$q_{wp} = \frac{4k_h l^2}{3B\left[ln\left(\frac{n}{s}\right) + \frac{k_h}{k_s} ln(s) - \frac{17}{12} + \frac{2l^2 \pi k_h}{3q_{wa}} \right]} \tag{2.65}$$

The model developed in this study was refined using a single drain model of 5 m long, and both elastic and elasto-plastic analyses were applied to predict its performance. Excellent agreement was obtained between axisymmetric and plane strain models especially with varied discharge capacity q_{wp} as shown in Figure 2.20, for elasto-plastic analysis. The well resistance matching also results in a more realistic excess pore water pressure variation with depth as shown in Figure 2.21, for elastic analysis. It can be seen that the varied discharge capacity yielded a more uniform and closer match between axisymmetric and plane strain methods compared to constant discharge capacity assumption.

The model described above was calibrated verified with the performance of an embankment stabilised with vertical drains founded in Muar clay, Malaysia. This study shows that the vertical drains not only increase the settlement rate, but also reduce the lateral deformation. A more realistic excess pore pressure distribution was also obtained when the well resistance and clogging were introduced in the analysis.

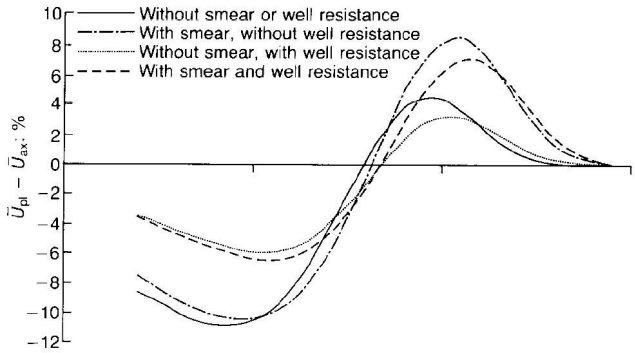

Figure 2.19(a) Result of axisymmetric and matched plane strain for Porto Tolle embankment: average surface settlement (Hird et al., 1992; Hird et al., 1995)

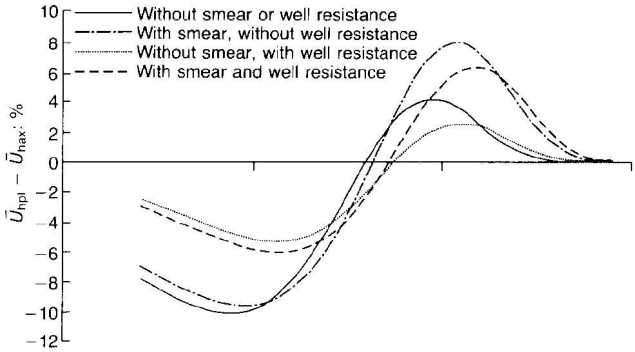

Figure 2.19(b) Result of axisymmetric and matched plane strain for Porto Tolle embankment: excess pore pressure (Hird et al., 1992; Hird et al., 1995)

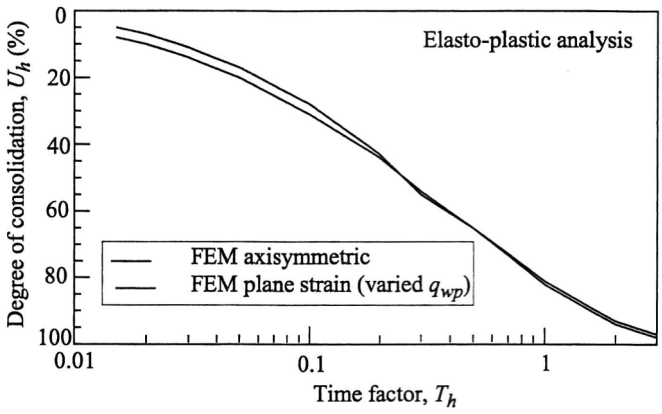

Figure 2.20 Comparison of average degree of horizontal consolidation (Chai et al., 1995)

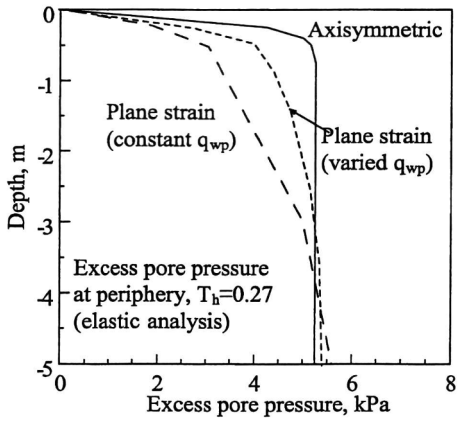

Figure 2.21 Comparison of excess pore pressure variation with depth (Chai et al., 1995)

2.10.4 Deformation as a Stability Indicator

Indraratna et al. (1997, 2005a, 2005b) investigated the effect of ground improvement by preloading together with geo-grid and vertical band drains, as well as sand compaction piles constructed on Muar clay, Malaysia. The settlement and lateral displacement of the soft clay foundation were analysed using the plane strain finite element formulation, and the findings were compared to the field measurements. In order to conduct a two-dimensional plane strain analysis, the vertical drain system was converted into an equivalent drainage wall as explained earlier (see Figure 2.11).

The analysis employed critical state soil mechanics, and the deformations were predicted on the basis of the fully coupled (Biot) consolidation model incorporated in the finite element code CRISP (Britto and Gunn, 1987). In the analysis, the soil underneath the embankment was discrete using linear strain quadrilateral (LSQ) elements. The vertical drains were modelled as ideal and non-ideal drains, where in the former, the well resistance factor was ignored. This study shows that the accurate prediction of lateral displacement depends on the correct assessment of the value of the Cam-clay parameter λ, the shear resistance at the embankment-foundation interface and the nature of assumptions made in the modelling of drains and sand piles. The actual soil properties are influenced by the working stress range and the assumed stress path of the sub-soil at a given depth. The normally consolidated parameters associated with the

Cam-clay theories over-estimate lateral displacement and settlements, if the applied stresses are smaller than the pre-consolidation pressure.

Table 2.2 Effect of ground improvement on normalised deformation factors (Indraratna et al., 1997).

Ground Improvement Scheme	α	β_1	β_2
Sand compaction piles for pile/soil stiffness ratio of 5 (h=9.8m, including 1m sand layer)	0.185	0.018	0.097
Geogrid and vertical band drains in square patterns at 2.0m spacing (h=8.7m)	0.141	0.021	0.149
Vertical band drains in triangular pattern at 1.3m spacing (h=4.75m)	0.127	0.035	0.275
Embankment rapidly constructed to failure on untreated foundation (h=5.5m)	0.695	0.089	0.128

The performance of vertical band drains and sand compaction piles was compared based on normalised deformation as shown in Table 2.2. The ratio of maximum lateral displacement to fill height (β_1) and the ratio of maximum settlement to fill height (β_2) were considered as stability indicators. In comparison with an unstabilised embankment constructed to failure (Indraratna et al., 1992), the stabilised foundations are characterised by considerably smaller values for α and β_1, highlighting their obvious implication on stability. The normalised settlement (β_2) on its own does not seem to be a proper indicator of instability. The foundation having SCP gives the lowest values of β_1 and β_2, clearly suggesting the benefits of sand compaction piles over the band drains.

2.10.5 Application of Vacuum Pressure

Finite element analysis was applied by Bergado et al. (1998) to analyse the performance of embankment stabilised with vertical drains, where a combined preload and vacuum pressure were utilised at the Second Bangkok International Airport site. A simple approximate method for modelling the effect of PVD as proposed by Chai and Miura (1997) was incorporated in this study. PVD increases the mass permeability in the vertical direction. Consequently, it is possible to establish a value of permeability of the

natural subsoil and the radial permeability towards the PVD. This equivalent vertical permeability (K_{ve}) is derived, based on equal average degree of consolidation. The approximate average degree of vertical consolidation U_v is given by:

$$U_v = 1 - exp(-3.54)T_v \tag{2.66}$$

where, T_v is the dimensionless time factor.

The equivalent vertical permeability, K_{ve} can be expressed as:

$$K_{ve} = \left(1 + \frac{2.26L^2K_h}{FD_e^2K_v}\right)K_v \tag{2.67}$$

where,

$$F = ln\left(\frac{D_e}{d_w}\right) + \left(\frac{K_h}{K_s} - 1\right)ln\left(\frac{d_s}{d_w}\right) - 0.75 + \frac{2\pi L^2K_h}{3q_w} \tag{2.68}$$

In Equation 2.68, D_e is the equivalent diameter of a unit PVD influence zone; d_s is the equivalent diameter of the disturbed zone; d_w is the equivalent diameter of PVD; K_h and K_s are the undisturbed and disturbed horizontal permeability of the surrounding soil, respectively; L is the length for one-way drainage, and q_w is discharge capacity of PVD. The effects of smear and well resistance have been incorporated in the derivation of the equivalent vertical permeability.

Two full-scale test embankments, TV1 and TV2 each with base area of 40 x 40 m were analysed by Bergado et al. (1998). The PVDs were installed to a depth of 15 m and 12 m for embankment TV1 and TV2, respectively. The design parameters are shown in Table 2.3, and the typical cross section of embankment TV1 is shown in Figure 2.22. It can be concluded from this study that the vacuum assisted consolidation has been

effectively utilised for both embankments TV1 and TV2. The performance of embankment TV2 with vacuum preloading (compared to the embankment at the same site without vacuum preloading), showed an acceleration in the rate of settlement of about 60% and a reduction in the period of preloading by about 4 months.

Table 2.3 Parameters of vertical drains

Spacing, S	1.0 m (triangular pattern)
Diameter of drain, d_w	50 mm
Diameter of smear zone, d_s	300 mm
Ratio of K_h / K_s	10
Drainage length, l	15 m for TV1 and 12 m for TV2
Discharge capacity, q_w (per drain)	50 m^3/year

2.10.6 Equivalent Plane Strain Modelling

An attempt was made by Indraratna and Redana (1997) to analyse the effect of smear zone and well resistance in a vertical drain using a 2D plane strain finite element model employing a modified Cam-clay theory. This was executed by converting the vertical drain system into equivalent parallel drain walls by adjusting the spacing of the drains and the coefficient of permeability of the soil as discussed earlier (Equations 2.36 to 2.44; Section 2.6.4). The transformed permeability coefficient was then incorporated in the finite element code, CRISP through appropriate subroutines.

In order to verify the proposed model, a finite element analysis was executed for both axisymmetric and equivalent plane strain models. As an example, a unit drain was considered with a drain installed to a depth of 5 m under the ground surface at 1.2 m spacing. The model parameters and the soil properties are given in Table 2.4.

In the analysis with smear, the size of the smear zone was taken to be 5 times the size of the mandrel based on the experimental results. For the verification of the model a simplified permeability variation was assumed as shown in Figure 2.23, where the coefficient of permeability within the smear zone was taken to be constant. A higher permeability coefficient was used for the undisturbed zone. Figure 2.23 shows both the

assumed axisymmetric and the converted plane strain permeability values.

Table 2.4 Model parameters and soil properties

Spacing, S	1.2m
Radius of drain, r_w	0.03m
Radius of mandrel	0.05m
Ratio of K_h / K_v in undisturbed zone	2
Ratio of K_h / K_v in smear zone	1
Plane strain permeability in undisturbed zone, k_{hp}	2.97×10^{-9} m/s
Plane strain permeability in smear zone, k'_{hp}	5.02×10^{-10} m/s
Radius of unit cell	0.6m
Gradient of volume vs. log pressure relation for consolidation, λ	0.2
Gradient of volume vs. log pressure relation for swelling, κ	0.04
Slope for critical state line, M	1.0
Void ratio at unit consolidation pressure, e_{cs}	2
Poisson's ratio, ν	0.25
Saturated unit weight of the soil, γ_{sat}	18 kN/m^3

The results of both axisymmetric and plane strain analysis are plotted in Figure 2.24, where the average degree of radial consolidation U_h (%) is plotted against the time factor T_h for perfect drain conditions. As illustrated in Figure 2.24, the proposed plane strain analysis gives a good agreement with the axisymmetric analysis. The maximum difference between the two methods is less than 5%. The well resistance can also be included using Equation 2.41. Figures 2.25 and 2.26 illustrate the settlements and excess pore pressure variations with time for single drains including smear plus well resistance. Once again, very good agreement between the axisymmetric model and the equivalent plane strain model is found. It is important to note that the inclusion of well resistance reduces the errors, notably in excess pore pressures.

Based on the above single drain analysis, Figures 2.24 and 2.26 provide concrete evidence that the equivalent (converted) plane strain model is an excellent substitute for the axisymmetric model. In finite element modelling, the 2-D, plane strain analysis is expected to cut down the computational time considerably, in comparison with the time taken by 3-D, axisymmetric model, especially in the case of multi drain analysis.

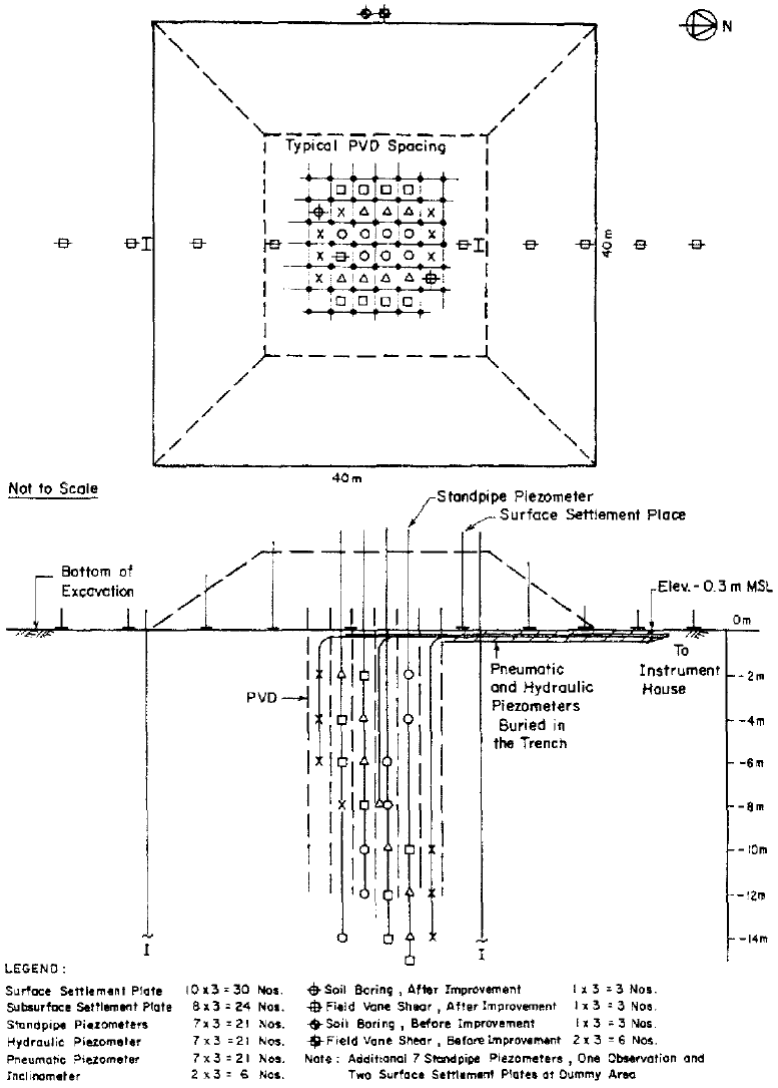

Figure 2.22 Cross-section of embankment TV1 with 15 m long PVD and location of monitoring instruments (Bergado et al., 1998; Bergado et al., 2002)

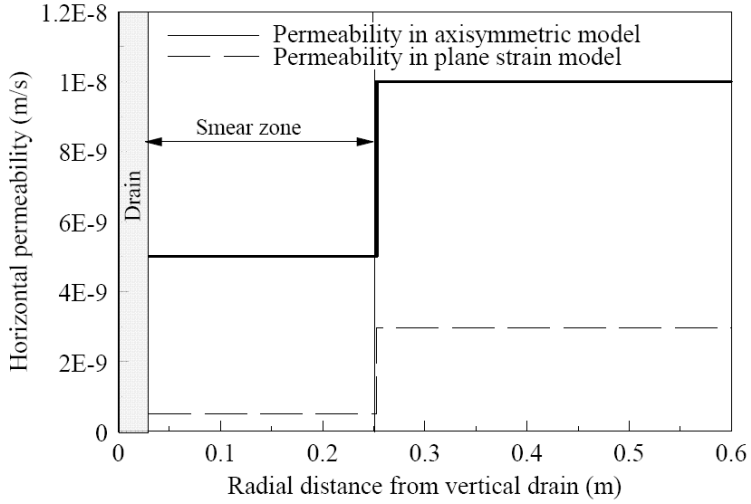

Figure 2.23 Simplified variation of permeability within and out side smear zone

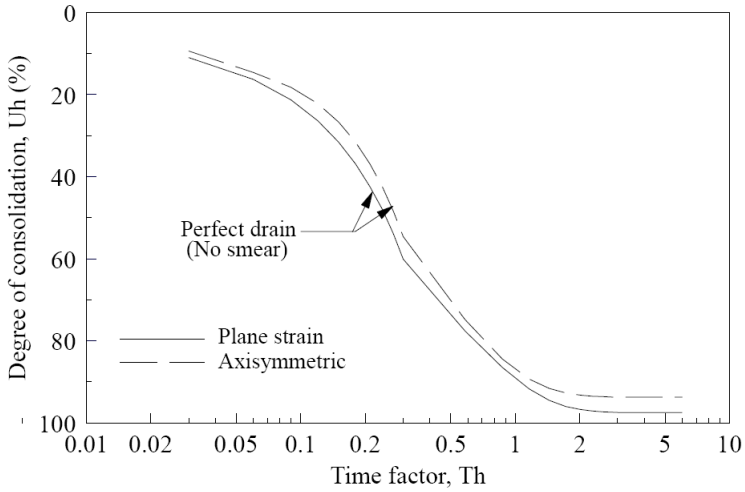

Figure 2.24 Average degree of consolidation vs time factor

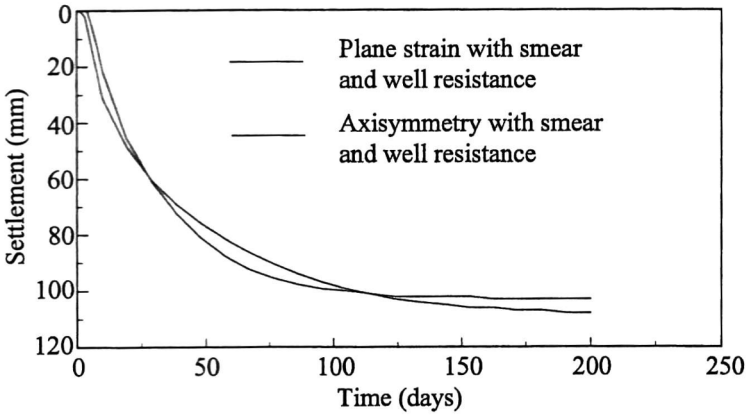

Figure 2.25 Comparison of the average surface settlement for axisymmetric and equivalent plane strain analyses with smear and well resistance (Indraratna et. al., 2000)

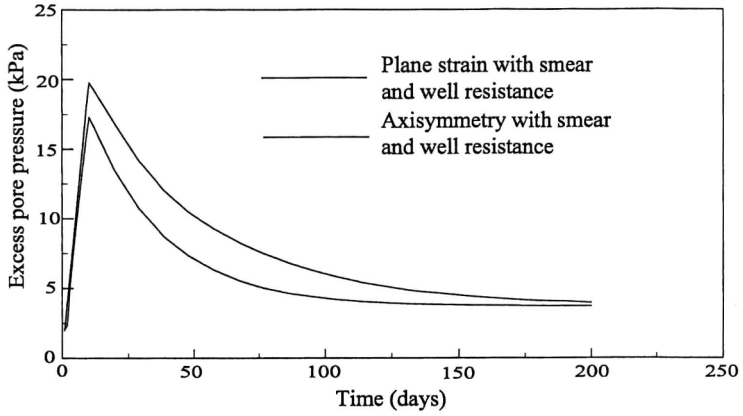

Figure 2.26 Comparison of the excess pore pressure for axisymmetric and equivalent plane strain analyses with smear and well resistance (Indraratna et. al., 2000)

2.11 Application of Numerical Modelling and Field Observation

2.11.1 Application of Numerical Modelling in Practice

Indraratna and Redana (1995, 1999, 2000) analysed the performance of several test embankments using their plane strain model. Figures 2.27(a) and 2.27(b) summarises

the typical subsoil profile, modified Cam-clay parameters and the effective stress conditions in the site. The unit weight of the weathered crust is about 18 kN/m^3 and the lowest unit weight of the soil is about 14.3 kN/m^3 at a depth of 7 m.

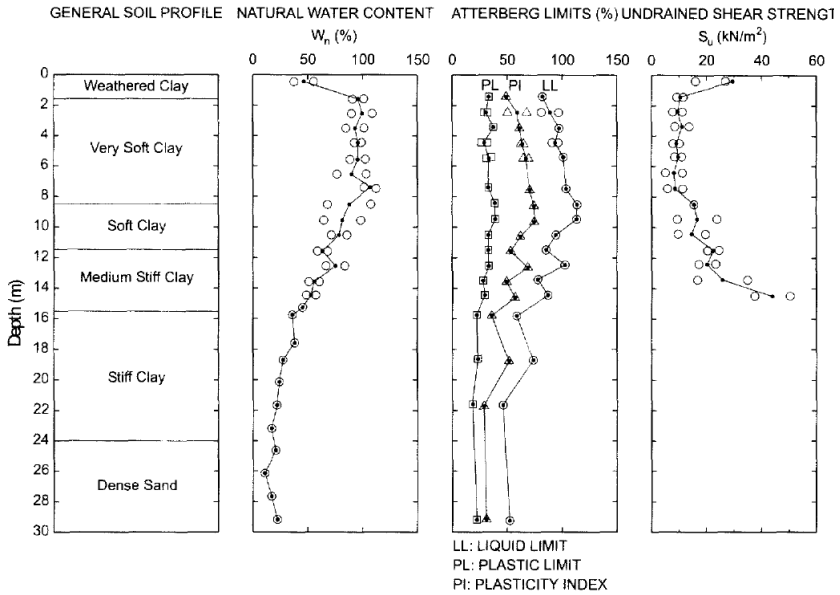

Figure 2.27(a) Sub-soil profile in Second Bangkok International Airport, (AIT, 1995; Bergado et al., 2002).

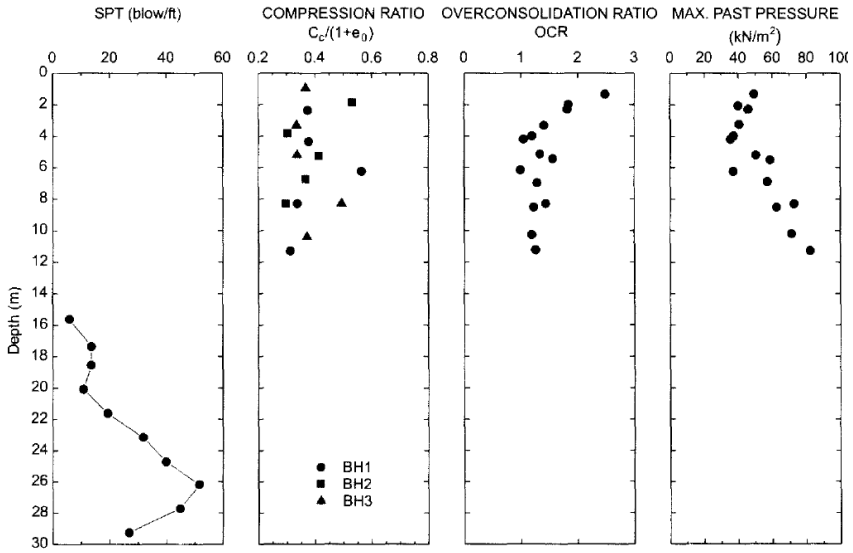

Figure 2.27(b) Cam-clay parameters and stress condition used in numerical analysis, Second Bangkok International Airport, (AIT, 1995; Bergado et al., 2002).

The typical finite element meshes for embankments employing the multi-drain analysis are given in Figures 2.28 and 2.29. The foundation is discretised into linear strain quadrilateral (LSQ) elements. For the zone stabilised with Prefabricated Vertical Drains (PVD), a finer mesh was used so that each drain element includes the smear zone on

either side of the PVD. The location of inclinometers and piezometers is accurately defined in the mesh, with the measurement points placed on the mesh nodes. The piezometer locations are shown in the insert of each mesh. The embankment load is applied in stages (i.e. sequential construction). Figure 2.30 indicates the rate of loading and the construction history of a typical embankment

The numerical analysis was based on the modified Cam-clay model (Roscoe and Burland, 1968) incorporated in the finite element code, CRISP92 (Britto and Gunn, 1987). The equivalent plane strain values were calculated based on Equations 2.42 and 2.43 (Indraratna and Redana, 1997). After a few trials to include the effect of well resistance, the minimum discharge capacity (q_w) was estimated to model the settlements and pore water pressure dissipation.

The results of the plane strain analysis of a typical embankment together with the measured settlements are plotted in Figure 2.31. The analysis based on 'perfect drain' conditions (i.e. no smear, complete pore pressure dissipation) over-predicts the measured settlement, but the inclusion of smear effect improves the accuracy of the predictions. The inclusion of the effects of smear and well resistance underestimate the measured settlements. In terms of settlements, the role of well resistance could be regarded as insignificant, in comparison with the smear effect.

The measured and predicted excess pore pressures along the centre-line of the embankment at a depth of 2 m below the ground surface are compared in Figure 2.32. In the 'smear only' analysis, the pore water pressure increase is well predicted during Stage 1 and Stage 2 loading. However after Stage 3 loading, the predicted pore pressure is significantly smaller than the field measurements. As expected, the perfect drain predictions underestimate the actual pore pressures. The inclusion of the effects of smear and well resistance gives a better prediction of the pore water pressure dissipation

for all stages of loading.

The prediction of settlement along the ground surface from the centre-line of a typical embankment after 400 days is shown in Figure 2.33.At the embankment centre-line, the limited available data agree well with the settlement profile. Also heave could be predicted beyond the toe of the embankment, i.e. at about 42 m away from the centre-line. Measured and predicted lateral deformation for the inclinometer installed away from the centreline of the embankment is shown in Figure 2.34. The lateral displacements at 44 days and 294 days after loading are well predicted when both the effects of smear and well resistance are included. As shown in Figure 2.34, the inclusion of smear effect by itself underestimates the magnitude of lateral displacement. The 'perfect drain' condition yields the smallest lateral deformation. It is verified that the presence of PVD is expected to reduce the lateral movement of soft clay under embankment loading.

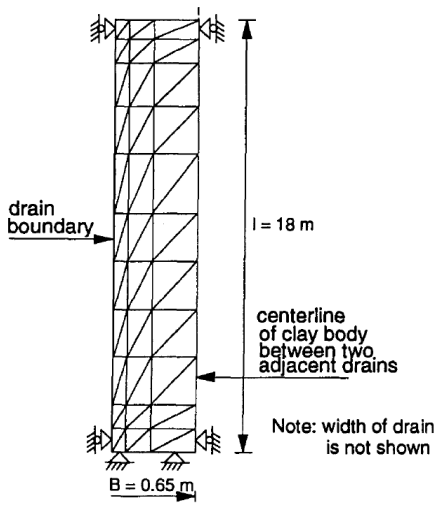

Figure 2.28 Finite element mesh of embankment for plane strain analysis with variable drain lengths (Indraratna and Redana, 1997, 2000)

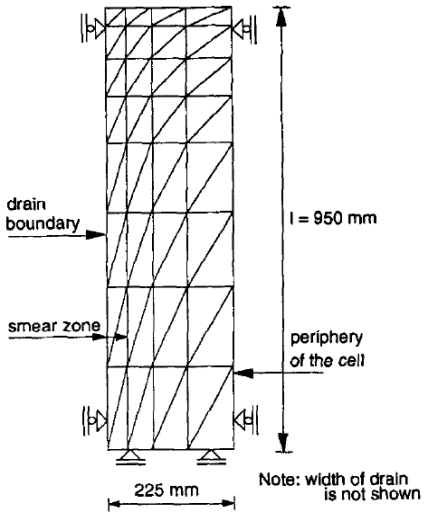

Figure 2.29 Finite element mesh of the embankment for plane strain analysis with constant drain length (Indraratna and Redana, 1997; Indraratna and Redana, 2000).

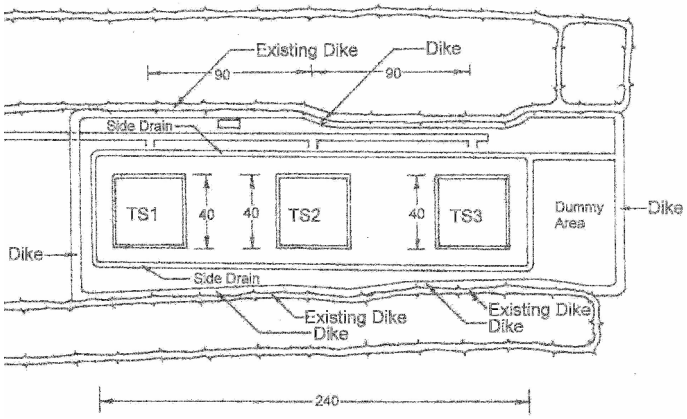

Figure 2.30(a) Site plan of test embankments TS1, TS2 and TS3 at Second Bangkok International Airport (AIT, 1995; Balasubramaniam et al., 2005)

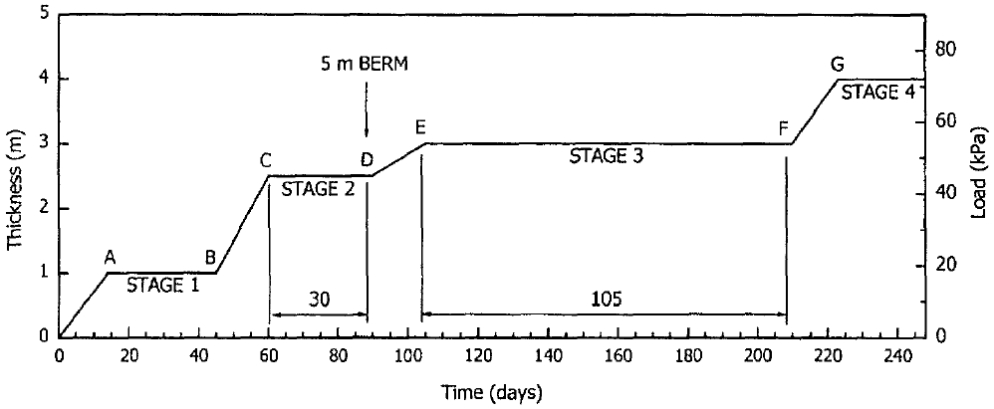

Figure 2.30(b) Construction loading history for embankments TS1, TS2 and TS3 at Second Bangkok International Airport (AIT, 1995; Bergado et al., 2002)

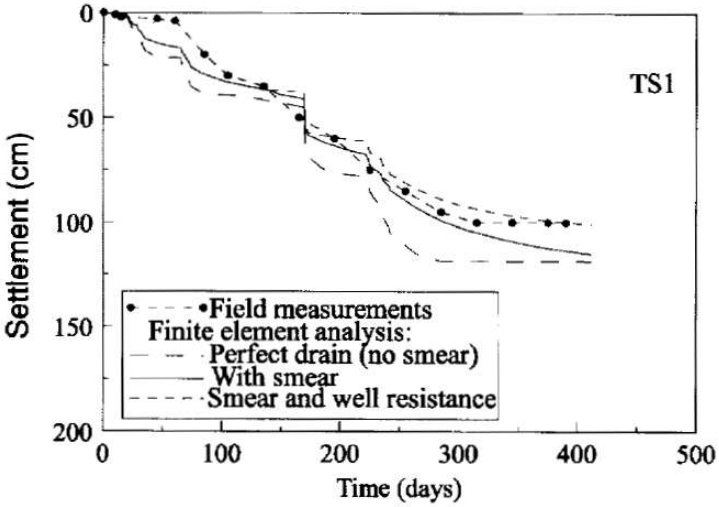

Figure 2.31(a) Surface settlement at the centre-line for embankment TS1, Second Bangkok International Airport (Indraratna and Redana, 2000)

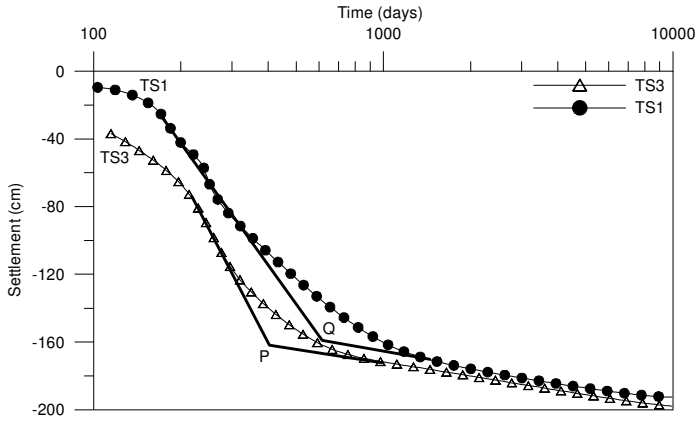

Figure 2.31(b) Surface settlement at the centre-line for embankment TS1 and TS3, Second Bangkok International Airport (Balasubramaniam et al., 2005)

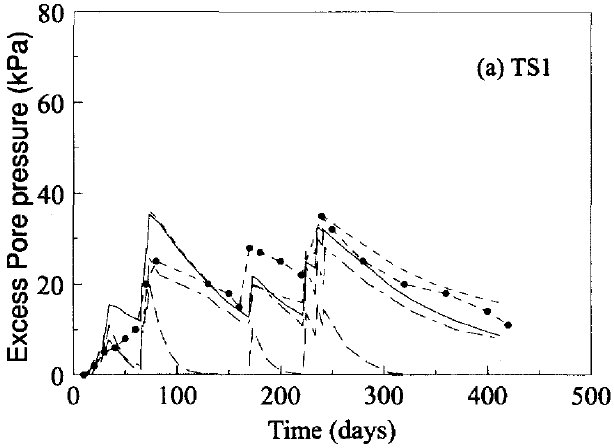

Figure 2.32 variation of excess pore water pressures at 8 m depth below ground level at the centre-line for embankment TS1 (Indraratna and Redana, 2000)

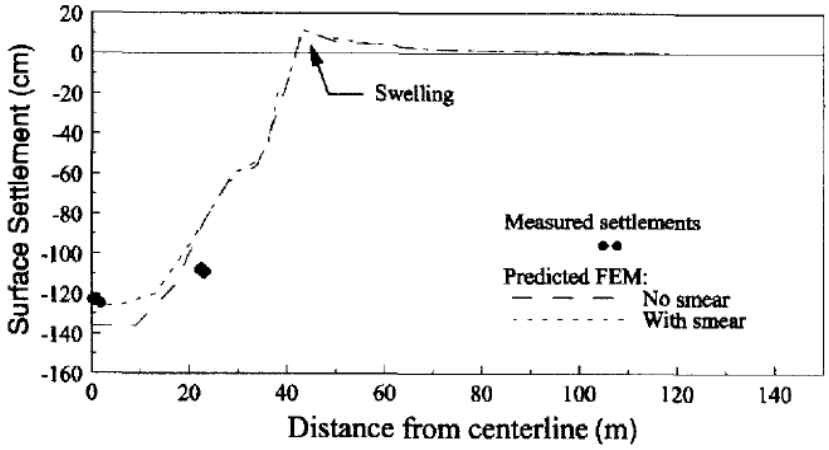

Figure 2.33 Surface settlement profiles after 400 days, Muar clay, Malaysia (Indraratna and Redana, 1999)

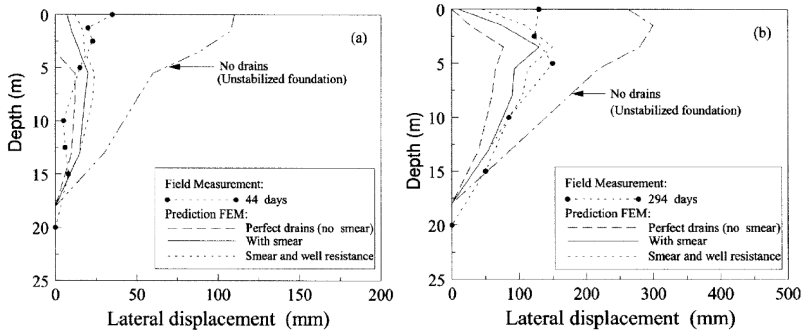

Figure 2.34 Lateral displacement profiles at 23 m away from centerline of embankments a) after 44 days, and b) after 294 days (Indraratna and Redana, 1999)

2.11.2 Field Observation in Practice

Ground improvement projects are implemented to eliminate further settlement. Degree of consolidation can be used to assess the performance related to specified load, and can be carried out by analysing instrumented data (or from field monitoring data). Bo et al. (2003) presented several case studies in Singapore, Hong Kong and China, where vertical drain are installed and field observation data are analysed. Yong and Lee (1997) also presented case histories of vertical drain application in highway embankment construction, which showed the importance of field observations. Chu and Choa (1995) highlighted the importance of the quality of vertical drain and field observation in a land reclamation project in Singapore.

Ohta et al. (2005) also presently a case history with of 5 pre-loading highway embankments placed on very uniform soft Ariake Clay in Japan. Comparison of field

observation data and computer simulation results were presented, where they concluded that field observation data would enhance the performance of computer simulation by calibrating input data closer to the reality results.

Akai and Tanaka (1999) reported a case history of Kansai International Airport in Osaka and the field measurements were described. Also, Akai (2000) reported the settlement of the offshore airport.

With particular reference to land reclamation projects in Singapore, Choa et al. (1995) and Bo et al., (1998) have in-depth descriptions of the investigation, design and construction processes involved. Bo et al (1998) reported the instrumentation and monitoring work for land reclamation project in Changi. Bo and Choa (2002) reported a well documented study on the land reclamation project.

Hudson (1990) presented several geotechnical aspects of the North–South Expressway in Malaysia. Loganathan et al. (1993) reported some findings on embankment monitoring in Muar Site of Malaysia, which were useful for the planning and design of the North–South Expressway. Bujang et al. (1995) investigated the properties of Marine Clay in Malaysia for the North-South Expressway. Later, Bujang (1996) presented the observed settlement of a studied site in the North-South Expressway.

2.12 Physical Densification – Stone Columns

Stone column are an extension of the vibro-compaction method used to treat non-cohesive soils. Conceived in Germany in the mid 1930s, the value of compaction by a poker vibrator for loose sands was endorsed more than 30 years ago by its choice for major structures, notably in Europe and USA. Within the past 30 years, the value of stone columns to reinforce cohesive soils for foundation has been generally recognised (Greenwood and Kirsch, 1984). These are conveniently constructed by the same poker vibrators. The stone column technique developed mainly in Europe and is now

increasingly used in USA primarily for embankments and roadwork.

For cohesive soils such as soft clay, vibration alone will not improve the soil, so it was a natural and practical development to introduce coarse granular backfill into the vibroflot bore. Granular fill columns form a composite with the soil, and are similar to piles (Holtz, 1989; Moseley and Pribe, 1993). Another method of accelerating the consolidation rate of soft marine clays is to install stone columns. Stone columns are extensively used to improve the bearing capacity of poor ground and reduce settlement of structures built on them (Lee and Pande, 1998). Stone columns consist of crushed rock, generally have a diameter which ranges between 0.6 to 1.0m and may be as long as 20m (Mitchell, 1981). Stone columns are normally installed in either a square or triangular pattern; with centre to centre spacing of 1.5 to 3.5m (Mitchell, 1981).

2.12.1 Stone Column Installation

The replacement and/or displacement method is commonly used to install stone columns. The replacement method involves replacing the in-situ soil with stone columns. A vibratory probe (vibroflot), accompanied by a water jet, is used to create the holes for the columns. This technique is suitable when the ground water level is high and the in-situ soil is relatively soft (Lee and Pande, 1998). The displacement method is utilised when the water table is low and the in-situ soil is firm. It involves using a vibratory probe, which uses compressed air, to displace the natural soil laterally.

2.12.2 Benefits of Stone Column

There are numerous benefits of installing stone columns, which include:

1. Substantial increase in the shear strength of the original ground (Cooper et al., 1999).
2. Enhanced drainage of excess pore water, as stone columns have high permeability by comparison with clay (Wood et al., 2000).

3. Higher frictional strength and stiffness than soft clay i.e. they behave more like a pile foundation.

4. Resist shear in the horizontal and inclined directions (Mitchell, 1981).

Stone columns are also very effective in accelerating the rate of consolidation, if the horizontal coefficient of consolidation (c_h) is much greater than the vertical (c_v). This is because the drainage path in the radial direction is considerably reduced.

2.12.3 Stone Column Models

The degree of consolidation of a soil cylinder with stone columns can be determined using Barron's classical consolidation formula or by a simple one-dimensional analysis.

Barron (1947) presented an expression to determine the degree of consolidation (U) of a cylindrical block of clay surrounding vertical drains/stone columns:

$$U = 1 - exp\left(-\frac{2T_r}{F}\right) \tag{2.69}$$

$$F = \frac{ln\ \chi}{1-\chi^2} - \frac{3-\chi^{-2}}{4} \tag{2.70}$$

Wood et al. (2000) proposed a simple one-dimensional analysis which can be used to estimate the degree of consolidation (U) in a cylindrical soil region around a vertical drain (as shown in Figure 2.35). To determine the degree of consolidation, the radial variation in pore pressure must first be established, and is given in Equation 2.71. Integrating Equation 2.71 over the radius will give an estimation of the average pore pressure (u_{av}). An average degree of consolidation (U_{av}) can then be obtained when the average pore pressure is compared with Equation 2.72.

$$u = \frac{\gamma_w \varepsilon}{4k_h}\left[2R^2\, ln\left(\frac{r}{r_c}\right) - \left(r^2 - r_c^2\right)\right] \tag{2.71}$$

$$U_{av} = 1 - \frac{F}{2T_r} \tag{2.72}$$

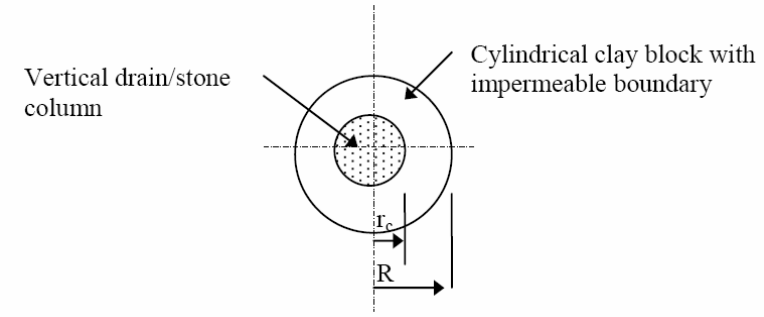

Figure 2.35 Sectional view of vertical drain or stone column (Wood et al., 2000)

2.12.4 Engineering Behaviour of Composite Ground

Bergado et al. (1996) presented a theory to determine the settlement and stability of ground reinforced with stone columns. The theory is based on the stress concentration in the granular pile. Figure 2.36 illustrates a diagram of the composite ground. Each stone column is separated into its own unit cell (as shown in Figure 2.36(a)). The unit cell is defined as the cylinder with an influence zone diameter (D) enclosing the tributary soil and one stone column. The area replacement ratio is the ratio of the granular pile area (A_s) over the whole area of the equivalent cylindrical unit within the unit cell (Bergado et al., 1996).

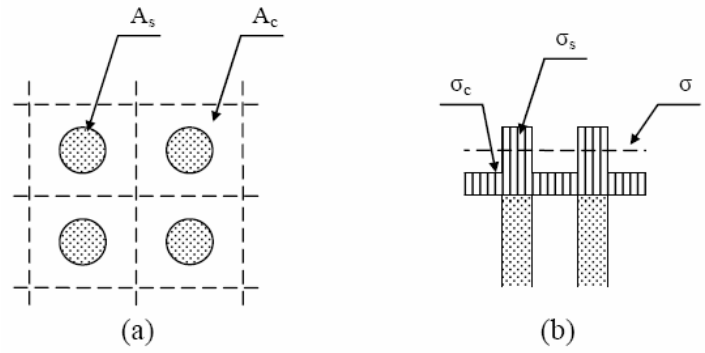

Figure 2.36 Diagram of composite ground (Bergado et al., 1996)

$$a_s = \frac{A_s}{A_s + A_c} \tag{2.73}$$

This ratio can also be expressed in terms of the stone column diameter (D_s) and spacing (S). The area replacement ratio for stone columns installed in a square and equilateral triangular pattern is respectively.

$$a_s = \frac{\pi}{4}\left(\frac{D_s}{S}\right)^2 \tag{2.74}$$

$$a_s = \frac{\pi}{2\sqrt{3}}\left(\frac{D_s}{S}\right)^2 \tag{2.75}$$

The distribution of the stress in the stone column (σ_s), clayey ground (σ_c) and average stress (σ) is illustrated in Figure 2.36(b). Studies have shown that when ground reinforced with stone columns is loaded, stress concentrations develop in the column accompanied by a reduction in stress in the surrounding clayey ground. This can be explained by the fact that, when loaded, the vertical settlement of the stone column and the surrounding soil is approximately the same, causing the occurrence of stress concentration in the column which is stiffer than the surrounding cohesive soil (Bergado et al., 1996). A stress concentration factor (n) is used to express the distribution of vertical stress within the unit cell.

$$n = \frac{\sigma_s}{\sigma_c} \tag{2.76}$$

The relative stiffness of the stone column and surrounding soil is affected by the magnitude of the stress concentration. The average stress (σ) over the unit cell area is given by:

$$\sigma = \sigma_s a_s + \sigma_c (1 - a_s) \tag{2.77}$$

The stress in the stone column (σ_s) and stress in the surrounding clayey ground (σ_c) is then given as follow:

$$\sigma_s = \frac{n\sigma}{1+(n-1)a_s} = \mu_s \sigma \tag{2.78}$$

$$\sigma_c = \frac{\sigma}{1+(n-1)a_s} = \mu_c \sigma \tag{2.79}$$

Most of the approaches in estimating settlement of ground reinforced with stone columns assume an infinitely wide, loaded area reinforced with granular piles having a constant diameter and spacing. Further, Bergado et al. (1996) presented the following expression to determine the settlement (S_t) of ground reinforced with stone columns.

$$S_t = m_v(\mu_c \sigma)H \tag{2.80}$$

Installing stone columns, beneath a road embankment constructed on soft marine clay can increase its overall stability. The three most commonly used methods of analysing the stability of composite ground are the profile, average shear strength and lumped parameter method. The profile method involves converting each row of the stone columns into an equivalent continuous strip of width (w) (as shown in Figure 2.37). The actual geometry and material properties are then used to analyse each strip of cohesion less and cohesive soils.

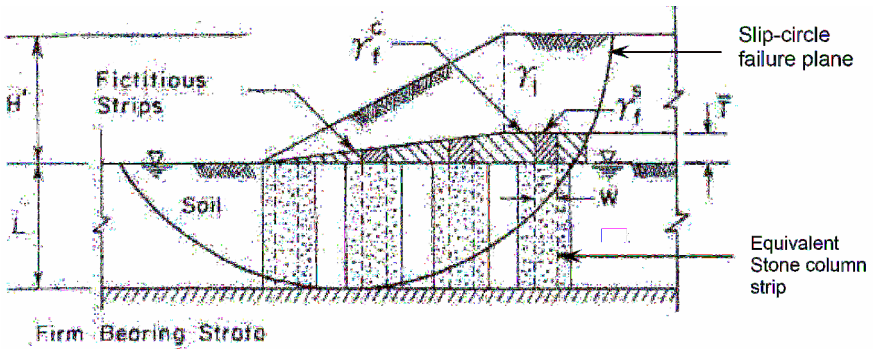

Figure 2.37 Granular pile strip idealization and fictitious soil layer for slope stability analysis (Bergado et al., 1996)

In order to produce an economical design, the stress concentrations which develop in the piles must be taken into consideration (Bergado et al., 1996). The stress concentration in the stone column increases the magnitude resisting shear force acting along the slip-circle failure plane. Thin fictitious strips of soil are placed above the in-situ soil and stone columns at the embankment interface to model the effect of the stress concentration in the column. The weights of the fictitious soil strips placed above the stone columns are relatively large to cause the desired stress concentration. The weight of the clayey ground and stone column fictitious strip are given as follow:

$$\gamma_f^c = \frac{(\mu_c - 1)\gamma_1 H'}{\overline{T}} \tag{2.81}$$

$$\gamma_f^s = \frac{(\mu_s - 1)\gamma_1 H'}{\overline{T}} \tag{2.82}$$

It should be noted that the fictitious strips placed above the in-situ soil and granular piles have no shear strength (Bergado et al., 1996). Also limits must be imposed on the grid size of slip-circle centres and radius, to ensure that the critical slip-circle isn't affected by the fictitious interface layer. The average shear strength method is widely used in stability analysis for sand compaction piles (Barksdale and Bachus, 1983; Bergado et al., 1996). This technique considers the weighted average of the material properties inside the unit cell; which is appealing for hand calculations. The distribution of stress within the unit cell is illustrated when referring to Figure 2.38. The effective stresses in the stone column and total stress in the surrounding soil is illustrated as follow:

$$\sigma_z^s = \gamma_s z + \sigma\mu_s \tag{2.83}$$

$$\sigma_z^c = \gamma_c z + \sigma\mu_c \tag{2.84}$$

The shear strength of the stone column and the surrounding soil is respectively determined by:

$$\tau_s = \left(\sigma_z^s \cos^2 \beta\right) \tan \varphi_s \tag{2.85}$$

$$\tau_c = c + \left(\sigma_z^c \cos^2 \beta\right) \tan \varphi_c \tag{2.86}$$

The weighted average shear strength (τ) and weight average unit weight (γ_{avg}) within the unit cell is given by:

$$\tau = (1 - a_s)\tau_c + a_s \tau_s \tag{2.87}$$

$$\gamma_{avg} = \gamma_s a_s + \gamma_c a_c \tag{2.88}$$

The shear strength parameters for use in this technique are:

$$c_{avg} = c(a_s) \tag{2.89}$$

$$(\tan \varphi)_{avg} = \frac{\gamma_s a_s \tan \varphi_s + \gamma_c a_c \tan \varphi_c}{\gamma_{avg}} \tag{2.90}$$

The lumped parameter technique is used to establish the factor of safety (SF) of the embankment and is given by the following expression:

$$SF = \frac{RM + \Delta RM}{DM + \Delta DM} \tag{2.91}$$

The resisting moment (RM) and driving moment (DM) are first calculated for the condition of no stone columns. These terms are then recalculated considering the effect of the stone columns.

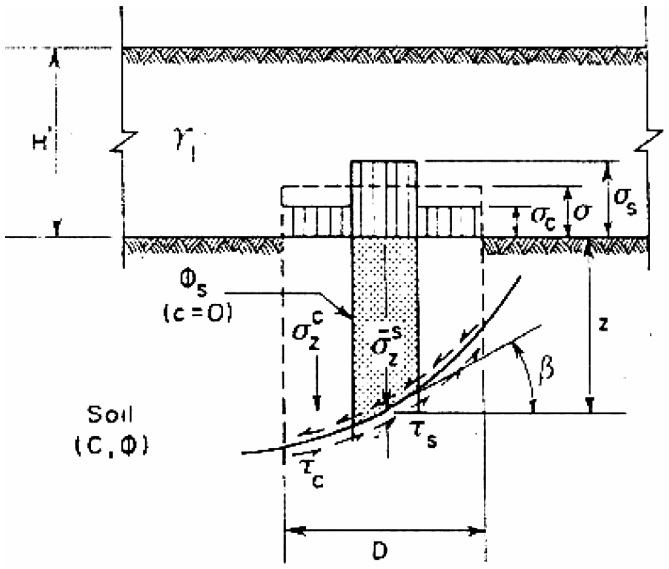

Figure 2.38 Average stress method of stability analysis (Bergado et al., 1996)

2.12.5 Factors Influencing Stone Column Efficiency

Hughes and Withers (1974) and Hughes et al. (1975) studied the behaviour of single stone columns, and they used laboratory radiography to observe the deformations occurring in and around a column of sand loaded within a cylindrical chamber containing clay (Wood et al., 2000). Hughes and Withers (1974) concluded that stone column bulging deformation occurs within four column diameters, measured from the column's surface, and the capacity of stone column can be assumed by observing the behaviour of bulging stone columns as they expand radially into the surrounding clay. In their research of stone columns, Wood et al. (2000) established that the length of a stone column can reduce the mechanism of deformation to a point. Beyond this point, increasing the column length gives no further advantage. Further, stone columns are also affected by smear and well resistance, in a similar manner as are prefabricated vertical drains. Wood et al. (2000) proposed the following four failure modes of stone columns:

1. Stone columns can fail by bulging, if it is not prevented from expanding radially by adjacent columns (as shown in Figure 2.39(a)).

2. If a column has little lateral restraint and is subjected to high loads, it may fail by a diagonal shear plane (as shown in Figure 2.39(b)).

3. Stone columns can fail by penetration through an underlying soft clay layer (as shown in Figure 2.39(c)).

4. A slender stone column can fail if it's laterally loaded (as shown in Figure 2.39(d)).

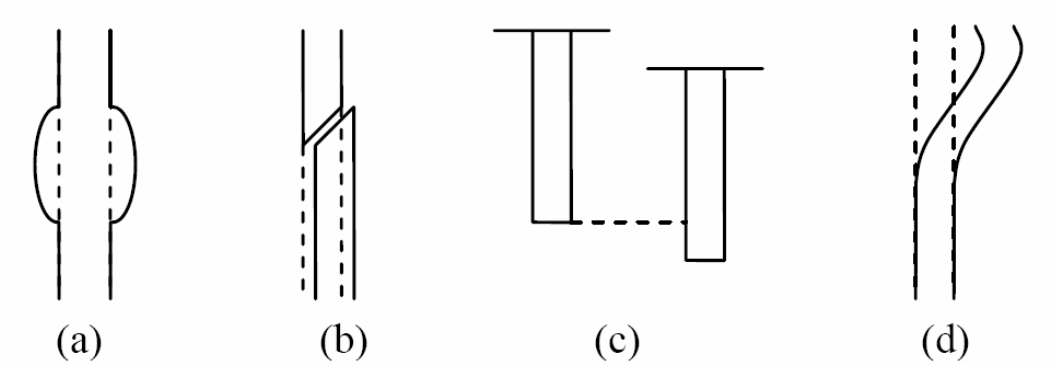

Figure 2.39 Four failure modes of stone columns (Wood et al., 2000)

2.12.6 Mechanism and Performance of Stone Columns

Stone column are usually installed in a triangular or square grid pattern ay typical centre to centre spacings of 1 to 3.5 m, and usually 15 and 35 percent of the volume of the soft soil is replaced by stone (Barksdale and Bachus, 1983). The presence of the column creates a composite material of lower overall compressibility and higher shear strength than the in-situ soil. Confinement, and thus stiffness of the stone, is provided by the lateral stress within the weak soil. Upon application of vertical stress at the ground surface, the stone and weak soil move downward together resulting in an important concentration of stress within the stone column, this concentration being primarily due to the column being stiffer than soil.

When an axial load is applied at the top of a single stone column, a large bulge is produced beneath the surface. This bulge in turn, increases the lateral stress within the clay which provides additional confinement for the stone. An equilibrium state is

eventually reached, resulting in reduction in vertical movement, when compared with the untreated ground. When an embankment is constructed over the soft ground, lateral spreading of ground occurs beneath the embankment. This reduces the confinement of the stone column. Additionally, at higher stress levels, relative displacement (slip) may also occur between the stone column and the surrounding soil. The occurrence of either lateral spreading or slip can thus result in greater settlement of stone column treated ground than would otherwise occur.

2.12.7 Consolidation Rate of Stone Column

Stone columns, one of the most commonly used soil improvement techniques, have been utilized worldwide to increase bearing capacity and reduce total and differential settlements of superstructures constructed on soft clays. A number of publications have been written on the development of theoretical solutions for estimating bearing capacity and settlement of reinforced foundations by stone columns (Aboshi et al. 1979; Barksdale and Bachus 1983; Priebe 1995). Therefore, these topics will not be explored in this paper. Field observations showed that stone columns could also accelerate the rate of consolidation of soft clays (Munfakh et al., 1983; Han and Ye, 1992). Field pore water pressure measurement under an embankment indicated that a homogenous clay stratum outside a stone column treated area only completed 25% primary consolidation when the stone column area had reached 100% primary consolidation (Munfakh et al. 1983). Han and Ye (1992) also reported that the rates of settlement of two similar buildings, one on an unreinforced foundation and the other on a stone column reinforced foundation on the same site, reached 66 and 95%, respectively over the same time period (480 days). The acceleration of the consolidation rate was accredited to stone columns for providing a drainage path and relieving excess pore water pressures by transferring the load from the soil. A numerical study demonstrated that an increase

of stone column-soil modular ratio can increase the rate of consolidation of soft clays under a rigid raft but not under a flexible raft (Balaam and Booker, 1981). The numerical solutions are excellent but need high computational efforts, which may not be convenient for practitioners.

Stone columns and the surrounding soil deform equally, as was the case of equal vertical strain investigated by Barron (1947). Some studies also found that the effectiveness of a stone column as a drainage path might be degraded because installation of the stone column could disturb the surrounding soil, and fine-grained soils could be mixed into the column (Barksdale and Bachus, 1983).

2.12.8 Barron's (1947) Solutions

Barron (1947) proposed a solution which dealt with consolidation of fine-grained soils by drain wells. Stone columns and drained wells have two major differences. First, stone columns have a larger drained elastic modulus than the surrounding soft clay. Barksdale and Bachus (1983) showed that, typical "elastic modulus ratios" of stone column in soft clay ranges from 10 to 20. As pointed out by Lane (1948), Barron's solution ignored the effect of the stiffness difference between the sand well and the surrounding soil on the consolidation rate. Second, stone columns have a smaller diameter ratio (influence diameter/column diameter) than drain wells. Typical diameter ratios for stone columns range from 1.5 to 5. However, the values for well diameter ratios used by Barron (1947) ranged from 5 to 100. In his derivation, Barron (1947) assumed that: (1) water in a saturated soil is incompressible, and at the moment of loading, excess pore water pressure carries all the vertical loads; (2) soil mass only deforms vertically; (3) each drain well has a circular influence zone; and (4) loads distribute uniformly over the compressible soil zone. Considering that the reduction of soil volume is equal to the discharge of water from the soil, a partial differential

equation for axisymmetric flow yields.

2.13 Chemical Admixture Stabilisation

Chemical admixture stabilisation has been extensively used in both shallow and deep applications to improve inherent soil properties, such as strength and deformation behaviour. The most commonly used admixtures are cement, lime, and bituminous compounds.

The main aims of admixture stabilisation are:

i. an increment of strength;

ii. a reduction in compressibility;

iii. improvement of shrink/swell characteristics;

iv. reduction of permeability; and,

v. increased soil durability.

The development of higher strength and stiffness is achieved by:

i. reduction of void space;

ii. bonding particles and aggregates together;

iii. maintenance of flocculent structures; and,

iv. prevention of swelling.

Shallow stabilisation with chemical admixtures has long been used to improve the performance of base course and subgrade materials in the construction of road pavements. It is considered a cost-effective method of improving long term performance and reducing whole-of-life costs of heavily trafficked pavements (Austroads, 1998). The increased bearing capacity of cement-modified subgrade allows a reduction in the thickness of the base course required to ensure prolonged

serviceability.

The use of chemical admixture stabilisation has more recently been extended to greater depths in which cement or lime columns act as a type of soil reinforcement. These processes were developed in the 1960s simultaneously, yet somewhat independently, at the Swedish Geotechnical Institute and at the Port and Harbour Research Institute in Japan (Holm, 1999). Cement columns were preliminarily reported to be successfully executed in practise in the early 1980s in a method known as DJM (Dry Jet Mixing).

The Swedish Geotechnical Institute, together with Linden-Alimak AB and Professor Bengt Broms, has done extensive work on the usage of lime columns for foundation and earthworks in soft clays (Bergado et al, 1996; Holm, 2001). Modern applications of deep mixing of in-situ soils with chemical admixtures proceeded in Japan in the late 1970s to improve soft ground for port and harbour structures. This technique has been expanded to applications in embankments, buildings, and storage tanks (see Figure 2.40). Broms (1986) suggested that it is preferable to use cement instead of lime in Southeast Asia, for the following reasons: lime is considerable more expensive in this region; unslaked lime is difficult to store in a hot, humid climate; greater strength can be generated with cement; and, there is a limit to the strength gains induced by lime stabilisation. It could be inferred that this statement would be also relevant to Australian conditions, particularly in northern parts such as Queensland.

2.13.1 Mechanism of Soil-Cement Stabilisation

Cement interacts with clay to alter its properties in two ways. Initially cement reacts with soil pore water in a process known as hydration. The primary products of hydration are formed virtually immediately upon mixing the two substances to produce the most substantial strength gains exhibited in cement stabilisation. The secondary product of hydration is hydrated lime, which induces a gradual rise in the soil-cement

pH to eventually dissolve and chemically alter soil minerals. This secondary reaction occurs over time to produce additional bonding and strength.

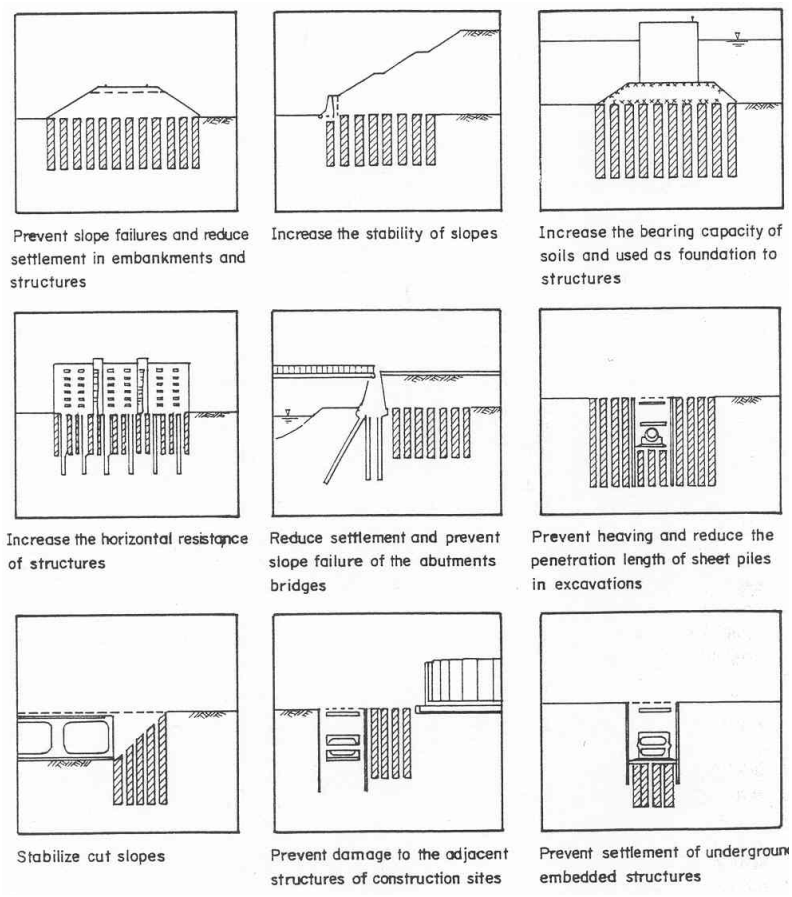

Figure 2.40 Applications of deep cement mixing (Bergado et al, 1996)

The reactions which take place in soil-cement stabilisation can be represented in the following qualitative equations (Bergado et al, 1996). Only tricalcium silicate (C_3S) has been considered, as it is the primary cementitious constituent of OPC.

$$C_3S + H_2O \rightarrow C_3\,S_2\,H_x \textit{ (tobermorite gel)} + Ca(OH)_2 \textit{ (hydrated lime)} \qquad (2.92)$$

$$Ca(OH)_2 \rightarrow Ca^{++} + 2(OH)^- \qquad (2.93)$$

$$Ca^{++} + 2(OH)^- + SiO_2 \textit{ (soil silica)} \rightarrow \text{CSH} \qquad (2.94)$$

$$Ca^{++} + 2(OH)^- + Al_2\,O_3 \textit{ (soil alumina)} \rightarrow \text{CAH} \qquad (2.95)$$

2.13.1.1 Primary Cementitious Products

When cement encounters soil pore water, the chemical process of hydration rapidly occurs (Equation 2.92). The direct products of hydration are: hydrated calcium silicates (C_2SH_x, $C_3S_2H_x$); hydrated calcium aluminates (C_3AH_x, C_4AH_x); and hydrated lime $Ca(OH)_2$. Hydrated calcium silicates and aluminates are the main cementitious products, with the hydrated lime being deposited as a separate crystalline solid phase. These cementitious particles bind with adjacent cement grains during curing to form a hardened skeleton matrix, which encloses unaltered soil particles.

2.13.1.2 Secondary Cementitious Products

The hydration of cement also leads to a rise in pore water pH, caused by the dissociation of the hydrated lime. This induced alkalinity dissolves the inherently acidic soil silica and alumina from both clay minerals and amorphous materials on the surface of the clay particles, in a manner similar to the classical weak acid - strong base reaction (Equations 2.93, 2.94, and 2.95). The hydrous silica and alumina then gradually react with the calcium ions liberated by the hydrolysis of cement, forming secondary insoluble cementitious compounds which harden when cured. This results in the soil experiencing further gains in bondage, strength and volume stability.

However, following the pozzolanic reaction of lime, the subsequent pH drop tends to promote the hydrolysis of $C_3S_2H_x$, to revert back to CSH and lime (Equation 2.96).

$$C_3\ S_2\ H_x \rightarrow C_3S_2H_x\ \textit{(hydrated gel)} + Ca(OH)_2 \qquad (2.96)$$

The formation of CSH is beneficial only if it is formed by the pozzolanic reaction of lime and soil particles. It becomes detrimental when CSH is formed at the expense of the formation of the $C_3S_2H_x$, whose strength generating characteristics are superior to those of CSH (Bergado et al, 1996).

In conclusion, fine clay soil that is combined with cement is modified by the formation of "primary" and "secondary" cementitious agents. The primary hydration products harden rapidly into high-strength compounds, while the secondary cementitious products increase the strength and durability of the stabilised soil over time to further enhance the bond strength between the particles.

2.13.2 Structure of Clay-Cement Skeleton Matrix

From the fundamental reactions between clay minerals and cementations products, the structure of clay-cement skeleton matrix can be described as follows. Since the particles of cement are very large in relation to those of clay, a clay-cement skeleton matrix and a clay matrix are most likely to form. The skeletal units contain a core, consisting of hydrated cement gel, to which layers of modified clay particles are added.

Modification of the clay is caused by the dissolution of its inherent silicates and aluminates and the amorphous components in the alkaline environment, due to the presence highly reactive $Ca(OH)_2$. This dissolved material associates with calcium ions, producing additional cementations which in turn bind with adjacent clay particles. These substances accumulate around the cement grains to create aggregations, packing some slightly modified clay in the space between the individual particles (Bergado et al, 1996).

Generally, the grain size of a soil dictates the amount of cement needed for complete stabilisation. Soils with smaller particles have a greater overall surface area, requiring more cement particles to acquire the ultimate strength gains.

2.13.3 Schematic Illustrations of Cement-Improved Soil

The hardening process commences immediately upon mixing soil with cement slurry. Despite thorough mixing, clay particles tend to form a cluster which is surrounded by

the slurry. The hardening agent produces the hydrated calcium silicate, hydrated calcium aluminates and calcium hydroxide and forms hardened cement bodies. Saitoh et al. (1985) showed the arrangement of cohesive soil and hardening agent that has formed a hardened body (Figure 2.41). It can therefore be inferred that the strength of the improved soil depends upon the strength characteristics of both hardened bodies.

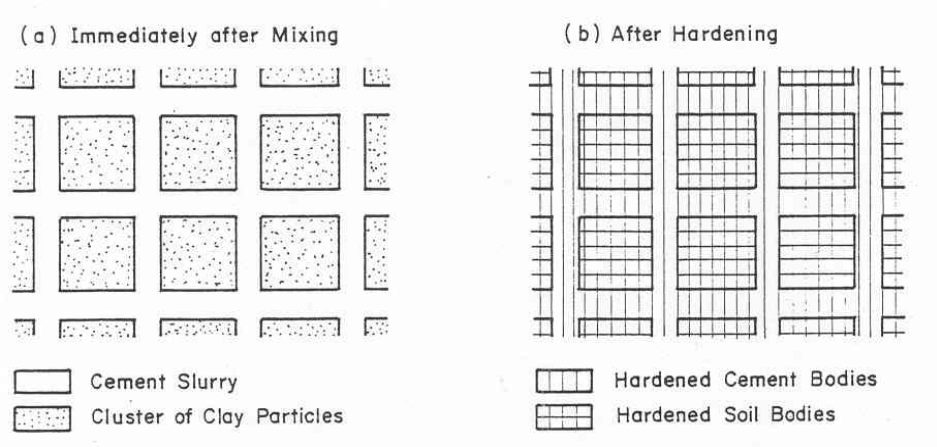

Figure 2.41 Schematic illustrations of cement improved soil (Saitoh et al, 1985)

2.13.4 Influences on Hardening of Cement Treated Clays

The hardening characteristics of cement treated soil mixtures are influenced by a number of factors (see Figure 2.42). Due to the multitude of alternatives and combinations, it is impractical to define the various mechanical properties as functions of these factors. However there are some predominant factors presented below, providing information outlining order-of-dominance value and the effects these factors on the strength and stiffness of the cemented clay (Bergado et al, 1996).

2.13.4.1 Type of Cement

The differences in improvement of cement treated clays have been investigated by Bergado et al (1996). It was shown that stabilisation by GB (General Blended) cements can be superior to that by GP Cements. However, ordinary Portland cements remain the most common cement used in soil stabilisation, due to their wide availability and cheaper cost when compared to other cement types.

2.13.4.2 Cement Content

In general, it has been found that the greater the cement content, the greater the strength of the cement-treated clay. In this respect, cement-treated clays differ from those similarly treated with lime. Lime-treated clay reaches a maximum strength limit at an optimum addition content, whereas cement-stabilised clay will generally continue to strengthen at higher cement contents.

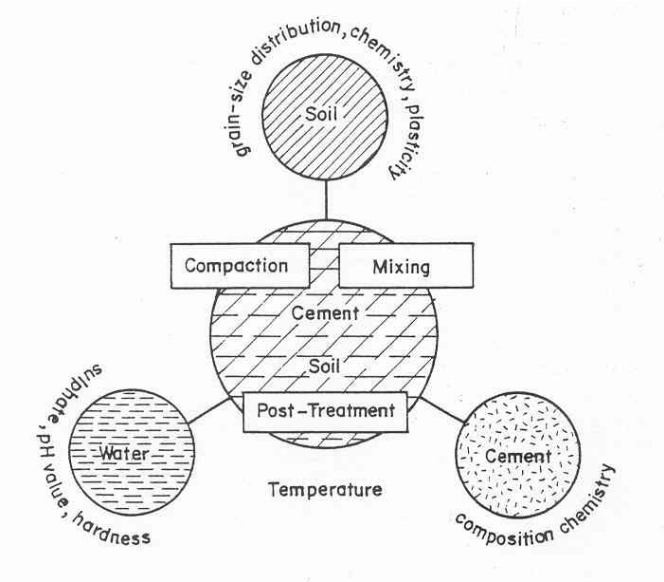

Figure 2.42 Factors affecting properties of cement treated soils (Kezdi, 1979)

2.13.4.3 Curing Time

In a manner similar to that of concrete, the shear strength of cement-treated clay increases with time. The rate of strength increase is rapid in the early stages of the curing period, thereafter decreasing with time. The rate of increase of strength is greater in cement-treated clay, than in lime-treated clay.

2.13.4.4 Soil Type

The effectiveness of cement and lime decreases with increasing water content and organic content. The improvement decreases generally with increasing plasticity index of the clay. The strength increase resulting from cement stabilisation of organic soils can be quite low, but is still generally more effective than lime stabilisation. In soil of

very high activity, the increase in shear strength upon cement mixing is low. This is the opposite order to that of lime treatment, since the strength of lime treated clay depends mainly on the participation of clay particles in the pozzolanic reaction. But in the case of cement treated clay, it depends mainly on cementation from the cement hydration on contact with pore waters (Bergado et al, 1996).

2.13.4.5 Curing Temperature

Increasing temperatures tend to accelerate the hydration reaction in cement-soil stabilisation, thus increasing the rate of strength gain. The solubility of clay mineral silicates and aluminates also increases at higher temperatures, promoting accelerated formation of the fore-mentioned secondary cementitious products and ongoing strength gains.

2.13.4.6 Soil Minerals

In the case of soil with higher pozzolanic reactivity, the strength gained by cement addition is governed by the strength characteristics of the hardened cement bodies. But in the case of soils with low pozzolanic reactivity, strength gains are governed by the strength characteristics of the hardened soil bodies (Saitoh et al, 1985). It follows that, if improvement conditions are identical, greater strength will be induced from the soil with higher pozzolanic reactivity. The amount of secondary cementitious materials produced during the pozzolanic reaction of the clay particles and hydrated lime is dependent upon the amount and mineral composition of the clay fraction as well as the amorphous silica and alumina present in the soil.

2.13.4.7 Soil pH

Solubility of the silicates and aluminates of the clay particles is increased at higher pH levels. This accelerates the long-term pozzolanic reactions that produce secondary

cementitious materials (Bergado et al, 1996). Therefore soil pH has some impact on the ongoing strength gain exhibited in cement-treated soil.

2.13.5 Field Application of Chemical Treated Clay for Shallow Stabilisation

Shallow stabilisation techniques are widely used for the improvement of road subgrade and base course material. Surface stabilisation involves the mixing of a borrow soil and binder material, and subsequent compaction of the mixture at the optimum water content. Chemical admixtures (mainly cement or lime) are used to improve the properties of soil by ion exchange and cementation reactions.

This method is usually performed using in-situ stabilisation equipment, essentially comprising an additive tanker/spreader and a stabilising mixer or reclaimer/stabiliser. The purpose of the spreader is to hold and distribute the chemical additive to be incorporated. The purpose of the stabiliser mixer is to thoroughly mix this additive into the host material. In the case of a reclaimer/stabiliser, the machine is also designed to reclaim and pulverise the existing soil. Conventional reclaimer/stabilisers can penetrate and improve depths of up to 400 mm for widths of 1.8 - 2.4 metres.

The use of cement as a stabilising agent has two important effects on soil behaviour. It greatly reduces the moisture susceptibility of some soils, giving enhanced volume and strength stability under variable moisture conditions. It also causes the development of interparticular bonds in granular, endowing the stabilised material with tensile strength and high elastic modulas. While these characteristics can offer many possibilities, other factors can limit its applications, including construction requirements, traffic loading, shrinkage characteristics, etc (Austroads, 1998).

2.13.6 Deep Mixing Method

Deep stabilisation with calcium hydroxide originated in the USA around 1960 on an experimental basis. The technique was further developed by researchers in Japan and Sweden, with unslaked lime or cement being mixed with soft soil in a columnar arrangement, and so dubbed the Deep Mixing Method (DMM) of ground improvement (Holm, 2001; Jelisic and Leppänen, 2003). The deep mixing method is an in-situ soil mixing technology that mixes existing soil with cementitious materials using mixing shafts consisting of auger cutting heads, discontinuous auger flights, and mixing paddles (see Figure 2.43). Mixing equipment varies from single to eight shaft configurations depending on the purpose of the deep mixing (Terashi, 1997; Stocker and Seidel, 2005).

Bredenberg (1999) reported that the idea of injecting dry quick lime into soil to form a vertical column was in Scandinavia first presented by Mr Kjeld Paus of Sweden in 1967. Mr Paus believed that the drying and strengthening effects he observed as a road engineer performing surface stabilisation, could also work if the quick lime was mixed vertically. It was considered desirable to use dry binder, as opposed to slurry, to allow it to undergo its initial pozzolanic lime-water reaction with the soil pore water. Transporting lime in pipes with air also proved a better alternative to water in cold climates with sub-zero temperature ranges (Bredenberg, 1999).

As detailed in Terashi (1997) and Yang (1997), the development and research on deep mixing for the purpose of stabilising soft marine soils with lime in harbours and below the sea floor before the construction of harbour facilities originated with laboratory model tests in 1967 by the Port and Harbour Research Institute of the Japanese Ministry of Transportation. This research progressed to become feasible for full-scale construction by 1974 known as the Deep Lime Mixing method (DLM). By 1975, based

on the DLM technology, the Cement Deep Mixing method (CDP) had been developed using cement grout as the stabilising agent.

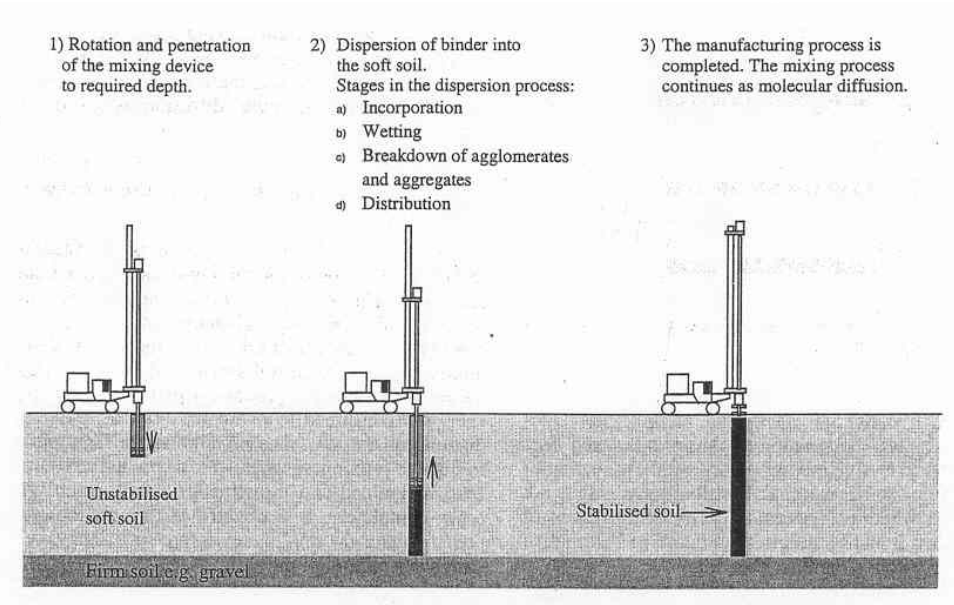

Figure 2.43(a) Schematic illustration of deep soil mixing (Larsson et al, 1999)

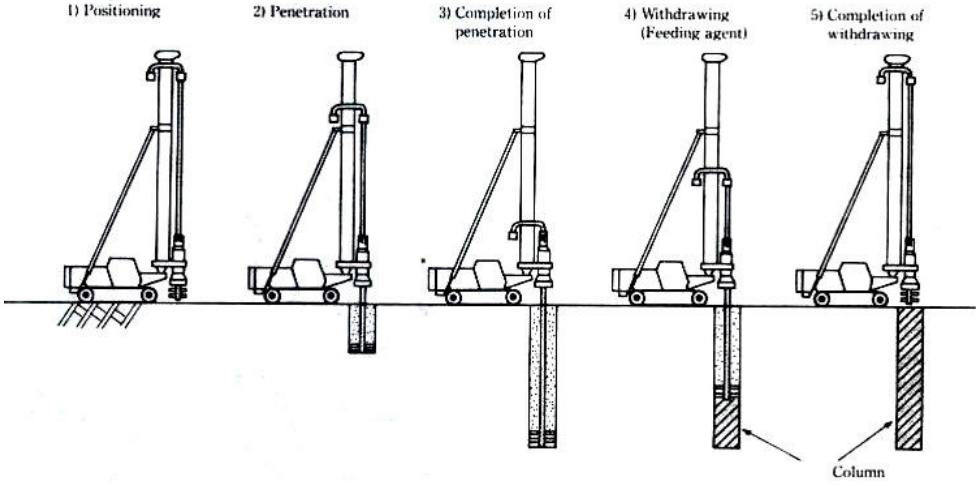

Figure 2.43(b) Construction sequence for deep mix stabilization (Porbaha, 2000)

Parallel to the development of the CDM method in coastal engineering applications, Seiko Kogyo Co. Ltd. of Osaka, Japan began research and development of the Soil Mix Wall (SMW) method in 1972 for the purpose of treating soil on land along a single row to produce a soil-cement wall. The SMW was first used in full-scale construction in 1976 in Japan. CDP and SMW methods are advantageous in that the mixing apparatus is relatively light, making it easy to transport and manoeuvre. Another advantage is that

the diameter of the improved column tends to vary with depth according to the variation of subsoil shear strength. This can create greater load transfer at the interface of improved column and surrounding soil (Terashi, 1997).

Figure 2.43(c) Deep dry mixing equipment (Massarsch, 2005)

In 1976, the Japanese Ministry of Construction's Civil Engineering Research Institute started researching deep mixing using dry cementitious powders. Termed the Deep Jet Mixing (DJM) method, it became commercially viable by 1981. The admixture is transported through a pipe with the aid of compressed air and mixed with the clay mechanically by cross jet mixing (Yasui et al., 2005). In this method no water is used and so the improvement is generally higher than the slurry system. Due to difficulties transporting the dry cement by air, the applications of DJM are somewhat limited in comparison with CDM and SMW methods. A more recent advance in deep soil mixing is the combination of dry jet and mechanical mixing procedures. This innovation comprises the central portion of the soil-cement column being produced by mechanical mixing, while the outer zone formed by cross jet mixing (Terashi, 1997). The largest project using deep soil mixing ever performed in the United States, and among the largest in the world, is the Central Artery Project in Boston. Several slurry and dry mixing techniques were used to form columns, grids, blocks, and stabilising walls

(including jet grouting and mechanical mixing) within large deposits of very soft Boston Blue Clay (Esrig, 1999).

2.13.7 Previous Laboratory Studies on Cement Treated Clay

2.13.7.1 General

Mitchell (1981) conducted a comprehensive review of the strength characteristics of cement stabilised soil. The unconfined compressive strength (q_u) was reported as increasing linearly with the cement content percentage (A_w). The increase is more pronounced for coarse-grained soil than for silts and clays. Like q_u, other strength parameters such as cohesion intercept (c) and the internal friction angle (ϕ) increase with A_w and curing time. The following relationship between curing time and unconfined compressive strength was developed (Bergado et al, 1996).

$$q_u(t) = q_u(t_0) + K \log \frac{t}{t_0} \tag{2.97}$$

where: $q_u(t)$ = Unconfined Compressive Strength at t days, kPa
$q_u(t_0)$ = Unconfined Compressive Strength at t_0 days, kPa
K = $70A_w$ for fine-grained soil, $480A_w$ for granular soils
A_w = Cement content, % by mass
t = Curing time
t_0 = Reference time

Several laboratory studies have been performed on cement-stabilised soils using a variety of test methods to document the effects of cement additions on particular clay specimens. These procedures include combinations of unconfined compression tests, drained and undrained triaxial compression tests, oedometer consolidation and constant stress ratio tests. Numerous parameters have been examined, such as cement content, curing times, moisture and temperature effects, etc.

While these reports have comprehensively detailed properties evident in particular clay specimens, dissimilarities among results indicate their limited applicability in a broad sense. This is likely to be due to the wide range of chemical constituents found in different soils, with varying minerals making up the respective clay fractions. The rate and magnitude of chemical reactions between the cement and the soil minerals varies accordingly. This is less evident in the case of cement compared to lime due to the consistent cement-water hydration reaction, however still considerable.

Therefore data gleaned from studies in a particular laboratory study may not be applicable to clay soils from elsewhere in the world. This indicates the need for some degree of laboratory testing of a clay soil to verify or adapt existing design and construction practices for cement stabilisation at that location. Very little research on this subject has been documented for Australian clays, and more particularly, the south-east Queensland region's estuarine clay deposits. The following is a summary of several laboratory studies undertaken in other parts of the world.

2.13.7.2 Soft Bangkok Clay, Thailand

At the Asian Institute of Technology, Uddin (1995) conducted research on the engineering characteristics of cement treated soft Bangkok clay under unconfined compression, oedometer, constant stress ratio tests, drained and undrained triaxial tests. The study addressed the effect of the variability in terms of hardening agent quantity, the pre-shear consolidation pressure, the stress conditions imposed during testing, the drainage condition, and the time dimension. The oedometer tests revealed that the addition of cement caused substantial improvement of consolidation properties. Normalised intrinsic compression curves offered confirmation of the hardening effect in the void index plane. It was observed that the main effect of cement treatment is to

modify the behaviour of the soft clay from a normally-consolidated to an over-consolidated state (Uddin et al., 1997).

The base soil used in this study was soft Bangkok clay, taken from a site within the Asian Institute of Technology campus at depths of 3 to 4 metres. Properties of this virgin soil are shown below in Table 2.5. Physical properties of the subsequently cement treated samples are then detailed in Table 2.6.

The effect of cement content ($\mathbf{A_w}$) and curing time (**t**) on the liquid limit was deemed insignificant, in contrast to the plastic limit which was observed to increase. Water content was reported to decrease by 5-10% immediately after mixing, with sharp reduction in moisture occurring up to around 12.5% cement additions and curing times of approximately 10 weeks. Investigations showed that the gradients of unit weight vs cement content plots were found to be almost constant, but with increasing sharply up to twelve weeks curing time and decreasing thereafter.

From unconfined compression tests, stress-strain curves for treated samples were found to increase rapidly up to the peak compressive strength, then suddenly decrease to very low residual values upon further straining. The effectiveness of cement treatment on Bangkok clay is illustrated below in Figure 2.44, depicting the relationship between the unconfined compressive strength ($\mathbf{q_u}$), and cement content ($\mathbf{A_w}$).

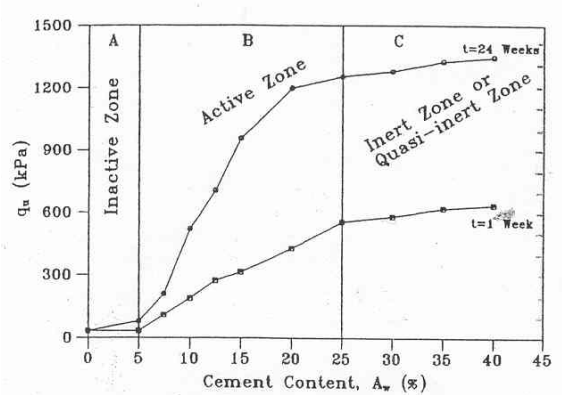

Figure 2.44 Influence of cement content on UCS of Bangkok clay (Uddin, 1995)

Table 2.5 Physical Properties of the Soft Bangkok Clay

Clay	69%	Water Content	76-84%
Silt	28%	Total Unit Weight (kN/m^3)	14.3
Sand	3%	Dry Unit Weight (kN/m^3)	7.73
Liquid Limit	103%	Initial Void Ratio, e	2.2
Plastic Limit	43%	Activity	0.87
Plasticity Index	60%	Sensitivity	7.3
Liquidity Index	0.62	Organic Content	5.6%

Table 2.6 Physical Properties of the Cement Treated Soft Bangkok Clay

Cement Content (%)	Curing Time (months)	Total Unit Weight (kN/m^3)	Dry Unit Weight (kN/m^3)	Void Ratio	Water Content (%)
5	1	14.85-15.12	8.16-8.67	2.03-2.22	73.4-83.8
7.5	1	14.90-15.25	8.31-8.76	1.99-2.15	72.9-81.4
10	1	14.95-15.43	8.44-8.90	1.93-2.09	69.3-78.5
12.5	1	15.03-15.52	8.49-9.21	1.90-2.06	68.5-77.7
15	1	15.04-15.40	8.60-9.05	1.87-2.02	66.8-75.4
5	2	14.90-15.51	8.28-8.98	1.99-2.16	71.7-80.9
7.5	2	14.97-15.55	8.32-9.10	1.92-2.12	70.9-80.0
10	2	15.00-15.48	8.62-9.15	1.91-2.05	69.2-77.5
12.5	2	15.05-15.60	8.68-9.22	1.85-1.98	67.7-74.2
15	2	15.28-15.61	8.81-9.31	1.82-1.95	67.1-73.5
Untreated	0, 1 & 3	14.10-14.96	7.74-8.24	2.20-2.44	81.6-86.0

From oedometer testing, the void ratio/ axial stress plot illustrated above in Figure 2.45 was produced. It demonstrates the similarity in the shapes of the void ratio-axial stress curves for 1 to 6 month curing periods. The (e, log σ_v) relationships show that the treated curve crosses the untreated curve well before its preconsolidation pressure and then is displaced from the untreated curve with increasing σ_v values. This indicates lower compressibility for treated samples, compared to untreated. With increasing cement contents, both an enhancement of preconsolidation pressure and a decrease of compression index were evident, accompanied by a gradual reduction in compressibility. This gradual compressibility decline was also obvious as curing time progressed.

Uddin (1995) observed that at low cement contents ($A_w \leq 5\%$), increased curing time did not develop considerable hardening effects in the clay matrix. It was also reported that gains in hardening potential were made more significant by increasing cement

content (e.g. 5 to 7.5%) than by prolonging curing time (e.g. 1 to 2 months). Subsequently it was postulated that the cement content of a sample is a much more active parameter than curing time, in terms of compressibility. The sensitivity of the clay diminished dramatically with cement treatment. At large strains, cohesion of the treated clay became negligible and was observed to act as purely frictional material.

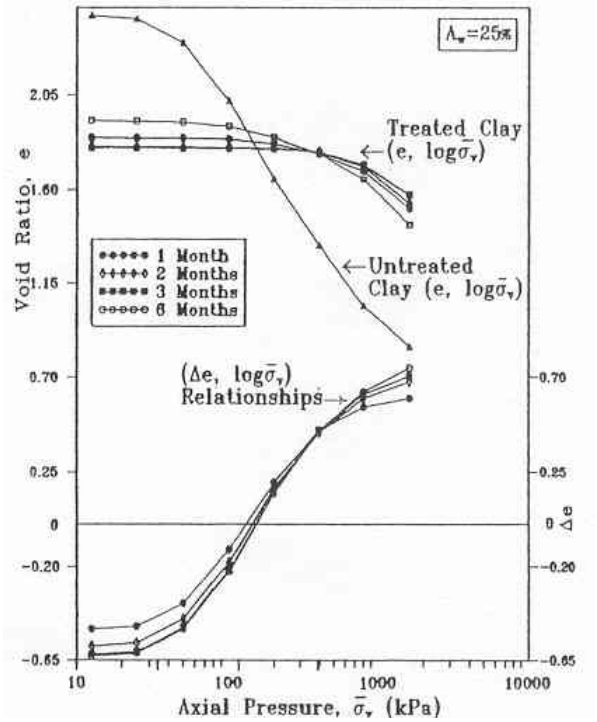

Figure 2.45 (Δe, log σ_v) Relationship at 25% cement content for Bangkok clay (Uddin, 1995)

2.13.7.3 Boston Blue Clay, USA

Esrig (1999) reported results of laboratory testing undertaken on chemically treated samples of Boston blue clay, as part of the fore-mentioned Central Artery Project. The primary purpose of the laboratory testing was to determine the appropriate stabilising agent to utilise on the large project, although other parameters including curing time, temperature effects and soil type were also examined. The unconfined compressive strength of cement treated Boston blue clay was observed to increase with time, at a very similar rate to other blended binders when normalised to the strength at 28 days.

2.13.7.4 Scandinavian Studies

Ahnberg and Holm (1999) of Sweden documented laboratory studies of organic Scandinavian soil mixed with cement and other stabilising agents. The majority of their efforts centred around determining appropriate binders for use with highly organic peat and "gyttja", a local type of organic clay. In the Scandinavian studies, the majority of sample sites were deposits of primarily organic peat but some were "gyttja" clay with organic contents of around 10% (Hansbo and Massarsch, 2005). This equates to the highest organic content likely to be encountered with southeast Queensland soft estuarine clays, however the water contents of these samples were much greater, up to 250%. Therefore it is difficult to directly compare these results with those gained from comparative Australian research.

Nonetheless, these studies indicate minimal strength increase with time after 28 days when using low binder contents ($\leq$ 100 kg/m^3). It was also observed that the strength increase with time grows with increasing quantities of stabilising agent for most of the different binder types. The effect of temperature was discussed, stressing the notion that increased curing temperature results in a higher rate of strength increase.

2.13.8 Lime as Stabilising Agent

Lime is found in all geological formations, all over the world. Lime is an effective stabilizing agent for soft soils and can be used to improve their workability, limit volumetric changes, and increase strength.

Lime has many different manufacturing and environmental applications. Its largest construction related use is for stabilization of foundation soils and materials that underlie highway and airfield pavements, building structures, drainage canals, and earth dams. In 2003, more than 1.6 million metric tons of lime was used for soil stabilisation in the U.S. (Miller, 2004).

Lime is a broad term which is used to describe calcium oxide (CaO) – quicklime; calcium hydroxide $Ca(OH)_2$ – slaked or hydrated-lime; and calcium carbonate ($CaCO_3$) – carbonate of lime. The relation between these three types of lime can be represented by the following equations.

$$CaCO_3 + HEAT = CaO + CO_2 \quad (2.98)$$

$$CaO + H_2O = Ca(OH)_2 + HEAT \quad (2.99)$$

$$Ca(OH)_2 + CO_2 = CaCO_3 + H_2O \quad (2.100)$$

When lime is added to a clay soil it has an immediate effect on the properties of the soil as cation exchange begins to take place between the metallic ions associated with the surface of the clay particles and the calcium ions of the lime. Clay particles are surrounded by a diffuse hydrous double layer which is modified by the ion exchange of calcium. This alters the density of the electrical charge around the clay particles which leads to them being attracted closer to each other to form floccules, the process being termed flocculation. It is the process which is primarily responsible for the modification of the engineering properties of clay soils when they are treated with lime (Sherwood, 1993).

Treatment with lime has been mainly used in the field of highways, railroads and airport constructions in order to improve the mechanical properties of the bearing layers. The use of lime stabilisation has more recently been extended to greater depth in which lime columns act as a type of soil reinforcement. Layers of lime stabilised clays, with their high strength and high modulus, can also function as a rigid crust which is useful in spreading the applied loads to the subsoil.

The addition of chemical agents to soil in the application of in-situ mix method was first conducted in both Sweden and Japan in the 1970's. Toth (1993) referred to Japanese development of chemical addition and deep mixing method to improve engineering properties of soft cohesive soils for depths up to 50 meters. These early application were

carried out on harbour structures. The most common agents used for soil stabilisation are cement and lime. Lime and cement soil stabilisation is used widely in Scandinavia for soft clays and organic soils to improve stability and reduce settlement on road and rail road embankments and to increase the stability of shallow trenches.

The final properties of stabilised soils depend on the type of additive used and amount of additive and the initial properties of the soil sample. The properties significantly change with time, i.e. the increase in strength with time after addition. Pozzolan as a finely divided silicaceous or aluminous material which, in the presence of water and calcium hydroxide, will form cemented products such as calcium or aluminate-silicate-hydrates. Thus clay, which is the source of silica and alumina, is, by this definition a pozzolan and a contributor to the pozzolanic reactions believed to occur during lime stabilisation.

Significant research has been done on additives for soil stabilisation such as gypsum, flyash, granulated blast furnace slags which have been found to have the ability to enhance the pozzolanic reactions which occur during lime stabilisation. The most appropriate stabilizer is a function of soil type and objective. Lime is normally the most cost effective stabilizer for highly plastic clays while cement is more appropriate for use with course grained materials. Flyash is more of an intermediate material.

2.13.8.1 Chemical and Mechanical Interaction of Chemically Improved Soils

When mixing the additive with the soil chemical reactions will start immediately, but these reactions will differ with the type of additive. Cement will form a lattice between the soil granules due to the initial hydration process of the cement. This differs with the addition of lime as it will react with the chemical components of the soil. Lime based additives will continue reactions with the soil for several months. Initially the water content will reduce in the mix due to the hydration process. This lime will also react

with the clay minerals and calcium ions will diffuse from high concentrations of binder, both with stabilised regions and also adjacent areas of soil not originally involved with the stabilising process. This in turn improves a greater area of soil not over time. The geo-mechanical properties of chemically improved soil depend on the type of binder. It is generally noticed that the strength and brittleness of the improved soil increase with the increasing amount of cement although the ductility of the soil will increase with the increasing amount of lime.

2.13.8.2 Lime Addition to Clay

Lime has been successfully used as an additive to the soil to improve soil behaviour. Cation exchange is considered to be one of the important reactions responsible for the improvement in the soil characteristics. Lime-clay reactions occur via two distinct processes (Boardman, 2001): (i) rapid ion exchange reactions known as soil improvement or modification and (ii) slower soil-lime pozzolanic reactions known as stabilization/solidification. Lime modification reactions occur from replacement of exchangeable ions of the soil with calcium ions released by lime. The increased exchangeable calcium ion concentration increases the flocculation of clay particles and transforms the plastic soil to a granular and less plastic material. Lime stabilization/solidification occurs at lime additions in excess of the Initial Consumption of Lime value.

2.13.8.3 Mechanism of Lime Stabilization

When lime is added to a clay soil it has an immediate effect on the properties of the soil as cation exchange begins to take place between the metallic ions associated with the surface of the clay particles and the calcium ions of the lime.

The major strength gain of lime treated clay is mainly derived from three reactions, namely; hydration of soil, ion exchange, and pozzolanic reaction. Other mechanisms

such as carbonation cause minor strength increase and can be neglected. Short term reactions include hydration (for quicklime) and flocculation (ion exchange). Longer term reactions are cementation and carbonation.

(i) Hydration

A large amount of heat is released when quicklime (CaO) is mixed with clay. This is due to the hydration of quicklime with the pore water of the soil. The increase in temperature can, at times, be so high that the pore water starts to boil (Broms, 1984). An immediate reduction of natural water contents occurs when quicklime is mixed with cohesive soil, as water is consumed in the hydration process. Moreover, a considerably larger amount of the pore water evaporates because of the heavy heat release, i.e., as the hydration of the quicklime proceeds and the temperature increases, the amount of pore water is reduced. This drying action is particularly beneficial in the treatment of the moist clays. Thus, if a reduction of the natural water content in a cohesive soil is desirable, quicklime (or unslaked lime) instead of calcium hydroxide is used. It is important that the water content of the base clay must be sufficient for the complete slakening of the quicklime. Furthermore, to make the ion exchange possible between calcium ions of hydrated lime and the alkali ions of the clay minerals, there must be enough water after the evaporation caused by the heat release at the slakening of the quicklime.

The calcium hydroxide, $Ca(OH)_2$, from the hydration of quicklime or when using calcium hydroxide as the stabilizer, dissociates in the water, increasing the electrolytic concentration and dissolving the SiO_2 and Al_2O_3 from the clay particles.

$$Ca(OH)_2 \text{ ---------- } Ca^{++} + 2(OH)^- \qquad (2.101)$$

This process will result in ion exchange, flocculation and pozzolanic reactions.

(ii) Ion Exchange and Flocculation

This process is primarily responsible for the modification of the engineering properties of clay soils when they are treated with lime. When lime is mixed with clay, Sodium and other cations absorbed to the clay mineral surfaces are exchanged with calcium. This change in cation complex affects the structural component of the clay mineral. Within a short time after mixing, the calcium hydroxide is transformed again due to the presence of carbonic acid (H2CO3) in the soil (Kezdi, 1979). The presence of carbonic acid in the soil is due to the reaction of carbon dioxide of the air in the soil and the free water. The reaction results in the dissociation of the lime into "Ca^{++}(or Mg^{++}) and $(OH)^{-}$" which modifies the electrical surface forces of the clay minerals. A transformation of the soil structure begins, i.e., flocculation and coagulation of soil particles into larger sized aggregates or grains and an associated increase in the plastic limit. Lime causes the clay to coagulate, aggregate or flocculate.

$$Ca^{++} + \text{Clay} = Ca^{++} \text{ exchanged with ions } (K^{+},\ Na^{+}) \qquad (2.102)$$

(iii) Pozzolanic Reaction

The shear strength of the stabilized soil gradually increases with time mainly due to pozzolanic reactions. Calcium hydroxide in the soil water reacts with the silicates and aluminates (pozzolans) in the clay to form cementing materials or binders, consisting of calcium silicates and/or aluminate hydrates. The dissolved Ca^{++} ions react with the dissolved SiO_2 and Al_2O_3 from the clay particle's surface and form hydrated gels, resulting in the combination of the soil particles.

$$Ca^{++} + 2(OH)^{-} + SiO_2 = \text{CSH (calcium silicate hydrates)} \qquad (2.103)$$

$$Ca^{++} + 2(OH)^{-} + Al_2O_3 = \text{CAH (calcium aluminate hydrates)} \qquad (2.103)$$

The gel of calcium silicate (and/or aluminate hydrates) from above reaction, which is insoluble in water and binding the soil particles together. This gel thus constitutes an enveloping and binding seam (see Figure 2.46). From this figure, it can also be seen that

the silicate can only be formed if there is sufficient water to enable the transfer of Ca^{+} and OH^{-} ions to the surface of the clay material.

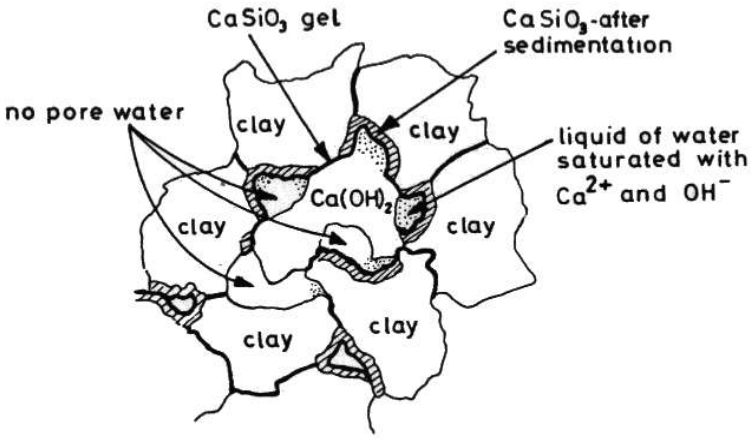

Figure 2.46 Principle of soil stability with lime (Ingles and Metcalf, 1972)

(iv) Carbonation

Reaction of lime with carbon dioxide in the open air or in voids of the ground forms a relatively weak cementing agent. This may be beneficial where lime is plentiful; the $CaCo_3$ formed will not react any further with the soil.

2.13.8.4 Factors that Affect Hardening of Soil-Lime

(i) Type of Lime

The efficiency of lime stabilization depends on the type of lime material used. Quicklime is generally more effective than hydrated lime (Kezdi, 1979); since water will be absorbed from the soil and more importantly, the hydration will cause an increase in temperature which is favorable to strength gain (Broms, 1984).

(ii) Lime Content

The strength of lime soil mixtures increases as the lime content is increased. There appears to be no optimum lime content which produces a maximum strength in a lime stabilized soil under all conditions. However, Eades and Grim (1966) suggested that the amount of lime consumed by a soil after one hour affords a quick method of

determining the percentage of lime required for stabilization. McDowell (1966) pointed out that short-time or quick tests probably will not identify optimum lime contents, but are essential in checking against the use of non-reactive soils for treatment of lime. On the other hand, while long-term tests would do a better job of identifying optimum lime contents, they may be impractical from the standpoint of time, and may even suggest the use of insufficient amounts of lime due to the ideal conditions under which they are run. Hilt and Davidson (1960) gave a correlation which showed that the amount of lime fixation is in proportion to the type and amount of clay present and is independent of the absorbed cation present in the clays.

(iii) Curing Time

The shear strength of the stabilized soil gradually increases with time through pozzolanic reactions when the lime reacts with the silicates and aluminates in the soil (Broms, 1984). The rate of increase is generally rapid at the early stage of curing time; thereafter, the rate of increase in strength decreases with time. Lime has an initial reaction with soil taking place during the first 48-72 hours after mixing, and a secondary reaction which starts after this period and continues indefinitely (Taylor and Arman, 1960).

Several attempts have been made to express the strength of lime stabilized soils as a function of curing time. Broms (1984) found that the shear strength of stabilized soil as determined by unconfined compression tests increased linearly with time when plotted in log-log scale (log c_u, log t). Brandl (1981) and Okamura and Terashi (1975), however, found that the time-dependent increase in shear strength was approximately linear with the logarithm of time.

(iv) Type of Soil

For lime treatment to be successful, the clay content of the soil should not be less than 20% and the sum of the silt and clay fractions should preferably exceed 35%, which is normally the case when the plasticity index of the soil is larger than 10 (Broms, 1984). The shear strength increase of the stabilized soil is highly dependent on pozzolanic reactions, i.e., the reactions of lime with silicates and aluminates in the soil.

(v) Clay Mineral

Eades and Grim (1966) reported that the quantity of lime needed to effectively treat clay is dependant on the type of clay mineral present. They observed that although kaolinites, illites, montmorillonites and other mixed-layered clays all react with lime to give greater strengths, the quantity of lime needed to treat clay is dependent on the type of mineral present. Hilt and Davidson (1960) found that from the unconfirmed compression test results, kaolinitic and montmorillonitic clayey soils are effectively stabilized with lime alone, whereas illitic clays require addition of flyash to obtain a significant strength gain.

2.13.9 Previous Laboratory Studies of Lime Stabilisation

2.13.9.1 Lime Stabilization of Soft Bangkok Clay

Bangkok clay is well known for its low strength and high compressibility. In this region, there are extensive deposits of soft marine clay which encounter problems in settlement and stability. The sub-soil conditions in the Bangkok area are typical of deltaic plains. The geotechnical problems encountered there are often associated with the presence of a relatively thick layer of soft clay (about 10 metres) with low strength and high compressibility. Various ground improvement techniques are increasingly properties of the soil and to minimize the settlement to within the tolerable values.

Extensively laboratory studies on the use of lime stabilized columns have been carried out at the Asian Institute of Technology (Balasubramaniam et al. 1988, 1989). Addition

of 5 to 10% quicklime is the optimum mix proportion for the soft Bangkok clay. The addition of quicklime increased the unconfined compressive strength to about 5 times and increased the pre-consolidation by as much as 3 times. The vertical coefficient of consolidation also increased by 10 to 40 times and the effective strength parameters also increased, especially the angle of internal friction from 24° to 40°.

2.13.9.2 Strength Characteristic of Lime-Treated Clay Minerals

Bell (1996) investigated the strength and deformation characteristic of lime treated minerals in clay deposits, namely, kaolinite, montmorillonite and quartz. The study investigates the amount of strength increase in a clay soil that can be produced by adding lime is dependent on the pozzolans present. When the desirable pozzolans are available, they react readily with lime to improve the strength of soil-lime mixtures. Nonetheless it would appear that the absolute amount of silica or alumina required to sustain pozzolanic reaction in soils is relatively small. Hence clays generally show a significant increase in strength when lime is used for stabilization.

Expansive clays respond more quickly to strength increase. For instance, montmorillonite showed a rapid initial increase in unconfined compressive strength with small additions of lime (Figure 2.47).

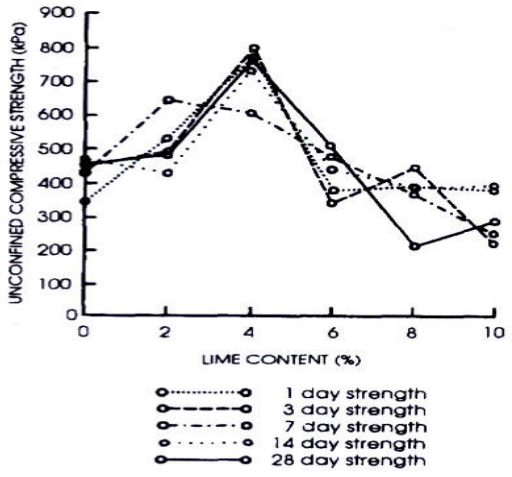

Figure 2.47 Unconfined compressive strength of montmorillonite with various additions of lime (Bell, 1996)

Its lime strength optimum was around 4% compared with that of kaolinite which varied between 4 and 6%, whilst that of quartz ranged between 4 and 8%. The addition of small amounts of lime to kaolinite and quartz also give rise to notable increase in unconfined compressive strength. Furthermore, montmorillonite mixed with a low lime content attained maximum strength in less time than one to which a higher content of lime had been added. Indeed strength does not increase linearly with lime content, and excessive addition of lime reduces strength. This is due to the fact that lime itself has neither appreciable friction nor cohesion.

2.13.10 Lime - Column Method

Cylindrical column can be formed in clay soils by mixing the clay with lime. This increases the permeability of the columns to between 100 and 1000 times greater than that of the surrounding clay (Broms and Boman, 1975). Hence the lime columns act as vertical drains, as well as reinforcing the soil. One lime column of 500mm diameter has the same drainage capacity as three 100 mm wide band drains. One of the advantages of lime column is that their installation creates little disturbance in the surrounding soil, which enhances their performance as a drain.

Lime columns are used extensively in Sweden, Norway and Finland for the following purposes.

i. To improve the total and differential settlements of light structures (one- to two- storey buildings).

ii. To increase the settlement rate and control the settlements of relatively heavy structures.

iii. To improve the stability of embankments, slopes, trenches and deep cuts.

iv. To reduce the vibrations from, for example, traffic, blasting, pile driving,etc.

Both the total and the differential settlements can be controlled with lime columns as discussed by Holm (1999). The settlements will be small as long as the axial load in the columns is less than the creep limit. With concrete or steel piles the total weight of the building has to be considered to control the settlements. The lime column method is therefore often an economical alternative to piles and floating foundations especially for light structures even when the thickness of the compressible strata below the structure is large.

For road embankments and dykes constructed on soft clay, the lime column method is often an economical alternative to sand or band drains. The spacing of the lime column can be relatively large diameter (0.5-0.6) and the relatively small disturbance of the soil caused by the installation of the columns. The consolidation time is reduced further by the reduction of the compressibility of the soil by the columns.

2.14 Concluding Remarks

In Southeast Queensland, many road embankments are constructed on soft estuarine clays (or marine clay) of low strength and high compressibility. Structures built on these sites are subject to damage from differential settlement. Pre-loading in combination with prefabricated vertical drains and stone columns and deep mixing methods are all examples of soil improvement techniques.

In this chapter, typical characteristics of clay deposits have been introduced. Geological and geotechnical descriptions of Southeast Queensland soft estuarine clays have been provided, in addition to geological maps detailing the distribution of these clay deposits throughout the region.

Application and analysis of vertical drains are presented. Vertical drains have been widely used to accelerate the rate of primary consolidation. However, it is difficult to predict the settlements and pore pressures accurately due to the complexity of estimating the correct values of soil parameters inside and outside smear zone.

Stone column applications and assessment methods are also discussed. Fundamental concepts of cement-soil stabilisation have been detailed, including: cement and lime chemistry; cement-soil and lime-soil interactions; mechanisms of hardening; and, controlling factors in hardening. Previous laboratory studies were summarised and relevant test data presented for research conducted in Southeast Asia, USA, and Scandinavia.

Generic construction implications of soft clay foundations have been discussed, as have the general principles of ground improvement. The multitude of available ground improvement options have been reviewed, encompassing densification, replacement, reinforcement and solidification techniques.

CHAPTER 3

METHODOLOGY AND THEORETICAL CONSIDERATIONS

3.1 Introduction

To achieve the objective of analysing field behaviour of motorway embankments, a systematic procedure taken:

i. Collection of field monitoring data

ii. Practical approaches to analysis the field data

iii. Numerical modelling of the case studies

Field Deformation Analysis (FDA) is a practical method, which can quantify the settlement components of an embankment foundation during loading and consolidation stages. The common soil parameters such as undrained shear strength and the coefficient of consolidation could be back calculated by achieving the monitoring data from full-scale trial embankments. The methods adopted for back-calculating the related soil parameters from full-scale tests are described in the subsequent sections. These methods are easy to use in practice. The prediction of the maximum settlement, excess pore pressures and the lateral displacements by FEM analysis are also illustrated.

3.2 Field Deformation Analysis (FDA)

3.2.1 General

Loganathan (1992) has proposed the field deformation analysis (FDA) method to quantify the settlement components of an embankment foundation. Normally, the following four settlement components are involved.

a) Loading Stage

   Immediate settlement

   Consolidation settlement

b) Consolidation Stage

Consolidation settlement

Creep settlement

During and after embankment loading, the actual settlement mechanism and the embankment behaviour can be predicted accurately by computing these settlement components. In this study, however, only the total settlement in the consolidation stage will be considered. The immediate settlement is neglected, as the width of the embankment is higher than the thickness of the soft compressible layer.

3.2.2 General Theoretical Background

From the vertical and lateral deformation characteristics of soft soil foundations subjected to embankment loading, properties of soft soil, drainage conditions and method of construction, the basis of this method has been derived. Considerable volume change in the clays below an embankment occur according to the magnitude of the applied surcharge and the duration of the consolidation time. In embankment foundations, with time the settlement and lateral displacements are associated with volume change, which takes place vertically and laterally. The undrained settlement takes place without any volume change, and thus the volume of soil displaced by vertical settlement is the same as the volume generated by lateral movement. During the consolidation stage, the vertical and lateral volume changes vary in different manner with the dissipation of the pore pressure. By using concept of volume changes, the settlement components can be separated for both loading and consolidation stages.

3.3 Graphical Evaluation of Settlement Records (Asaoka's Method)

Asaoka (1978) suggested a graphical procedure as one possible way to solve the recurrence relation. The usefulness of this procedure has been results appear to have

been obtained with settlement records of test embankments on soft clay deposits (Magnan and Mieussens, 1980; Magna and Deroy, 1980).

The steps in the graphical procedure used by Magnan and Mieussens (1980) are as follow:

1) The observed time-settlement curve plotted to an arithmetic scale is divided into equal time intervals, Δt, (usually Δt is between 30 and 100 days). The settlements S_1, S_2, … corresponding to the times t_1, t_2, … are read off and tabulated

2) The settlement values S_1, S_2, … are plotted as points (S_{i-1}, S_i) in a coordinate system with axes $S_{i-1}$and S_i, as shown in Figure 3.1. the 45^o line $S_i = S_{i-1}$ is also drawn.

3) A strength line (l) is fitted through the points. The point where this line intersects the 45^o line gives the final consolidation settlement, S_{100}. The slope β_1 is related to the coefficient of consolidation, c_v, by:

$$c_v = \frac{5}{12} h^2 \frac{ln\,\beta_1}{\Delta t} \tag{3.1}$$

and therefore indicates the rate of settlement. The slope, β1, depends on the time steps, Δt, selected and decreases when Δt increases

In some cases, it occurs that the data points are better fitted by two straight lines (I) and (II), as shown in Figure 3.2. The second straight line, (II), corresponds to the tail of the settlement curve, and thus represents secondary compression. In the case of multi-stage loading, a straight line corresponding to each loading stage can be fitted. If the time between the load increments is large, a secondary compression line can also be drawn. Figure 3.2 shows a case of a load applied in three stages with secondary compression at

the end of the third stage. In some rare cases, according to Magnan and Deroy (1980), it is difficult to define a straight line through the points.

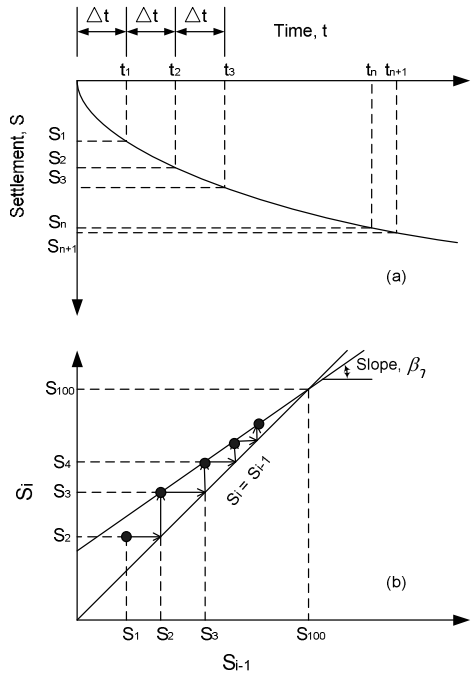

Figure 3.1 Asaoka's Method: (a) partition of settlement record into equal time intervals, (b) plot of settlement values and fitting of straight line (Magnan and Deroy, 1980)

3.4 Consolidation with vertical drains

Barron (1948) presented the first exhaustive theory to describe the consolidation phenomenon with vertical drains. In the case of equal strain, the differential equation governing consolidation is

$$\frac{\partial u}{\partial t} = c_h \left[\left(\frac{\partial^2 u}{\partial r^2} \right) + \frac{1}{r} \left(\frac{\partial u}{\partial r} \right) \right] \tag{3.2}$$

where u is the average excess pore pressure at any point and at any given time. r is the radial distance of the considered point from the centre of the drained soil cylinder; t is the time after an instantaneous increment in the vertical stress and c_h is the coefficient of horizontal consolidation.

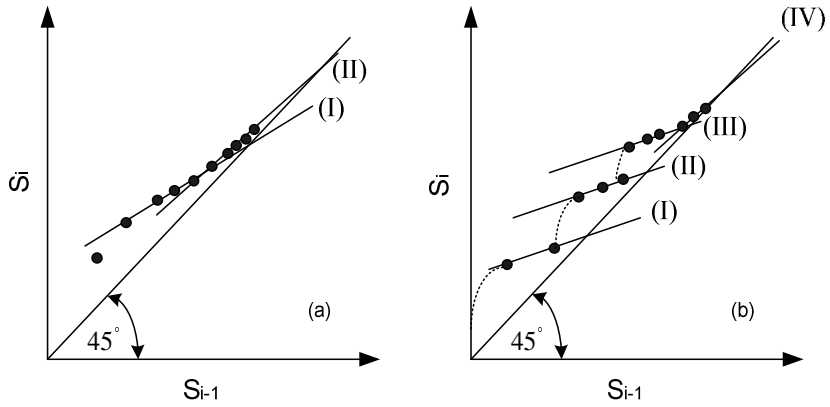

Figure 3.2 (a) Asaoka's Method for Single-stage Loading and Secondary Compression (b) Asaoka's Method for Multi-stage Loading and Secondary Compression occurring at the end of the third loading (Magnan and Deroy, 1980)

For the case of radial drainage only, the solution of Barron under ideal conditions with no smear and no well resistance is as follows:

$$U_h = 1 - exp\left(\frac{-8T_h}{F(n)}\right) \tag{3.3}$$

where

$$T_h = \frac{c_h}{D_e} \tag{3.4}$$

$$F(n) = \left(\frac{n^2}{1-n}\right)\left(n(n) - \frac{3}{4} + \frac{1}{n^2}\right) \tag{3.5}$$

D_e is the diameter of the equivalent cylinder, and d_w is the equivalent diameter of the drain, and n is the spacing ratio given as

$$n = \frac{D_e}{d_w} \tag{3.6}$$

Hansbo (1979) modified the equations developed by Barron for PVD applications. The modifications catered for the physical dimensions and the PVD characteristics and the effect of their installation. The modified expression for average degree of consolidation is given as

$$U_h = 1 - exp\left(\frac{-8T_h}{F}\right) \tag{3.7}$$

and

$$F = F(n) + F_s + F_r \tag{3.8}$$

where F is the factor that governs the cumulative effect due to the spacing of the drains, $F(n)$; for the smear effect, F_s; and well resistance, F_r. For spacing ratios n in the range of 20 or more the factor $F(n)$ simplifies to:

$$F(n) = ln\left(\frac{D_e}{d_w}\right) - \frac{3}{4} \tag{3.9}$$

To account for the effects of soil disturbance during installation of drains, a zone of disturbance with a reduced permeability is assumed in the vicinity of the drains. The smear effect factor is given as:

$$F_s = \left(\frac{k_h}{k_s} - 1\right) ln\left[\frac{d_s}{d_w}\right] \tag{3.10}$$

d_s is the diameter of the smeared zone around the drain; and k_h is the coefficient of permeability in the horizontal direction in the disturbed zone. Since the PVD have limited discharge capacities, Hansbo (1979) developed a drain resistance factor, F_r, assuming that Darcy's Law can be applied for flow along the vertical axis of the drain. The well-resistance factor is given as:

$$F_r = \pi z(l - z)\frac{k_h}{q_w} \tag{3.11}$$

z is the distance from the drainage end of the drain; l is twice the length of the drain, when drainage occurs at one end only; l is equal to the length of the drain when drainage occurs at both ends; k_h is the coefficient of permeability in the horizontal direction in the undisturbed soil; and q_w is the discharge capacity of the drain at a hydraulic gradient of one. Incorporating the effects of smear and well resistance, the

time t, to obtain a given degree of consolidation at an assumed spacing of PVD, is given as follows:

$$t = \left(\frac{D_e^2}{8c_h}\right)\left(F(n) + F_s + F_r\right) ln\left(\frac{1}{1-U_h}\right) \tag{3.12}$$

3.4.1 Drain Properties

The theory of consolidation with radial drainage assumes that the soil is drained by vertical drains with circular cross section. The equivalent diameter of a band shaped drain is defined as the diameter of a circular drain, which has the same theoretical radial drainage performance as the band-shaped drain. Subsequent studies of Rixner *et al*. (1986) supported by Hansbo (1979) says that the equivalent diameter preferable is

$$d_w = \frac{a+b}{2} \tag{3.13}$$

The discharge capacities of prefabricated drains are required to analyse the drain resistance factor and is usually obtained from the published results reported by the manufacturers.

3.4.2 Drain Influence Zone

The time to achieve a given percentage of consolidation is a function of the square of the equivalent diameter of soil cylinder, D_e. This variable is controllable, since it is a function of the drain spacing and pattern. Vertical drains are usually installed in square or triangular patterns .The spacing between the drains establishes D_e through the following relationships:

$$D_e = 1.13s \text{ ; (Square pattern)} \tag{3.14}$$

$$D_e = 1.06s \text{ ; (Triangular pattern)} \tag{3.15}$$

The square pattern has the advantage for easier layout and control. A square pattern is usually preferred. However, the triangular pattern provides more uniform consolidation between drains.

3.4.3 Well Resistance

Hansbo (1979) presented for equal-strain conditions, a closed –form solution which allows for ready computation of the effects of well resistance on drain performance. The finite drain permeability was considered by imposing the continuity equation of flow toward the drain. In this assumption, the flow rate in the considered section of the drain is equal to the maximum flow rate, which can be discharged through the drain. The discharge capacity of band drains varies considerably depending on the make of the drain and decreases with increasing lateral pressure. This is caused by either the squeezing in of the filter sleeve into the core channels, reducing the cross-sectional area of the channels or, for drains without a filter; the channels themselves are squeezed together.

Another important factor is the folding of the drain when subjected to large vertical strains. In this case the channels of flow would be reduced, thus reducing the discharge capacity. The sedimentation of fine particles in the flow channels may also decrease the discharge capacity. The introduction of the well resistance concept affects the value of the degree of consolidation, U_h, which is no longer constant with depth. Taking well resistance into consideration, the rate of radial consolidation is controlled not only by c_h and D_e but also by the ratio q_w / k_h. This factor may play a very important role when pre-fabricated vertical drains of great lengths are used; q_w / k_h is less than 500 m^2 ,when the time required to a specific degree of consolidation is increased. The influence of well resistance on the consolidation rate increases, when the drain length increases.

3.4.4 Smear effects and disturbance

The installation of drains results in the disturbance of the soil surrounding. The extent of disturbance depends on the mandrel size and shape, the soil macro-fabric and the installation procedure. To reduce the disturbance the mandrel cross-section should be

minimized and additional stiffness be provided. The diameter of the disturbed zone is given by

$$d_s = \frac{5d_m \text{ to } 6d_m}{2} \tag{3.16}$$

where d_m is the diameter of the circle with an equal area to the cross-sectional area of the mandrel. Hansbo (1979) recommended

$$d_s = 2d_m \tag{3.17}$$

3.4.5 Ratio of Permeabilities

For soils with pronounced macro-fabric, the permeability ratio (k_h / k_v) can be very high and even reach a value of ten. This greater vale of the horizontal permeability can be reduced or eliminated by the smear effects. Thus in the smeared zone the permeability can be taken as the vertical permeability value.

3.4.6 Coefficient of Radial Consolidation

The coefficient of radial consolidation can be evaluated from c_v values using the relation,

$$c_h = \left(\frac{k_h}{k_v}\right) c_v \tag{3.18}$$

3.4.7 Parameter Effects on Consolidation Time

With smear effects, the time for a given degree of consolidation is given by

$$t = \frac{D_e}{8c_h}\left[ln\left(\frac{D_e}{d_w}\right) - \frac{3}{4}\right] + \left(\frac{k_h}{k_s} - 1\right) ln\left(\frac{d_s}{d_w}\right) ln\left(\frac{1}{1-U_h}\right) \tag{3.19}$$

The value of c_h, which can vary by a factor of 10, has the most dominant effect on t. D_e can vary by a factor of about 2 to 3. It reflects the influence of the drain spacing. The effects of the properties of disturbed zones (k_s and d_s) can also be significant. The equivalent diameter of the drain, d_w, has only a minimal influence.

3.4.8 Rate of Consolidation

The principal objective of pre-loading with vertical drains is to achieve the desired degree of consolidation within a specified period of time. Both horizontal and vertical drainage takes place in the dissipation of the excess pore pressure and the resulting consolidation can be expressed as

$$U = 1 - (1 - U_h)(1 - U_v) \tag{3.20}$$

U_h average degree of consolidation in the horizontal direction and, U_v , the corresponding value in the vertical direction.

3.5 Back-calculation of c_h Values from Pore Pressure Measurements

From Hansbo (1979) equation, the following equation can be derived for the consolidation with prefabricated vertical drains (PVD).

$$1 - \frac{\Delta u_t}{\Delta u_0} = 1 - exp(-\alpha t) \tag{3.21}$$

$$\alpha = \frac{8 c_h}{D_e} \tag{3.22}$$

where, Δu_0 is the excess pore pressure at reference time ($t = 0$); Δu_t is the excess pore pressure at reference time t; D_e is the effective diameter of unit drain; α is the resistance factor for the effects of spacing, smear and well resistance (as explained earlier in Equation 3.8)

From Equation 3.20;

$$ln\left(\frac{\Delta u_0}{\Delta u_t}\right) = \alpha t \tag{3.23}$$

The values of α were therefore obtained as the slopes of the plot of $ln(\Delta u_0 / \Delta u_t)$ vs time. Knowing the value of α , c_h can be computed from Equation 3.22.

3.6 Finite Element Analysis

At present, there are many finite element codes that can be used in the analyses of embankments on soft ground. Of those, two programs namely: CRISP (developed originally at Cambridge University) and PLAXIS (Brinkgreve, 2002) have been employed generally, in the analysis of embankments on soft ground (Indraratna *et al*., 1994; Bergado *et al*., 2000; Bergado *et al*., 2002; Bergado *et al*., 2003; Tan and Kei, 2004). The PLAXIS finite element program was employed in this study.

Due to the fact that there is no field instrumentation in Section C, comparisons of the finite element analysis with the observed data are only made for Section A (with 1m triangular PVD spacing) and Section B (without PVD).

3.6.1 Model Generation in FEM Analysis and Input Parameters

As a result of the non-symmetry in the test embankment, full-scale geometry models were generated according to the actual trial embankment dimensions. For the model of Section A, the installed PVD were modelled using drains option provided in the PLAXIS manual. The drain option is normally used to prescribe lines inside the geometry model where excess pore pressures are set to zero.

The soil parts were modelled using 15-node triangular elements. The soil-soil shear surface and the soil-geotextile interfaces were considered by using 10-node interface elements. The boundary condition was assumed using standard fixity, which means a full fixity at the base of the geometry, and, roller conditions at the vertical sides. The Mohr-Coulomb's elastic perfectly plastic model was used for both back fill soil and the silty sand layer. The soft silty clay layer was modelled using soft soil model.

After the soil parameters were input, a simple finite element mesh was generated using the medium coarse setting.

According to the observations from the site investigation, the ground water level represented semi-permanent surface water in the area where the trial embankment was constructed. The ground water level in the PLAXIS analysis, therefore, was assumed to coincide with the ground surface. During the calculation process, all the boundaries are assumed as free draining so that the water can freely flow out of the all boundaries and the excess pore pressures can dissipate in all directions. In the current situation, however, both vertical boundaries of upper and lower soft silty clay layers were assumed to be closed because there is no free out flow at those boundaries.

3.6.2 Calculation Process

The calculation process in PLAXIS was divided in to 2 stages; calculation during the embankment construction (Stage 1) and the calculation after the end of construction (Stage 2). In the former calculation, the plastic calculation was adopted. The latter was calculated using consolidation analysis. In fact, during the embankment construction, consolidation settlement does occur. However, the construction time is short (approximately 65 days), and therefore the consolidation settlement during this time was assumed to be negligible. In stage 2 calculation, the progress of consolidation was modelled taking into consideration the development and dissipation of excess pore pressures.

3.7 Total Stress Analysis

The total stress analysis ($\phi_u = 0$) is used to find the factor of safety at the end of construction. The shear strength introduced in the stability calculation is thus the in-situ undrained shear strength of the clay, which existed prior to construction. For the analysis of embankment construction, the shear strength increases with time due to the dissipation of pore pressure after construction. As a result of this, the total stress analysis at the end of construction will be the most critical.

3.8 Safety Analysis (Phi-c Reduction) from PLAXIS

Phi-c reduction is an option available in PLAXIS to compute safety factors. The Phi-c reduction approach resembles the method of calculating safety factors as conventionally adopted in slip-circle analyses. In the Phi-c reduction approach the strength parameter $\tan\phi$ and c of the soil are successively reduced until failure of the structure occurs. The total multiplier ΣMsf is used to define the value of the soil strength parameters at the given stage in the analysis:

$$\sum Msf = \frac{\tan\phi_{input}}{\tan\phi_{reduced}} = \frac{c_{input}}{c_{reduced}} \tag{3.24}$$

where the strength parameters with the subscript input refer to the properties entered in the material sets and parameters with the subscript reduced refer to the reduced values used in the analysis. In contrast to other total multipliers, ΣMsf is set to 1.0 at the start of a calculation to set all material strengths to their unreduced values. The strength parameters are successively reduced automatically until failure of the structure occurs. At this point the factor of safety is given by:

$$SF = \frac{available\ strength}{strength\ at\ failure} = value\ of\ \sum Msf\ at\ failure \tag{3.25}$$

If a failure mechanism has not developed, then the calculation must be repeated with a larger number of addition steps.

CHAPTER 4

CASE STUDY 1: SUNSHINE MOTORWAY EMBANKMENT - ANALYSIS OF LABORATORY AND FIELD TEST DATA

4.1 Introduction

The Sunshine Motorway (Stage 2) Area 2 is a 4.7 km motorway which was subdivided into Area 2A (Ch28300 – Ch 29050) and Area 2B (Ch29050 – Ch33000). It extends north from Area 1 through cane farm lowlands with a minor swampy section adjacent to the Maroochy River before intersecting a terrain of higher relief to the South of West Coolum Road. The route then re-enters another small swampy area and further holding on South Coolum Road. Area 2 terminates approximately 1.5 km South of the Yandina-Coolum Road.

Due to the existence of soft sensitive marine clays in Area 2, the three sections –test embankment was required to ensure the satisfactory evolution of the design and construction procedures. To accelerate settlements and to improve the embankment stability prefabricated vertical drains (PVD), and, additional tensile strength as obtained from geogrids were incorporated in the fill material.

4.2 Project Description and Soil Conditions

4.2.1 Project Description

Along the adopted alignment, the Area 2A of Sunshine Motorway (Stage 2) has the deepest soft clay layers when compared to other areas. Thus, this area was later on being considered as an area for the test embankment. As can be seen from the Sunshine Motorway longitudinal profile (see Figure 4.1), the area 2A from Ch 28300 to Ch29050 show the deepest depth of soft clay extending to approximately 16.5m depth. In this area totally, 33 boreholes were drilled with depths ranging from 1.7 to 30 m. Besides the test embankment the other field tests included standard penetration tests (SPT),

electric static friction cone penetration tests, standard bridge probes, field shear vanes and seismic surveys.

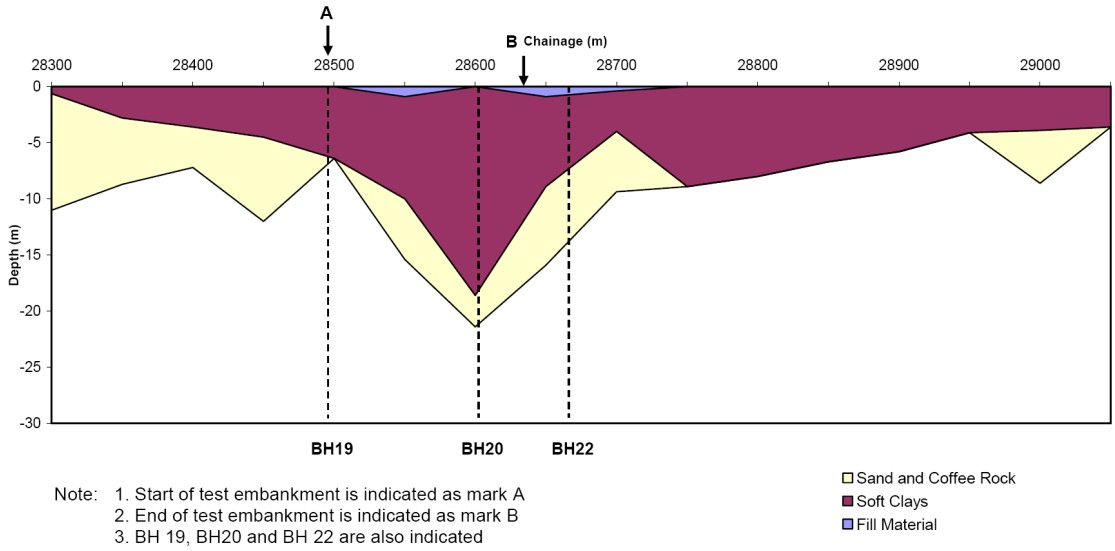

Figure 4.1 Sunshine Motorway Stage 2, Area 2 (Longitudinal Profile)

The soil strata can be classified into several layers. Field-testing has indicated a substantial deposit of vary soft, compressible organic silty clay between 4 and 10 m in thickness. This material is underlain by a very loose silty sand layer approximately 2 m in thickness. This in turn is underlain by moderately dense to dense sand (coffee rock) strata 4 – 6 m in thickness. Below these beds further loose to dense silty sands, sand and soft clay were intersected to a depth of at least 30 m.

Some variation to the sequence is possible between Ch28550 and Ch28650 where in BH20 the moderately dense to dense sand (coffee rock) layer was not found below the very soft silty clay.

4.2.2 Characteristics of the Bulk Earthworks

The bulk densities recorded from undisturbed tube samples averaged 19.9 kN/m^3 with a maximum value of 20.8 kN/m^3.

4.2.3 Ground Water

Ground water level observed during the investigation indicated the presence of semi-permanent surface water at the two swamp locations, including Ch28450 to Ch28650 (the area of test embankment) and Ch30350 to Ch30600. Elsewhere, the low lying areas of alluvium are seasonally wet above the organic hard pan (coffee rock) with water within 1m of the ground surface.

4.3 Summary of Test Embankment Design Philosophy

The particular features of the test embankment, which should be noted, are:

- 200 kN/m Tensile Strength Geogrid used throughout
- Section A and B in Figure 4.2(a) each 35m in length are the prime sections representing the design vertical drain spacing (1m of triangular pattern) and no drains respectively.
- Section C in Figure 4.2(a) (20m in length) representing an intermediate case with 2m triangular pattern drain spacing and less instruments
- Half cross-sections intensively instrumented to capture relevant data
- Design berm width of 5m on the instrumented side and 8m on the opposite side to force failure in the requisite direction
- Ends of the trial embankment designed and shaped to avoid end failure
- Instrumentation of reinforcement to directly determine forces and strains
- Careful location of instruments to capture critical data on foundation performance

Figure 4.2(a) illustrates the plan dimensions of the trial embankment.

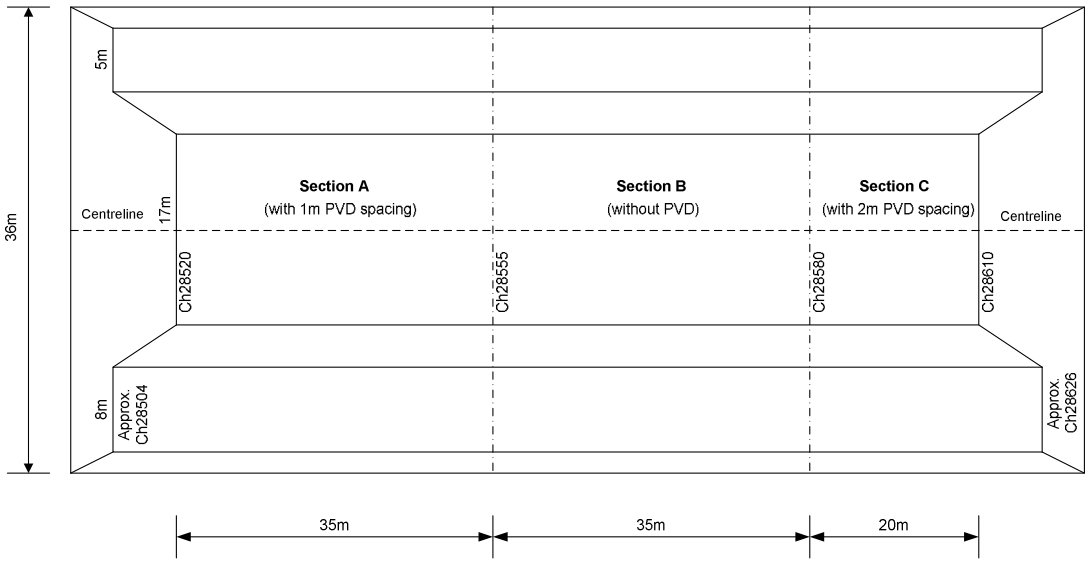

Figure 4.2(a) Locations and Dimensions of Test Embankment with Section A (with 1m PVD spacing), Section B (without PVD) and Section C (with 2m PVD spacing)

4.4 Scope of Instrumentation

The instrumentation layout has been designed to capture critical information regarding both the settlement and stability of the clay subsoils, the in-situ behaviour of the geogrid and the vertical pressures applied by the embankment trial loading. The location of field instrumentation is illustrated in Figures 4.12 to 4.14 for trial embankment sections A, B and C, respectively. The total numbers of instruments located in each section are detailed in Table 4.1. A brief description of the purpose of each type of instrument is given in section 4.4.1 – 4.4.4.

Table 4.1 Details of Instrumentation in Test Embankment

Instrument Type	***Section A***	***Section B***	***Section C***	***Total***
	Number of Instrumentation			
Inclinometer (I)	2	2	1	5
Horizontal Profile Gauge (HPG)	1	1	0	2
Sondex Settlement System (ME)	3	3	1	7
Piezometer 1 Standpipe (PS)	1	1	1	3
2 Vibrating Wire (PV)	11	11	6	18
3 Pneumatic (PP)	6	6	3	15

4.4.1 Inclinometers (I)

Inclinometers were located in the centre of the batter slope in section A and B and at the toe of the berm in section A, B and C to determine the extent of lateral ground

movements. The inclinometer equipment consisted of UPVC tubing (GSA Type 7010) with inner longitudinal tracks, which guided a torpedo type unit down the length of the tubing, thereby sensing the inclination in two planes at right angles to each other, at a reading interval of 0.5m. This inclinometer is displayed in terms of horizontal displacement on electronic readout equipment at ground level. The inner tracks of the tubing were positioned to run along centreline and comparing these profiles the horizontal displacement of the tube over a period of time has been determined.

The general method of installation entailed the drilling of a borehole of 114mm diameter (HW casing) through the soft soil strata into stable ground (at least 3.0m), which served to anchor the base of the tube. The overall design depth of installation was approx. 21.0m.

The borehole was backfilled with a weak cement/bentonite grout and the tubing lengths (3.0m) were coupled independently while being lowered down the borehole. Both tubes were filled with clean water during this procedure to counteract the buoyancy effect of the tubing. Even with both tubes full of water, a reasonable force was required to push the tubing down the borehole. Top caps were placed on both tubes and the HW casing removed.

As the layers of fill material were placed, hand compaction around the tubing was performed.

4.4.2 Horizontal Profile Gauges (HPG)

The horizontal profile gauge (HPG) comprises UPVC tubing of larger diameter but similar longitudinal tracking to that of inclinometer tubing, expansion joints and a dead end pulley assembly with a wire cable to pull the torpedo or Sondex inductance probe through the tubing.

This provides data for determining the profile of vertical settlement across the full width of the embankment and also lateral strains (see Figure 4.2(b)) at the top of soft clay foundation by the addition of the Sondex sensing ring.

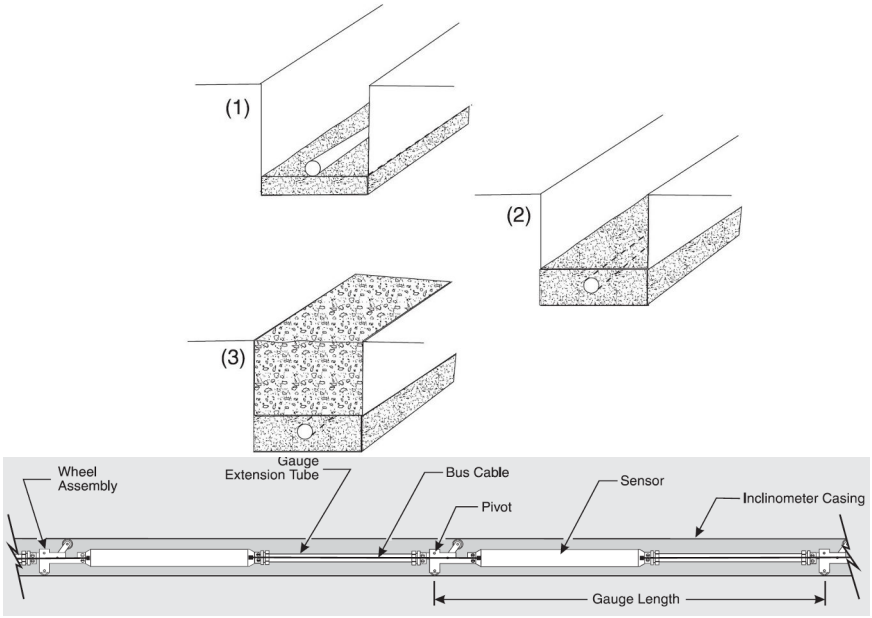

Figure 4.2(b) Sketch of Horizontal Profile Gauge (Slope Indicator, 2004)

The tubing, the dead end pulley and the return wire cable conduit were assembled on site and the 3m lengths of tubing coupled together. After that, the sensing rings were placed at approximately 3m intervals along the entire length of the tubing. Two expansion joints were placed at nominally 9.0m from each end to allow for lateral movements. A trench was prepared by a mini excavator to a depth of approximately 0.5m below the natural ground surface along the full width of the embankment and the tubing manhandled into position. Ideally sand or a similar type of bedding material should have been placed over the tubing whilst back filling, however due to the difficult nature of the site and the trench being inundated with water the trench was back filled with only the naturally excavated material. The dead end pulley assembly was buried on the eastern side of embankment and the open (access) end gradually rose out of the ground at the readout pulling back at 0.5m intervals and the data recorded on electronic readout equipment.

4.4.3 Sondex System

4.4.3.1 General

The Sondex system (see Figure 4.2(c)) is designed to measure differential movements between various locations. The system comprises 1) flexible corrugated pipe with stainless steel sensing rings at designated intervals; 2) UPVC, inclinometer or horizontal profile tubing to act as access for the probe; 3) an inductance probe which has a 35m cable and steel marking tape graduated in millimetres connected to an integral readout unit.

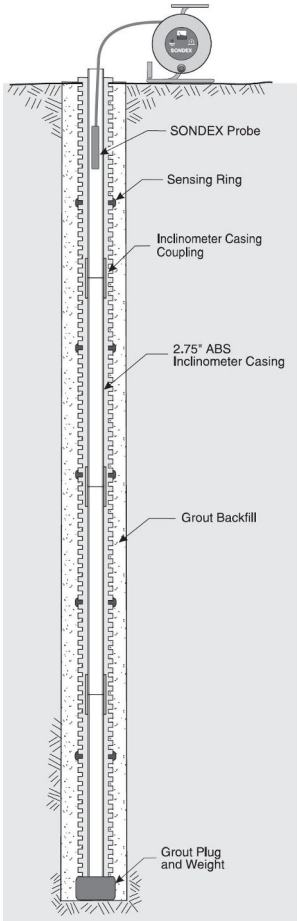

Figure 4.2(c) Sketch of Sondex System (Slope Indicator, 2004)

4.4.3.2 Vertical Settlements

Settlement of the surrounding ground causes compression of the corrugated pipe, which alters the levels of the sensing rings. The probe locates the position of the sensing rings relative to the lower most ring, which is assumed to be in a fixed position. To take

readings, the probe is lowered to the base of the tubing and raised slowly. The unit sounds a buzzer when passing through a sensing ring and the depth is noted on the steel marking tape. The installation procedure is similar to the inclinometer installation, as described in section 4.4.1. The access tube at the centre of the embankment consisted of a rigid UPVC tube, while at the edge of the embankment the inclinometer tubing was used. The access tube was fixed to the corrugated pipe at the base prior to installation.

4.4.3.3 Lateral Displacements

Lateral displacement of the surrounding ground causes movement of the corrugated pipe, which alters the location of the sensing rings. The probe locates the position of the sensing rings relative to the end of the tubing. The sensing rings were installed in conjunction with the Horizontal Profile Gauges (HPG). To take readings the probe is pulled through the horizontal profile tubing and slowly pulled back. The mechanism for this process is similar to reading the HPG. The unit sounds a buzzer when passed through a sensing ring and the horizontal location is noted on the steel marking tape.

4.4.4 Piezometers

4.4.4.1 Standard type

The standpipe piezometer is comprised of a UPVC tip 345mm in length with a number of uniform pore holes covering a 75-micron filter element. This is attached to 25mm UPVC tubing and positioned to the design depth. Measurement of water depths is taken by the use of a dipmeter unit while the RL of the top of the tubing is obtained by precise levelling relative to the PSM. Typical installation methods would normally require an appropriate grout, however due to the soft nature of the soil the standpipe was manually covered with a sand filled geotexile bag. Ground water levels at each section were determined from these units.

4.4.4.2 Vibrating Wire Type (PV)

The vibrating wire piezometers were GEOKON type 4500s, equipped with 50 micron sintered stainless steel fitters, prior to installation; the piezometers were de-aired by assembling the filters under water. Each piezometer was placed inside sand filled bag, manufactured from geotextile material typically used as a drainage membrane, such that the filter faced upwards. This ensured that gases did not get trapped inside the piezometer during installation and over the longer term due to organic or natural gases. Boreholes for installation of piezometers were of 89mm diameter (NW) and advanced to the required depth by wash boring with casing. Piezometers were placed in position and typical procedures for grouting the hole were employed. Accurate installation depths were determined.

The cables from the piezometers were located in trenches within the working platform and covered with 7mm screenings, and routed to the readout station adjacent to section B.

4.4.4.3 Pneumatic Type (PP)

The pneumatic piezometers were SINCO 5/8" diameter, equipped with 50 micron sintered stainless steel filters. Prior to installation, the piezometers were de-aired immersing the piezometer in water, with the filter facing upwards, for a period of 30 minutes. The installation procedure used was the same as for the vibrating wire piezometer. A readout station was set up adjacent to each section.

4.5 Construction Activities

4.5.1 Installation of Vertical Drains

Vertical drains were installed with a crawler-mounted machine from the working platform at approximately RL 1.0. The layout of the drains and the drain depths for Section A are in the range of 9 – 11m. In section C, it is understood that the drains were

driven the full length of the mandrel (11.0m) without encountering refusal. However, it is also understood that increased resistance was observed during the lower levels of drain installation on many of the drains indicating the presence of the underlying sand layer.

4.5.2 Installation of Reinforcement

Tensar ER200 is produced in roll lengths of approximately 60mm length x 1m widths. The rolls were laid out transversely to the alignment and cut such that 1 roll would provide two passes viz. the length of the grid in x-section was 30m, extending 15m from CL.

Simple manual attempts at tensioning the grid were made followed by pinning at the extremities to maintain tension. These procedures met with minimal success since the grid was not true in its longitudinal alignment, and would relax in sunlight due to thermal expansion. Adjacent edges of geogrid were tie-wired in an attempt to create a stable mass.

Tensioning was abandoned even though it was considered advantageous to the performance of the grid. In the absence of more effective tensioning, the decision to use 7mm screenings to cover the geogrid is considered important to the successful function of the grid.

4.5.3 Coverage of Geogrid

Prior to the placement of the earthworks proper, the geogrid was covered with a thin layer of 7mm screenings. This material was selected since is was considered that it would provide good interlock as well as being small enough to pass through the grid apertures and hence potentially fill any underlying voids. Generally, it is considered that the screenings served the purpose.

4.5.4 General Earth Works

Following the covering of the geogrid, earthworks were placed full width and in full-length runs in layers of 200-300mm thickness. The construction sequence of the trial embankment and the monitoring dates and earthworks placement history from the first date of earthworks until the date of earthworks completion is tabulated in Table 4.2. During the course of construction it was realized that the berm heights were effectively 1m above the prepared ground level of approximately RL 0.4. This compares with the design intent, which required 1.25m height berms above undisturbed natural surface level of approximately RL 0.55.

Table 4.2 Embankment Construction History

Date	**Approximate Embankment RL on CL**			**Comments**
	Section A	**Section B**	**Section C**	
14/4/92	1.0	1.0	1.0	1st day on site
15/4-30/4	1.0	1.0	1.0	Multiple readings on all instruments during installation
1/5	1.35	1.45	1.35	Geogrid covered with 7mm screenings and earthworks
5/5	1.35	1.45	1.35	
12/5	1.35	1.45	1.35	
26/5	1.35 (am)	1.45	1.35	
	1.35 (pm)	1.66	1.63	
27/5	* (am)	1.64	1.69	* additional layer placed approx. thickness 0.2m
	* (pm)	*	*	
28/5	1.78 (am)	2.10	1.90	Fill Placement/Multiple Readings
	2.25 (pm)			
29/5	2.34 (am)	1.96	1.90	Fill Placement/Multiple Readings
	2.69 (pm)	2.39	2.40	
30/5	2.69 (am)	2.70	2.75	Wet layer stripped
	2.72 (pm)	2.40	2.40	Section A replaced
1/6	2.64	2.67	2.98	Fill Placement/Multiple Readings
2/6	2.62	2.66	2.95	Regular Readings
3/6	2.60	2.65	2.94	Regular Readings
9/6	2.67	2.86	2.82	Fill Placement/Multiple Readings
10/6	3.05 (am)	3.10	3.16	Fill Placement/Multiple Readings
	3.26 (pm)	3.24	3.35	Earthworks Completed
11/6	3.26 (pm)	3.24	3.35	Start of Regular Readings

4.6 Interpretation of Data

The works contained in this chapter are in three parts. The first one is related to the soil profile close to the test embankment, the laboratory tests conducted on disturbed and undisturbed samples, and the interpretation of vanes tests data. The second part is the major one and it relates to a full interpretation of the settlement, the lateral deformation and pore pressures below the test embankment and the third one is on the back-analysis of the test embankment data using PLAXIS computer softwares. These sub-sections are listed below.

4.6.1 Soil Profiles, Laboratory Tests and In-situ Tests Data

This section includes the following work program

i. Defining the subsoil profile below the test embankment

ii. Delineating the index properties, unit weight and shear strength of the sub-soils in the test embankment location

iii. Interpretation of consolidation test data as tested on undisturbed samples taken in the location of the test embankment

iv. Analysis and synthesis of vane strength data at locations below the test embankment

4.6.2 Analysis of Data from the Test Embankment:

This section includes the following works.

i. Interpretation of the settlement records below the test embankment in the PVD sections (Sections A and C) and no PVD section (Section B)

ii. Interpretation of the excess pore pressure development and dissipation below the test embankment

iii. Analysis of the lateral deformation profiles below the test embankment.

4.6.3 PLAXIS analysis

A comparison of the observed settlement, pore pressures and lateral movements below the test embankment with those predicted by the PLAXIS analysis using coupled consolidation.

4.7 Interpretation of Laboratory and Field Vane Shear Tests.

4.7.1 Longitudinal Soil Profile and Cross Sections of the Test Embankment

Figure 4.1 delineates the sub-soil profile as interpreted by the Author from 33 Boreholes close to the proximity of the test embankment. The deepest thickness of the upper layer of soft clay is about 10.5m and this was followed by layers of sand and coffee rock. In the analysis, only the behavior of the soft clay is studied as this the critical layer with high compressibility leading to large settlement and low shear strength which poses the stability problems in embankment construction. The test embankment is closer to the location where the soft clay layer is deepest. The running chainage of the test embankment is from Ch28520 to Ch28610 marked as A and B in Figure 4.1. Three boreholes were found to be close to the test embankment and these were BH 19 (Ch28500), BH20 (Ch28600) and BH 22 (Ch28664). The longitudinal sections of the embankment, namely Section A (with PVD at 1.0m spacing), Section C (with PVD at 2.0m spacing) and Section B with no PVD are shown in Figure 4.2.The no-PVD section (Section B) is sandwiched between the other two sections (Section A and Section B with PVD at closer and wider spacing respectively.

4.7.2 Index properties, Unit Weight and Vane Shear Strength

Figure 4.3 indicates typical sub-soil layers in the swampy areas along the Sunshine Motorway. In this figure silty clay (CH) is noted up to about 8m depth followed by clayey silt (MH), silty clay (CH) and clayey sand up to 12m depth. The natural water content of all layers were substantially higher than the liquid limit and highest water

content is noted in the depth range 2-6.5m (maximum 120 pc), followed by lower water content of about 80 percent from 6.5 to 12 m. As such the weakest soft clay is encountered in the depth range of 2-6.5m and this layer is bound to be of low shear strength as revealed from the natural water content. The liquidity index of the clay will be higher than 1.0 as the natural water content is higher than the liquid limit. The plasticity index of the clay is uniform with depth and is about 40 percent.

Except for the upper shallow depth for rest of the depths, the unit weight ranged from 14.5 kN/m^3 to 15 kN/m^3. Such low unit bulk weight is an indication of the high water content. These properties were compiled in general for the Soft clay in the Sunshine Motorway, but the actual values very close to the test embankment may deviate to some extent as estuarine clays are bound to have variabilities in their properties at close proximity.

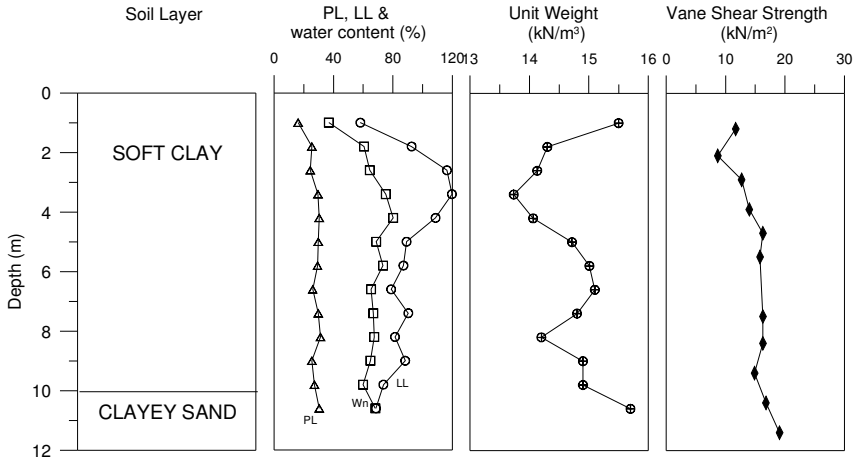

Figure 4.3 Index Properties, Unit Weight and Vane Shear Strength

4.7.3 Analysis of consolidation test data

From the borehole BH19 at Ch 28500, two series of consolidation tests were interpreted for samples taken from depths of 0.8 to 1.6m, and 4.0 to 4.8m respectively. From borehole BH20, three consolidation tests were analysed for samples taken at depths of 1.8 to 2.6m, 3.4 to 4.2m, and 8.2 to 9.0m. Similarly from borehole BH22, three tests were performed on samples taken at depths of 2.7 to 3.2m, 6.8 to 7.2m, and 8.2 to 9.0m.

The voids ratio-effective vertical stress relationships for these tests are presented in Figures 4.4(a) to 4.4(c). From these voids ratio-effective stress relations, values of the compression index (C_c), the coefficient of compressibility (a_v), the coefficient of volume decrease (m_v), the constraint modulus (D) and the coefficient of consolidation (c_v) were established as a function of the effective vertical stress. The compression indexes for all samples (see Figure 4.5) were found to initially increase with effective vertical stress and thereafter remain constant. Depending on the initial water content of the samples, the C_c values generally ranged from 0.5 to 1.0 at stresses in the normally consolidated range. The exception was sample taken at a depth of 8.2 to 9.0m, which indicated a C_c value of 1.5 in the normally consolidated range of stress levels. Figure 4.6 indicates that the a_v values generally decreased with increase in effective vertical stress. The trends in the a_v values indicate in spite of variations in C_c, the a_v values are more clustered within a narrow band. Figure 4.7 illustrates the variation of the coefficient of volume decrease m_v, with increase in effective vertical stress. The m_v values at the lower stress range seem to have a large variation from 1to 5 MN/m^2, but as the stress range increase from 50 to 100 kN/m^2, the m_v values ranged from 1 to 3 MN/m^2 for most samples. In this figure the m_v value as 2.2MN/m^2 and back-calculated from the centreline settlement of Section A of the test embankment is also shown. This will be discussed at a latter section under the interpretations of settlements below the test embankment.

An important finding emerged from these analysis is that the constraint modulus D, varied more or less linearly with increase in vertical effective stress with a lower bound linear relation and an upper bound linear relation as well. These bound values could give better estimation of the consolidation settlement when used in PLAXIS and other programs of similar structure. The variation of the coefficient of consolidation c_v, is presented in Figure 4.9. Except for one sample all other tests indicated c_v values in the range of 0.25 to 0.5 m^2/year. These values are extremely small and if reliable the

consolidation in the field will take a very long period of time. In general, the c_v value at the over-consolidated (OC) state should be higher than that at normally consolidated (NC) state. This is not reflected in most of the curves in Figure 4.9. The results presented in Figure 4.9 were factual as obtained from the laboratory.

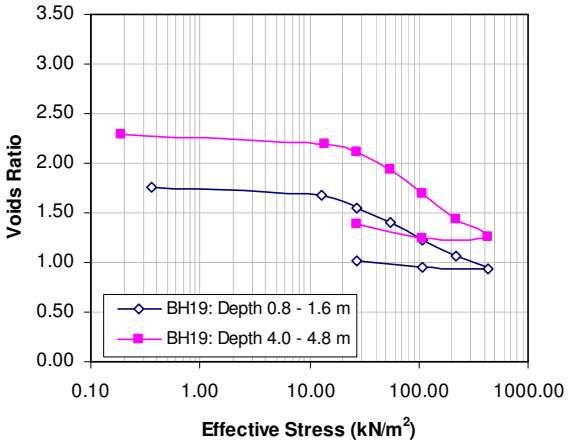

Figure 4.4(a) Voids Ratio – Effective Vertical Stress relationships (BH 19)

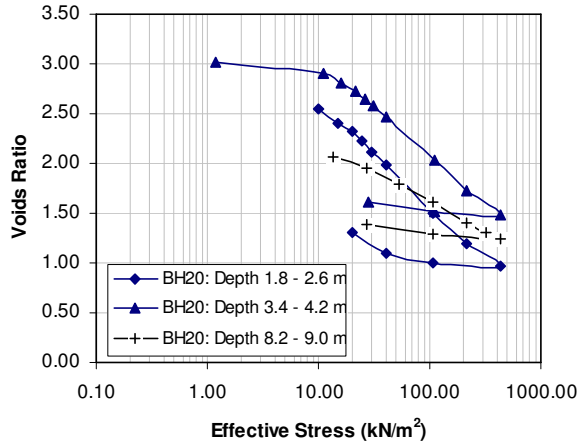

Figure 4.4(b) Voids Ratio – Effective Vertical Stress relationships (BH 20)

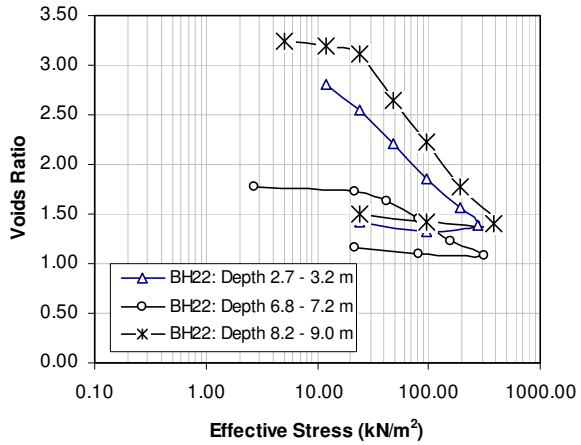

Figure 4.4(c) Voids Ratio – Effective Vertical Stress relationships (BH 22)

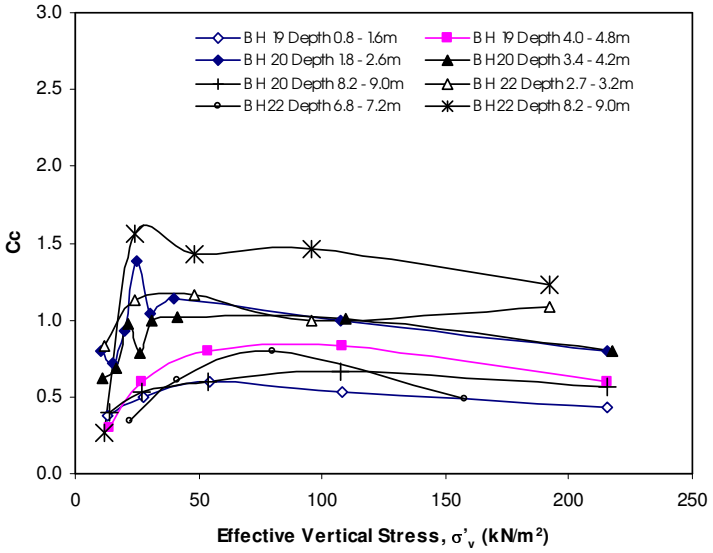

Figure 4.5 variation of Compression Index, C_C, with Effective Vertical Stress, σ'_v

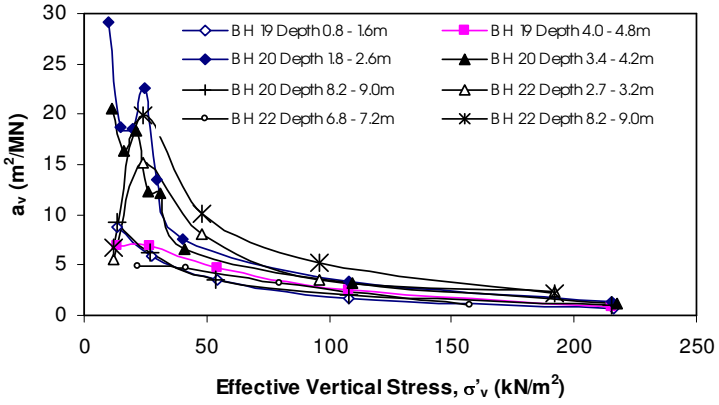

Figure 4.6 Variation of Coefficient of Compressibility, a_v, with Effective Vertical Stress, (σ'_v)

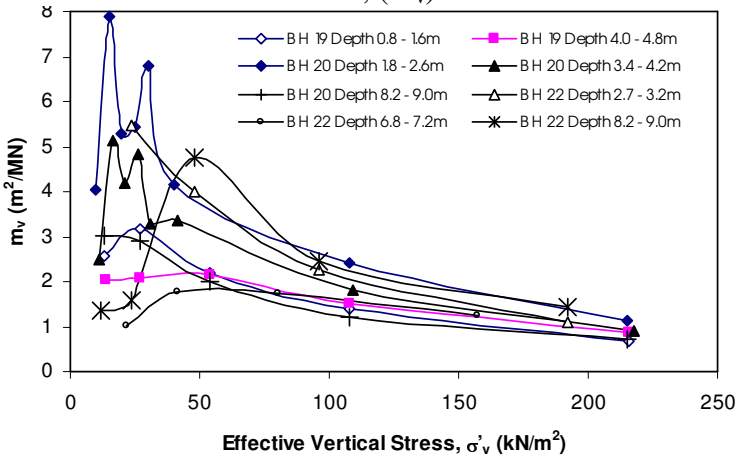

Figure 4.7 variation of Coefficient of Volume Decrease, m_v, with Effective Vertical Stress(σ'_v)

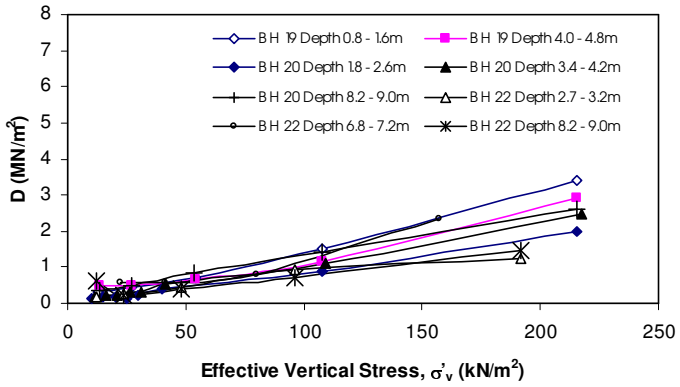

Figure 4.8 Variation of Constrained Modulus, D, with Effective Vertical Stress (σ'_v)

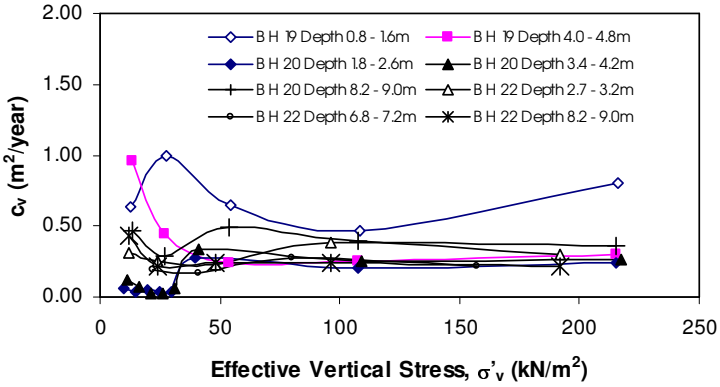

Figure 4.9 Variation of Coefficient of Consolidation, c_v, with Effective Vertical Stress (σ'_v)

The pre-consolidation pressure was estimated from all the voids ratio-effective vertical stress relations and the OCR values were then determined. The OCR values reduced with depth and at deeper depths the samples were normally consolidated with an OCR value of one (see Figure 4.10). All the values from the consolidation tests are tabulated in Table 4.3(a) to 4.3(h).

4.7.4 Vane shear strength

Altogether, six vane borings were done (see Table 4.4(a) to (c), and Figures 4.11(a) to 4.11(c)) close to the test embankment under all three sections. All six vane borings indicated the strength is about 15 kN/m^2 for all the depth range. Though the strength increases slightly with depth, but the increase is not substantial. Figures 4.11(a) to 4.11(c) contain the vane strength profile under each of Section A, Section B and Section C, respectively.

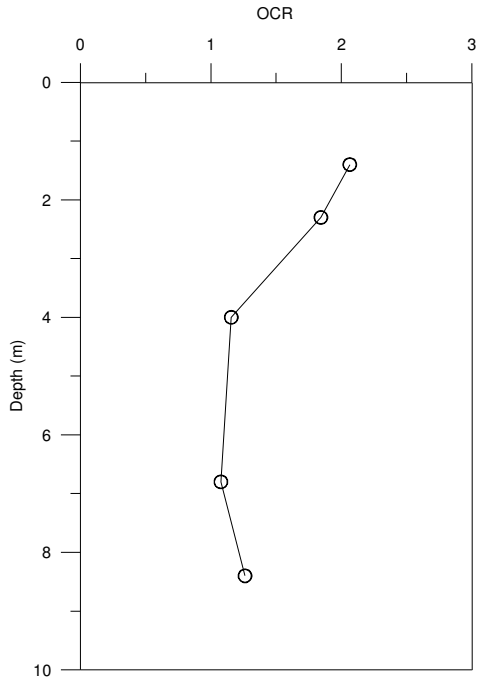

Figure 4.10 Variation of Over Consolidation Ratio with Depth

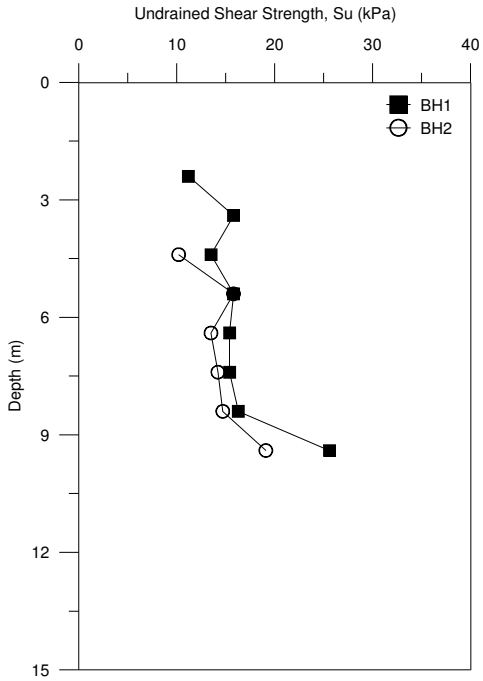

Figure 4.11(a) Variation of Undrained Shear Strength with Depth (BH1 and BH2 for Section A)

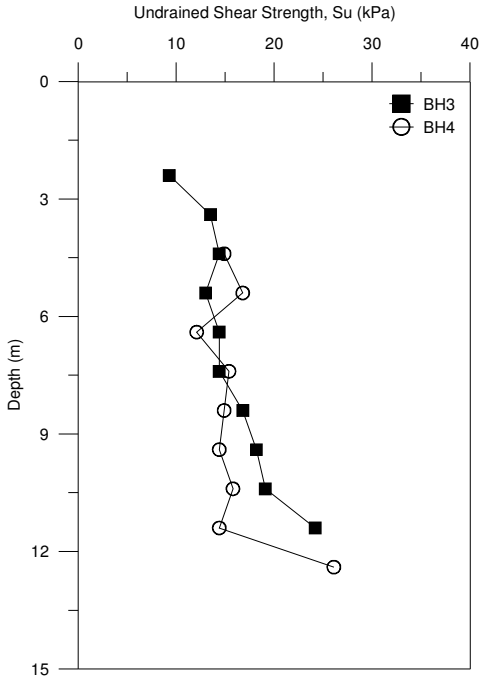

Figure 4.11(b) Variation of Undrained Shear Strength with Depth (BH3 and BH4 for Section B)

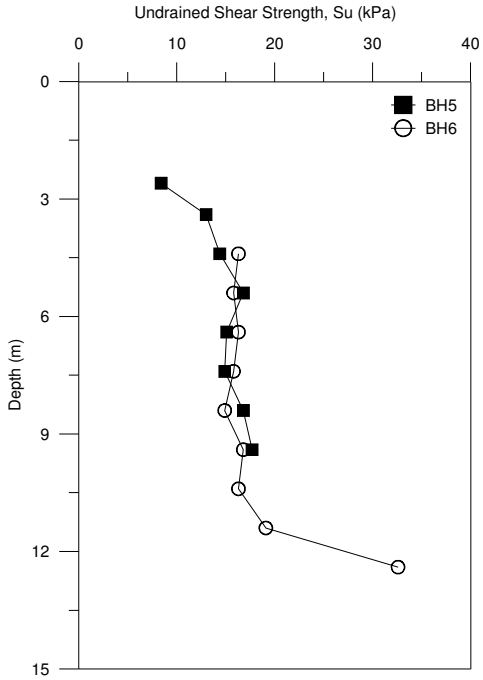

Figure 4.11(c) Variation of Undrained Shear Strength with Depth (BH5 and BH6 for Section C)

Table 4.3(a) Consolidation Parameters (Sample from BH19; Depth 0.8 – 1.6m)

Pressure (kPa)	*Compression Index; C_C*	*Coefficient of Compressibility; a_v (m^2/MN)*	*Coefficient of Volume Change; m_v (m^2/MN)*	*Constrained Modulus; D (MN/m^2)*	*Coefficient of Consolidation; c_v (m^2/year)*
0.4	0.06				
13.1	0.38	8.74	3.17	0.32	0.639
27.3	0.50	5.83	2.18	0.46	0.994
54.2	0.60	3.55	1.39	0.72	0.645
108.1	0.53	1.61	0.67	1.49	0.462
215.8	0.43	0.65	0.29	3.41	0.808
431.1	0.03	0.07	0.03	31.18	

Table 4.3(b) Consolidation Parameters (Sample from BH19; Depth 4.0 – 4.8m)

Pressure (kPa)	*Compression Index; C_C*	*Coefficient of Compressibility; a_v (m^2/MN)*	*Coefficient of Volume Change; m_v (m^2/MN)*	*Constrained Modulus; D (MN/m^2)*	*Coefficient of Consolidation; c_v (m^2/year)*
0.2	0.05				
13.6	0.30	6.86	2.09	0.48	0.958
27.1	0.60	6.88	2.15	0.47	0.440
54.0	0.80	4.73	1.52	0.66	0.243
107.9	0.83	2.53	0.86	1.16	0.256
215.6	0.60	0.92	0.34	2.92	0.298
431.0	0.25	0.02	0.010	100.00	

Table 4.3 (c) Consolidation Parameters (Sample from BH20; Depth 1.8 – 2.6m)

Pressure (kPa)	*Compression Index; C_C*	*Coefficient of Compressibility; a_v (m^2/MN)*	*Coefficient of Volume Change; m_v (m^2/MN)*	*Constrained Modulus; D (MN/m^2)*	*Coefficient of Consolidation; c_v (m^2/year)*
10.0	0.80	29.18	7.89	0.13	0.064
15.0	0.72	18.74	5.28	0.19	0.041
20.0	0.93	18.49	5.42	0.18	0.042
25.0	1.39	22.61	6.81	0.15	0.039
30.0	1.04	13.46	4.17	0.24	0.034
40.0	1.14	7.55	2.42	0.41	0.270
107.7	1.00	3.33	1.11	0.90	0.206
215.4	0.80	1.27	0.51	1.97	0.243
430.8	0.07	0.14	0.06	15.83	

Table 4.3 (d) Consolidation Parameters (Sample from BH20; Depth 3.4 – 4.2m)

Pressure (kPa)	*Compression Index; C_C*	*Coefficient of Compressibility; a_v (m^2/MN)*	*Coefficient of Volume Change; m_v (m^2/MN)*	*Constrained Modulus; D (MN/m^2)*	*Coefficient of Consolidation; c_v (m^2/year)*
2.7	0.08				
16.1	0.79	10.77	2.87	0.35	0.169
56.8	1.24	7.53	2.04	0.49	0.243
110.8	1.08	3.33	1.02	0.98	0.238
219.0	0.03	0.14	0.05	20.93	0.285

Table 4.3(e) Consolidation Parameters (Sample from BH20; Depths 8.2 – 9.0m)

Pressure (kPa)	*Compression Index; C_C*	*Coefficient of Compressibility; a_v (m^2/MN)*	*Coefficient of Volume Change; m_v (m^2/MN)*	*Constrained Modulus; D (MN/m^2)*	*Coefficient of Consolidation; c_v (m^2/year)*
13.4	0.13	3.05	1.05	0.95	0.97
26.9	0.20	2.26	0.80	1.25	0.527
53.9	0.93	5.31	1.91	0.52	0.189
107.7	0.76	2.38	0.88	1.14	0.248
215.4	0.56	0.87	0.36	2.80	0.382
430.8	0.07	0.13	0.06	16.48	

Table 4.3 (f) Consolidation Parameters (Sample from BH22; Depth 2.7 – 3.2m)

Pressure (kPa)	*Compression Index; C_C*	*Coefficient of Compressibility; a_v (m^2/MN)*	*Coefficient of Volume Change; m_v (m^2/MN)*	*Constrained Modulus; D (MN/m^2)*	*Coefficient of Consolidation; c_v (m^2/year)*
5.0					
12.0	0.83	5.48	0.83	0.18	0.314
24.0	1.13	15.16	1.13	0.25	0.247
48.0	1.16	8.06	1.16	0.44	0.229
96.0	1.00	3.51	1.00	0.92	0.386
192.0	1.09	2.29	1.09	1.25	0.304
275.0					

Table 4.3 (g) Consolidation Parameters (Sample from BH22; Depths 6.8 – 7.2m)

Pressure (kPa)	*Compression Index; C_C*	*Coefficient of Compressibility; a_v (m^2/MN)*	*Coefficient of Volume Change; m_v (m^2/MN)*	*Constrained Modulus; D (MN/m^2)*	*Coefficient of Consolidation; c_v (m^2/year)*
2.8	0.06				
22.0	0.34	4.96	1.79	0.56	0.188
41.4	0.61	4.68	1.72	0.58	0.166
80.1	0.79	3.24	1.23	0.81	0.280
157.4	0.49	1.04	0.43	2.35	0.211
312.0	0.04	0.13	0.06	17.19	

Table 4.3 (h) Consolidation Parameters (Sample from BH22; Depth 8.2 – 9.0m)

Pressure (kPa)	*Compression Index; C_C*	*Coefficient of Compressibility; a_v (m^2/MN)*	*Coefficient of Volume Change; m_v (m^2/MN)*	*Constrained Modulus; D (MN/m^2)*	*Coefficient of Consolidation; c_v (m^2/year)*
5.0					
12.0	1.08	6.73	0.27	0.63	0.427
24.0	1.38	19.96	1.56	0.21	0.214
48.0	1.68	10.11	1.43	0.41	0.244
96.0	1.98	5.20	1.46	0.70	0.234
192.0	2.28	2.23	1.23	1.44	0.214
384.0	2.58	0.04	0.02	69.41	

4.8 Embankment Data Analysis

4.8.1 Instrumentation Locations in Test Embankment

The details of the cross sections and the instrumentations used are shown in Figure 4.12 to 4.14. It is noted that sensitive soft silty clay extends to about 10m depth followed by a layer of sand 6m thick and below this is 2m of sensitive clay layer which again is followed by sand. In Figure 4.12, in Section A with close PVD, a hydraulic profile was used to measure the settlement below the entire test embankment. Two inclinometer casings XX and YY (see Figure 4.12) were installed on the left hand side, one (at XX) approximately at mid-slope of the embankment with maximum height (2.85m), while the other casing YY was installed close to the toe of the berm. The inclinometer casings in Section B (Figure 4.13) were also located in the same manner as for Section A. But for Section C (Figure 4.14) only one inclinometer casing YY was installed close to the toe. In Section A (Figure 4.12), a cluster of piezometers, seven in numbers were installed along the center line at varying depths ranging just below the surface to some 18m depth. Additionally two piezometers were installed close to location XX and six more were installed between the locations XX and YY. The arrangement of the piezometers in Section B (Figure 4.13) was very similar to those in Section A. However for Section C (Figure 4.14), only six piezometers were installed below the centreline,

and two others close to the location of the slope of the embankment with 2.85m high and the berm on the left hand side of the centreline.

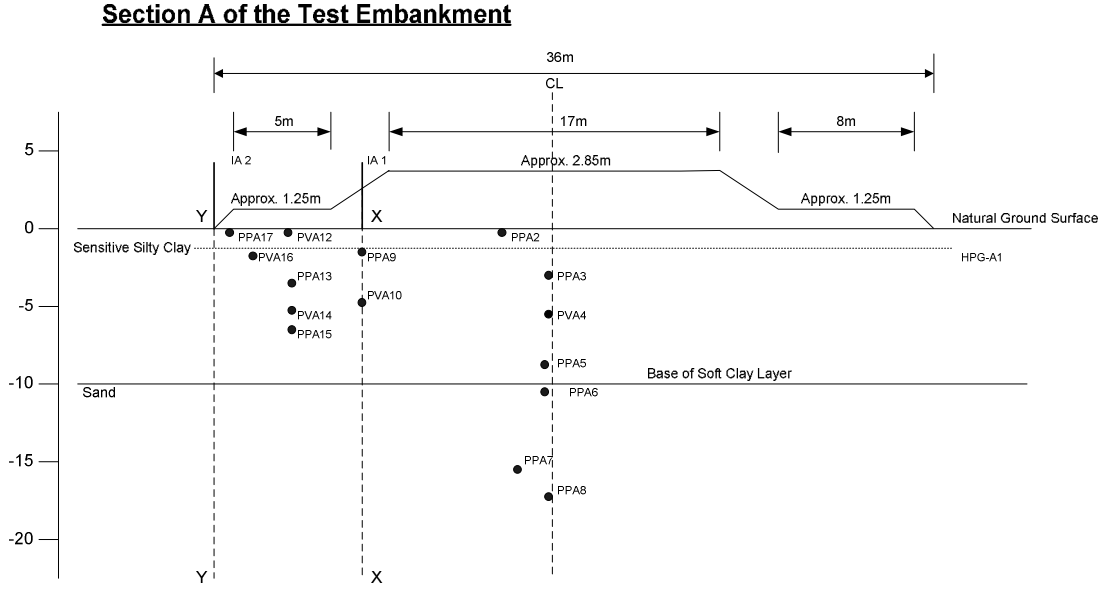

Figure 4.12 Section A - cross section showing instrumentation

4.8.2 Interpretation of Settlement Data

4.8.2.1 Surface Settlement across Section A and Section B

Horizontal profile gauges were only installed in Section A and Section B (see Figures. 4.12 and 4.13 respectively) to monitor the settlements across the cross sections with varying time ranging from one day to 2904 days. However, the settlement monitoring in Section B (without any PVD) only continued up to 724 days. These hydraulic profile gauge data are presented in Figures 4.15 and 4.16 for Section A and Section B respectively and were interpreted extensively. In both figures, the location marked EE correspond to the centreline of the embankment. Then the locations DD, CC, BB and AA were taken from the centre line to the left at distances of 5m, 10m, 15m and 20m respectively. Similarly the locations, FF, GG and HH were on the right hand side and at distances of 5m, 10m and 15m respectively.

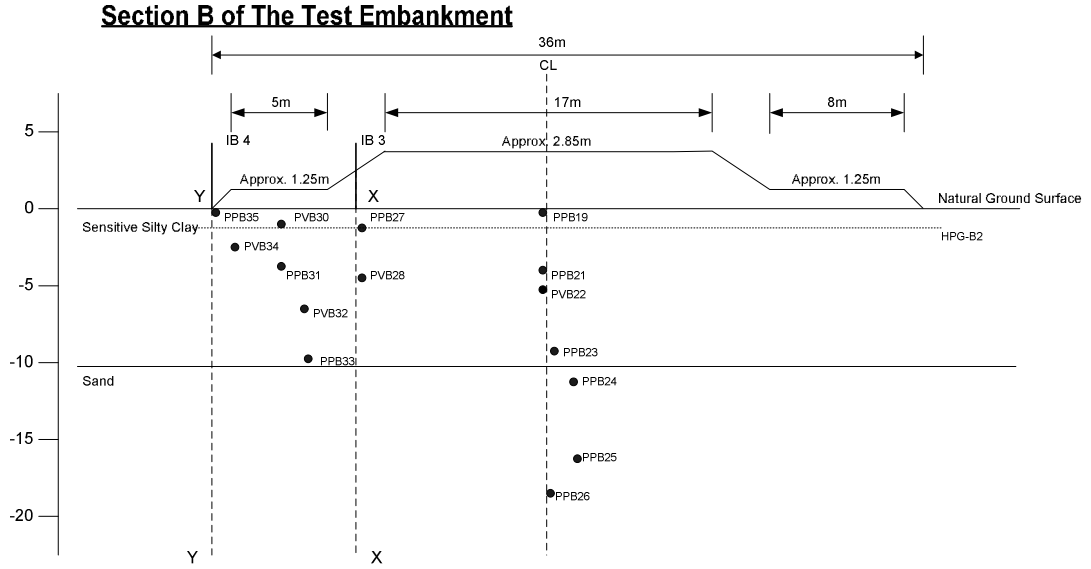

Figure 4.13 Section B - cross section showing instrumentation

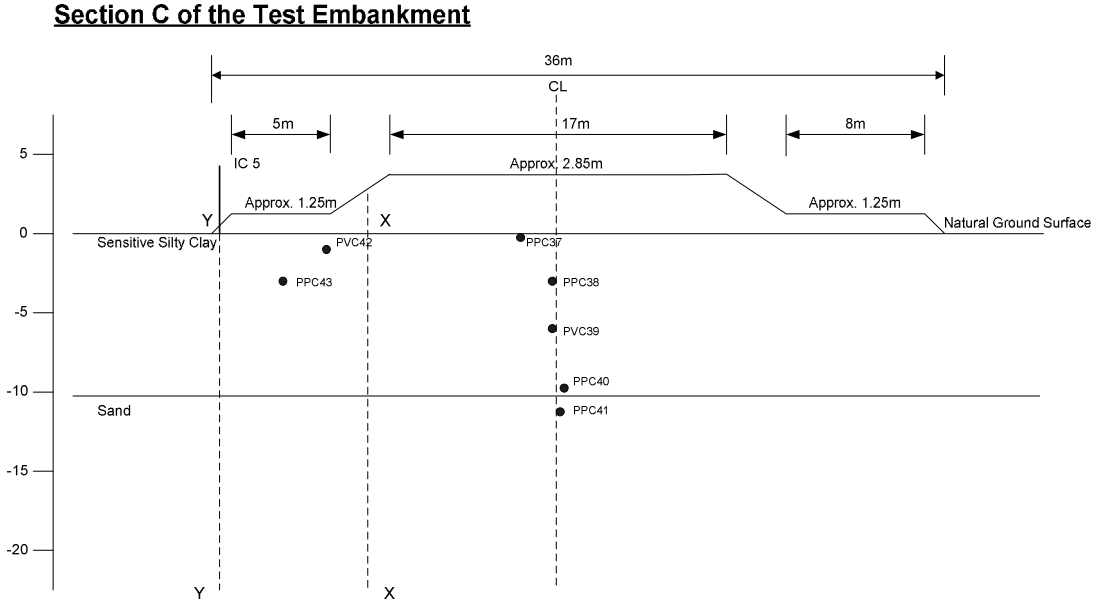

Figure 4.14 Section C - cross section showing instrumentation

In the interpretation of these hydraulic profile gauges, two distinct phenomena were noted. They are, Section A with the PVD, showed higher settlement at any time when compared with Section B without any PVD. This is illustrated in Figure 4.17 for times of approximately, 1 day, 62 days, 93 days and 533 days. At all times, Section A with PVD has experienced higher settlement than Section B. Also individual settlement –log time plots are plotted for all sections to show, that Section A with PVD experiencing greater settlement than Section B without PVD. It is clear that the use of vertical drains

has not accelerated settlements to any great extent. Assuming a drainage thickness of 5 m for Section B, the drainage times for Section A, in the idealised case should have been at least 25 times faster (assuming $c_v=c_h$). The ongoing settlement would suggest that, the close spacing of vertical drains has probably been wiped out by installation disturbance of the vertical drains in this sensitive clay.

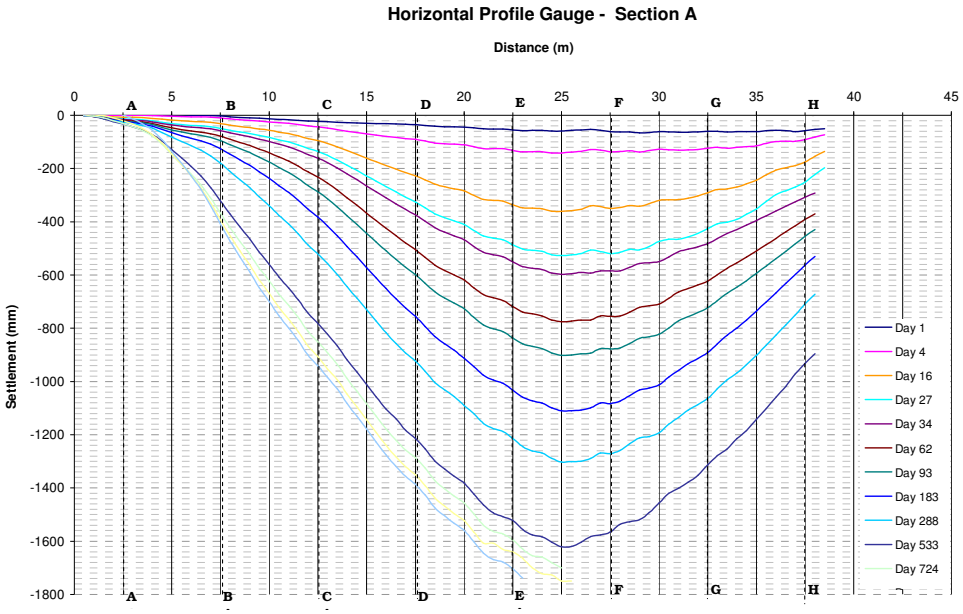

Figure 4.15 Surface settlements from horizontal profile gauge in Section A

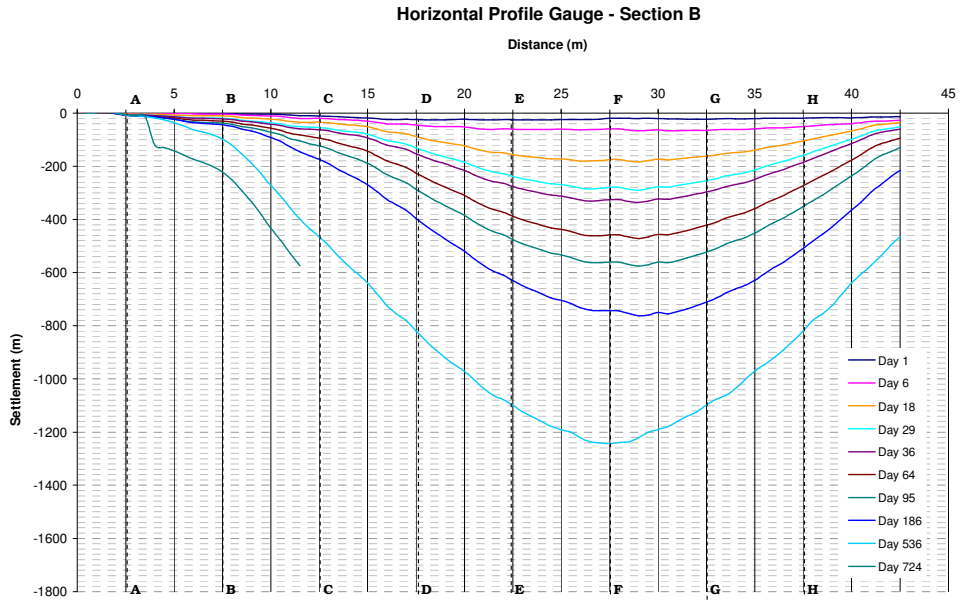

Figure 4.16 Surface settlements from horizontal profile gauge in Section B

4.8.2.2 Casagrande settlement-log time plot

The second phenomenon which is somewhat difficult to explain is that for Section A with the PVD, the curves in the settlement log time plots (Figure 4.18(a)) indicated that, 100 percent primary consolidation is over virtually for all sections, to the left of the centre line. But these plots indicated that the sections to the right of the centre line were unable to achieve 100 percent primary consolidation even with the use of PVD in closer spacing of 1.0m. This was established systematically, by plotting the settlement –log time plot of each location separately to the left and to the right of the centre line of Section A. The settlements for the centre line and the locations to the left are shown in Figure 4.18(a); those corresponding to the right are shown in Figure 4.18(b).

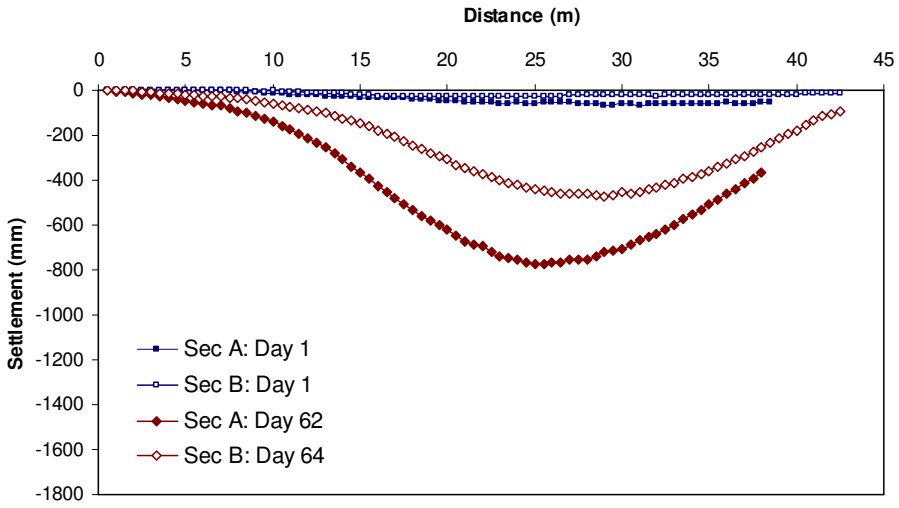

Figure 4.17(a) Surface settlements from horizontal profile gauge (Before End of Construction)

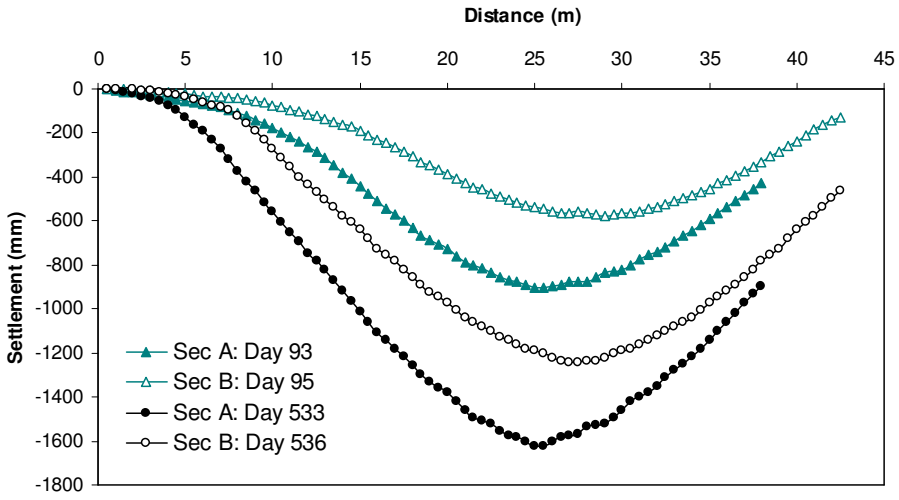

Figure 4.17(b) Surface settlements from horizontal profile gauge (After the End of Construction)

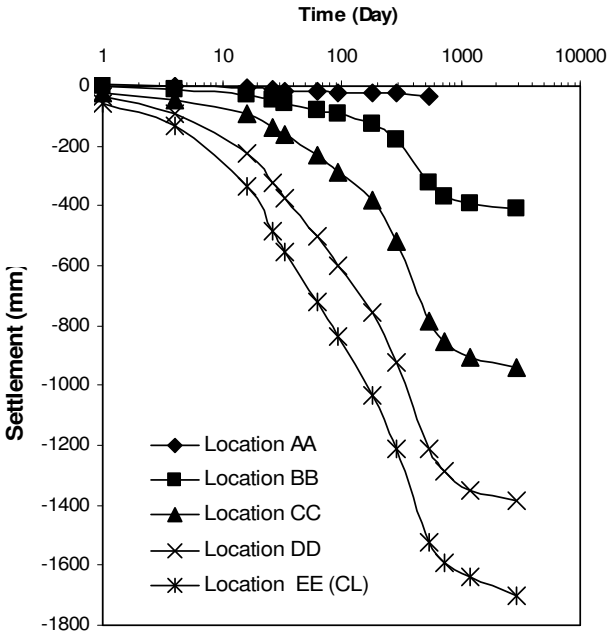

Figure 4.18(a) Variation of settlement with time along the Centreline and the Locations to the Left in Section A (100 pc Consolidation Completed)

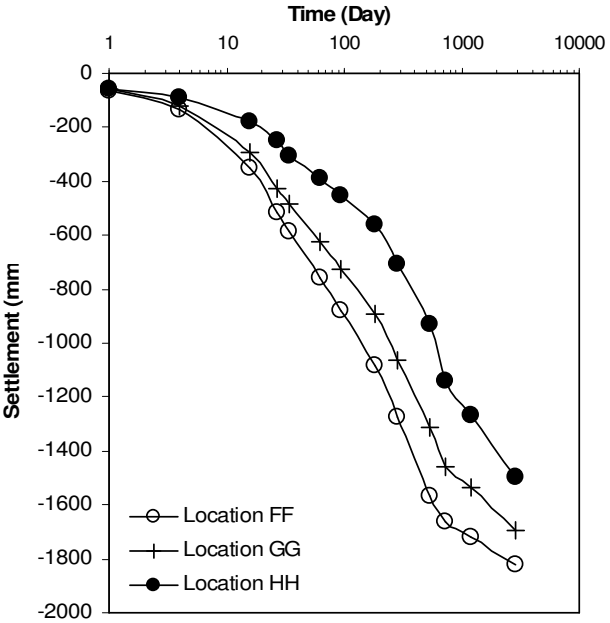

Figure 4.18(b) Variation of settlement with time at the Locations to the Right of Centreline in Section A (100 pc Consolidation Not Completed)

4.8.2.3 Asaoka Graphical method for Primary consolidation Settlement

When the settlement –log time plot do not show an S curve, and where the Casagrande method cannot be applied to estimate the 100 percent primary consolidation, the Aasoka plot as described in Section 4.3 was used to estimate the 100 percent primary consolidation. The results obtained by this method for Section A with PVD and on the

right hand side of the centreline are presented in Figure 4.19. It was observed later that the Asaoka Method at times give lower values for the ultimate settlement (that is one hundred percent consolidation settlement). This aspect will be discussed at a latter section.

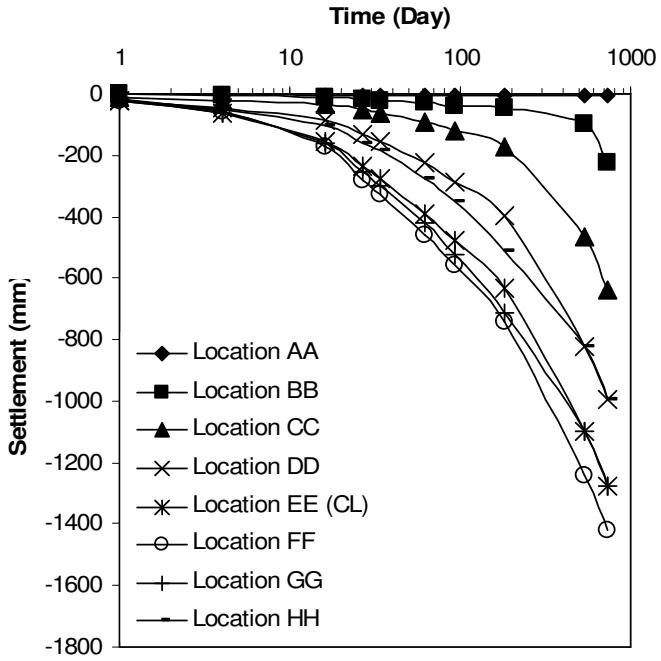

Figure 4.19 Variation of settlement with time in Section B (100 pc Consolidation Not Completed)

4.8.2.4 Values of Primary Consolidation from Casagrande and Asaoka Methods

Table 4.5 summarises the 100 percent settlement estimated from the Casagrande and Asaoka methods (see Figures 4.20(a) to 4.20(c)) for Section A and Section B respectively. These values indicate that even Section B is having proportionately higher settlements, even though no PVD were used. The major reason for this was perhaps due to the fact that the PVD Section A and Section C are on either side of the section B which have no PVD. Earlier work carried out at other sites in Southeast Asia and elsewhere indicated a better arrangement would have been to separately locate the PVD Sections and the no-PVD Section so that there is no interference effect. By not doing so at the test embankment in the Sunshine Motorway, the lateral drainage from the Section with no PVD (Section B) and through silt and sand lenses to the PVD in the drained sections have possibly occurred.

Table 4.4 (a) Field Vane Shear Strengths in Section A

Section	*A*	*A*
Vane Boring No.	*1*	*2*
Chainage	*28544*	*28544*
Offset	*15.4m Left*	*0.6m Right*
Location	*Berm*	*Embankment*
RL	*1.335*	*2.527*

Depth (m)	s_u (kN/m^2)	Depth (m)	s_u (kN/m^2)
2.4	11.2	4.4	10.2
3.4	15.8	5.4	15.8
4.4	13.5	6.4	13.5
5.4	15.8	7.4	14.2
6.4	15.4	8.4	14.7
7.4	15.4	9.4	19.1
8.4	16.3		
9.4	25.6		

Table 4.4 (b) Field Vane Shear Strengths in Section B

Section	*B*	*B*
Vane Boring No.	*3*	*4*
Chainage	*28578*	*28578*
Offset	*16.1m Left*	*0.0m*
Location	*Berm*	*Embankment*
RL	*1.543*	*2.685*

Depth (m)	s_u (kN/m^2)	Depth (m)	s_u (kN/m^2)
2.4	*9.3*	*4.4*	*14.9*
3.4	*13.5*	*5.4*	*16.8*
4.4	*14.4*	*6.4*	*12.1*
5.4	*13.0*	*7.4*	*15.4*
6.4	*14.4*	*8.4*	*14.9*
7.4	*14.4*	*9.4*	*14.4*
8.4	*16.8*	*10.4*	*15.8*
9.4	*18.2*	*11.4*	*14.4*
10.4	*19.1*	*12.4*	*26.1*
11.4	*24.2*		

Table 4.4 (c) Field Vane Shear Strengths in Section C

Section	*C*	*C*
Vane Boring No.	*5*	*6*
Chainage	*28604*	*28602*
Offset	*15.0m Left*	*1.2m Right*
Location	*Berm*	*Embankment*
RL	*1.425*	*2.600*

Depth (m)	s_u (kN/m^2)	Depth (m)	s_u (kN/m^2)
2.6	8.4	4.4	16.3
3.4	13.0	5.4	15.8
4.4	14.4	6.4	16.3
5.4	16.8	7.4	15.8
6.4	15.1	8.4	14.9
7.4	14.9	9.4	16.8
8.4	16.8	10.4	16.3
9.4	17.7	11.4	19.1
10.4	21.4	12.4	32.6

Table 4.5 (a) Ultimate Settlement (100 % Consolidation Settlement) in Section A

Location	*Casagrande's Method 100 pc Settlement (mm)*	*Asaoka's Method 100 pc Settlement (mm)*
CL	1570	-
5m Left from CL	1320	-
10m Left from CL	885	-
15m Left from CL	380	-
20m Left from CL	-	-
5m Right from CL	-	1506
10m Right from CL	-	1316
15m Right from CL	-	970

Table 4.5 (b) Ultimate Settlement (100 % Consolidation Settlement) in Section B

Location	*Casagrande's Method 100 pc Settlement (mm)*	*Asaoka's Method 100 pc Settlement (mm)*
CL	-	1200
5m Left from CL	-	1050
10m Left from CL	-	480
15m Left from CL	-	290
20m Left from CL	-	-
5m Right from CL	-	1200
10m Right from CL	-	1060
15m Right from CL	-	830

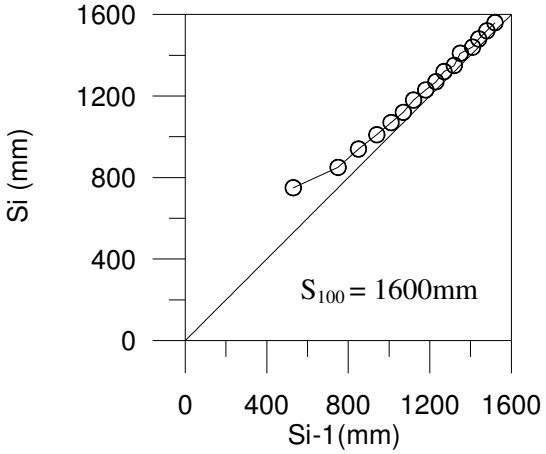

Figure 4.20 (a) Asaoka's Plot (at 5m Right from CL) in Section A

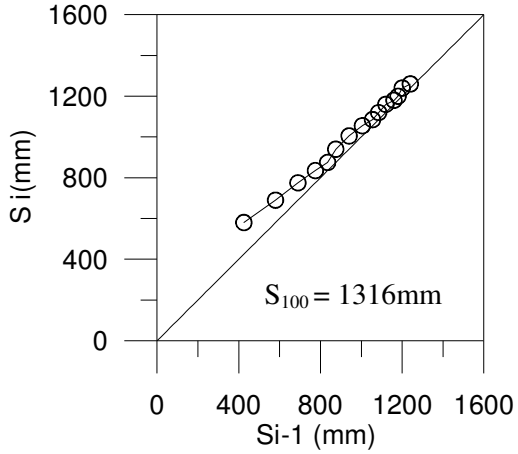

Figure 4.20 (b) Asaoka's Plot (at 10 Right from CL) in Section A

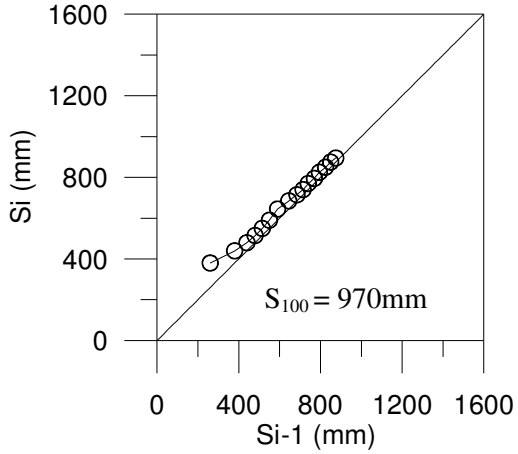

Figure 4.20 (c) Asaoka's Plot (at 15m Right from CL) in Section A

4.8.2.5 Back-calculated c_h values using Hansbo Equation

The Hansbo (1979) equation (see Chapter 3, Section 3.4) was used to back-calculate the coefficient of consolidation (c_h). The back-calculated results are presented in Tables 4.6 and 4.7, and Figure 4.21. In Figure 4.21(a) for the centre line and for the locations left of the centre line, the 100 percent primary consolidation was obtained using Casagrande

method of plotting settlement versus log time. Except for the centreline, for other locations to the left, the back calculated c_h values are generally less than 0.5 m^2/year. These values are close to the laboratory measured c_v values. However for the sections on the right hand side where Asaoka method was used to determine the 100 percent primary consolidation, the back calculated c_h values are generally found to decrease with increase in degree of consolidation. The reduction seems to be somewhat exponential in nature with increase in the degree of consolidation. Undoubtedly, the Asaoka method of determining the 100 percent degree of consolidation may as well not be as precise as the Casagrande method.

Table 4.6 Coefficient of Consolidation, c_h, Back-calculated from Field Settlement and Degree of Consolidation (Hansbo's Method, 1979)

Degree of Consolidation; U (%)	*c_h, (m^2/year)*						
	CL	5m Left	10m Left	15m Left	5m Right	10m Right	15m Right
10	1.07	0.53	0.43	0.53	2.67	3.56	3.56
20	1.13	0.75	0.45	0.38	1.74	1.74	1.13
30	1.21	0.52	0.52	0.24	1.64	1.51	1.17
40	1.04	0.52	0.35	0.22	1.36	1.23	0.91
50	0.70	0.47	0.31	0.23	1.13	0.98	0.58
60	0.72	0.43	0.32	0.25	0.90	0.72	0.47
70	0.58	0.39	0.34	0.25	0.71	0.60	0.46
80	0.54	0.41	0.38	0.35	0.66	0.58	0.45
90	0.54	0.47	0.43	0.34	0.65	0.58	0.50

Table 4.7 Coefficient of Consolidation, c_v, Back-calculated from Field Settlement and Degree of Consolidation (Hansbo's Method, 1979)

Degree of Consolidation; U (%)	*c_v, (m^2/year)*						
	CL	5m Left	10m Left	15m Left	5m Right	10m Right	15m Right
10	6.68	3.86	3.22	1.19	7.33	7.29	7.34
20	10.23	4.26	4.72	0.93	24.14	13.04	10.39
30	12.13	5.39	4.73	1.22	15.24	15.81	12.36
40	11.82	5.42	5.52	1.83	16.04	17.77	13.55
50	10.23	5.79	6.76	2.64	15.11	17.70	14.12
60	9.49	6.35	7.97	3.58	13.95	17.11	13.46
70	9.52	7.04	9.34	4.74	12.94	15.84	13.10
80	10.57	-	11.33	-	13.22	15.15	13.16
90	11.14	-	14.82	-	15.08	16.43	13.49

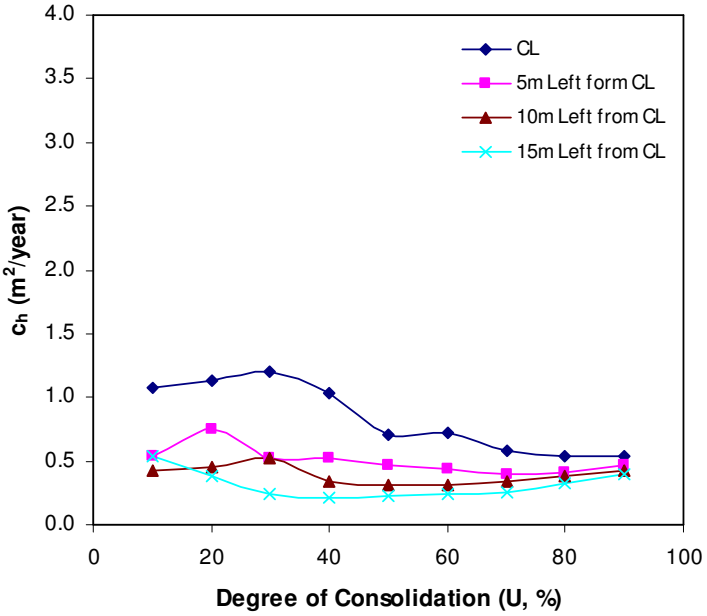

Figure 4.21(a) Variation of back-calculated Coefficient of Consolidation, $c_{h,}$ with Degree of Consolidation which reached 100% Consolidation in Section A

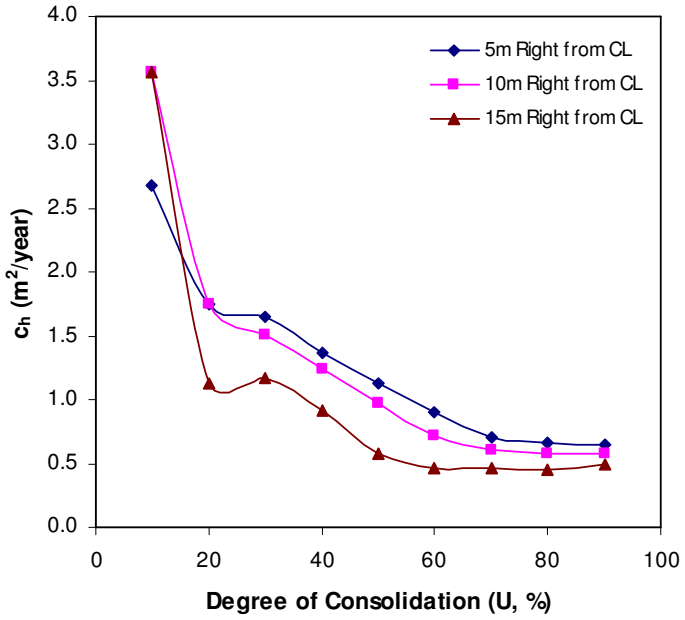

Figure 4.21(b) Variation of back-calculated Coefficient of Consolidation, $c_{h,}$ with Degree of Consolidation which did not reach 100% Consolidation in Section A

4.8.2.6 Back-calculated c_v Values from Section B

Section B was found to experience very large settlement even though this section did not have any PVD. Using the primary settlement experienced by this section and the coefficient of consolidation, c_v values were computed with double end drainage at the upper and lower end and with no lateral drainage (see Figure 4.22). It was found that to match the settlement in this section which has no PVD, the equivalent c_v values need to

be very high for the centre line section about 10 m^2/ year and this value reducing to the left of the embankment, while increasing to the right of the embankment to as much as 15 m^2/ year. This is of course a very coarse calculation and illustrates that Section B has artificially acquired a very high equivalent c_v to match its excessive settlement. This is due to the interference of Section A and Section C with PVD, while the no PVD section B is sandwiched between the two PVD Sections.

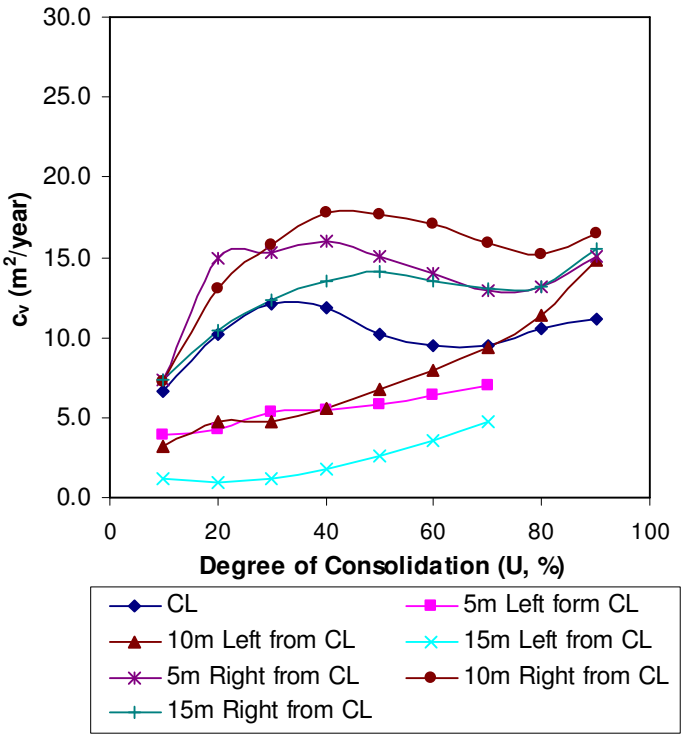

Figure 4.22 variation of back-calculated Coefficient of Consolidation, c_v, with Degree of Consolidation at Locations which did not Reach 100 pc Consolidation in Section B

4.8.2.7 Back-calculated m_v Value and Stresses across Section A and B.

From the ultimate settlement at the centre line in Section A, and using the surcharge pressure q of 57.5 kN/m^2, the field m_v value was back-calculated as 2.1 MN/m^2 and this value is plotted together with the laboratory determined values of m_v as presented in Figure 4.7. The m_v values from the laboratory tests are found to be higher than this field value at low effective vertical stress and lower than the field value at very high effective vertical stress.

Another interesting feature to note is the reduction in one hundred percent consolidation settlement at locations away from the centreline. Using the estimated one hundred percent consolidation settlement at locations other than the centre line, the effective vertical stress increment was computed and found to vary as shown in Figure 4.23.

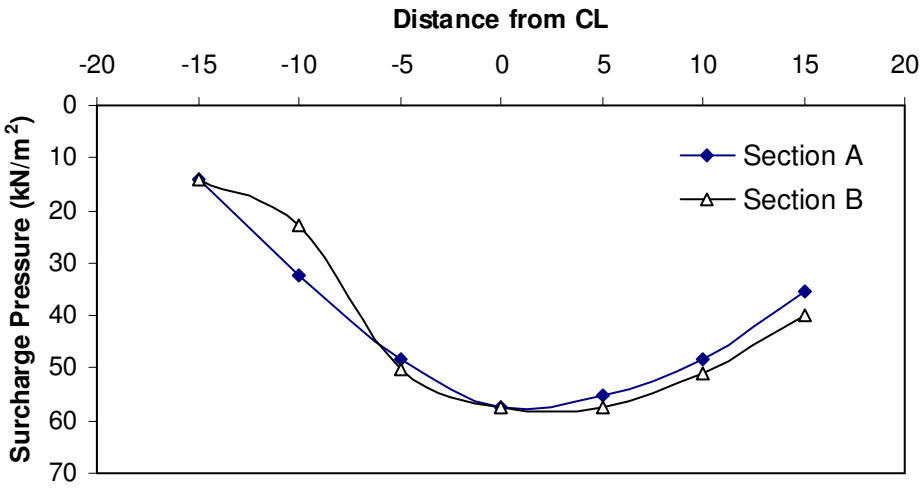

Figure 4.23 variation of Surcharge Pressure in Section A and Section B

4.8.2.8 Lateral Deformation from Inclinometer Measurements.

Lateral deformation profiles were determined at locations XX and YY (see Figures. 4.12 to 4.14). However only in Section A and Section B inclinometer casings were installed at the location XX. While for Section C, as well as for Section A and B, inclinometer casings were installed in YY. Figure 4.24 illustrates the lateral deformation profiles for Section A and Section B at location XX after one day, 62 days, 93 days and 526 days. Initially, Section A with PVD was found to develop more lateral deformation. Perhaps this may be due to the disturbance created by the installation of PVD. However at 526 days time both Section A and Section B have similar lateral deformation profiles at XX.

Similar comparisons were made for the lateral deformations at location YY. Even Section C has an inclinometer at YY, so it was possible to make comparisons of the

lateral deformation profiles for all three sections. The trend in the lateral deformation profiles presented in Figure 4.25 is more or less similar for all three Sections at the toe of the berm (YY). This perhaps indicates that all sections whether PVD were used or not have similar magnitude of lateral deformation. That would indicate, while the lateral deformation continue to take place during immediate settlement and also during undrained creep, the consolidation settlement seems more or less one dimensional in nature. So far there is no successful theory developed to predict undrained creep in test embankments on Soft clays. Loganathan *et al.* (1993) based on the work of Christian made an attempt to make such predictions for the series of test embankments at Muar Flat site in Malaysia.

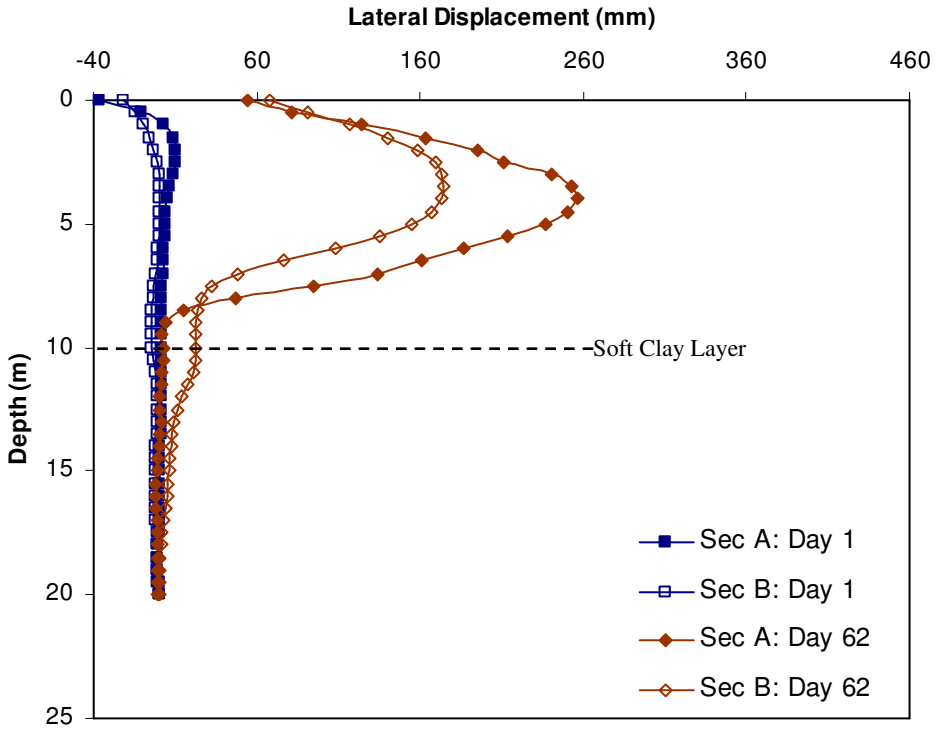

Figure 4.24 (a) variation of Lateral Displacements in Section A and Section B (Before the End of Construction) at Location XX

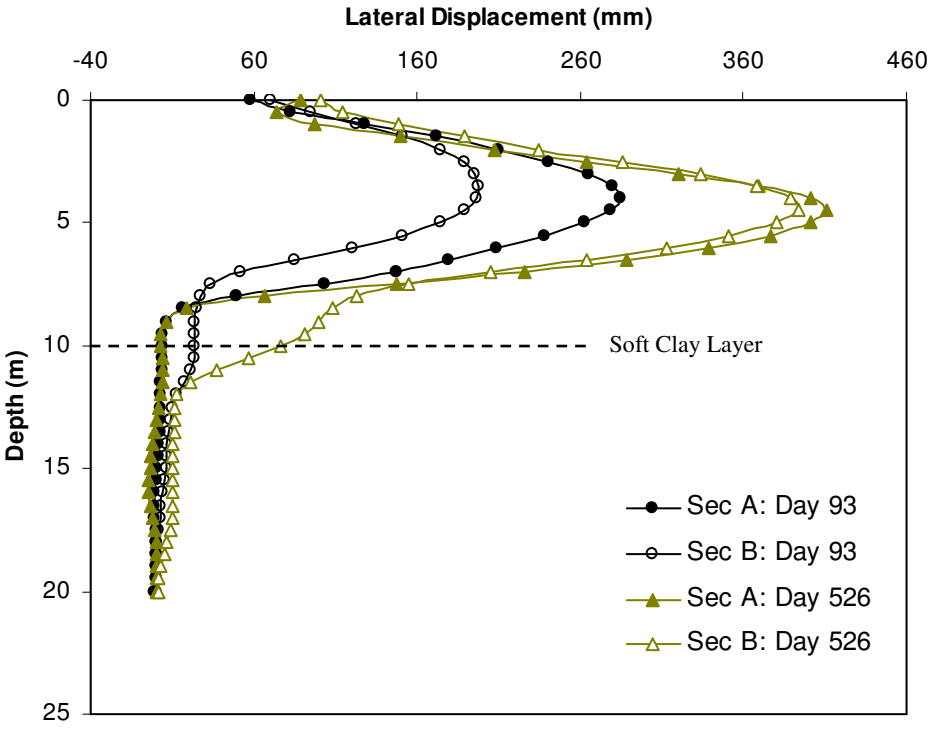

Figure 4.24 (b) variation of Lateral Displacements in Section A and Section B (After the End of Construction) at Location XX

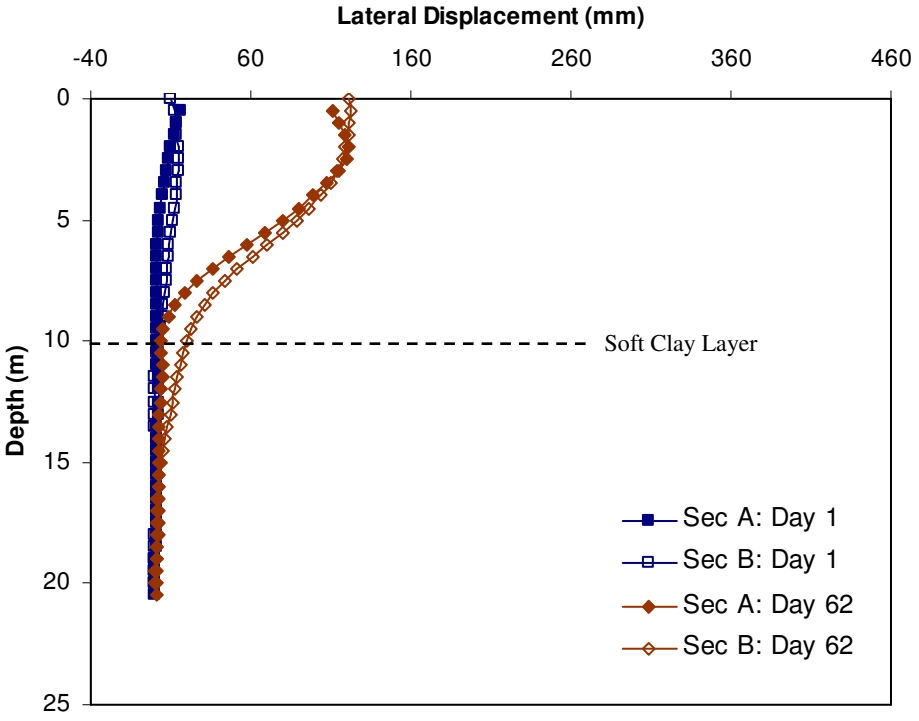

Figure 4.25 (a) variation of Lateral Displacements in Section A and Section B (Before the End of Construction) at Location YY

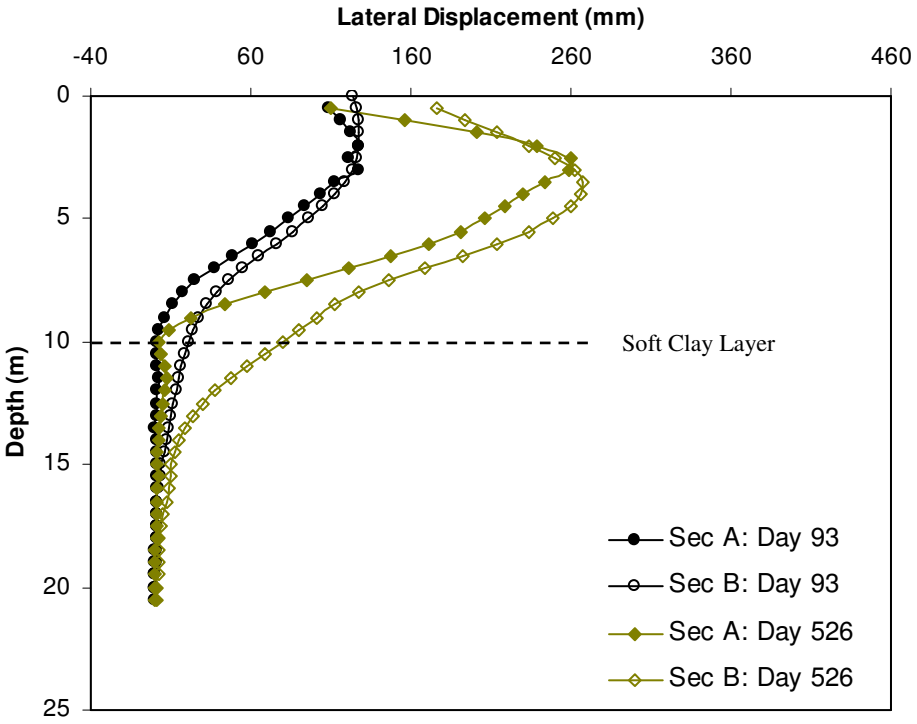

Figure 4.25 (b) variation of Lateral Displacements in Section A and Section B (Before the End of Construction) at Location YY

For Section A and Section B, at the location XX, Figure 4.26 gives a plot of the maximum lateral movement against the maximum settlement. It is interesting to note that the line OA with the higher slope indicate the initial maximum lateral movement profile. After that even Section B without any PVD have settlement which makes the slope in this plot smaller than that of OA, indicating substantial consolidation settlement has taken place. Of course the curve OA for Section A with PVD has the least slope (or decreasing slope with increasing settlement), this is an indication of higher settlement achieved with the use of the PVD.

4.8.2.9 Excess Pore Pressure Development and Dissipation

The locations of the Piezometers in Section A, Section B and Section C were shown in Figures 4.12 to 4.14. It should be noted that the designation PV is used for the vibrating wire piezometers and the symbol PVA means the vibrating wire piezometer PV in Section A. Similarly, the symbol PP means pneumatic piezometer, and thus PPA refers

to the pneumatic piezometer in Section A. Thus the last symbol of each piezometer designation indicates the relevant section in which the piezometer is located. The excess pore pressures were determined along three alignments in Section A. The construction sequence adopted is shown in Figure 4.27 (a). The excess pore pressures as indicated by Piezometers PVA4, PVA10 and PVA 14 are shown in Figure 4.27 (b). These piezometers are located around 5.5m depth and PVA4 is along the centre line of the Section, while PVA10 is along the location XX and PVA 14 is between locations XX and YY. It is noted that the Piezometer PVA4 along the centre line indicates maximum excess pore pressures and this is followed by Piezometer PVA 10 and the least excess pore pressure was indicated by Piezometer PVA 14. These measurements are in accordance with the excess stress at these points due to the embankment loading.

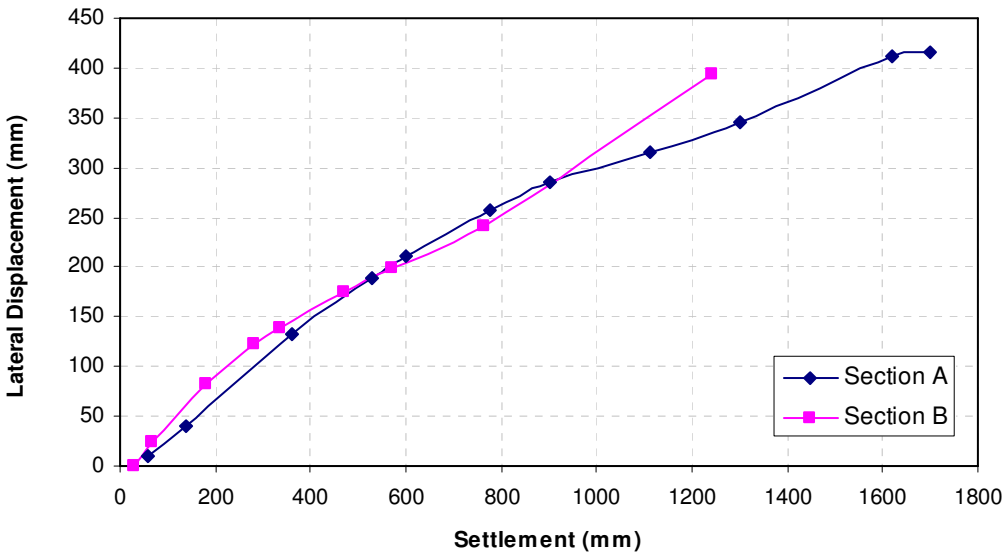

Figure 4.26 Plot of the Maximum Lateral Displacement against the Maximum settlement

For Section B too excess pore pressures are plotted in Figure 4.28(a) along the centre line as indicated by Piezometers PPB21 and PPB23 located at 4.5m and 9.5m depth respectively. Both piezometers indicate similar development of excess pore pressures and also dissipation pattern. Unlike the piezometers in Section A with PVD, the piezometers PPB21 and PPB 23 in Section B with no PVD did not indicate faster

dissipation of excess pore pressures. Similarly Figure 4.28(b) illustrates the excess pore pressures measured by Piezometers PVB30, PPB31, PVB32 and PPB33 which are located between locations XX and YY at depths of 1.5, 4, 7 and 10m respectively. Here again the trend in the development and dissipation of excess pore pressures are in accordance with their depths. At deeper depths lesser excess pore pressures are noted. Figure 4.28(c) indicates the pore pressures around 4.0 to 5m depths in the piezometers located along the centreline, location XX and in between location XX and YY. Here again the excess pore pressures along the centre line are higher than along the other locations close to the berm, though these piezometers are located at more or less the same depths.

For Section C, the excess pore pressures and their dissipation are shown in Figure 4.29(a) and 4.29(b). In Figure 4.29(a), the excess pore pressures as indicated by piezometers PVC39 and PVC40 located at depths of 7m and 10m respectively are shown, while Figure 4.29 (b) give the values indicated by piezometers PVC42 and PVC43 located at 1,5m and 4m depth between locations XX and YY.

The pore pressure dissipation in Section A with closer PVD is faster than the corresponding dissipation in Section C with wider PVD spacing and this again is faster than Section B with no PVD. The minimum acceptable drain spacing as reported elsewhere is also in the range of 1.0 m; this is to prevent excessive smearing effects at very close spacing lesser than 1.0m.

4.8.2.10 Coefficient of Consolidation c_h from Pore Pressure Dissipation

Hansbo (1979) equations (see Chapter 3, Section 3.4) are used to calculate the c_h values from pore pressure dissipation. These c_h values are then compared with the c_h values computed and presented in section 4.3.2.5. The comparison is only made along the

centreline of Section A. These results are included in Table 4.8 and are also presented in Figure 4.30.

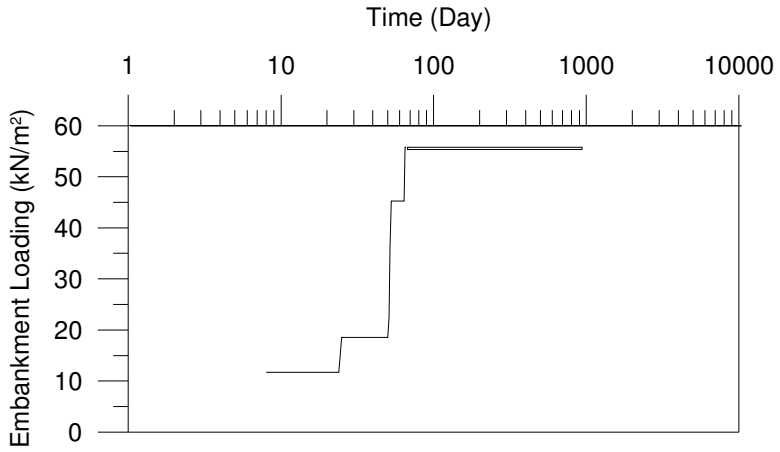

Figure 4.27(a) variation of excess pore pressure with time in Section A - Plot of Embankment Loading with time.

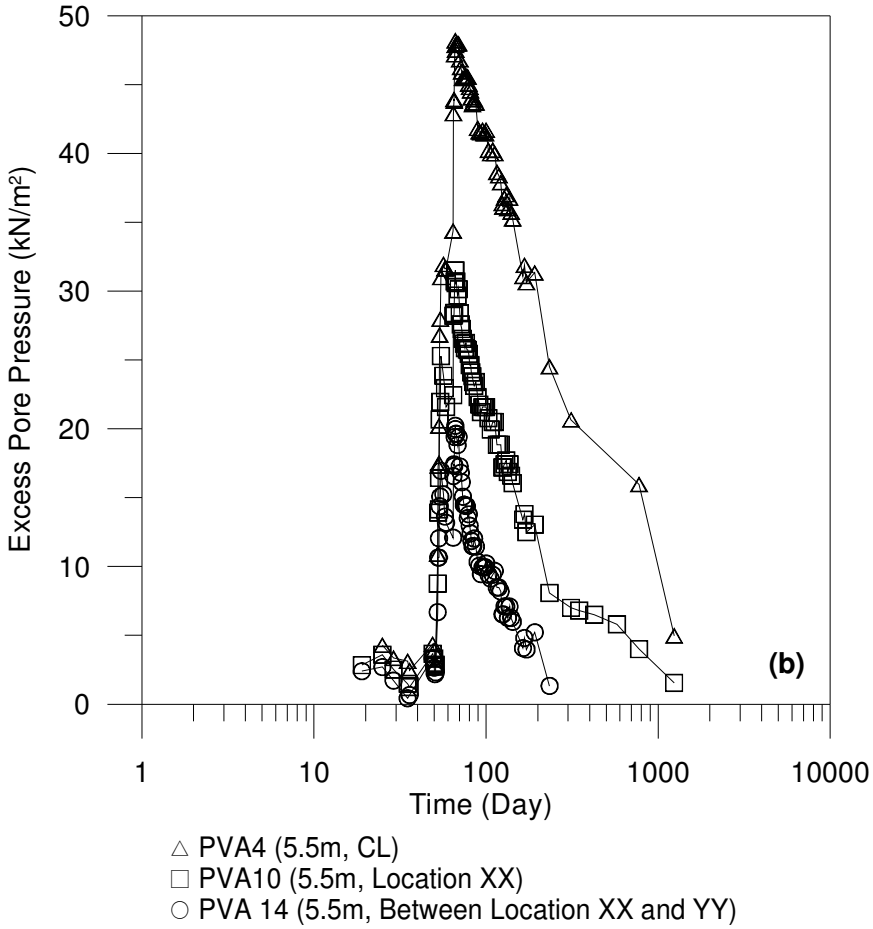

Figure 4.27(b) variation of excess pore pressure with time in Section A - Piezometers PVA4, PVA10 and PVA14.

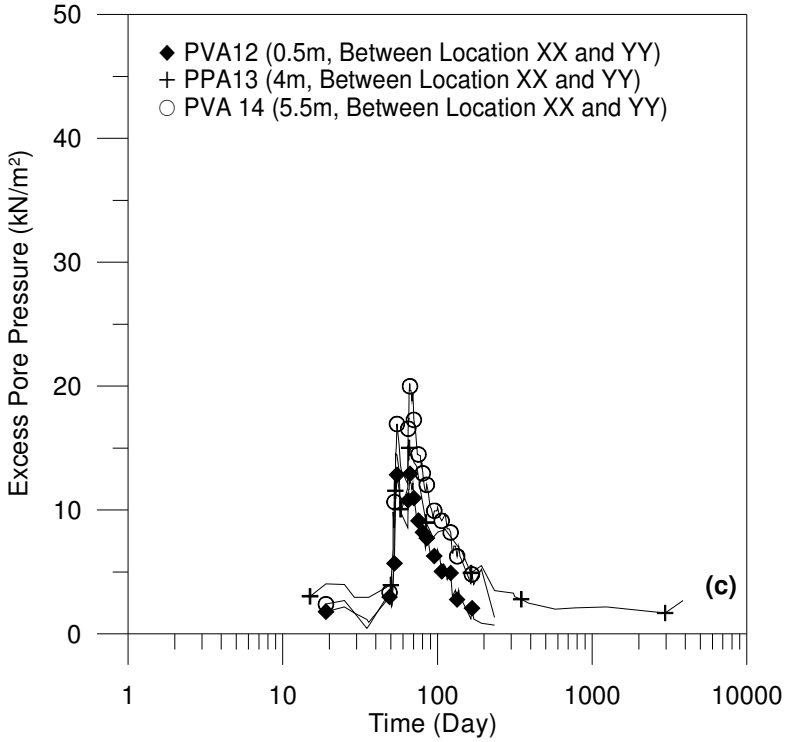

Figure 4.27(c) variation of excess pore pressure with time in Section A - Piezometers PVA12, PPA13 and PVA14

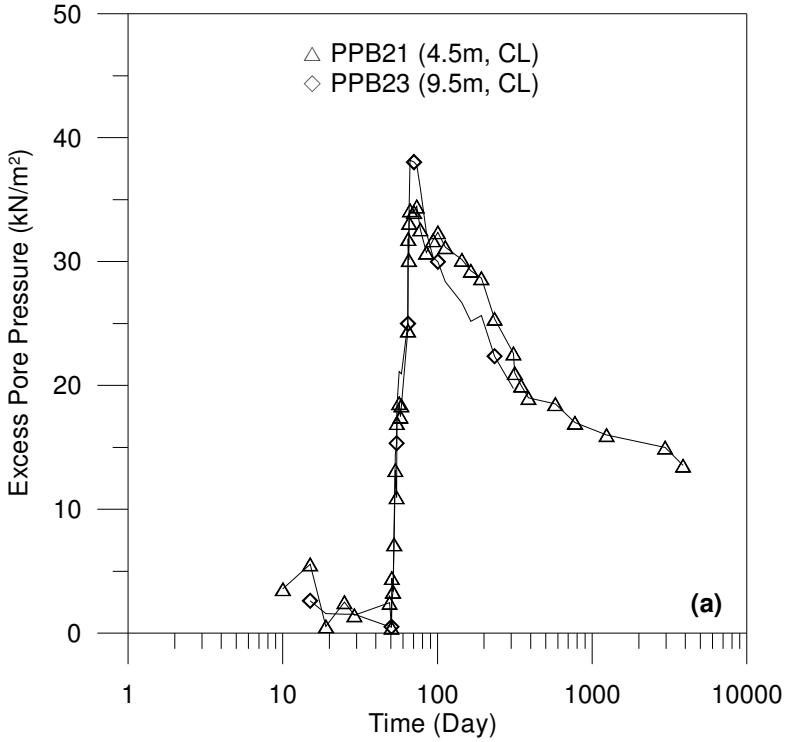

Figure 4.28(a) variation of excess pore pressure with time in Section B - Piezometers PPB21 and PPB23

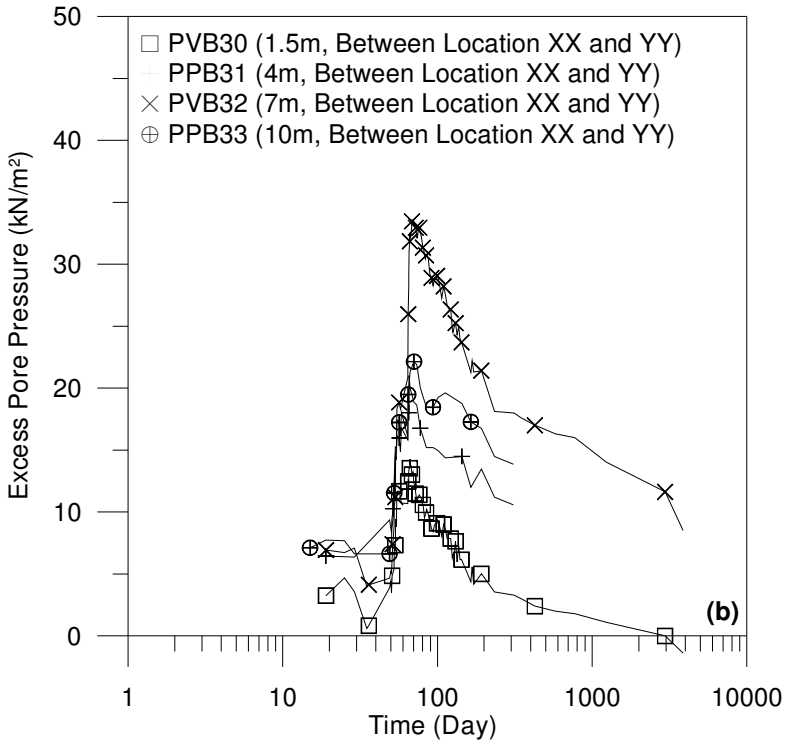

Figure 4.28(b) variation of excess pore pressure with time in Section B - Piezometers PVB30, PPB31, PVB32 and PPB33

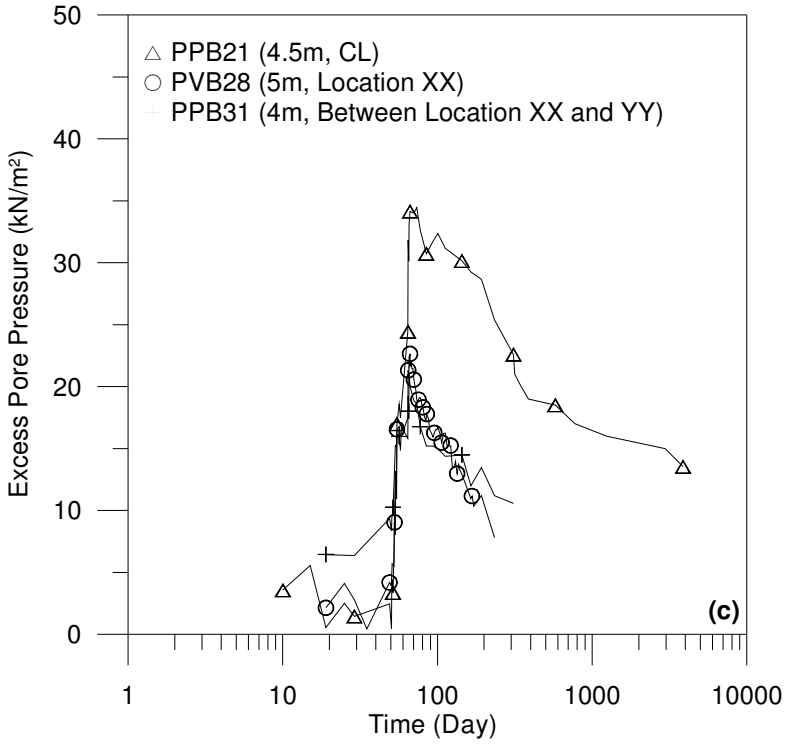

Figure 4.28(c) variation of excess pore pressure with time in Section B - Piezometers PPB21, PVB28 and PPB31

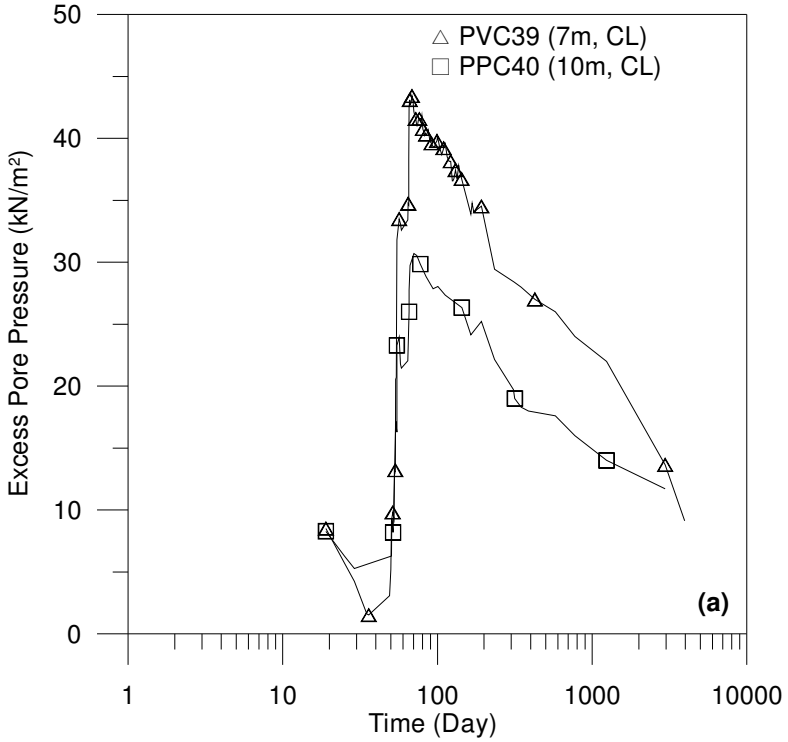

Figure 4.29(a) variation of excess pore pressure with time in Section C - Piezometers PPVC39 and PPC40

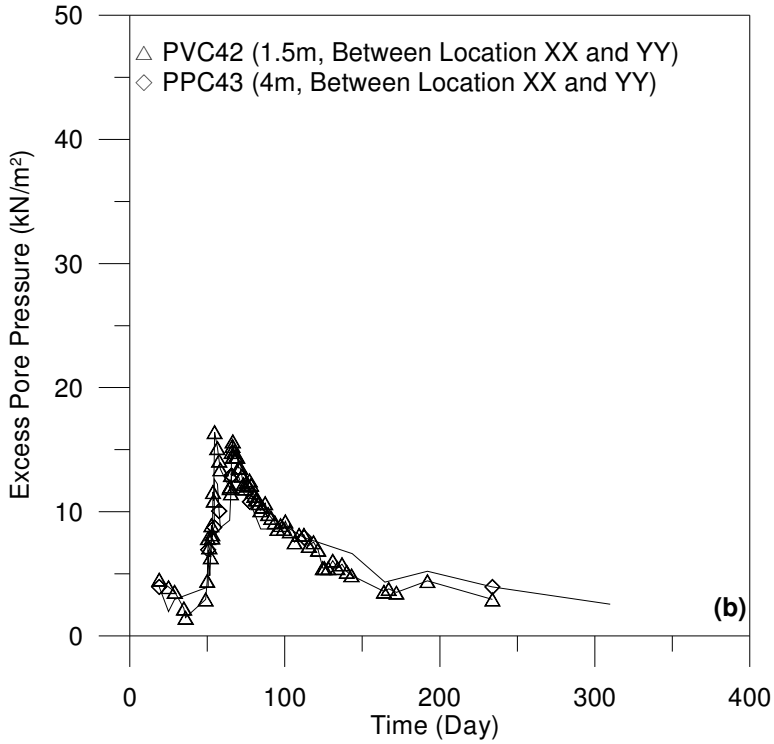

Figure 4.29(b) variation of excess pore pressure with time in Section C - Piezometers PVC42 and PVC43

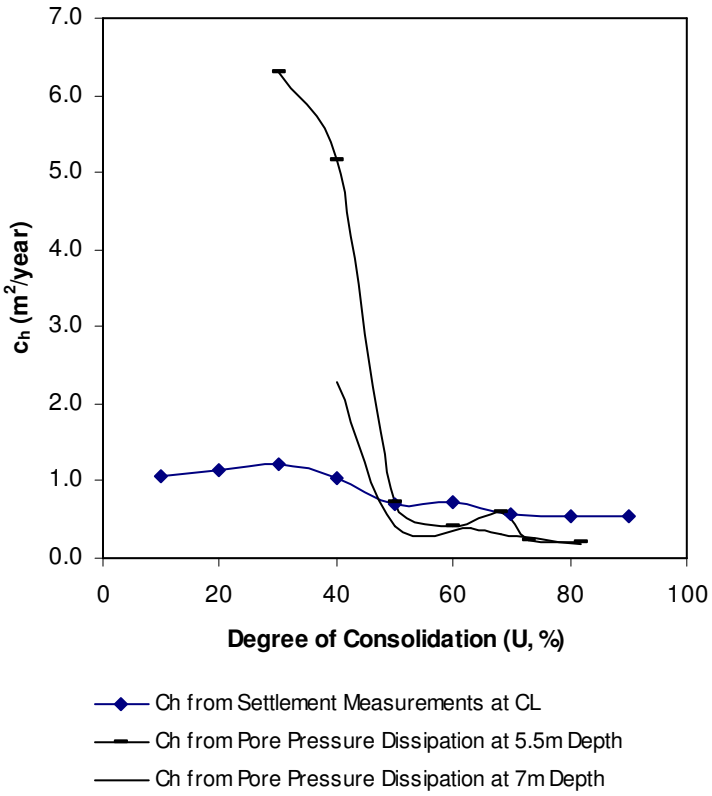

Figure 4.30 Comparison of back-calculated c_h from pore pressure Dissipation and c_h Values back-calculated from Degree of Consolidation (Section A)

Table 4.8 Coefficient of Consolidation, c_h, Back-calculated from Pore Pressure Dissipation (Hansbo's Method, 1979)

Depth (m)	*Time (Day)*	*Degree of Consolidation (%)*	*Coefficient of Consolidation, c_h (m^2/year)*
5.5	30	30	6.30
	50	40	5.16
	100	50	0.73
	130	60	0.42
	192	68	0.59
	234	73	0.24
	312	82	0.22
7.0	30	30	0.33
	50	40	2.28
	100	50	0.41
	143	63	0.38
	192	68	0.32
	310	82	0.18

4.9 Finite Element Analysis

4.9.1 Input parameters

A coupled consolidation analysis was performed using PLAXIS Version 8. The details of this Version of the program are described in Chapter 4, section 4.6. Thus these details will not be repeated here. The soft soil model (SSM) was used to model the soft clay and the Mohr coulomb model (M-C) was used to model the embankment material and sand. For SSM, the effective cohesion $\overline{c}$ was taken as zero and the angle of internal friction $\overline{\phi}$ was taken as 23 degrees. For the embankment material $\overline{c}$ was also zero and $\overline{\phi}$ was 35 degrees. For sand also, $\overline{c}$ is zero and $\overline{\phi}$ is 30 degrees.

SSM also needed values for λ^* and κ^* which are defined as the modified compression and swell indices respectively. The effective Poisson's ratio $\overline{\nu}$ for SSM is 0.33 and for sand is taken as 0.25. The corresponding value for the embankment material is 0.33. The drained modulus for sand is taken as 10,000 kN/m^{2}and for the embankment material as 12,000 kN/m^2. The vertical permeability k_v for soft clay is 0.3 x 10^{-4}m/day. The corresponding value for sand 8x10^{-2}m/day. The horizontal permeability was assumed to be equal to the vertical permeability. The bulk unit weight for soft clay is 15 kN/m^3 and for sand 19kN/m^3. The corresponding value for the embankment material is 20 kN/m^3. The input parameters so described above are tabulated in Table 4.9.

Table 4.9 Input Parameters for Coupled Consolidation Analysis Using PLAXIS

Depth (m)	*Soil Model*	*c' (kN/m^2)*	*ϕ' (^{o})*	*λ^**	*κ^**	*υ'*	*E (kN/m^2)*	*$K_v = K_h$ (10^{-4}m/day)*	*γ_{bulk} (kN/m^3)*
0.0-9.5	SSM	0	23	0.111	0.06	0.33	-	0.3	15
9.5-15.5	M-C	0	30	-	-	0.25	10000	800	19
15.5-20	SSM	0	23	0.111	0.06	0.33	-	0.3	15
Embankment Material	M-C	0	35	-	-	0.33	12000		20

Note: c' = shear strength intercept; E = modulus of elasticity; K_v = vertical permeability; K_h = horizontal permeability; γ_{dry} and γ_{wet} = dry and wet unit weight; ϕ' = effective angle of internal friction; λ^* = modified compression index ($\lambda^* = \lambda/(1+e)$, where λ is the compression index for SSM parameters and e is the void ratio); κ^* = modified swelling index ($\kappa^* = \kappa/(1+e)$, where κ is the swilling index for SSM parameters) υ' = Poisson's ratio. M-C = elastic-perfectly plastic Mohr-Coulomb; SSM = Soft Soil Model

This is the first time, a PLAXIS analysis was conducted on the test embankments in Southeast Queensland. Further refinement is needed for this type of sophisticated analysis and this is recommended as a future research topic. The preliminary results of the Finite Element Analysis using PLAXIS Version 8 for pore pressure dissipation; surface settlements and lateral displacements are presented in the subsequent sections. Also, comparisons are made between the FEM predictions and the field measurements.

The finite element mesh automatically created for section A and Section B by the PLAXIS program is shown in Figure 4.31. The no-flow boundaries adopted are shown in Figure 4.32.

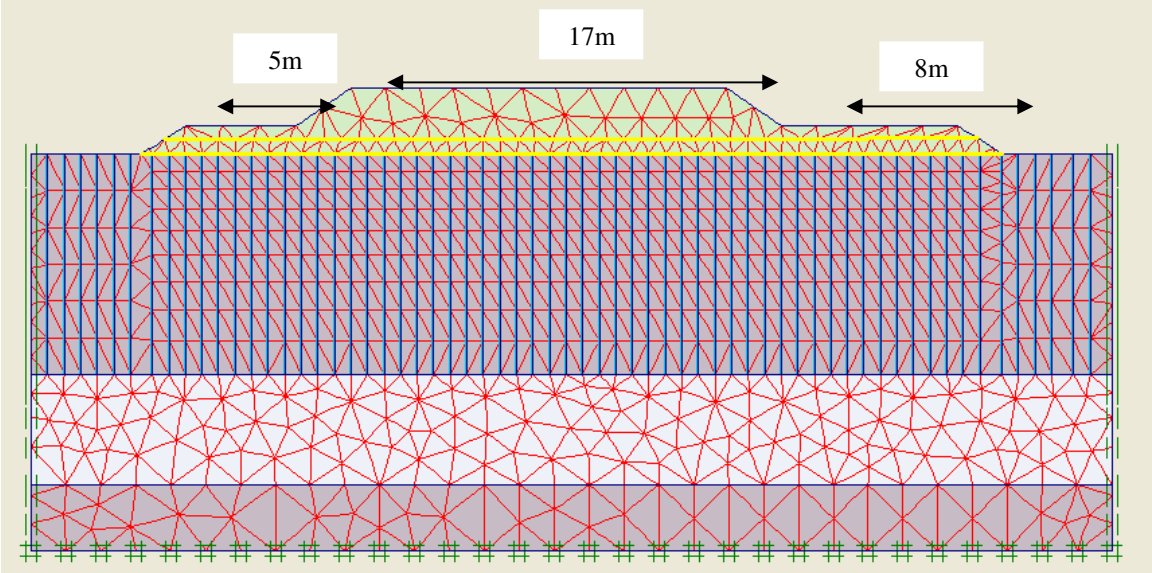

Figure 4.31 Finite Element Mesh Used in PLAXIS Program

4.9.2 Excess Pore Pressure Development and Dissipation

In the in the consolidation analysis using the PLAXIS program, the constant pore pressure boundaries without any lateral dissipation can be specified as closed flow boundaries (no flow of water is allowed across these boundaries). In the analysis of the test embankment 1, the vertical boundaries at both ends for the soft clay layers were assumed to be closed and no flow of water can take place in these boundaries.

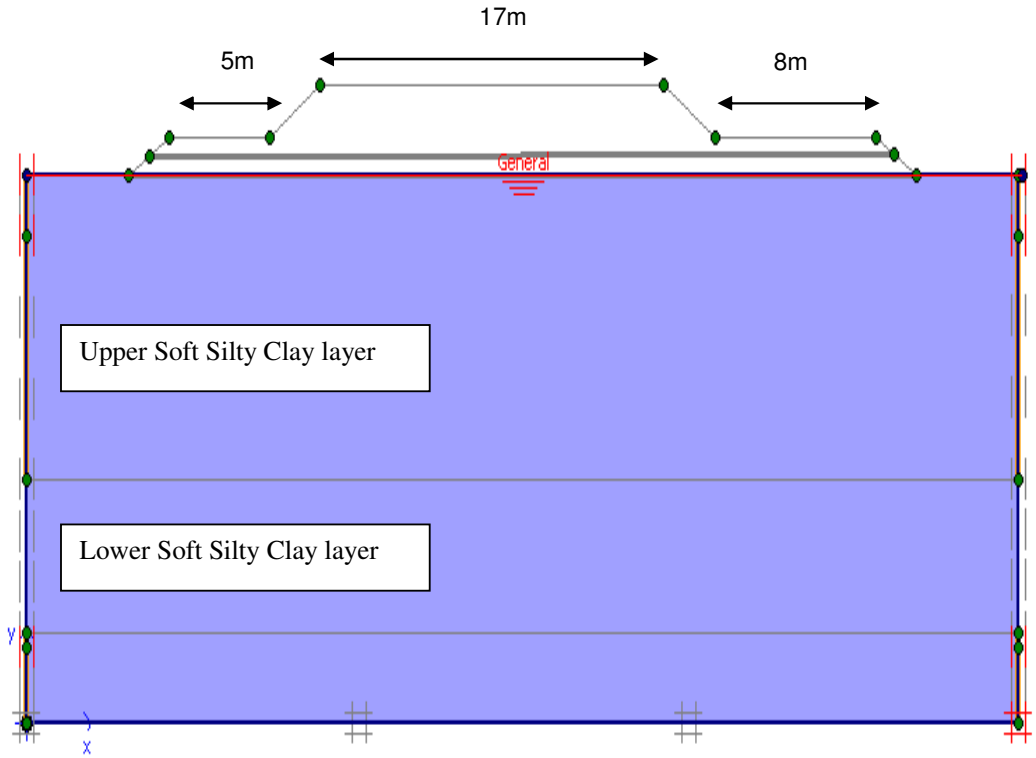

Figure 4.32 No-flow Boundary Conditions in Soft Clay Layers

In the two-dimensional plane strain analysis as carried out here using the PLAXIS Version 8 program, the pore pressure predictions are computed at depths, which are not necessarily at the exact location of the piezometer. As a result, the two-dimensional predictions can deviate to some extent from the measured values, but this deviation is small and can be ignored.

Figure 4.33 shows the predicted excess pore pressures and the measured values for the piezometers along the centre line of Section A at a depth of 4.5m and Section B at 4m respectively. It should be noted that for Section A the agreement of the prediction with the measured values is good, while for Section B the FEA analysis indicate very low dissipation of pore pressure, however, the measured values in the field show substantially higher pore pressure dissipation. This aspect has been discussed before and it was stated that Section A and Section C with PVD were interfering with section B with no PVD. This has resulted in larger consolidation settlement in Section B as well

as greater pore pressure dissipation, than what FEA can predict under idealized conditions. As stated before refined analysis are further recommended, incorporating the findings in this thesis of higher permeability and coefficient of consolidation due to interference of the PVD in Section A and Section C with Section B.

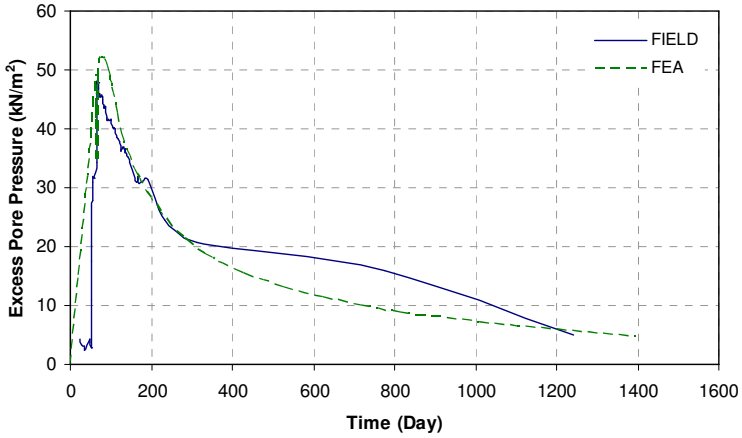

Figure 4.33(a) Comparison of predicted and observed pore pressure variation with time. Piezometer Response in Section A at 4.5m Depth

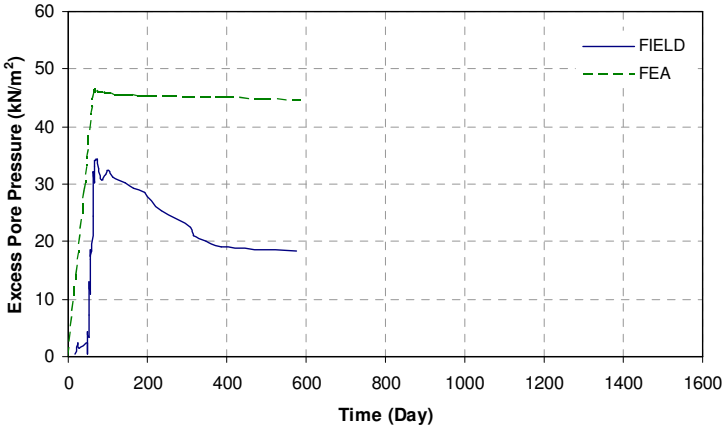

Figure 4.33(b) Comparison of predicted and observed pore pressure variation with time. Piezometer Response in Section B at 4.0m Depth

4.9.3 Settlements

The comparison between the computed values and the measured values of the surface settlements with time along the centreline for Section A and Section B are shown in Figure 4.34. In these figures the computed and measured values are shown up to 2700 days for Section A and only for 500 days for Section B. The field settlement was not recorded for Section B for a longer duration as for Section A. It appears that for the

preliminary analysis presented here, the computed values and the measured values are in good agreement.

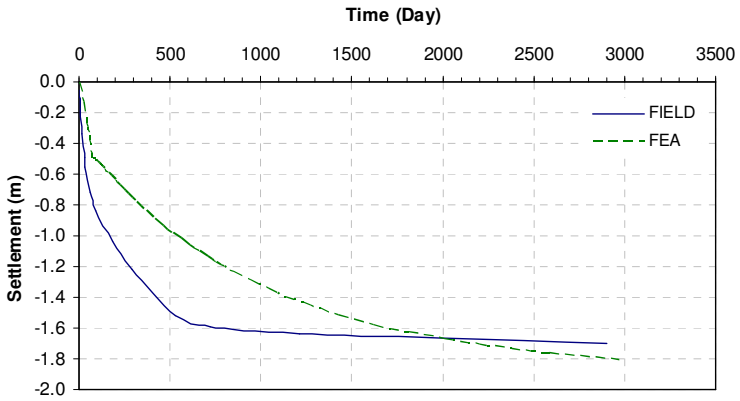

Figure 4.34(a) Observed and predicted surface settlement variation (at the Centreline) with time (Section A)

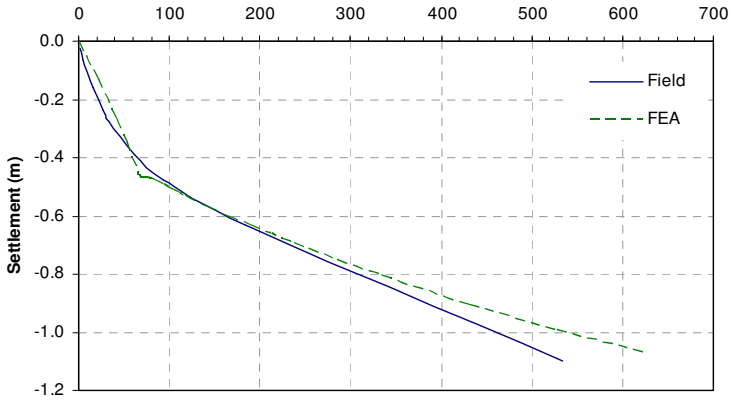

Figure 4.34(b) Observed and predicted surface settlement variation (at the Centreline) with time (Section B)

However extensive interpretations were made in the earlier sections where in it was noted that even for Section A with PVD, 100 percent consolidation was achieved along the centreline and those locations left to the centre line. But for locations right to the centre line for some reason or another, the 100 percent primary consolidation was not achieved. Also for Section B with no PVD, the PVD installed in Section A and Section C have created greater dissipation of pore pressures perhaps due to the presence of horizontal drainage layers through sand and silt seams. These observations are to be noted when subsequent PLAXIS runs are made in future refined research.

4.9.4 Lateral Displacements

One of the major problems of the SSM used in the PLAXIS program is that it cannot model, the undrained or drained creep. Most of the high embankments in soft clays

show continuous increase in the lateral deformation due to undrained creep. Loganathan *et al*. (1993), made a Field Deformation Analysis to incorporate such large undrained creep and its effect in the lateral deformation in test embankments. As such it should be anticipated that the current analysis has severe limitations in predicting continuous increase in lateral movements due to creep. Nevertheless the computed values are compared with the predicted values in Figure 4.35 for Section A. These comparisons are made at locations XX and YY (see Figure 4.12) for varying time intervals. Similar comparisons are made in Figure 4.36 for Section B.

4.10 Stability and Safety Analysis

4.10.1 General

Limit equilibrium analysis using method of slices has been widely used in solving slope stability problems. The main advantage of this method is that the solution can be obtained for the irregular slip surface with complicated cases of boundary loads, embankment configurations and nonhomogeneous foundation soils. Practically, this method is not often used for hand calculation and a computer program is needed.

Moreover, using the PLAXIS software, an alternate method of safety analysis known as Phi-c Reduction, can better estimate the limiting cohesion and angle of internal friction. . The basic approach adopted here is to reduce the soil strength until failure is reached. Thus factor of safety can be obtained from the ratio of the available strength to the strength at failure.

4.10.2 Stability Analysis Using Limit Equilibrium Method

The stability analyses of the embankment (with berms) on soft clay was performed using the limit equilibrium method and the most critical circle at the end of construction (Total Stress Analysis). The in-situ undrained shear strength obtained from vane shear tests (as shown in Table 4.4 and Figure 4.11 were used in the analysis. The unit weight of the soft clay is taken as 15 kN/m^3.

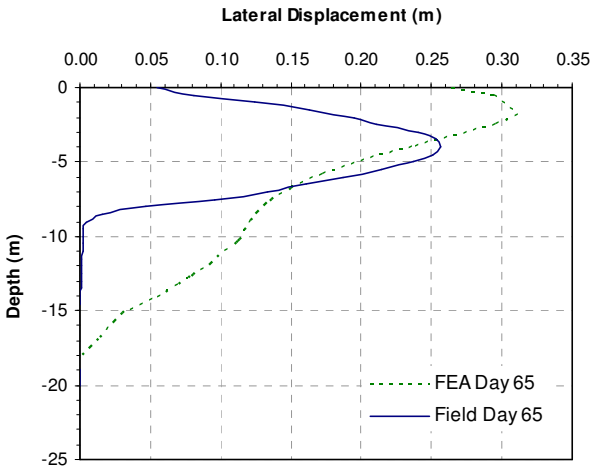

Figure 4.35(a) Comparison of predicted and observed lateral movement with time (Section A at Embankment Toe, Day 65)

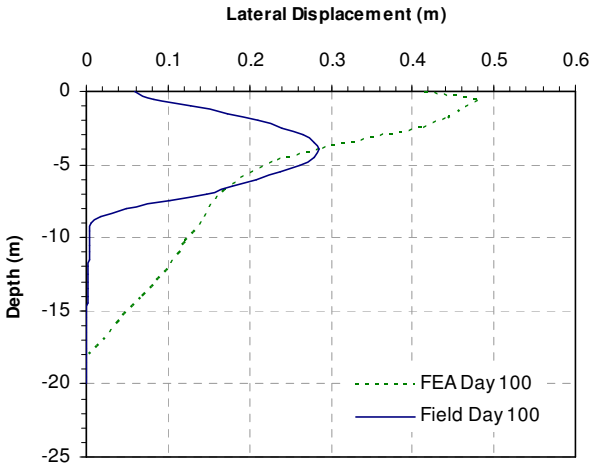

Figure 4.35(b) Comparison of predicted and observed lateral movement with time (Section A at Embankment Toe, Day 100)

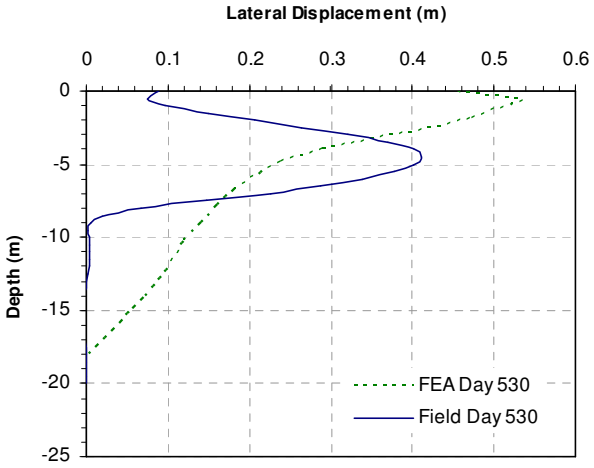

Figure 4.35(c) Comparison of predicted and observed lateral movement with time (Section A at Embankment Toe, Day 530)

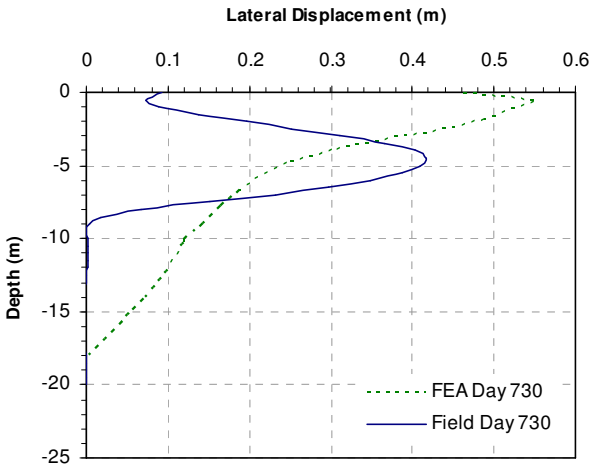

Figure 4.35(d) Comparison of predicted and observed lateral movement with time (Section A at Embankment Toe, Day 730)

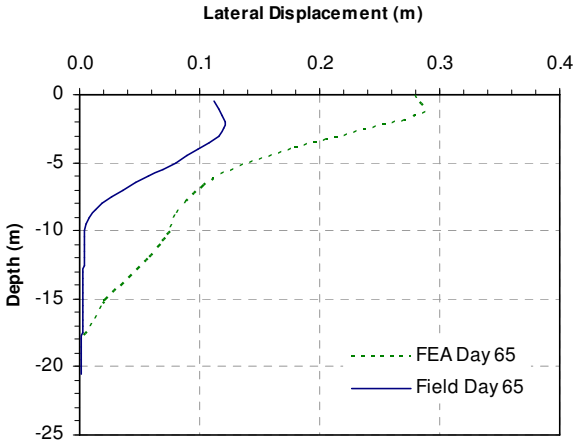

Figure 4.35(e) Comparison of predicted and observed lateral movement with time (Section A at Berm Toe, Day 65)

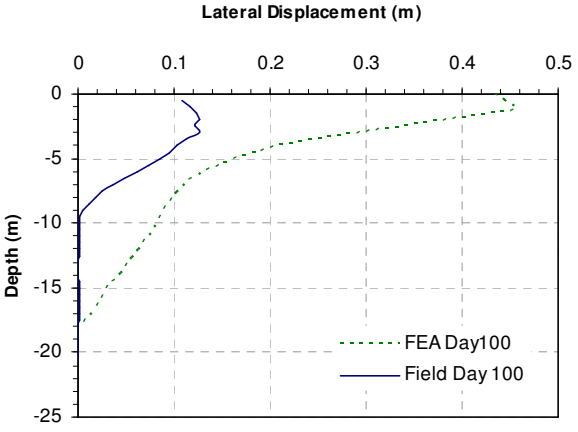

Figure 4.35(f) Comparison of predicted and observed lateral movement with time (Section A at Berm Toe, Day 100)

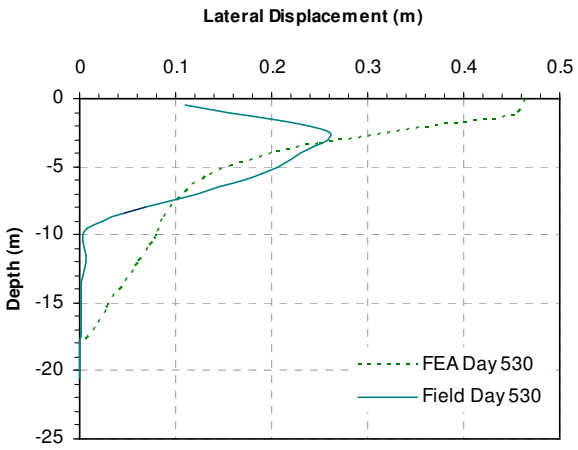

Figure 4.35(g) Comparison of predicted and observed lateral movement with time (Section A at Berm Toe, Day 530)

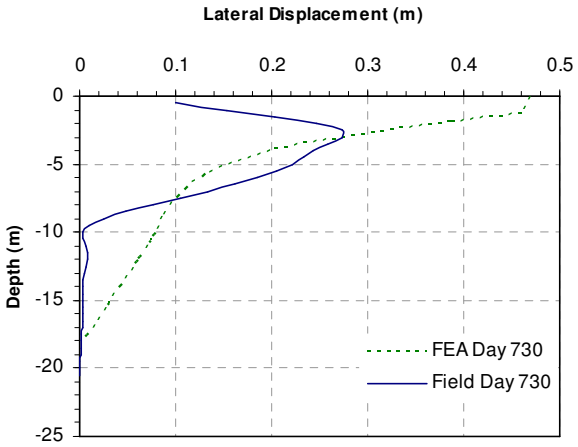

Figure 4.35(h) Comparison of predicted and observed lateral movement with time (Section A at Berm Toe, Day 730)

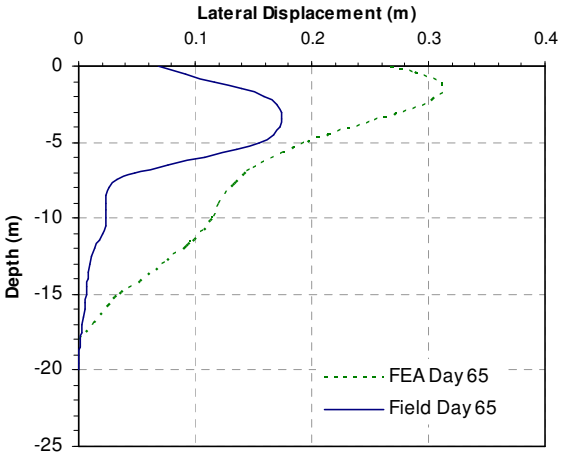

Figure 4.36(a) Comparison of predicted and observed lateral movement with time (Section B at Embankment Toe, Day 65)

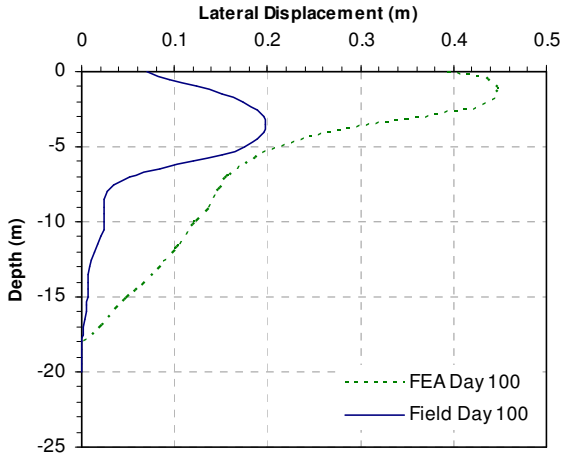

Figure 4.36(b) Comparison of predicted and observed lateral movement with time (Section B at Embankment Toe, Day 100)

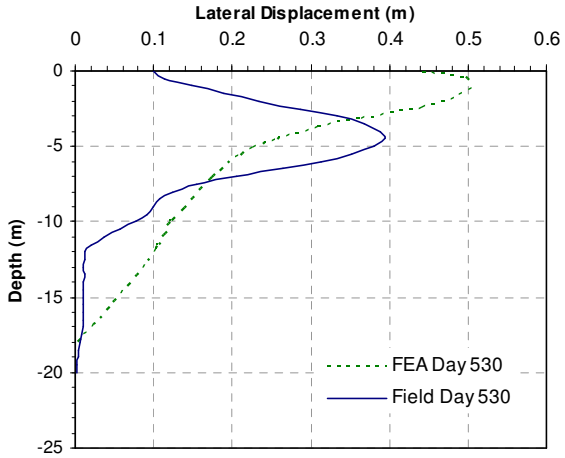

Figure 4.36(c) Comparison of predicted and observed lateral movement with time (Section B at Embankment Toe, Day 530)

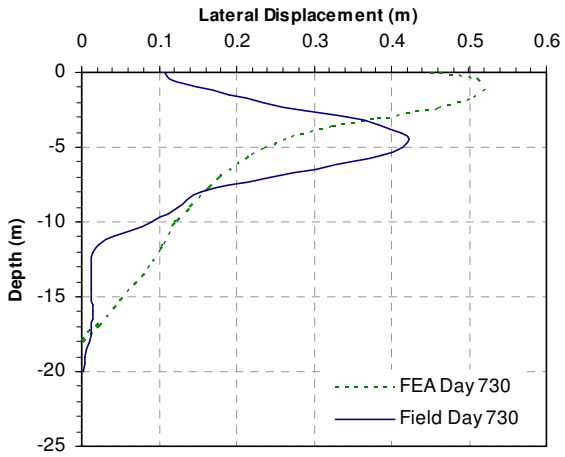

Figure 4.36(d) Comparison of predicted and observed lateral movement with time (Section B at Embankment Toe, Day 730)

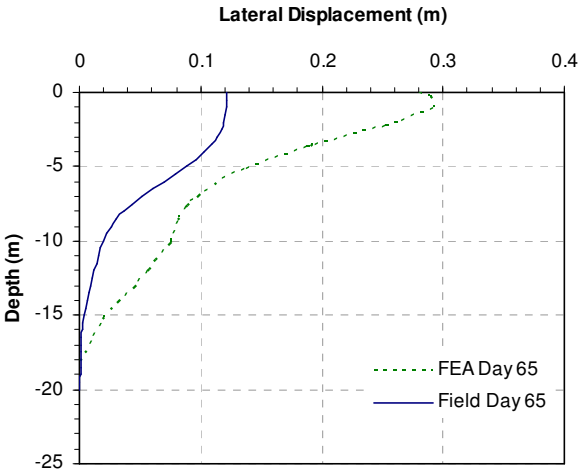

Figure 4.36(e) Comparison of predicted and observed lateral movement with time (Section B at Berm Toe, Day 65)

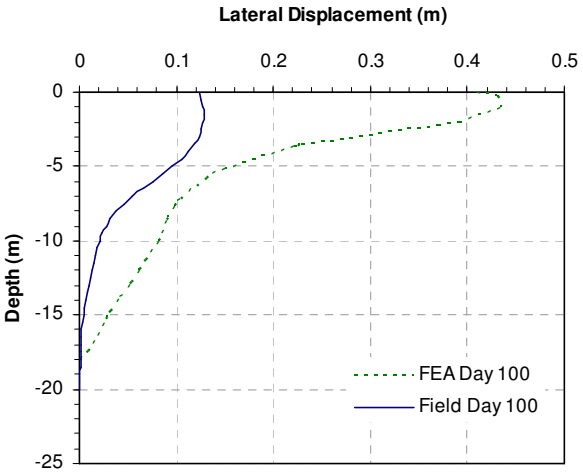

Figure 4.36(f) Comparison of predicted and observed lateral movement with time (Section B at Berm Toe, Day 100)

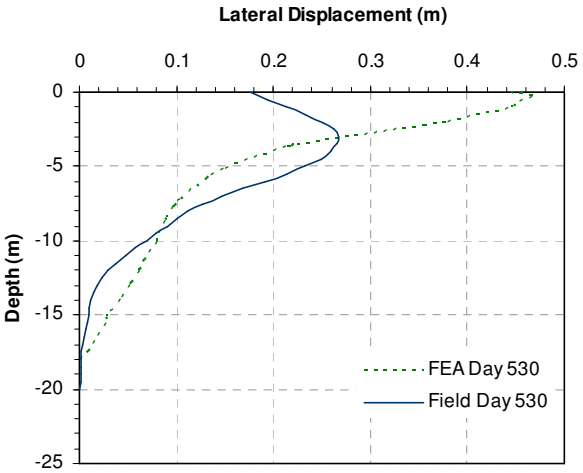

Figure 4.36(g) Comparison of predicted and observed lateral movement with time (Section B at Berm Toe, Day 530)

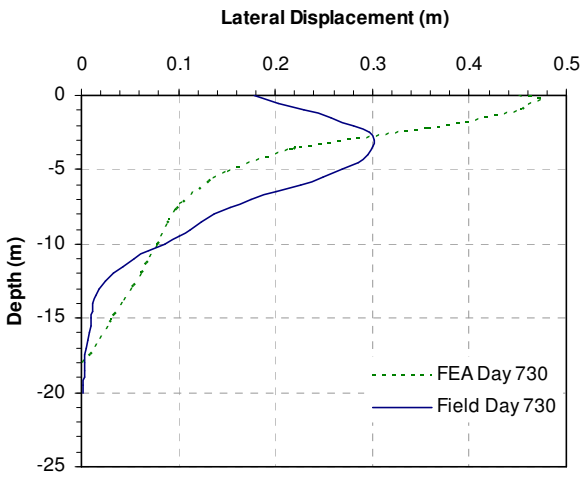

Figure 4.36(h) Comparison of predicted and observed lateral movement with time (Section B at Berm Toe, Day 730)

4.10.3 Safety Analysis (Phi-c Reduction) from PLAXIS

Displacements are generated during a phi-c-reduction calculation. In the factor of safety calculation, the total displacements do not have a physical meaning, but the incremental displacements in the final step (at failure) give an indication of the likely failure mechanism. The factor of safety can be obtained by plotting a curve in which the quantity ΣMsf is plotted against the displacement of a certain node. Σ Msf is defined as the ratio of the available strength to the reduced strength and is controlled by the reduction of tan $\overline{\phi}$ and $\overline{c}$. Plots of ΣMsf against the displacement (see Figure 4.37) represent the calculated factor of safety for Section A and B as 1.53 and 1.50, respectively.

4.11 Concluding Remarks

This chapter is devoted to the interpretation and analysis of the laboratory and field data in Sunshine Coast Motorway, and includes the following sections: (i) Defining the subsoil profile below the test embankment; (ii) Delineating the index properties, unit weight and shear strength of the sub-soils in the test embankment location; (iii) Interpretation of consolidation test data; (iv) Analysis and synthesis of vane strength data close to the test embankment; (v) Interpretation of the settlement records below the

test embankment in the PVD sections (Sections A and C) and no PVD section (Section B); (vi) Interpretation of the excess pore pressure development and dissipation below the test embankment; (vii) Analysis of the lateral deformation profiles below the test embankment; (viii) Compare the observed settlement, pore pressures and lateral movements below the test embankment with those predicted by the PLAXIS analysis using coupled consolidation.

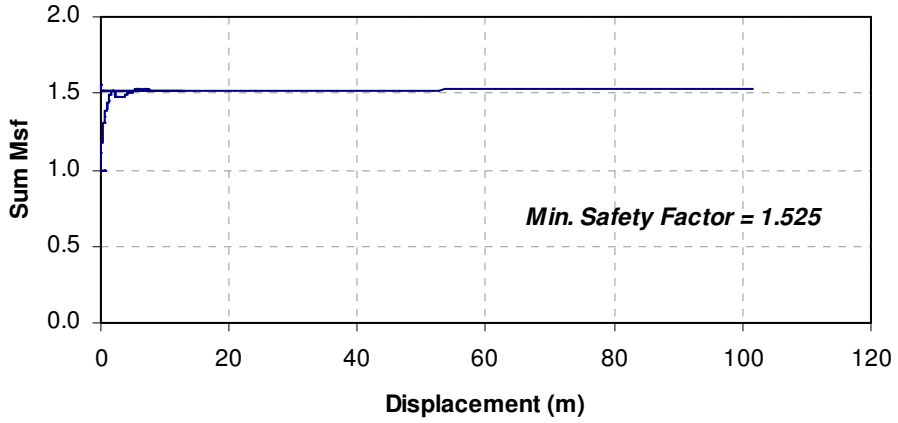

Figure 4.37 (a) Factor of Safety from PLAXIS Analysis, Section A

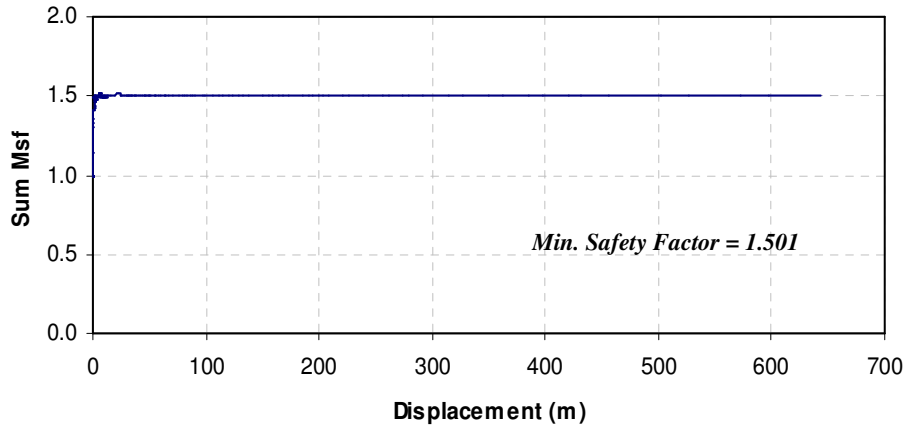

Figure 4.37 (b) Factor of Safety from PLAXIS Analysis, Section B

CHAPTER 5

CASE STUDY 2: PORT OF BRISBANE MOTORWAY EMBANKMENT - ANALYSIS OF LABORATORY AND FIELD TEST DATA

5.1 Introduction

Contained within Chapter 5, is information gathered in order to perform an analysis of the Port of Brisbane Motorway embankment in three parts. The first part of the analysis is related to the soil profile beneath the trial embankment and the results of in-situ and laboratory tests of soil conditions prior to construction. The second part relates to a full description of the motorway embankment and the instrumentation installed beneath at the surface and subsurface of the ground on which the embankments were constructed. This includes instruments installed to measure vertical settlement, lateral deformation and pore-water pressure dissipation below the motorway embankment before, during and after construction. Finally, in the third part, field data were interpreted. Further, the parameters required for performing the computer analysis are obtained and explained for their relevance. The settlement of the embankment will be back-analysed using PLAXIS.

5.2 General

The requirement of a thorough ground investigation in order to build the Port of Brisbane Motorway was necessary due to its location along the side of the Brisbane River. The Brisbane River is known to have problems with silt deposits due to large farming areas in the Darling Downs. Sedimentary erosion of the rich soils in the catchment area have constantly being filling the river with soil. The Brisbane River turns tidal before entering the CBD and winds its way through low lying flood-prone lands into Morton Bay. Over thousands of years the Brisbane River will have changed paths of flow leaving behind large deposits of soft soils. The Port of Brisbane Motorway

is approximately 8 km in length and connects the Gateway Motorway with the Port of Brisbane.

5.3 Soil Profile

5.3.1 Longitudinal Section

The Port of Brisbane Motorway is built over deep layers of highly sensitive soft soils. Figure 5.1 shows a cross section of the motorway with running chainage from CH750 to CH1320 along control line MC10 where deep clay layers were evident problems and where the test embankments are located. In this cross section the natural soil profile to a depth of 40 meters showing the existence of multi stratum sub soil conditions can be seen. Silty clay deposits up to 22 meters in depth are the critical soil layer for this investigation due to their highly compressible nature which poses the embankment construction problem. The silty clay overlies a layer of sand and gravel before reaching a layer of sandstone. The sand and gravel layer is highly compacted and can be assumed to be incompressible. Due to the great depths of the soft soil the properties are likely to change with depth.

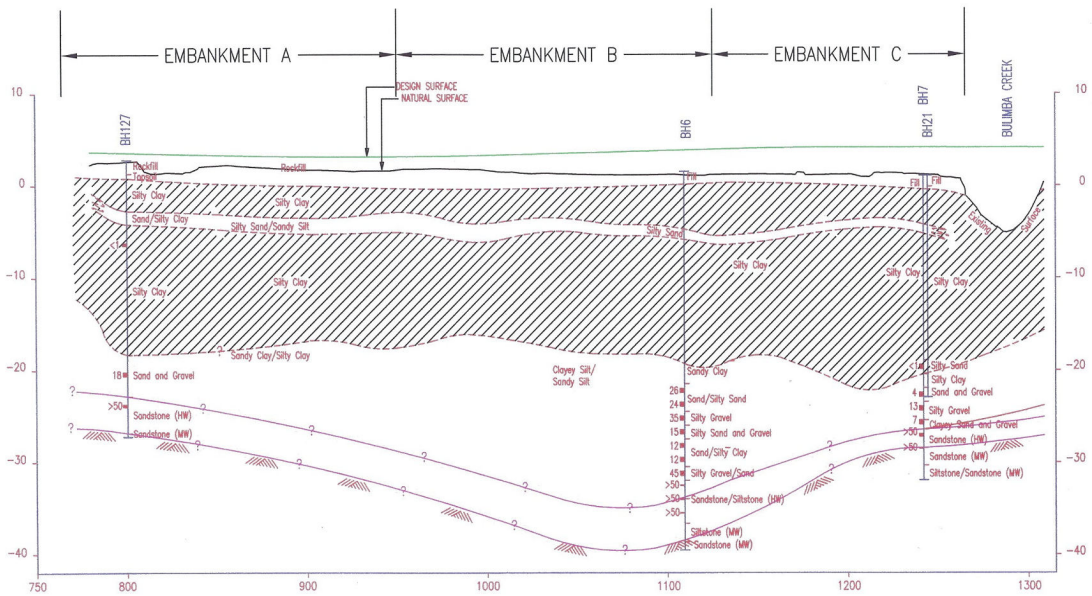

Figure 5.1 Longitudinal Profile of the Port of Brisbane Motorway from CH750 to CH1320.

5.3.2 Index Properties, Unit Weight and Vane Shear Strength

A total of 22 boreholes were drilled along the alignment these were strategically placed at the locations of proposed structures and because of this, boreholes drilled beneath the trial embankments were limited. The relevant boreholes for each embankment are BH127 (CH804) for Embankment A, BH6 (CH1114) for Embankment B and Boreholes BH21 (CH1240), BH7 (CH1244) for Embankment C. The results of the boreholes were presented in Report, R3285 (2002) prepared by QDMR.

From the combined results of BH7 and 21 a good understanding of the soil properties can be obtained with good accuracy. Figure 5.2 shows the laboratory test results for plastic limit (PL), liquid limit (LL), water content, unit weight and from in-situ tests the vane shear strength profile of the soil condition. From Figure 5.2 it can be seen that the plastic limit has a minimum of 22.6 % at a depth of 6.4 meters and a maximum of 39.8 % at a depth of 16.4 meters. The liquid limit varies from a maximum of 66 % at a depth of 12.4 meters to a minimum of 45 % at a depth of 6.4 meters. The water content has a maximum of 81 % at a depth of 2.4 meters and a minimum of 53 % at a depth of 6.4 meters. The high water content at the top of the soil profile suggests that the expected settlement will be also greatest at the top of the soil profile. The minimum unit weight of 15.6 kN/m^3 is at the top of the soil profile depth 2.4 meters where the maximum water content is located and the maximum unit weight of 17.2 kN/m^3 is at a depth of 6.4 meters were the minimum water content occurs. The relationship between the water content and the unit weight can also be seen as water content increases unit weight decreases and as water content decreases unit weight increases. The result of this relationship gives the unit weight curve a mirrored appearance to that of the water content curve.

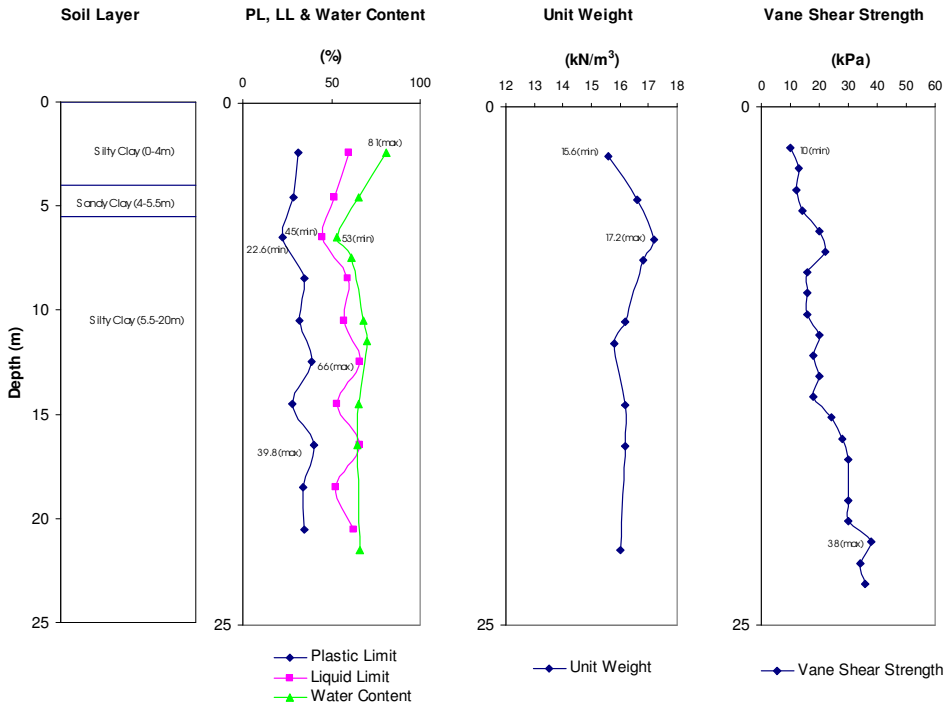

Figure 5.2 Index Properties, Unit Weight and Vane Shear Strength

The in-situ results of the vane shear strength give a minimum value of 10 kPa at a depth of 2 meters and a maximum of 38 kPa at a depth of 21 meters. It can be seen from the curve of vane shear strength that the strength increases with depth this is as expected due to increase in compressive stress with depth of the soil layer.

5.3.3 Ground Water

The ground water level was found to be at a depth of 1 meter for the whole site. This was also seen to remain unchanged for the duration of the construction period.

5.4 Embankment Details

5.4.1 Ground improvement

The variation in ground improvement is the reason the three sections; embankment A, embankment B and embankment C have been selected for analysis. These embankments incorporated 3 separate methods of ground improvement. Section A used sand drains in a triangular pattern with a spacing of 3 meters, Section B had sand drains in a triangular pattern with 1.5 meter spacing and Section C had sand drains in a triangular pattern with

1.5 meter spacing. All sand drains installed were of 66 mm diameter and used well graded sand for optimum efficiency.

5.4.2 Characteristics of the Bulk Earthworks

The characteristics of the material used as bulk earthworks were found to have a bulk density $\gamma_{Bulk} = 20$ kN/m^2. Along with the unit weight of the embankment material used the Poisson's ratio, $v = 0.3$, Young's Modulus, $E = 7.5$ MPa, the cohesion, $c = 13.5$ kN/m^2, and the friction angle, $\phi = 35$ degrees, were also obtained.

5.4.3 Dimensions and location

The dimensions and location of the three motorway embankment can be seen in Figure 5.3. Embankment A was 160 meters in length starting at CH790 and finishing at CH950. Embankment B is in between embankment A and embankment C and is 184 meters in length finishing at CH1134. Embankment C is 104 meters in length starting from embankment B and finishing at CH1238. The width of the motorway varies from 32 meters in width to 26 meters in width for the stretches of straight road. Embankment A starts at the location of turning point for the road network which required the embankment is to be wider than the other embankments. All three trial embankments were built with 1:2 battered sides.

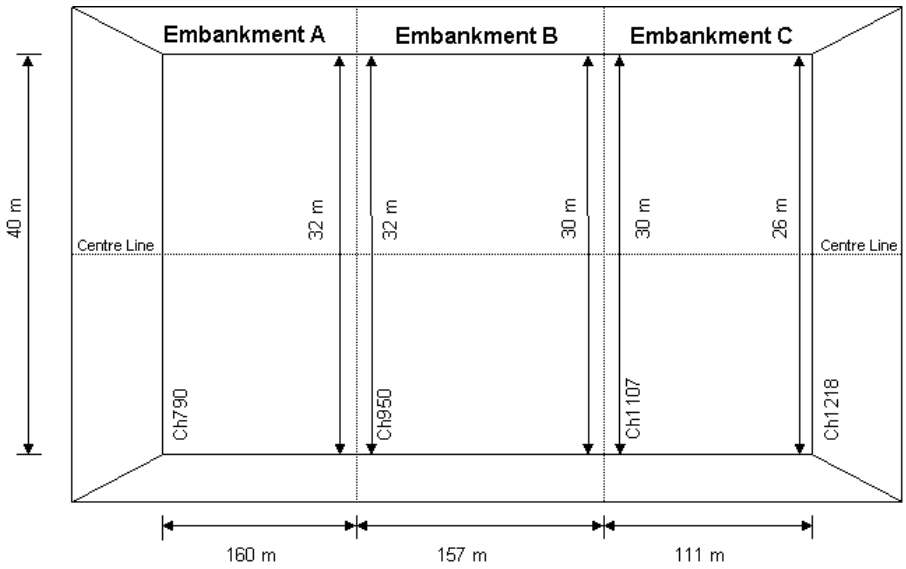

Figure 5.3 Locations and dimensions of trial embankment A, B and C

5.4.4 Construction Sequence

The construction sequence for each embankment section is illustrated in Figure 5.4. The embankment reduced level (RL) readings were taken at similar intervals to the instrument readings and at varying chainages for each trial embankment. Because the trial embankments are unusually long in length, ranging from 111 meters for embankment C to 160 meters for embankment A, the construction schedule varied from one point in a trial embankment to another. Averaging of the construction schedule can be assumed an accurate assumption for the entire embankment as overall variations to the construction schedule of each trial embankment were only minor when compared to the average.

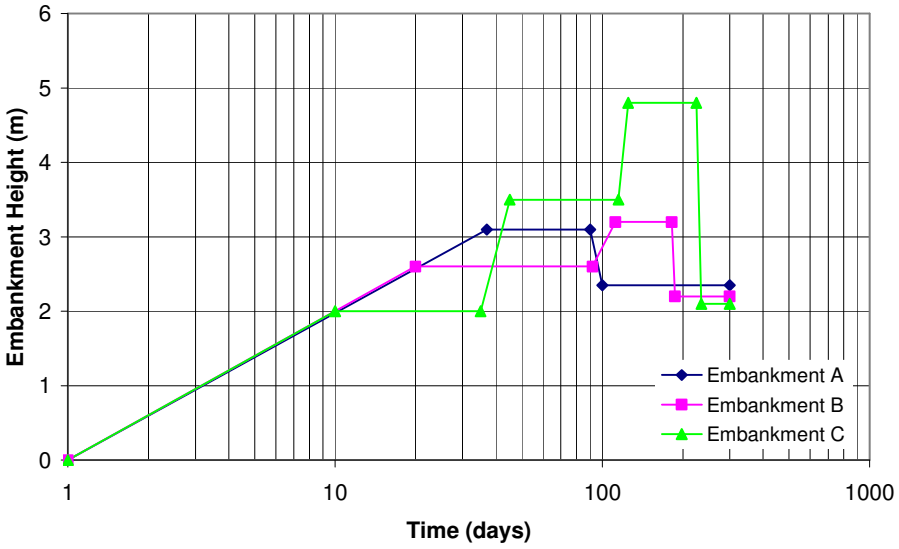

Figure 5.4 Embankment construction sequence

It can be seen from Figure 5.4 that the schedule varies for each embankment. The height to which an embankment can be built depends on the foundation soil parameters. Settlement of the soil layer results in an increase in the strength of the soil layer allowing for a further increase to the height of the embankment.

From Figure 5.4 it can be seen that the construction of embankment A was in one stage the embankment was built to a height of 3.1 meters in 37 days. Embankment B was built in two stages the first stage of construction was to a height of 2.6 meters in 20 days,

after allowing the embankment to settle for 72 days stage two increased the height to 3.2 meters in a further 20 days. Embankment C was the most complicated of the three construction schedules and consisted of 3 stages of construction. The first stage was to build to a height of 2 meters in 10 days followed by 25 days of allowing the embankment to settle. The construction then continued to a height of 3.5 meters in 10 days and once again the embankment was allowed to settle for a further 70 days until the final stage of construction finally reaching a height of 4.8 meters in a further 10 days.

5.5 Field Instruments

Figures 5.5 to 5.7 show the cross-section of each trial embankment and location of the instruments installed to monitor the vertical deformation, lateral deformation and pore-water dissipation. Table 5.1 gives a summary of the instruments contained with in the three trial embankments.

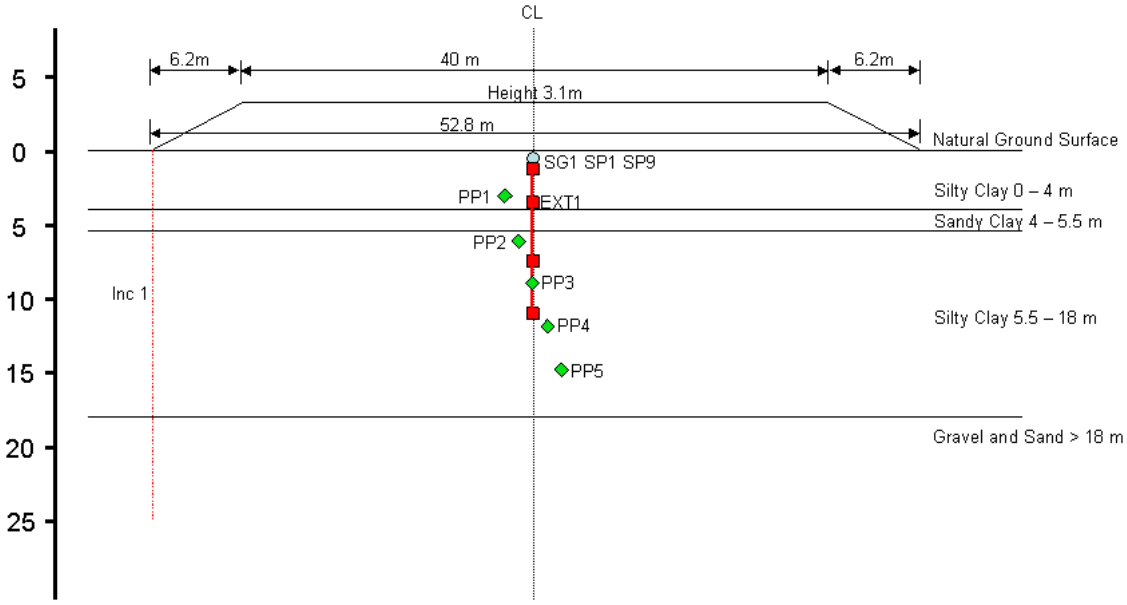

Figure 5.5 Embankment A CH790 –CH950: Cross Section Showing Instrumentation

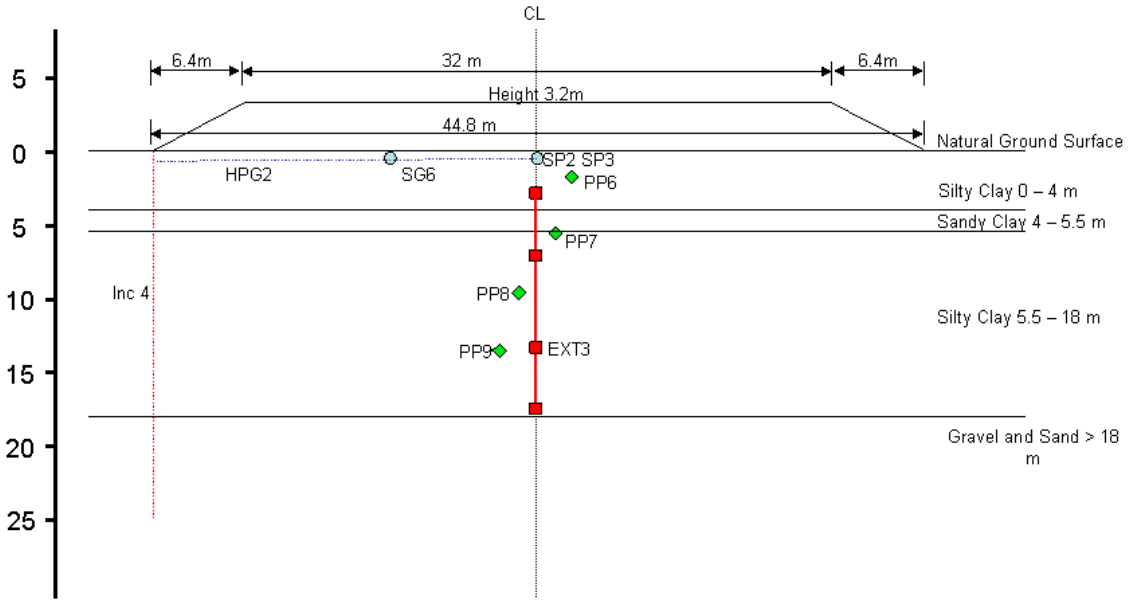

Figure 5.6 Embankment B CH950 – CH1107: Cross Section Showing Instrumentation

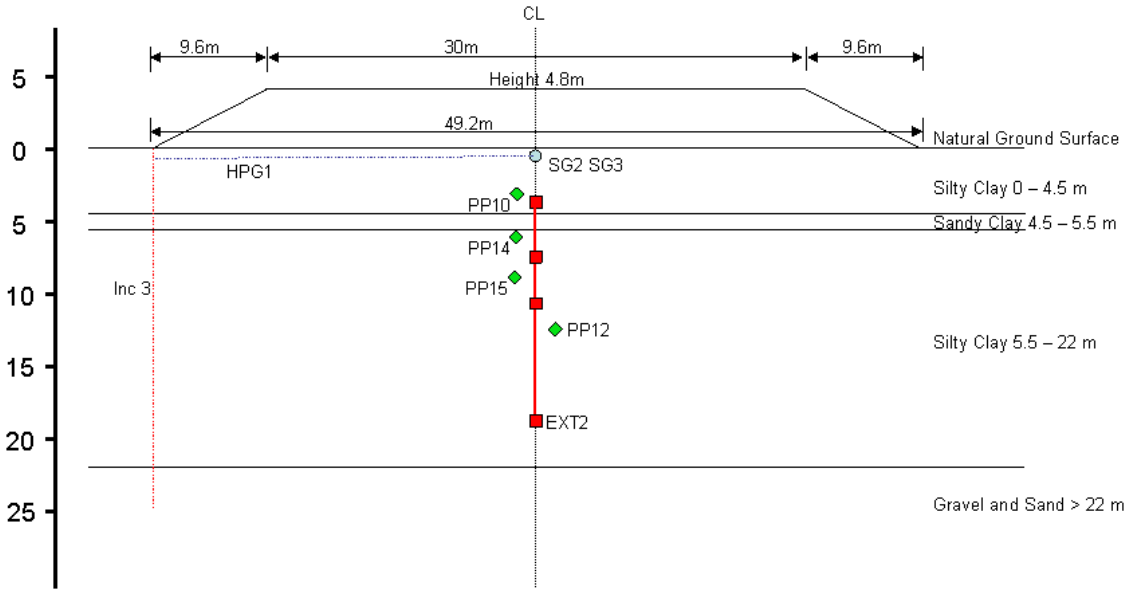

Figure 5.7 Embankment C CH1107 CH1218: Cross Section Showing Instrumentation

Table 5.1 Embankment Instrumentation

Instrument Type	Number of Instruments			
	Embankment A	Embankment B	Embankment C	Total
Inclinometer (INC)	1	1	1	3
Horizontal Profile Gauge (HPG)	0	1	1	2
Settlement Gauge (SG)	1	1	2	4
Settlement Plate (SP)	2	2	0	4
Extensometer (EXT)	1	1	1	3
Pneumatic Piezometer (PP)	5	4	4	13

5.5.1 Vertical Deformation

Many instruments incorporated in the Port of Brisbane Motorway were used to monitor the vertical settlement of the soil layer induced by the trial embankments. The instruments include; settlement plates, settlement gauges, horizontal profile gauges and extensometer magnets. All three trial embankments had settlement plates or settlement gauges installed at the surface of the soil layer. Horizontal profile gauges were only installed at the surface of the soil layer for embankments B and C. Embankment A had no horizontal profile gauge installed. The extensometer magnets were installed to measure the vertical settlement at varying depths beneath the centre line of each embankment.

5.5.2 Horizontal Deformation

Borehole inclinometers were incorporated to measure the horizontal deformation of the soil layer due to initial settlement. Borehole casings were installed at the toe of all three trial embankments. The inclinometer is lowered into the borehole casing and gives readings about a parallel axis and a perpendicular axis to the trial embankment. It is the perpendicular axis that is of importance as this is the axis that measures horizontal deformation.

5.5.3 Porewater Dissipation

Excess pore-water pressure created from the constructed trial embankment caused the water to flow from areas of high pressure to low pressure. This dissipation of the pore-water was monitored by the use of piezometers. The Port of Brisbane Motorway installed pneumeric piezometers at varying location and depths within each of the three trial embankments.

5.6 Analysis of Laboratory and Field Vane Shear Tests

Queensland Department of Main Roads (QDMR) conducted consolidation tests on samples extracted from various boreholes for varying depths with in the soil layer. The consolidation test data were used to obtain the consolidation parameters; compression index, coefficient of compressibility, coefficient of volume change, constrained modulus and coefficient of consolidation when varying levels of pressure were applied. QDMR also conducted in-situ undrained shear strength tests by the use of piezocone penetrometers (PCP's). From the results of the PCP tests varying values of the shear strength with depth were obtained. These results are also important in understanding the strengths of the soil and the extent to which the soft soil's (low strength) extended. The field vane shear tests are presented in Figure 5.2.

5.6.1 Analysis of Laboratory Consolidation Test Data

As mentioned previously, the analysis of laboratory data was conducted from boreholes taken closest to the centreline for each trial embankment. The location of each borehole can be seen in the longitudinal cross section of the Port of Brisbane Motorway in Figure 5.1.

For Embankment A from borehole BH127 at CH804, two series of consolidation tests were analysed for samples taken from depths of 3 meters and 6 meters respectively. For Embankment B from BH6 at CH1114, three series of consolidation tests were analysed for samples taken at depths of 5-5.4 meters, 10-10.4 meters and 15-15.4 meters respectively. For Embankment C from boreholes BH7 (CH1240) and BH21 (CH1244) the consolidation test data was analysed. From BH7 two series of consolidation tests were analysed with the samples taken at depths of 2.5-2.9 meters and 5.5-5.9 meters respectively, From BH21 four series of consolidation tests were analysed with the

samples taken at depths of 6-6.4 meters, 11-11.4 meters, 16-16.4 meters and 21-21.4 meters respectively.

From the relationship of voids ratio to average pressure, values of the consolidation parameters; compression index, C_c, coefficient of compressibility, a_v, coefficient of volume change, m_v, constrained modulus, D and coefficient of consolidation, c_v, were established.

For Embankment A the results at a depth of 6 meters exhibited the highest compressibility thus having the lowest strength properties. For Embankments B and C the same is true at depths of 5-5.4 meters and 5.5-5.9 meters respectively. Embankment C also shows signs of high compressibility at 21-21.4 meters depth.

5.6.2 Over Consolidated Ratio

The over consolidated ratio (OCR) is the maximum value of effective stress the soil has been subject to in the past divided by the present value of effective stress the soil is subject to. Craig (1999) explained that the relationship between voids ratio and effective stress depends on the stress history of the soil. If the present effective stress is the maximum to which the soil has ever been subjected, the soil is said to be normally consolidated. If on the other hand, the effective stress at some time in the past has been greater than the present value, the soil is said to be over consolidated.

By combined use of boreholes 7 and 21 the profile of the, over consolidated ratio of the soil was obtained. As can be seen in Figure 5.8, the soil had the highest over consolidated ratio of 2.48 at a depth of 2.5 meters. The minimum over consolidated ratio of 1.28 occurred at a depth of 6 meters. The voids ratio was plotted against pressure to obtain the values for the past pressure.

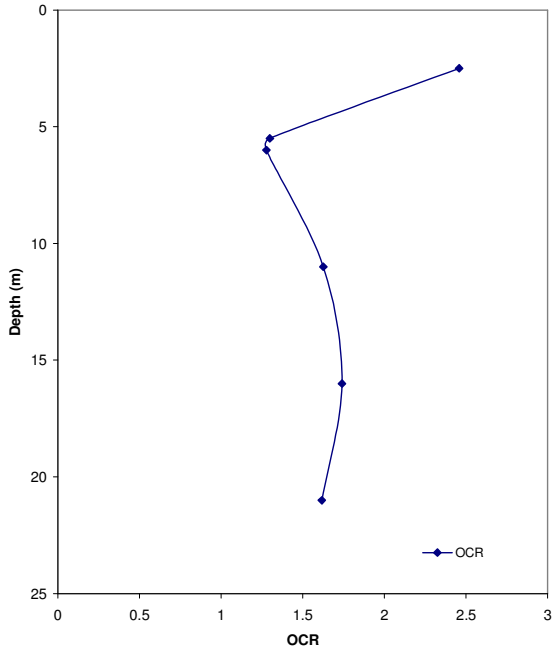

Figure 5.8 Variation in Over Consolidated Ratio (OCR) with Depth

5.6.3 Vane Shear Strength

Numerous piezocone penetrometer (PCP) tests were carried out at the site of the Port of Brisbane Motorway. The PCP closest to the centreline of each embankment was selected for analysis. For Embankment A PCP201 at CH915 was analysed, for Embankment B PCP203 at CH990 was analysed and for Embankment C PCP207 at CH1220 was analysed. The variations of undrained shear strength (obtained from field vane tests) with depth for each embankment can be seen in Figures 5.9(a) to 5.9(c).

For all three trial embankments the founding soft soil's shear strength increased gradually with depth to a maximum value of 50 kPa. From the results of the PCP tests it should be noted that for all three embankments the founding soil shear strength once past 50 kPa increased dramatically almost instantaneously. This increase in strength properties suggests a change in the soil stratum indicating the end of the soft soil layer and was therefore not included in Figure 5.9. The depths of the soft soils were shown to extend 21, 20 and 22 meters for Embankments A, B and C respectively. This is as

expected in Embankment B and C however in Embankment A the depth of soft soil was not expected to extend to depths greater than 20 meters.

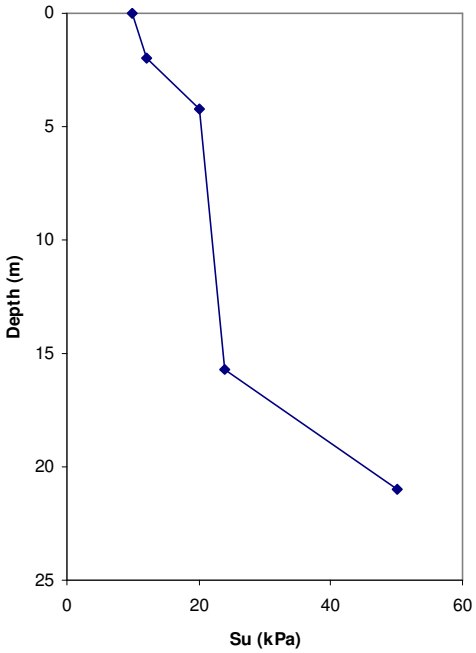

Figure 5.9(a) Variation of Undrained Shear Strength (Field Vane test) with depth (Embankment A)

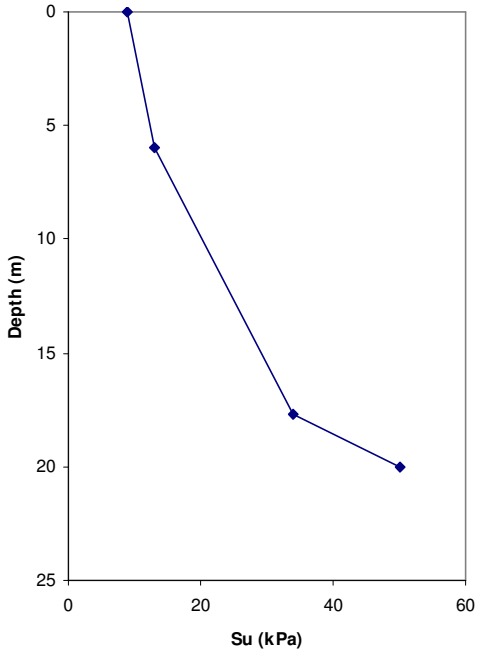

Figure 5.9(b) Variation of Undrained Shear Strength (Field Vane test) with depth (Embankment B)

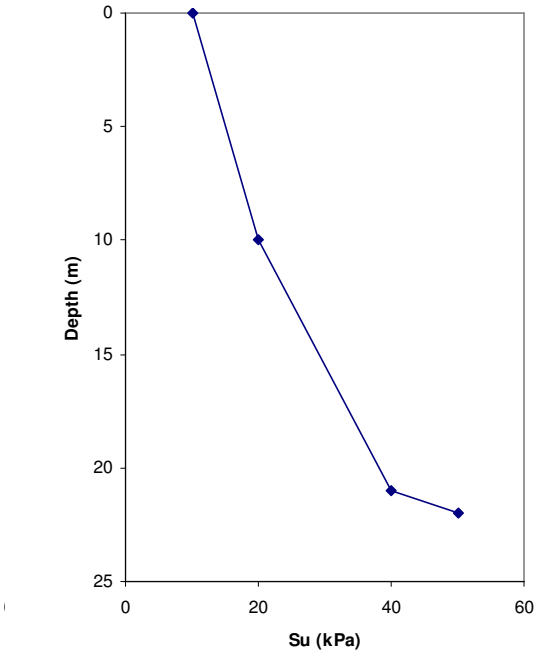

Figure 5.9(c) Variation of Undrained Shear Strength (Field Vane test) with depth (Embankment C)

5.7 Field Deformation Analysis

The results of constant monitoring of field instruments by the QDMR were presented in the geotechnical reports provided. The information collected by the QDMR has been systematically sorted and entered into spreadsheets by the author for analysis. Analysis is made on the vertical deformation (settlement), horizontal deformation and porewater dissipation that occurred due to the construction of the trial embankments.

5.7.1 Vertical Deformation

From the settlement gauges, settlement plates, extensometer magnets and horizontal profile gauges installed within each of the embankment sections, suitable values of the coefficient of consolidation (c_v) were obtained using Taylor's method of consolidation. The procedure and methodology behind Taylor's method of consolidation is explained in Chapter 3. Tables 5.2 - 5.4 show the location of each instrument with in its embankment and the corresponding c_v value obtained.

Table 5.2 Obtained Values of Coefficient of Consolidation for Embankment A

Embankment A CH790-CH950				
Instrumentation	Chainage	Depth of installation (m)	t_{90} (days)	c_v (m^2/year)
Settlement Gauge 1	796	0	61	11.44
Settlement Plate 1	890	0	63	11.02
Settlement Plate 9	940	0	56	12.38
Extensometer 1 Magnet 2	793	12.23	104	6.69
Extensometer 1 Magnet 3	793	7.41	104	6.69
Extensometer 1 Magnet 4	793	3.38	96	7.25
Extensometer 1 Magnet 5	793	0.5	86	8.41

Table 5.3 Obtained Values of Coefficient of Consolidation for Embankment B

Embankment B CH950-CH1107				
Instrumentation	Chainage	Depth of installation (m)	t_{90} (days)	c_v (m^2/year)
Settlement Gauge 6	1078	0	196	0.82
Settlement Plate 2	990	0	64	2.72
Settlement Plate 3	1070	0	79	2.20
Extensometer 3 Magnet 6	1040	3.11	60	2.86
HPG2 Location AA	1040	0	195	0.89
HPG2 Location BB	1040	0	196	0.86
HPG2 Location DD	1040	0	204	0.85

Table 5.4 Obtained Values of Coefficient of Consolidation for Embankment C

Embankment C CH1107-CH1218				
Instrumentation	Chainage	Depth of installation (m)	t_{90} (days)	c_v (m^2/year)
Settlement Gauge 2	1175	0	59	2.98
Settlement Gauge 3	1114	0	77	2.25
Extensometer 2 Magnet 3	1210	7.65	61	2.86
Extensometer 2 Magnet 4	1210	3.91	67	2.59
HPG1 Location AA	1210	0	47	3.66
HPG1 Location CC	1210	0	84	2.06
HPG1 Location DD	1210	0	112	1.55

Tables 5.2 - 5.4 clearly shows that the results for the coefficient of consolidation obtained from beneath Embankment A are considerably higher than those of Embankments B and C. This is due to the spacing of the vertical drains installed within the embankment, Embankment A had drains at 3 meter spacing and Embankments B and C had drains at 1.5 meter spacings. However, Embankment A seemed to settle at the same rate as Embankments B and C.

A comparison is also made between results from the settlement gauges and plates on the settlement that occurred with in each of the three trial embankments. In Figures 5.10 to

5.12, it can be seen that a quality correlation between reading for settlement and rate of settlement occurs within each of the trial embankments for varying locations along the longitudinal chainage.

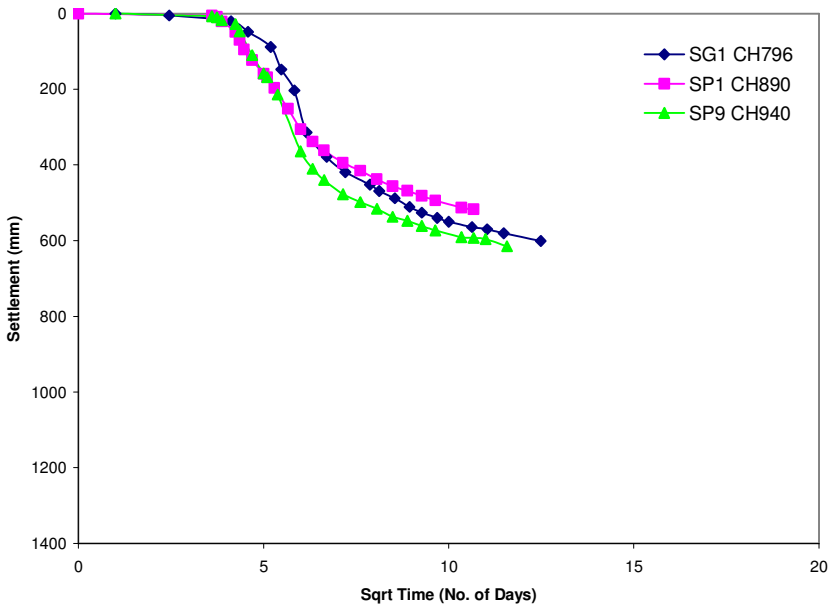

Figure 5.10 Comparison of measured surface settlement at Centre Line of Embankment A

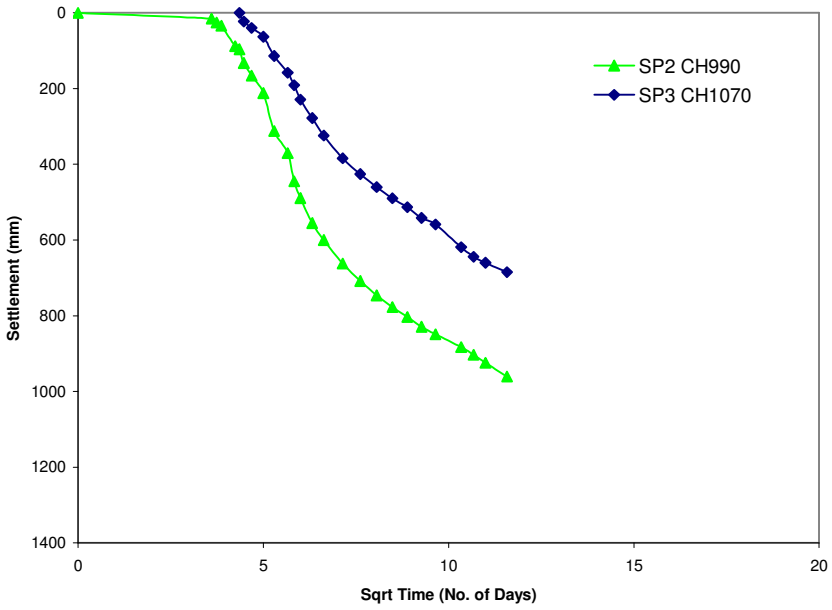

Figure 5.11 Comparison of Measured Surface settlement at Centre Line of Embankment B

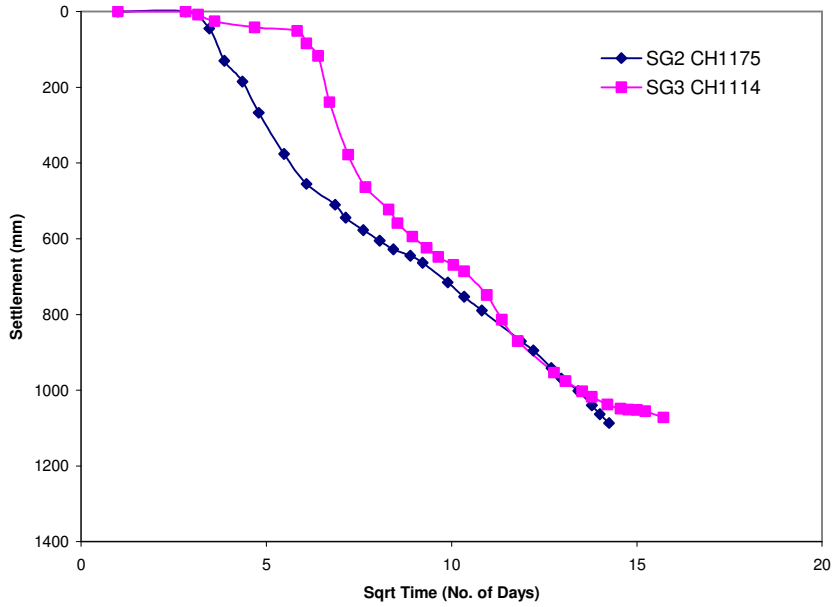

Figure 5.12 Comparison of Measured Surface settlement at Centre Line of Embankment C

5.7.2 Settlement Profile

The settlement beneath the trial embankments across the cross section were monitored with the use of a horizontal profile gauge. Horizontal profile gauges were installed in trial Embankments B and C only. Figures 5.13 and 5.14 showed the results of readings from the horizontal profile gauge with varying time intervals. HPG1 in Embankment C was monitored from 2 days, through to 251 days after the commencement of construction. HPG2 in Embankment B was monitored from 80 days, through to 207 days after the commencement of construction.

A comparison of surface settlement is made between Embankment B and Embankment C at 80 days and at 207 days after commencement of construction during and after construction of the embankment was complete and can be seen in Figures 5.15 and 5.16. From the comparison the surface settlement of Embankment C can be seen to be considerably higher than that of Embankment B. This is due to the higher surcharge pressure applied to trial Embankment C.

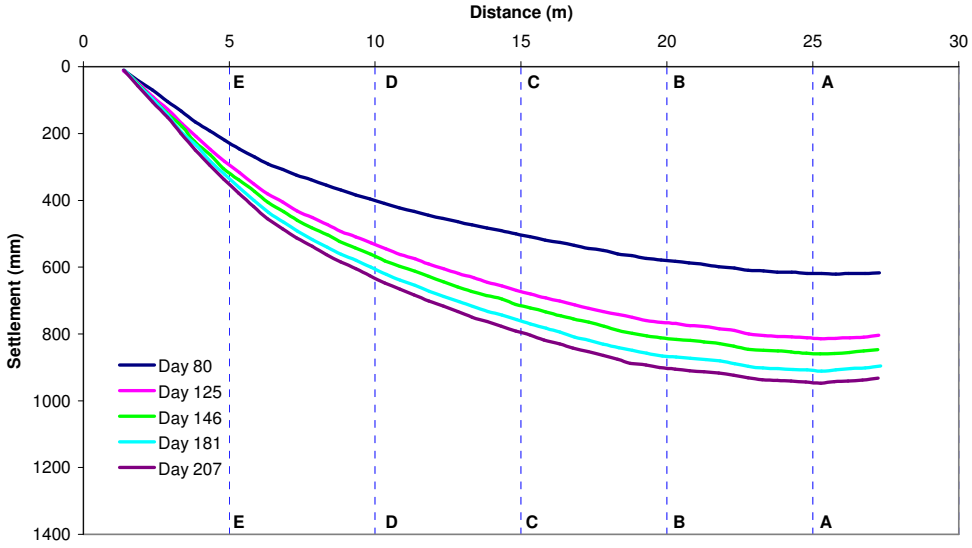

Figure 5.13 variation of settlement along Cross Section for Embankment B from horizontal profile gauge HPG2 CH1040

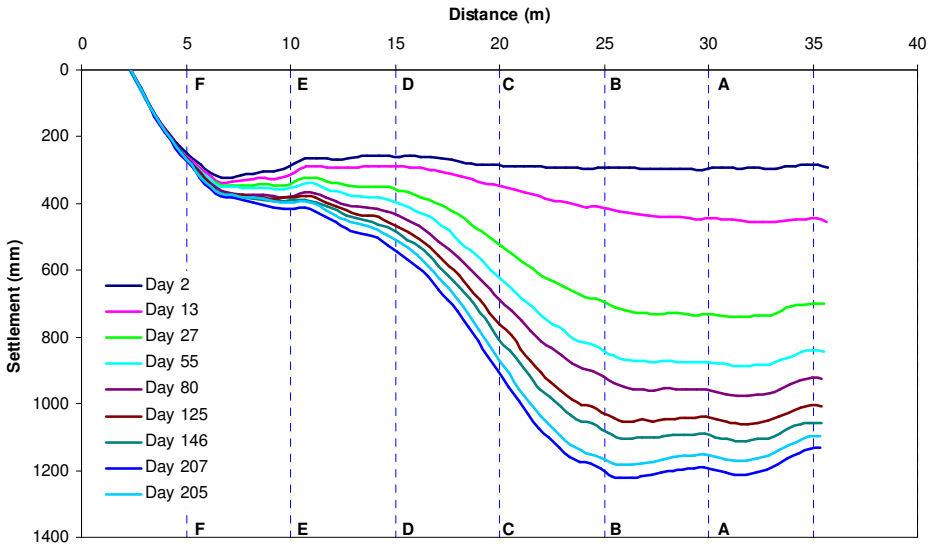

Figure 5.14 variation of settlement along Cross Section for Embankment C from horizontal profile gauge HPG1 CH1210

In Figures 5.13 and 5.14, the location marked AA is the centreline for the horizontal profile gauges, locations were then marked BB, CC, DD, EE, and FF for locations 5, 10, 15, 20 and 25 meters left of the centreline. At these locations settlement versus time plots were obtained to identify if 100% consolidation is being reached. From Figures 5.17 and 5.18 it can be seen for, HPG2 locations AA, BB and DD and for HPG1 location AA, CC, DD and EE respectively, that 100 percent consolidation is being reached. The coefficient of consolidation, c_v for the locations showing 100%

consolidation were obtained using Taylor's method, the results can be seen in Tables 5.2 to 5.4.

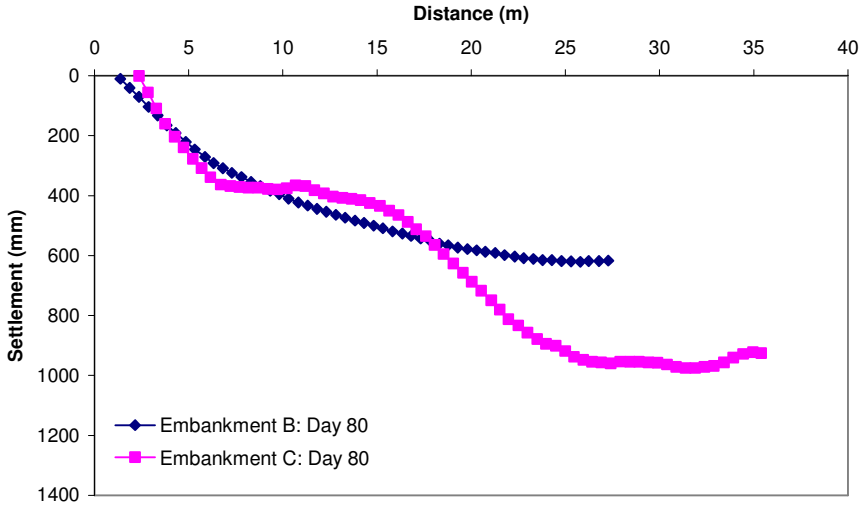

Figure 5.15 Comparisons of Surface settlement for Embankment B and C (Before End of Construction)

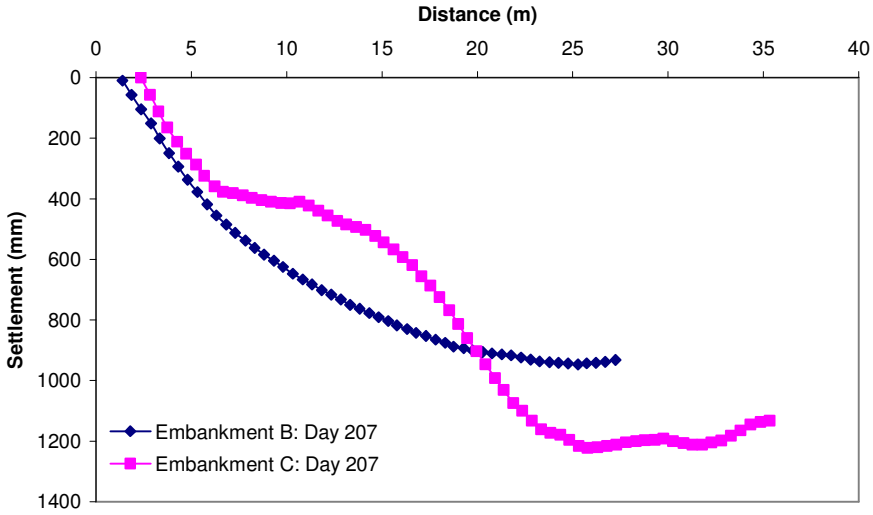

Figure 5.16 Comparison of Surface settlement for Embankment B and C (After End of Construction)

5.7.3 Settlement at Varying Depths

The settlement of the soil layers at varying depths were monitored with the aid of four extensometer magnets installed beneath each embankment. For Embankment A magnets 2, 3, 4 and 5 were installed at 12.23, 7.41, 3.38 and 0.5 meters depth respectively. For Embankment B magnets 2, 3, 5 and 6 were installed at depths of 17.9, 14.92, 7.16 and 3.11 meters depth respectively. For Embankment C magnets 1, 2, 3 and 4 were installed at depths of 18.9, 10.55, 7.65 and 3.91 meters depth respectively.

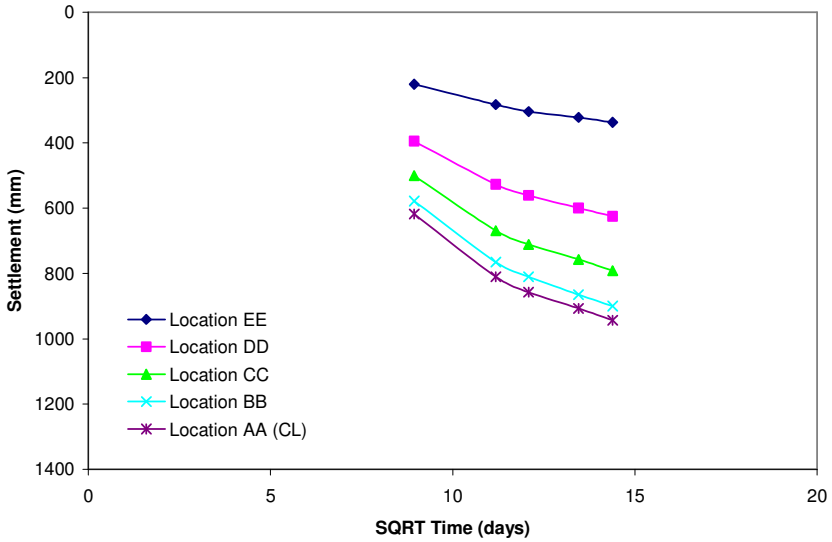

Figure 5.17 variation of settlement with time along the Centre Line and the Locations to the Left in Embankment B taken from HPG2 CH1040

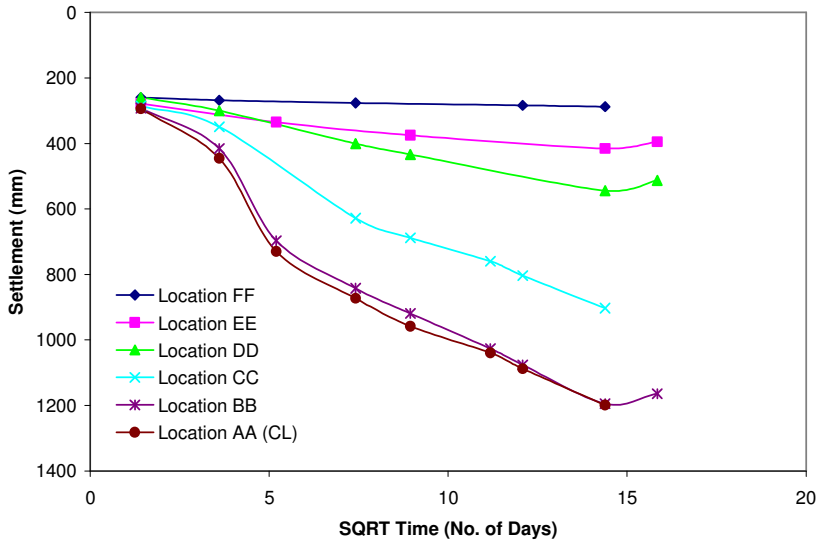

Figure 5.18 variation of settlement with time along the Centre Line and the Locations to the Left in Embankment C Taken from HPG1 CH1210

For all three trial embankments it can be seen in Figures 5.19(a) to 5.19(c) that the settlement decreases with depth in the soil layer. A comparison of the settlement for Embankments A, B and C was made at 3.38, 3.11 and 3.91 meters depth respectively and also at 7.41, 7.16 and 7.65 meters depth respectively. From this comparison it can be seen in Figures 5.20(a) and 5.20(b) that both Embankments B and C show larger settlement compared to that of Embankment A. These results are as expect due to the reduced spacing pattern of the vertical drains installed in Embankment B and C and the higher surcharge load applied to Embankment B and C.

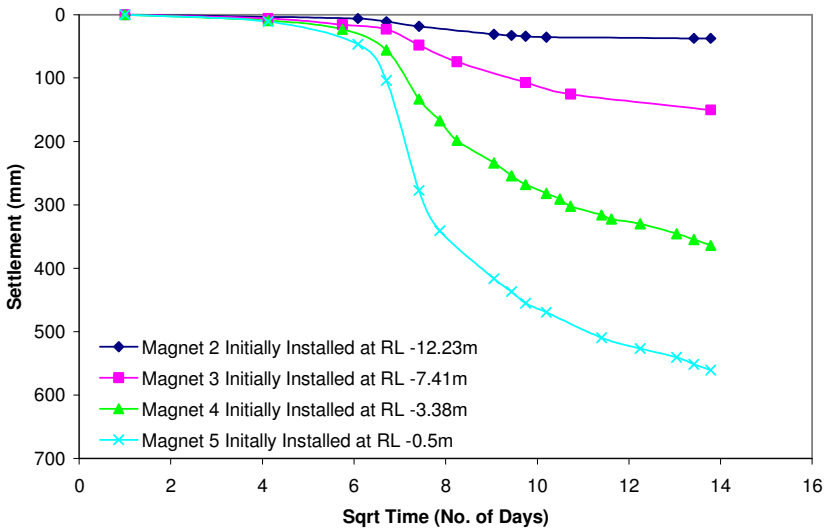

Figure 5.19(a) Field Measurements from Extensometer EXT1 Embankment A CH793

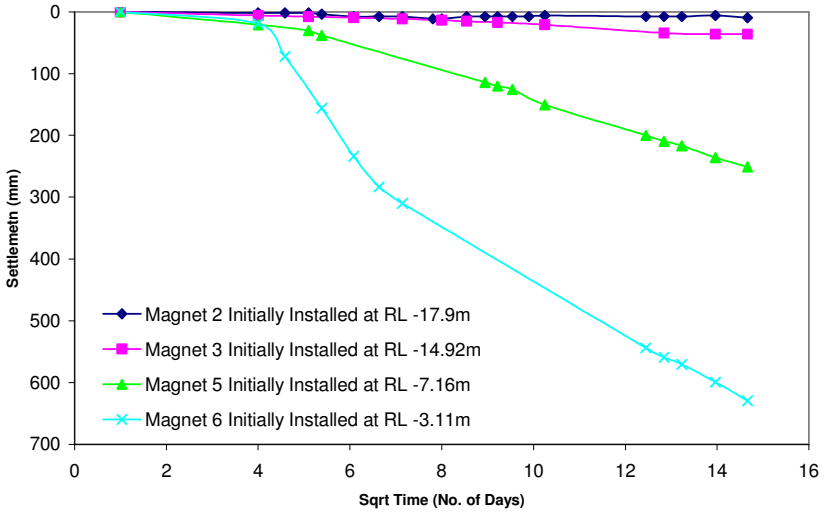

Figure 5.19(b) Field Measurements from Extensometer EXT3 Embankment B CH1040

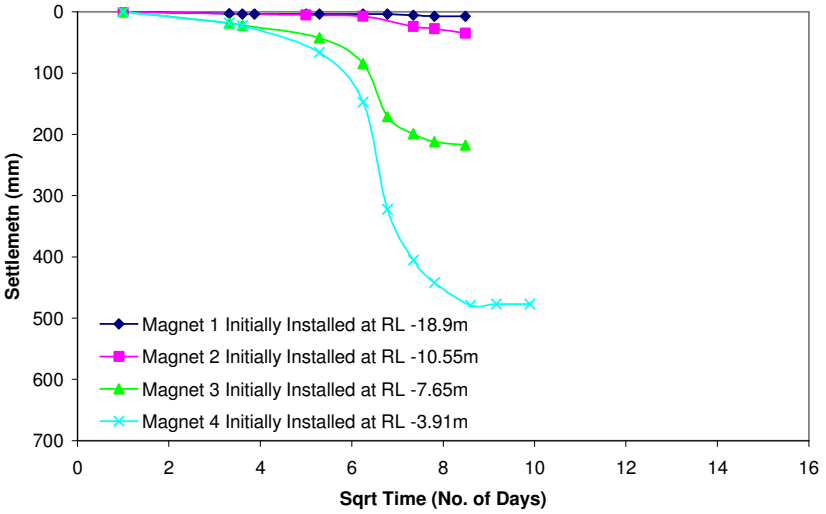

Figure 5.19(c) Field Measurements from Extensometer EXT2 Embankment C CH1210

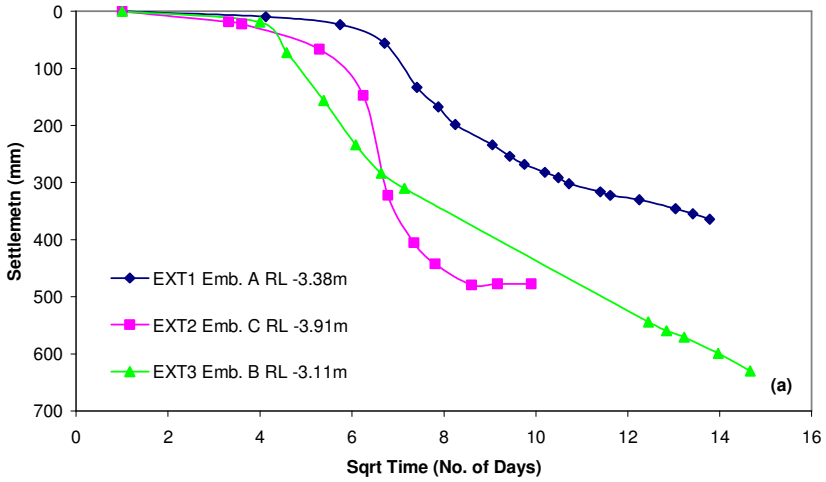

Figure 5.20(a) settlement of Trial Embankments A, B and C Between 3 and 4 meters Depth

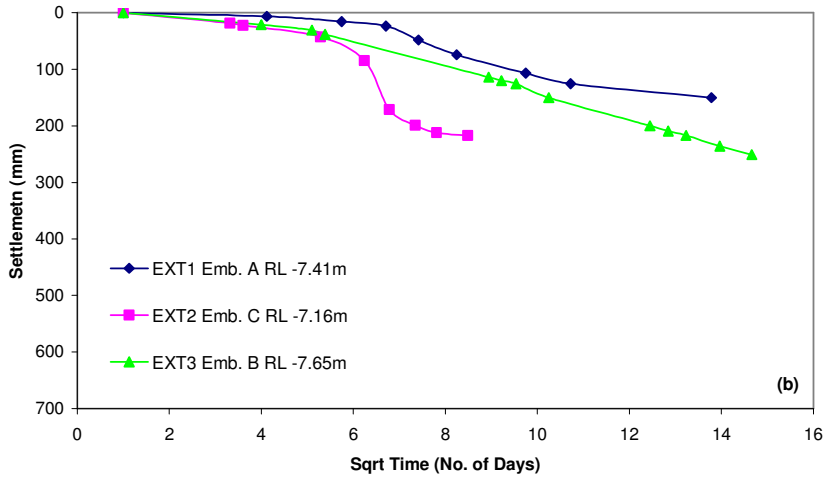

Figure 5.20(b) settlement of Trial Embankments A, B and C between 7 and 8 meters Depth

5.7.4 Lateral Deformation

Inclinometers installed at the toe of each embankment gave readings of the lateral deformation that occurred due to construction of the trial embankments. The results of inclinometer readings with increased time can be seen in Figures 5.21 to 5.23. Inclinometer INC1 installed beneath the toe of Embankment A reached a maximum lateral deformation of 134.5 mm at a depth in the soil layer of 2.64 meters 179 days after construction commenced, the deformation reduced after reaching the maximum of 134.5 mm to 128 mm at 210 days before increasing again to a deflection of 131 mm at 240 days. This increase suggests that an increase in the load was introduced between

day 210 and day 240 although no report of the increase was evident in the corresponding construction sequence.

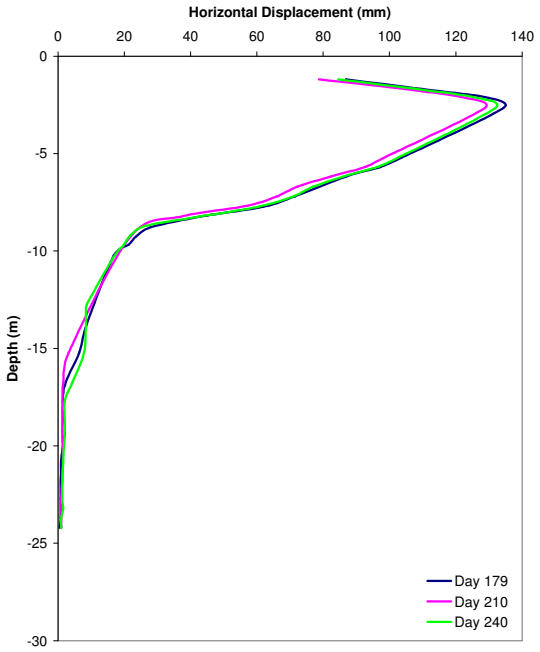

Figure 5.21 Field Measurement variation of horizontal Deformation with Depth from Inclinometer INC1 Embankment A.

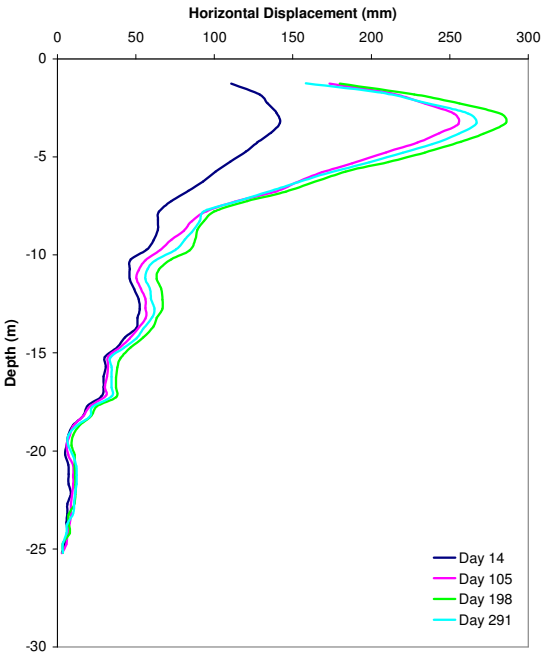

Figure 5.22 Field Measurement variation of horizontal Deformation with Depth from Inclinometer INC4 Embankment B.

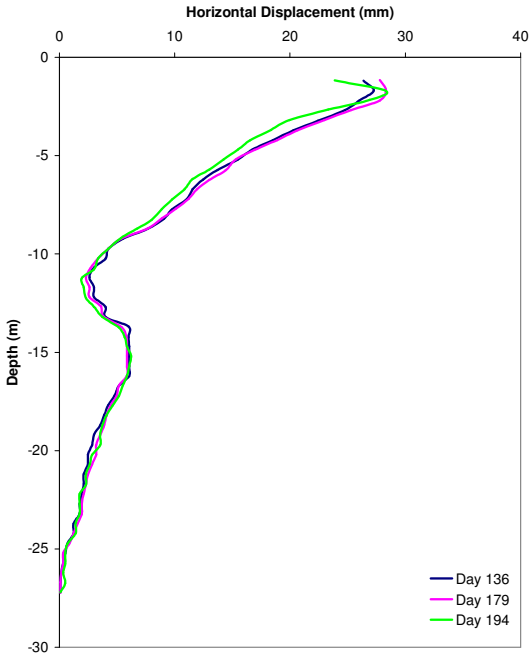

Figure 5.23 Field Measurement variation of horizontal Deformation with Depth from Inclinometer INC3 Embankment C.

Inclinometer INC4 installed at the toe of Embankment B reached a maximum lateral deformation of 286 mm at a depth of 3.27 meters 198 days after construction commenced. As in Embankment A the deformation reduced after reaching a maximum deflection of 286 mm to 266 mm 291 days after construction. Inclinometer INC3 installed at the toe of Embankment C reached a maximum deformation of 28.3 mm at a depth of 1.72 meters 194 days after construction commenced. The deformation of this inclinometer is inconsistent with that of Embankment A and Embankment B suggesting that it was installed an unknown distance from the toe of the embankment.

A comparison of the lateral displacement for Embankments A, B and C at 179, 198 and 179 days after the start of construction respectively, can be seen in Figure 5.24. From this it can be seen that the lateral deformation between embankments varies greatly. The lateral deformation of Embankment A and Embankment B was expected to be similar because the embankments were constructed to heights of 3.1 and 3.2 meters respectively, however it can be seen that the lateral deformation of Embankment B is 151.5 mm, more than double the total lateral deformation of Embankment A. A possible

explanation for this result is the rate at which the embankments were constructed. Embankment A was constructed at 0.084 m/day while Embankment B was constructed at 0.13 m/day and 0.03 m/day for stage 1 and stage 2 respectively. The stage 1 construction rate of Embankment B is far greater then that of Embankment A, which potentially could result in the increase lateral deformation. Another important factor to consider is the amount of settlement that occurred in between Stage 1 and Stage 2 constructions for Embankment B this settlement would not be accounted for in the total embankment height thus the embankment may have in fact been built to a total greater height when accounting for the settlement that occurred. The lateral deformation of Embankment C is minimal in comparison with that of Embankments A and B, however the expected lateral deformation of Embankment C is greater than that expected from Embankments A and B because of the greater surcharge load applied. Therefore as stated previously results of this nature suggest that inclinometer INC3 was installed an unknown distance from the toe of the embankment.

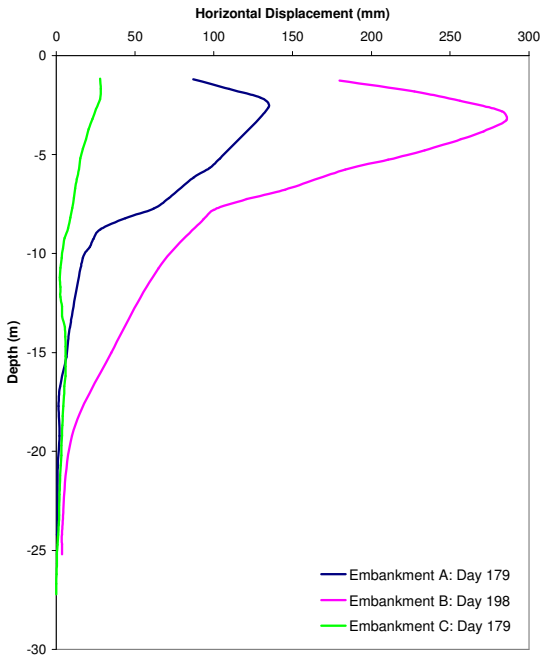

Figure 5.24 Comparisons of horizontal Deformation of Embankment A, B and C after End of Construction

5.7.5 Piezometers

Results of monitoring of the pneumatic piezometers can be seen in Figures 5.25 to 5.27. These figures also show the monitoring results beneath the construction sequence. By displaying the piezometer readings beneath the construction sequence it can be clearly seen that the piezometer readings exhibit increased excess porewater pressure at periods of increased surcharge.

PP1 – PP5 installed in Embankment B range from depths of 0.79 meters to 12.79 meters. PP6 – PP9 installed in Embankment B gave readings varying from depths of 2.10 meters to 14 meters. PP10 - PP11 and PP14 – PP15 installed in Embankment C gave readings varying in depths of 3.3 meters to 9.9 meters. The readings of the piezometers in Embankment A show the largest increase of excess porewater pressure of 55.58 kPa in PP3 installed at a depth of 6.79 meters. Embankment B's increase in excess porewater pressure reached a maximum of 45.59 kPa in PP6 installed at a depth of 2.1 meters after the second stage of loading. Embankment C's increase in excess porewater pressure reached a maximum of 39 kPa in PP10 on the second stage of loading installed at a depth of 3.3 meters.

Embankment B reached a maximum excess porewater pressure of 41.79 kPa in PP6 installed at depth of 2.1 meters after Stage 1 of construction and a maximum excess porewater pressure of 45.59 kPa after Stage 2 of construction.

The reason why the increased excess porewater pressure reached a larger maximum in Embankment A is because a construction height increase of 3.1 meters was applied in one stage. For Embankment B the maximum height increase of 2.6 meters occurred in the first loading. After this loading stage the porewater was allowed to dissipate for 72 days before increasing the height of the embankment was increased to 3.2 meters. The excess pore pressure induced by the first stage of loading had not completely dissipated

and this is why with the increase of a further 0.6 meters the maximum excess porewater pressure was obtained. For Embankment C the excess porewater pressure created after the Stages 1, 2 and 3 of loading were 16.3 kPa in PP14 installed at a depth of 6.2 meters, 36.93 kPa in PP10 installed at a depth of 3.3 meters and 32.93 kPa also in PP10. Embankment C although built to the greatest height was given the most time to settle for all three of the trial embankments a total of 95 days compared to 72 days for Embankment B before construction was completed. Embankment A had no settlement time before the end of construction as the embankment was built in one stage.

5.8 Back Calculated Coefficient of Horizontal Consolidation

From results of instruments installed to observe the settlement of the trial embankments, values for the coefficient of horizontal consolidation, c_h, can be back-calculated. Because the dissipation of the pore-water is primarily through the vertical drains, water is assumed to flow horizontally or radially through the soil layer. The results of laboratory tests only achieve values for the coefficient of vertical consolidation, c_v. By developing a relationship between the back-calculated values of the coefficients of horizontal and vertical consolidation an accurate prediction of the values for horizontal permeability can be made.

The results of the coefficient of horizontal consolidation for varying degrees of consolidation can be seen in Figures 5.28(a) to 5.28(c). From both Embankment B and C the back calculated c_v values can be seen to increase semi-linearly to maximums of around 0.4 to 1 m^2/year at 90% degree of consolidation. The same is similar for Embankment A where by the back calculated c_v values can be seen to decrease semi-linearly to maximum back calculated c_v values at 90% degree of consolidation, however the rate is greatly increased reaching maximums between 0.7 to 2 m^2/year.

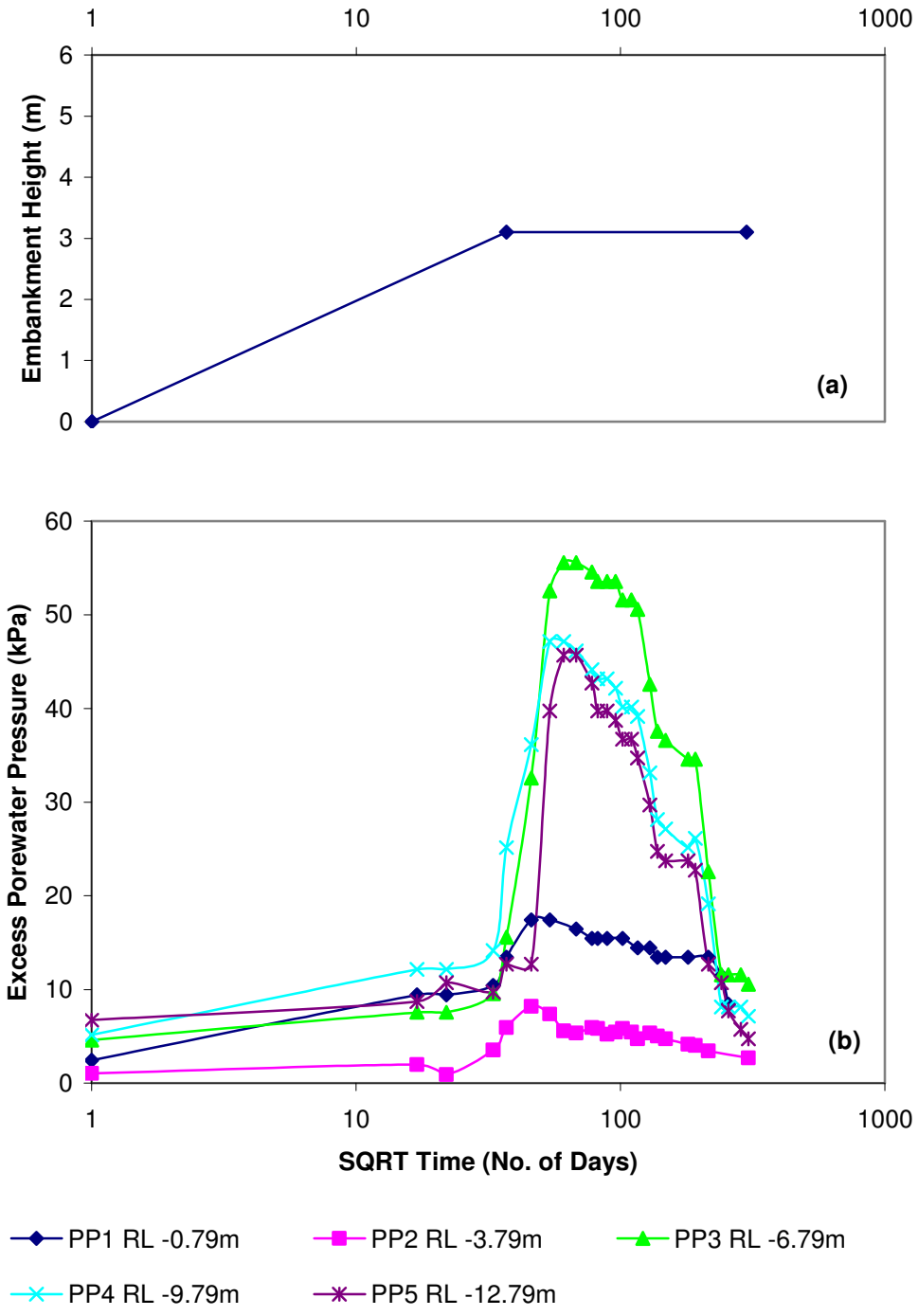

Figure 5.25 variation of excess Pore-water Pressure with time in Embankment A CH794. (a) Plot of Embankment Loading with time; (b) Piezometers PP1, PP2, PP3, PP4 and PP5.

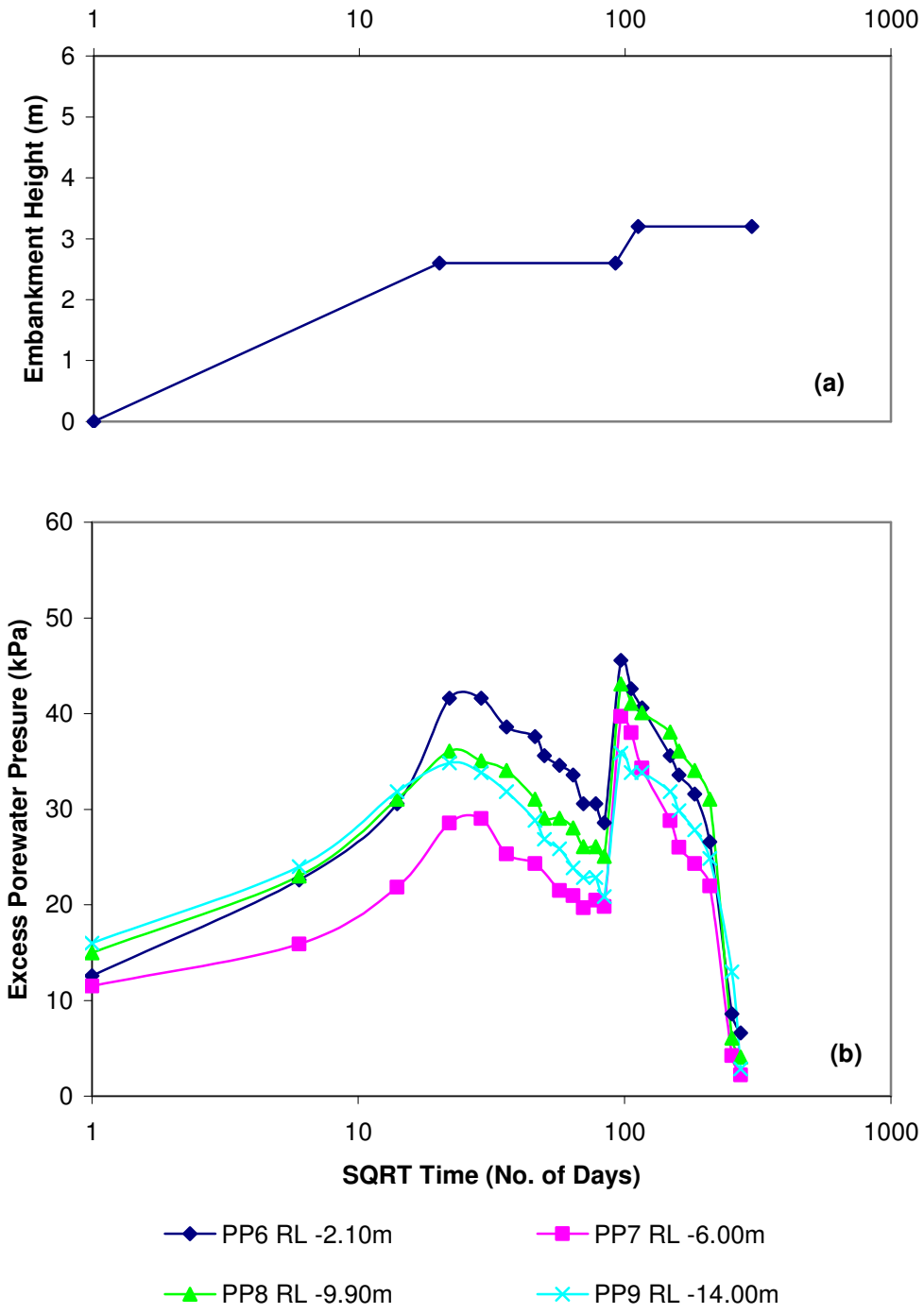

Figure 5.26 variation of excess Pore-water Pressure with time in Embankment B CH1040. (a)Plot of Embankment Loading with time; (b)Piezometers PP6, PP7, PP8 and PP9.

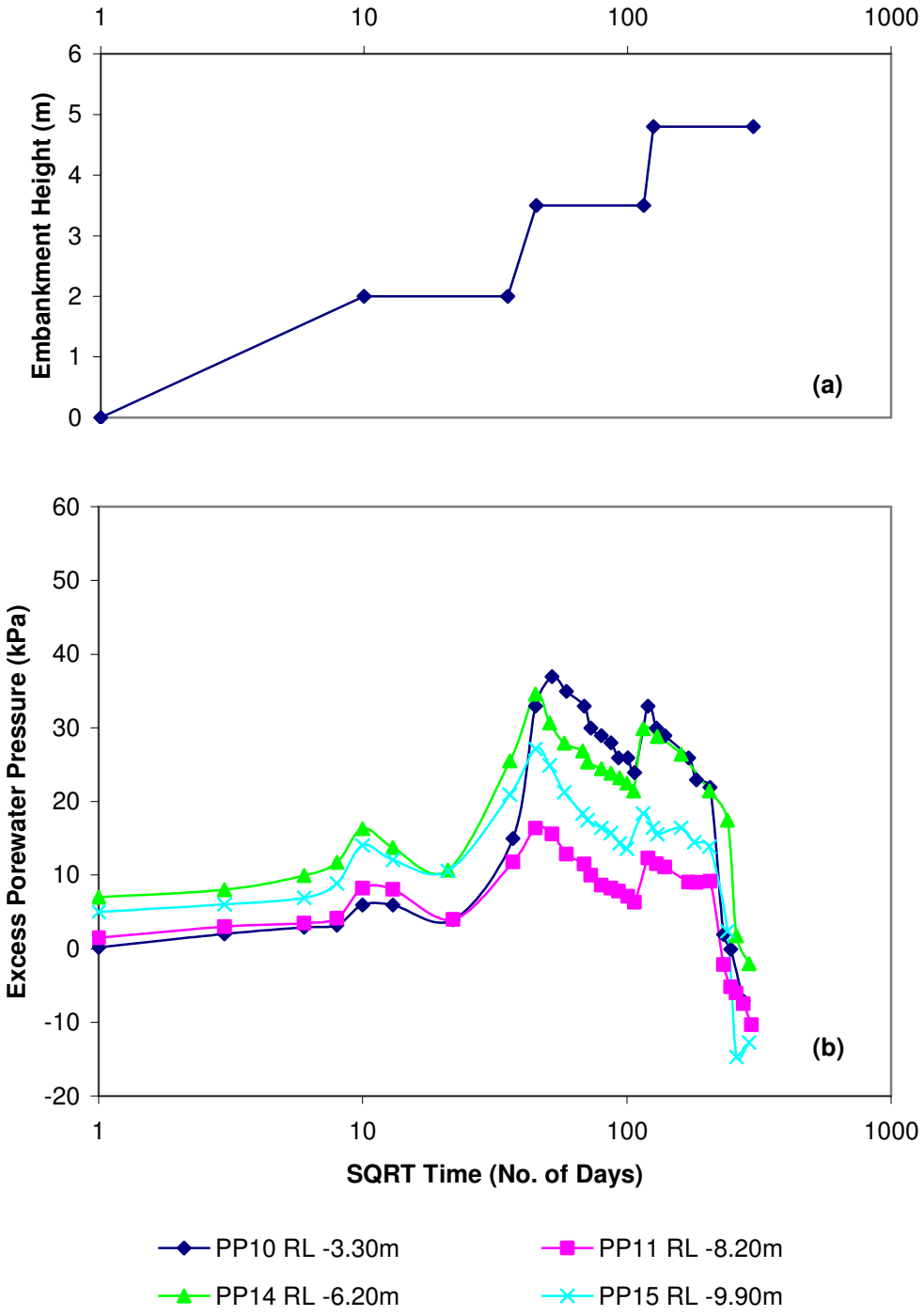

Figure 5.27 variation of excess Pore-water Pressure with time in Embankment C CH1170. (a) Plot of Embankment Loading with time; (b) Piezometers PP10, PP11, PP14 and PP15

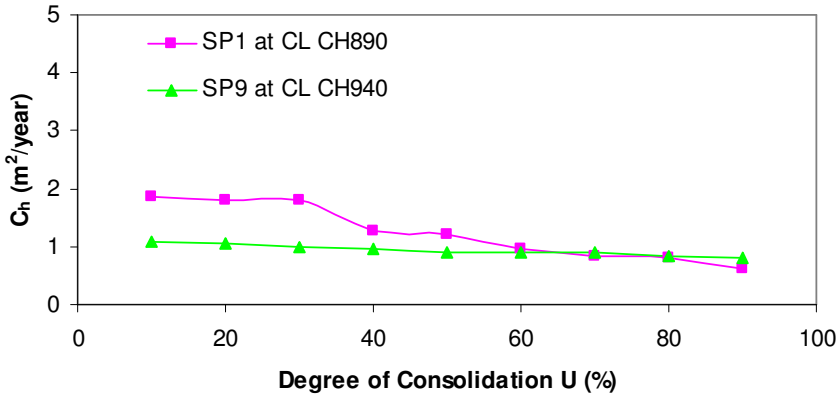

Figure 5.28(a) variation of back-calculated Coefficient of Consolidation, c_h, with Degree of Consolidation for Different Chainages (Embankment A).

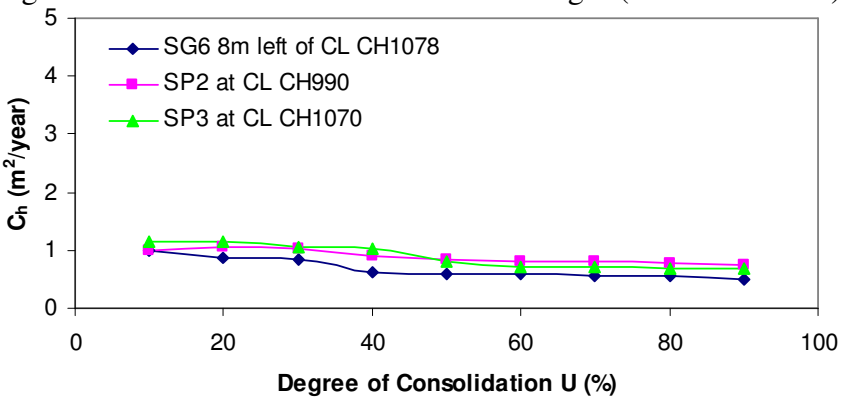

Figure 5.28(b) variation of back-calculated Coefficient of Consolidation, c_h, with Degree of Consolidation for Different Chainages (Embankment B).

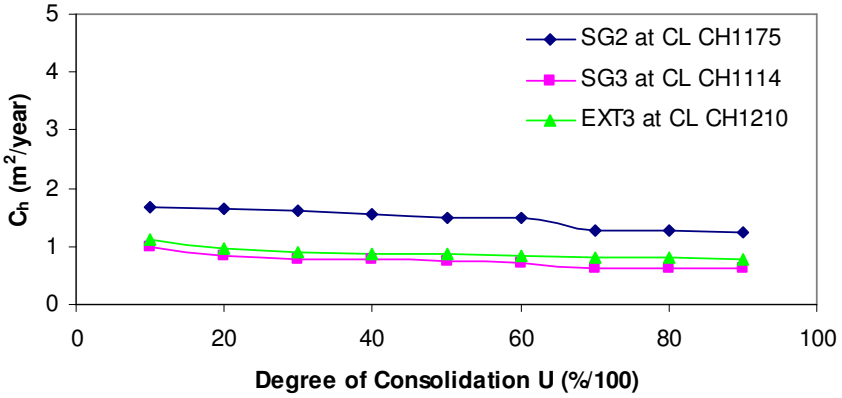

Figure 5.28(c) variation of back-calculated Coefficient of Consolidation, c_h, with Degree of Consolidation for Different Chainages (Embankment C).

5.9 PLAXIS Finite Element Analysis

In this section, the results from a computer analysis using PLAXIS Version 8 program whose parameters were obtained using results of the laboratory test data are compared to the results obtained from the field measurements. The comparison is between vertical

deformation and excess porewater pressure prediction as created by the construction of the three trial embankments.

5.9.1 Mesh Generation and Pressure Boundaries

PLAXIS analysis required the generation of the finite element mesh and pressure boundaries. The mesh is generated using the generate mesh commend in the PLAXIS program. In Figures 5.29(a) to 5.29(c), the mesh generated by the PLAXIS program for each trial embankment can be seen. Boundary conditions can be specified by the user in the PLAXIS program. For this symmetrical consolidation analysis the conditions requiring specification included, the vertical drains, ground water level and the flow boundaries. The vertical drains were used to define areas of zero pore pressure, PLAXIS program includes a feature for the installation of vertical drains whereby lines representing the drain wells can be installed. Ground water level can be specified by the ground water command. The boundary flow at all perimeters of the PLAXIS program are assumed free draining, this assumption can be overridden by installing closed flow boundary plates (no flow of water is allowed across these boundaries). The pressure boundaries are displayed in Figure 5.30.

5.9.2 Vertical Deformation

From the results of PLAXIS program an accurate comparison of settlement was able to be made. The comparison for each trial embankment was made for surface settlement and settlement between 3 and 4 meters depth with in the soil layer. In Figure 5.31 – 5.36 it can be seen that PLAXIS program over predicted the surface settlement and the settlement at depths between 3-4 meters for all three trial embankments. Although PLAXIS program is seen to over predict the settlement the results between predicted and measured settlement are in good agreement. Displayed in all curves produced by

PLAXIS program, an increased in the time required for 100% consolidation to be completed can be seen.

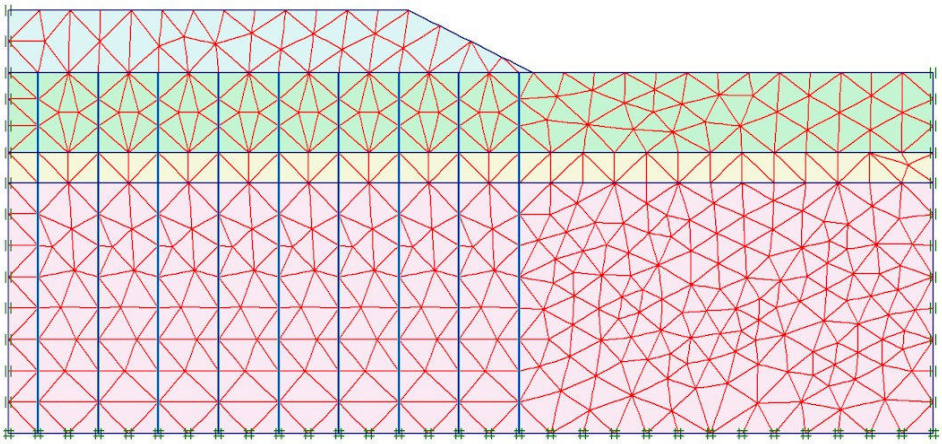

Figure 5.29(a) Finite Element Mesh Used in PLAXIS Program for Embankment A

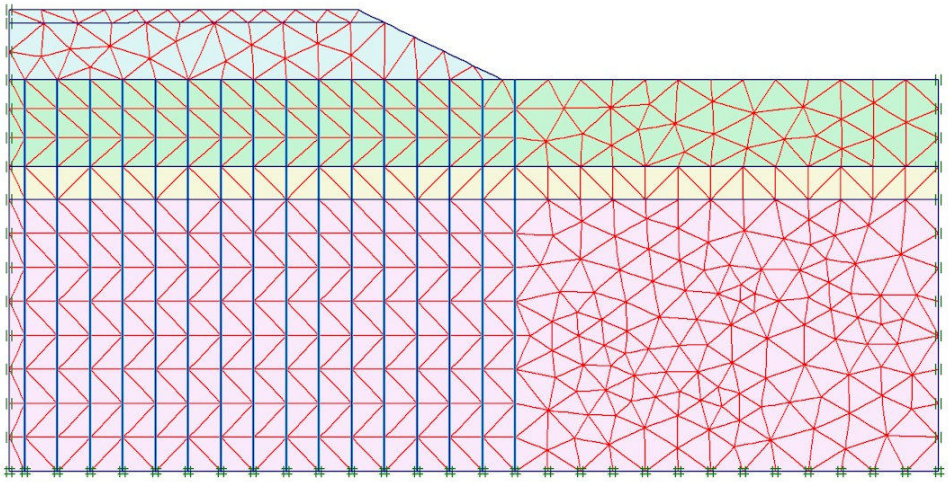

Figure 5.29(b) Finite Element Mesh Used in PLAXIS Program for Embankment B

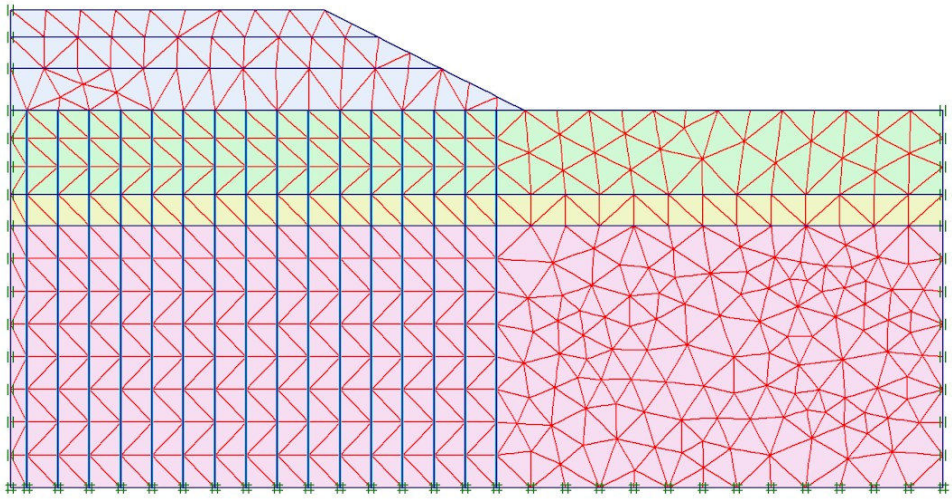

Figure 5.29(c) Finite Element Mesh Used in PLAXIS Program for Embankment C

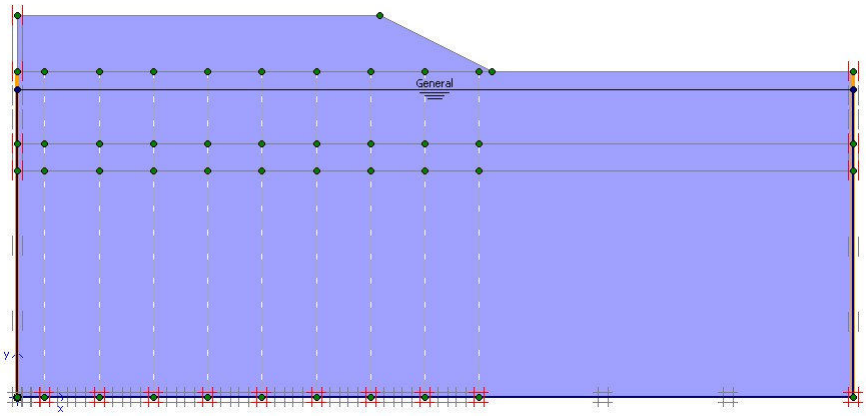

Figure 5.30(a) No-Flow Boundary Conditions in Soft Soil Layers for Embankment A

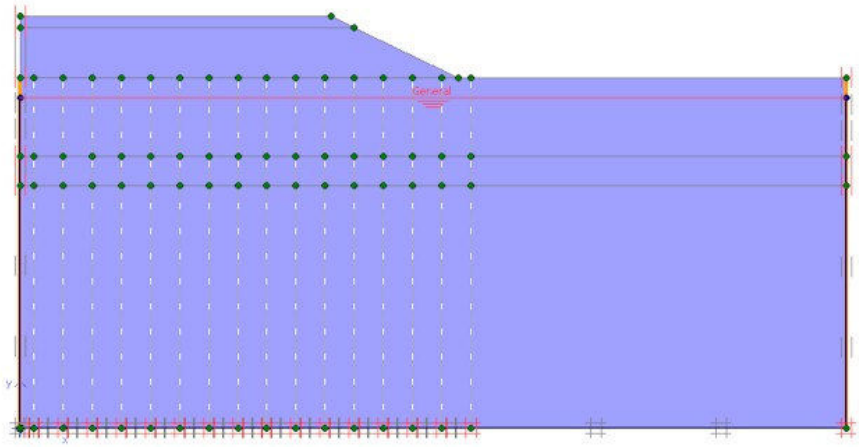

Figure 5.30(b) No-Flow Boundary Conditions in Soft Soil Layers for Embankment B

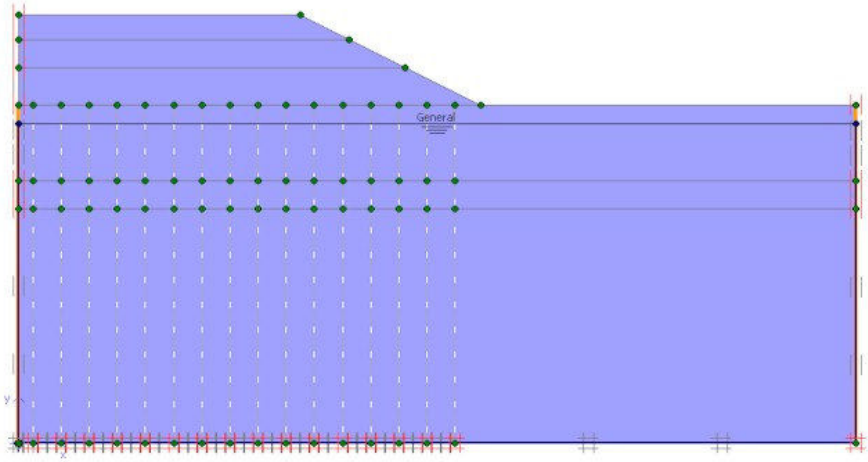

Figure 5.30(c) No-Flow Boundary Conditions in Soft Soil Layers for Embankment C

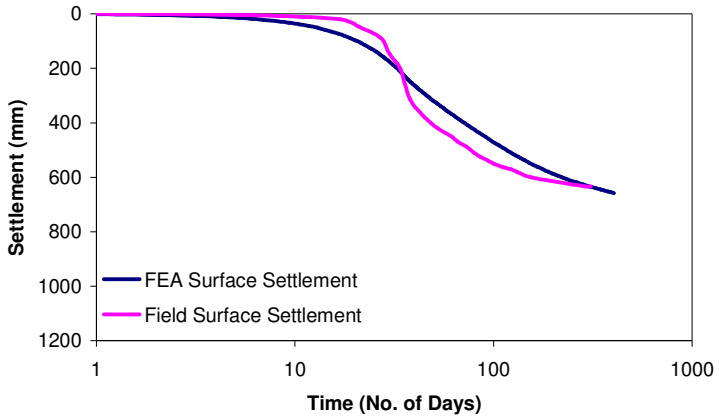

Figure 5.31 Observed and predicted surface settlement variation at the Centre Line with time for Embankment A

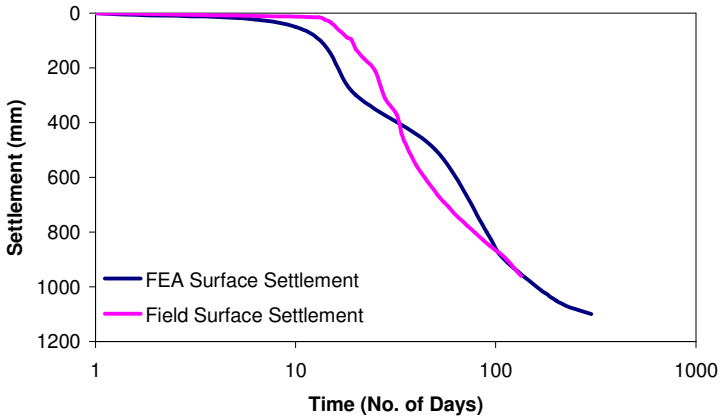

Figure 5.32 Observed and predicted surface settlement variation at the Centre Line with time for Embankment B

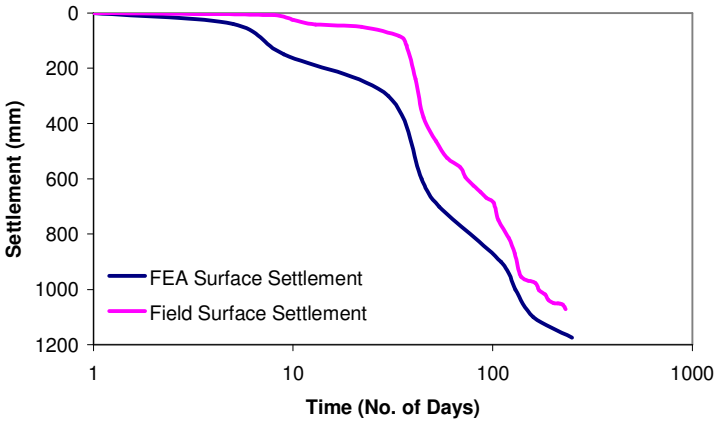

Figure 5.33 Observed and predicted surface settlement variation at the Centre Line with time for Embankment C

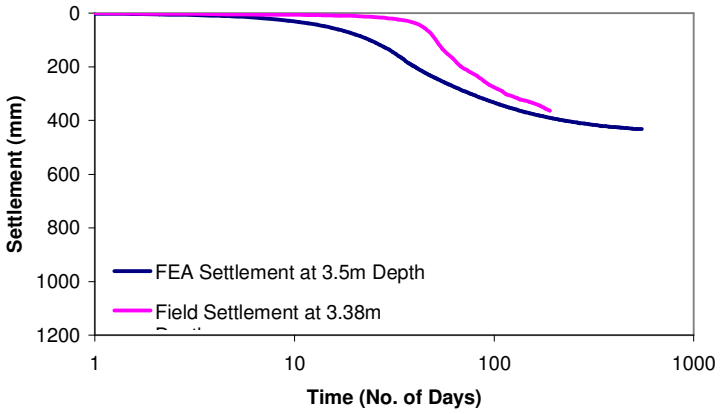

Figure 5.34 Observed and Predicted settlement at 3-4m Depth variation at the Centre Line with time for Embankment A

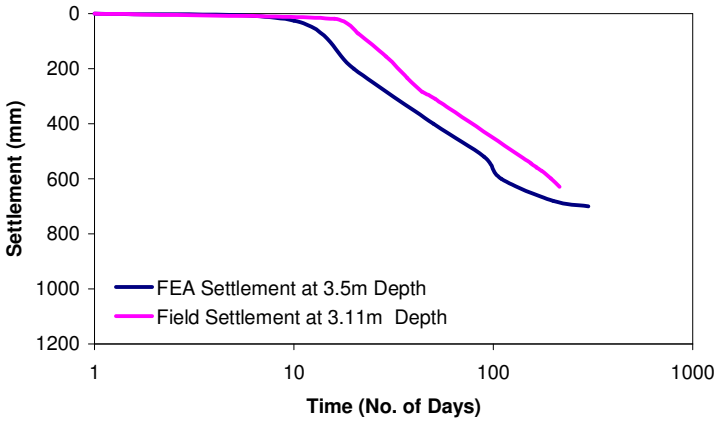

Figure 5.35 Observed and Predicted settlement at 3-4m Depth variation at the Centre Line with time for Embankment B

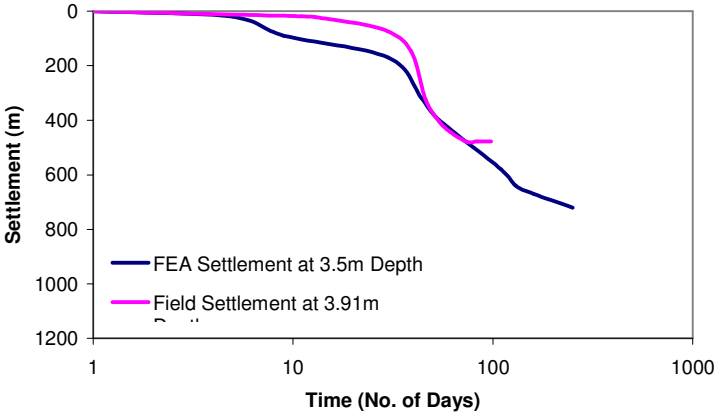

Figure 5.36 Observed and Predicted settlement at 3-4m Depth variation at the Centre Line with time for Embankment C

5.9.3 Excess Pore-water Pressure Development and Dissipation

Figures 5.37 - 5.39 shows the results of the compared predicted and measured pore-water pressure generation and dissipation with time in the three trial embankments. It

can be seen that a good agreement between the measured and predicted increases and decreases is obtained. For all three trial embankments the predicted pore pressure is greater than the measured pore pressure and that the dissipation of the pore pressure is more gradual for the predicted results. The result of this decreased pore pressure dissipation is a decrease in the accuracy of pore pressure readings for more construction sequences. This is evident in Embankments A and B where the prediction of pore pressure for the first stage of loading is in excellent agreement. After a pause between settlements the measure pore pressure dissipation is higher than the predicted, after the first stage the predicted values increase with inaccuracy because after the pause they are already above, this can be seen clearly for Embankments B and C for the second and third stage of construction.

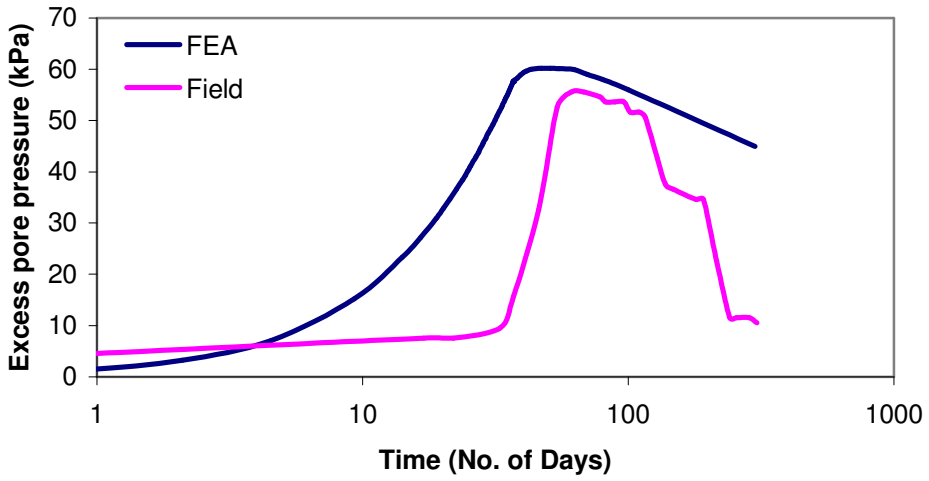

Figure 5.37 Comparison of Observed and Predicted pore pressure variation with time for Embankment A

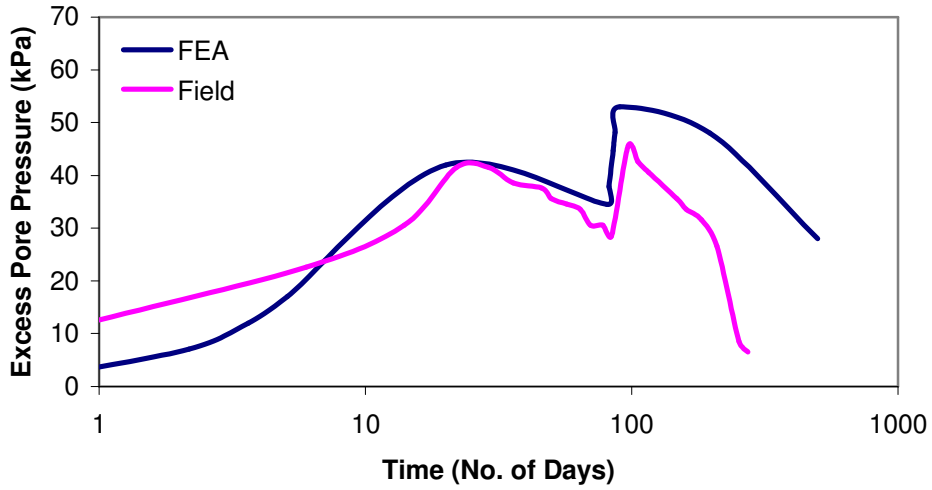

Figure 5.38 Comparison of Observed and Predicted pore pressure variation with time for Embankment B

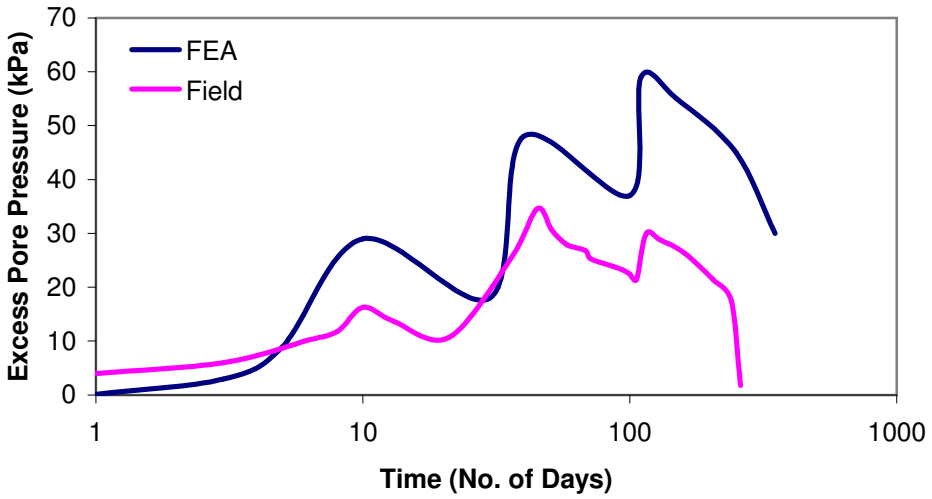

Figure 5.39 Comparison of Observed and Predicted pore pressure variation with time for Embankment C

5.10 Concluding Remarks

Vertical drains at different spacing with and without polystyrene platform foundations were installed beneath the Port of Brisbane Motorway trial embankment. From the comparison of field measurements and predicted performance obtained by using PLAXIS finite element software, it can be concluded that vertical drains installed at closer spacing effectively increase settlement of the soft clays.

CHAPTER 6

CASE STUDY 3: GOLD COAST HIGHWAY EMBANKMENT - ANALYSIS OF LABORATORY AND FIELD TEST DATA

6.1 Introduction

This chapter presents the soil characteristics of the site where the trial embankment was built. Included in this section are the in-situ conditions before the embankment was constructed and the subsequent conditions after the embankment was built. From the laboratory results, the one dimensional settlement of the embankment was predicted. The vertical settlement (both surface and sub-surface), horizontal settlement profile, lateral displacement and excess pore pressure plots, determined from the in-situ field equipment, are provided.

The Coombabah Creek trial embankment is located in a marine environment. It passes through a low lying wetland reserve. The soil found here is predominately soft organic marine clay. Before the trial embankment was constructed, numerous bore holes were drilled and undisturbed soil samples taken, to assess the soil characteristics. These characteristic were then utilised in the design and construction of the trial embankment. During the construction of the embankment, field instrumentation was installed to monitor the performance of the embankment, both during and after it was built.

Further, in this chapter, a detailed analysis of all laboratory and instrumentation data is provided. Insight is given into the measured behaviour of the trial embankment. Comparisons are made between the monitored field performances of the embankment, against the expected behaviour as envisaged during the design stage. The performance of the trial embankment was also assessed using commercial Geotechnical Engineering software packages (PLAXIS).

6.2 Longitudinal Soil Profile

The trial embankment was built along the deepest section of the very soft to soft organic clay layer, which extended to a maximum depth of 13.5m (as shown in Figure 6.1(a)). Underlying this layer is a moderately dense to dense sandy sediment strata. On either side of these strata are stiff-hard clay/silty clay. The longitudinal profile of the soil stratum is displayed in Figure 6.1(a).

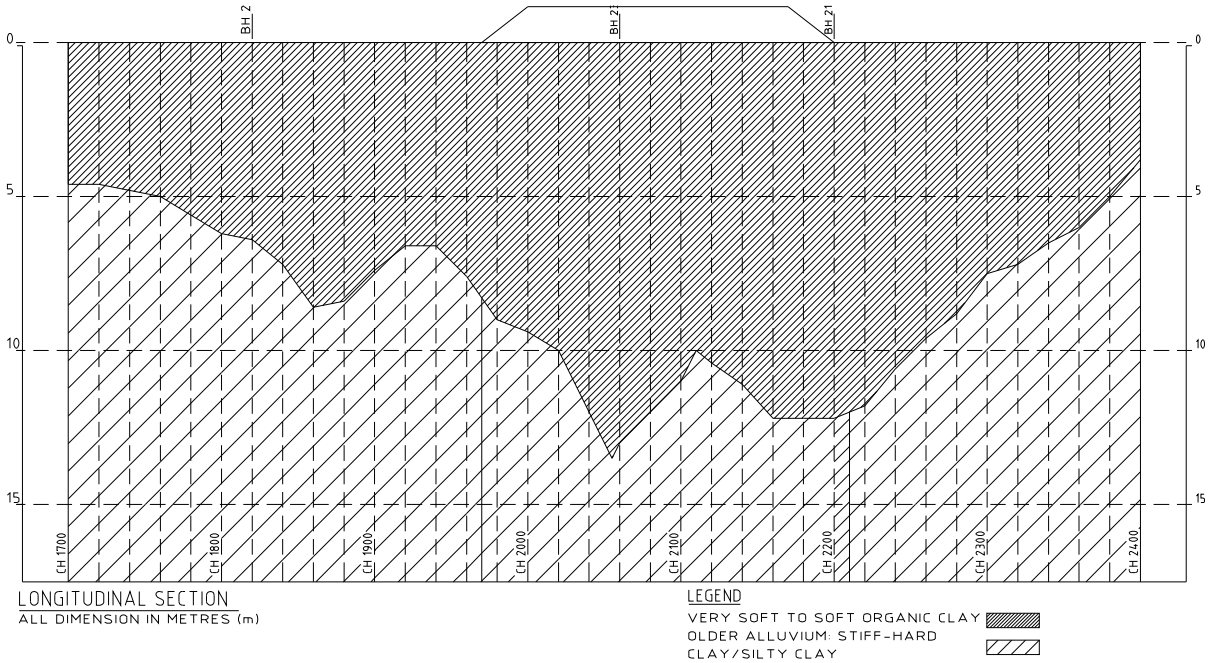

Figure 6.1(a) Longitudinal soil profile of test site

6.3 Embankment Geometry and Construction Schedule

One trial embankment was constructed along the Gold Coast Highway. This embankment was divided into three sections – section (1) contained no ground improvement, section (2) had stone columns at 2m spacing and section (3) had stone columns at 3m spacing. The stone columns had a diameter of 1m and were 16m long. The Coombabah Creek embankment was constructed in two stages. Stage one construction was 2m high, while stage two constructions varied for each section. Beneath the embankment, Geogrid was placed to reinforce the embankment. The geometry of the trial embankment is illustrated on Figure 6.1(b).

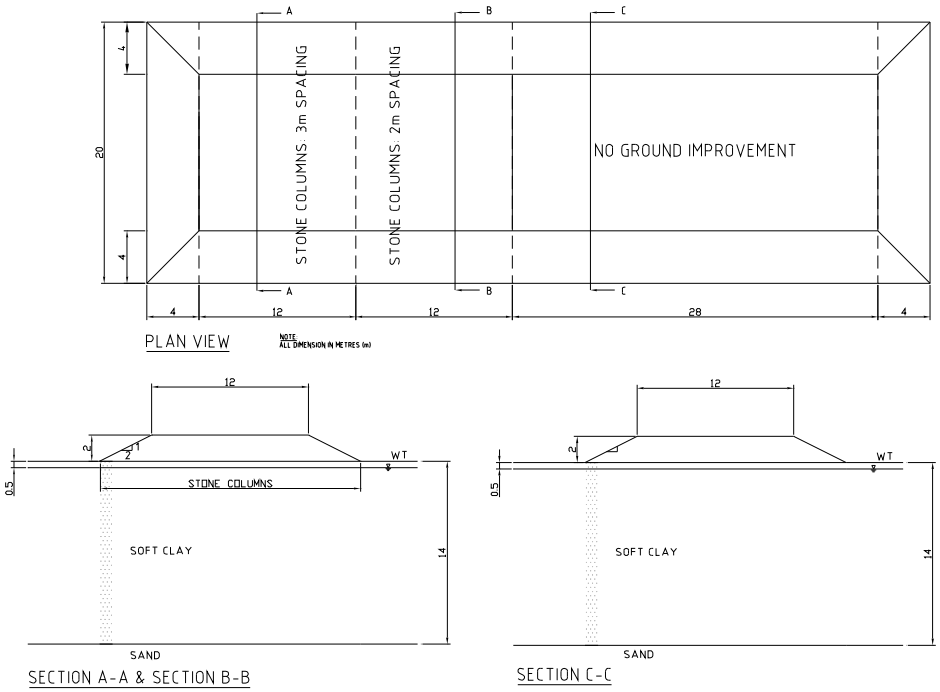

Figure 6.1(b) Trial embankment geometry

The exact construction schedule of the trial embankment is unknown from the Queensland Department of Main Roads (QDMR) reports. Knowledge from the Principal Geotechnical Testing Officer at QDMR suggests that it took 35 days to construct each stage and there was a period of 100 days (consolidation period) between each stage (as shown in Figure 6.1(c)).

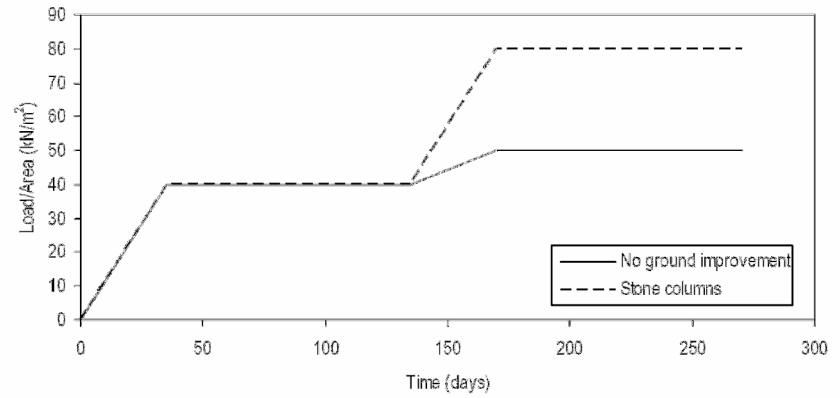

Figure 6.1(c) Construction schedule

6.4 In-situ Field Conditions

Numerous bore holes were drilled along the site where the trial embankment was built. From the bore holes, undistributed soil samples were taken, at various depths, to

determine the nature of the soil stratum. As shown in Figure 6.2(a), laboratory tests were used to establish liquid limit, moisture content, plastic limit, and soil sensitivity profile. Further, Figure 6.2(b) gives the wet density (γ_{wet}) profile of the soft organic clay at the test site. The undrained shear strength (Su) of the soft clay was also determined at various depths (as shown in Figure 6.2).

Once the wet density (γ_{wet}) is known the total vertical stress (σ_v), pore pressure (u) and effective vertical stress ($\sigma_v^{'}$) can then be calculated for the condition before the embankment is constructed. The raw data used to produce these plots is displayed in Table 6.1. The coloured figures in Table 6.1 are obtained from the stated bore holes. The uncoloured figures are the assumed distribution.

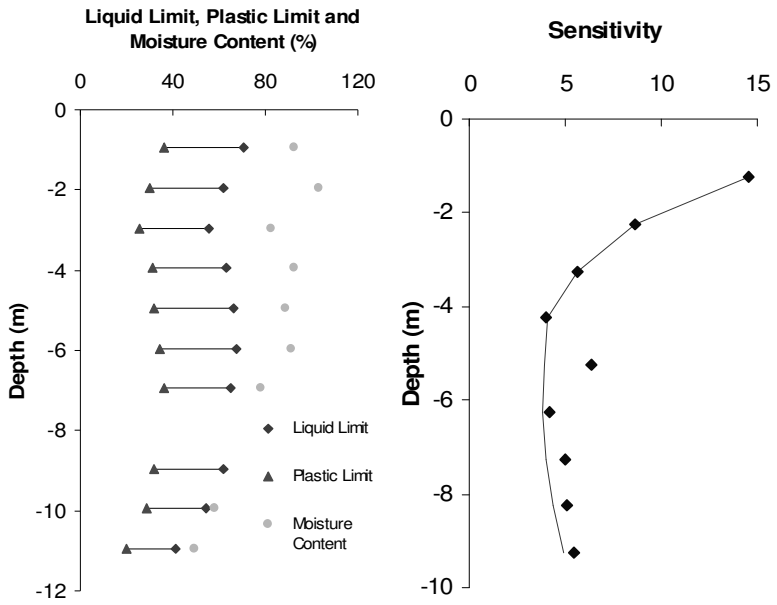

Figure 6.2(a) Liquid limit, moisture content, plastic limit, undrained strength and soil sensitivity profile.

Oedometer consolidation tests were also undertaken, in the laboratory, to assess the compressibility characteristics of the soft organic clay. Figure 6.3 illustrates the compression curves for five different soil samples taken from bore holes located along the Gold Coast highway site at Coombabah Creek. From these curves the coefficient of volume decrease (m_v) and coefficient of consolidation (c_v) can be determined.

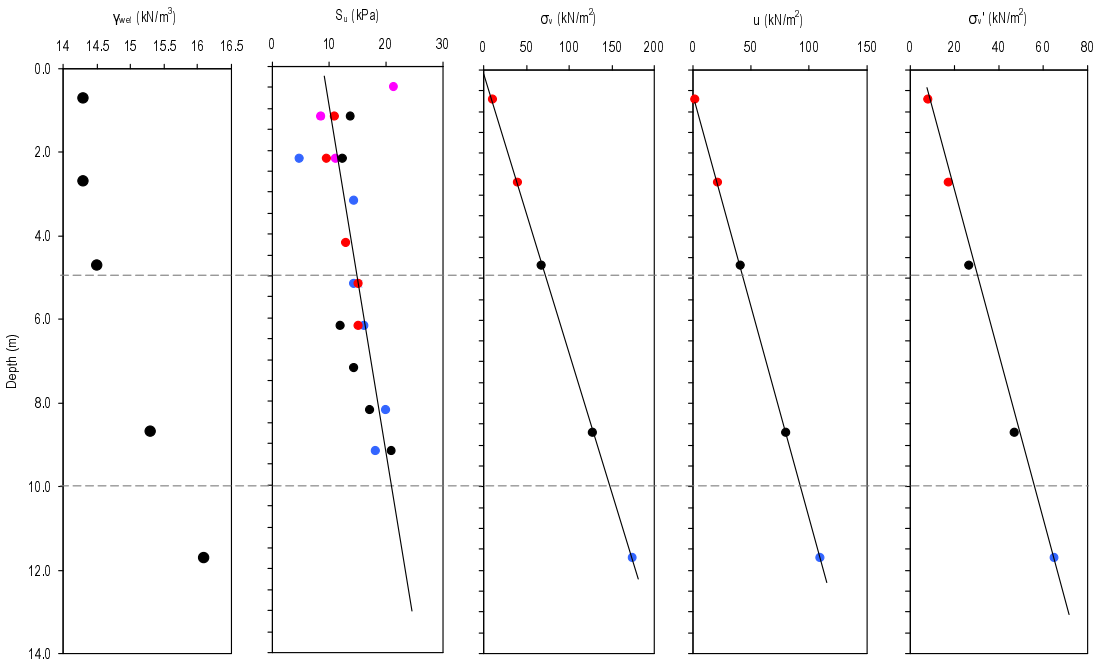

Figure 6.2(b) In-situ field conditions

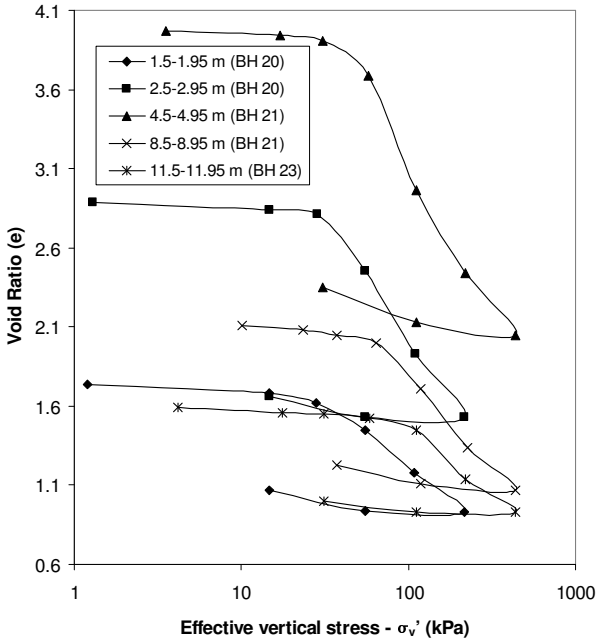

Figure 6.3 Consolidation curves at various depths

6.5 Conditions after Embankment Construction

The weight of the trial embankment causes an increase in the vertical stress in the soft clay layer. This increase in stress and/or incremental stress ($\Delta\sigma_v$) decreases with depth below the embankment. The following expression was used to determine the vertical stress in a semi-finite mass due to embankment loading. Incremental stress at point A due to embankment loading (Das, 1997) shown in Figure 6.7 and is given as follow:

$$\Delta\sigma_v = \frac{q}{\pi}\left[\left(\frac{a+b}{a}\right)(\alpha_1+\alpha_2)-\frac{b}{a}\alpha_2\right] \tag{6.1}$$

The increase in vertical stress was calculated for each stage construction height of the trial embankment. In determining the incremental stress ($\Delta\sigma_v$) the unit weight of the trial embankment was taken as 20kN/m^3. For the condition of one-dimensional consolidation, the total effective ($\Delta\sigma_v + \sigma_v^{'}$) stress in the soft clay layer is the summation of the in-situ vertical stress and incremental vertical stress for each depth. A plot of the incremental and total effective stress is shown in Figures 6.4, 6.5, and 6.6 for each construction stage.

Table 6.1 In-situ field conditions

Depth (m)	γ_{wet} (kN/m^3)	s_u (kPa)	σ_v (kN/m^2)	u (kN/m^2)	$\sigma_v^{'}$ (kN/m^2)
1.0	14.3	8.50	14.30	4.90	9.40
2.0	14.3	10.00	28.60	14.71	13.89
3.0	14.3	11.00	42.90	24.52	18.38
4.0	14.4	12.50	57.60	34.32	23.28
5.0	14.5	14.00	72.50	44.13	28.37
6.0	14.7	15.00	88.20	53.94	34.26
7.0	14.9	16.50	104.30	63.75	40.55
8.0	15.1	17.50	120.80	73.55	47.25
9.0	15.3	18.50	137.70	83.36	54.34
10.0	15.6	20.00	156.00	93.17	62.83
11.0	15.9	21.50	174.90	102.97	71.93
12.0	16.1	22.50	193.20	112.78	80.42
13.0	16.3	24.00	211.90	122.59	89.31
14.0	16.5	25.00	231.00	132.39	98.61

Once the total effective stress beneath the embankment is known, the coefficient of volume decrease (m_v) can be determined. Using Figure 6.3 and the following expression:

$$m_v = \frac{1}{1+e_0}\left(\frac{e_0-e_1}{\sigma_1^{'}-\sigma_0^{'}}\right) \tag{6.2}$$

The coefficient of volume decrease (m_v) was calculated for various depth intervals beneath the trial embankment.

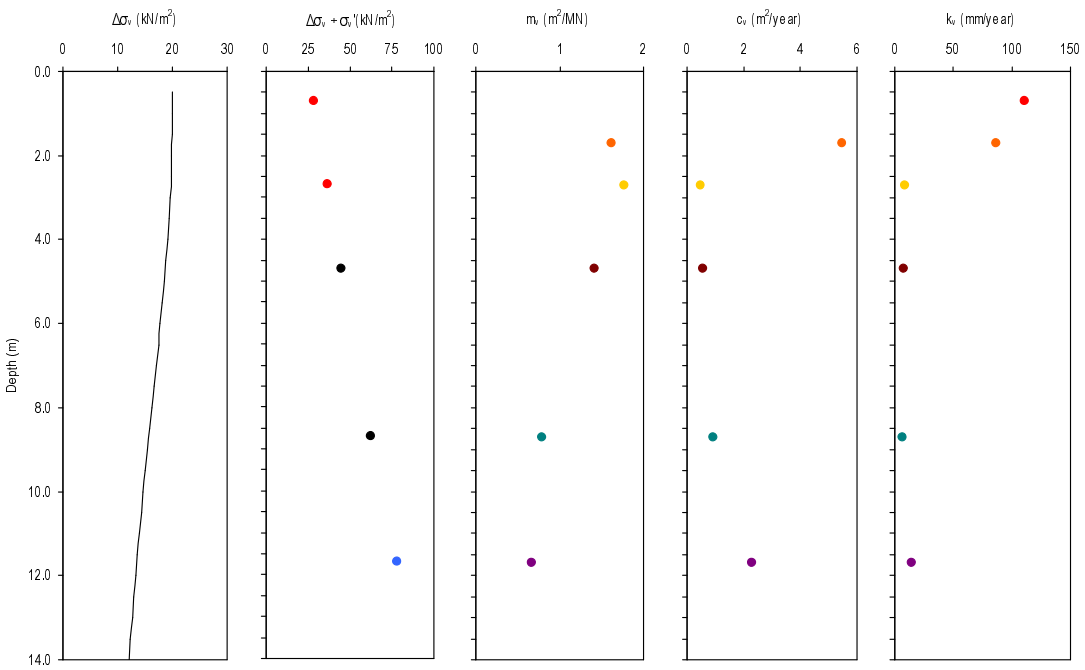

Figure 6.4 Stage 1 construction (Embankment height = 2m)

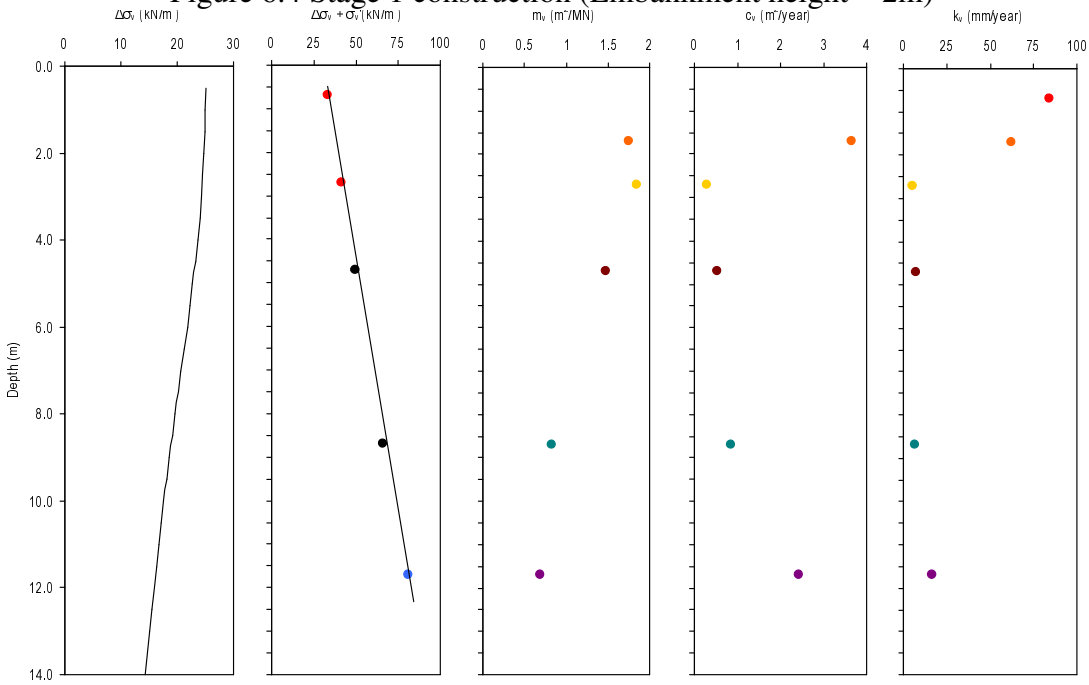

Figure 6.5 Stage 2 construction (Embankment height = 2.5m)

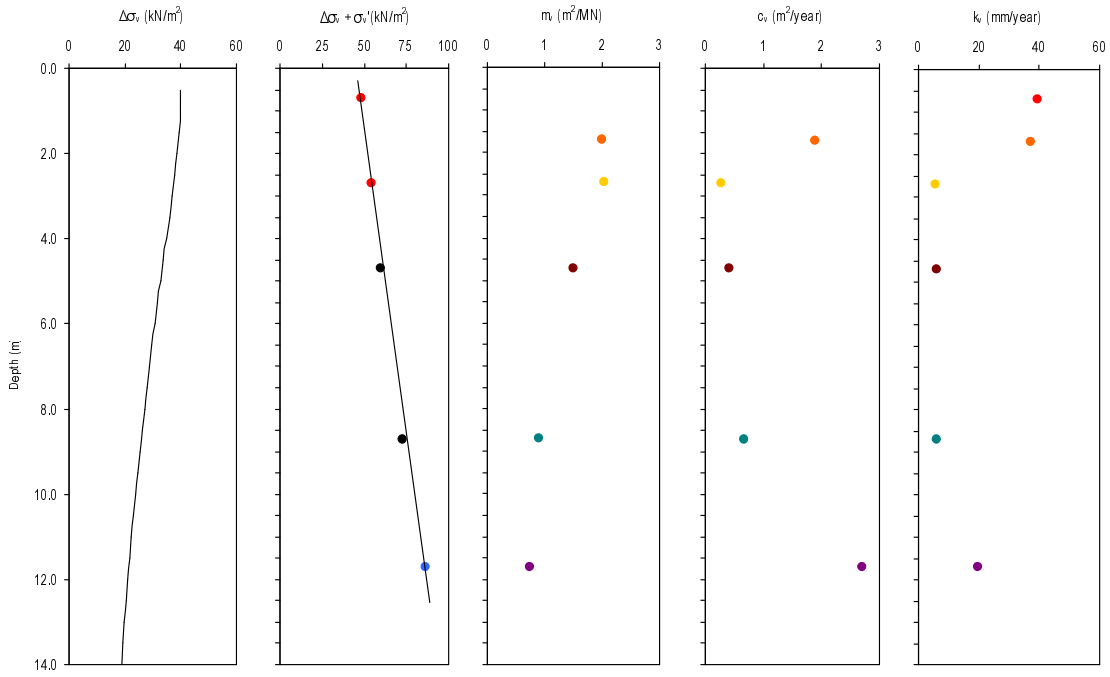

Figure 6.6 Stage 2 construction (Embankment height = 4m)

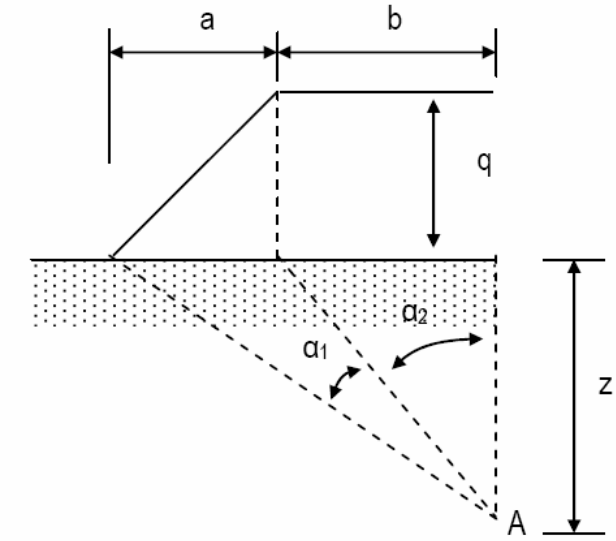

Figure 6.7 Vertical stress due to embankment loading (Das, 1997)

The coefficient of consolidation (c_v) was also determined for various depth intervals beneath the embankment. These values were determined by linear interpolating between the QDMR laboratory c_v values and the total effective stress values beneath the embankment.

With the coefficient of volume decrease (m_v) and coefficient of consolidation (c_v) known, the coefficient of permeability (k_v) for each depth interval can be calculated from the following euqation:

$$k_v = c_v \bullet m_v \bullet \gamma_w \tag{6.3}$$

The variation of m_v, c_v and k_v with depth is shown in Figures 6.4 (c), (d) and (e), Figures 6.5 (c), (d) and (e), and Figures 6.6 (c), (d) and (e) for each construction stage, respectively. The raw data used to produce these plots is displayed in Table 6.2, 6.3 and 6.4. The coloured figures in these tables are obtained from the stated bore holes. The uncoloured figures are the assumed distribution.

It can be seen, when referring to Figures 6.4, 6.5 and 6.6, that the coefficient of volume decrease (m_v), coefficient of consolidation (c_v) and coefficient of permeability (k_v) varies with depth. A single value for each of these parameters is required for the total soft clay strata. To determine the equivalent coefficient of volume decrease (m_v), coefficient of permeability (k_v) and coefficient of consolidation (c_v) for the whole clay layer the following procedure was followed:

i. Integrate the area under the incremental stress depth curves using the trapezoidal rule (Table 6.5), as displayed below

$$Area = \Delta\sigma_v H = \frac{\Delta H}{2}\left(\Delta\sigma_0 + 2\Delta\sigma_1 + 2\Delta\sigma_2 + \cdots + 2\Delta\sigma_{n-1} + \Delta\sigma_n\right) \tag{6.4}$$

ii. Determine the total settlement of the clay layer (Table 6.6) by summing the vertical settlement in the depth intervals, using the following expression:

$$\rho_c = \sum_{i=1}^{n} m_{vi}\Delta H_i \Delta\sigma_{vi} \tag{6.5}$$

iii. Once these two parameters are known, the equivalent coefficient of volume decrease (m_v) can be determined from the proceeding expression:

$$M_v = \frac{\rho_c}{Area} \tag{6.6}$$

iv. The equivalent coefficient of permeability (k_v) for the soft clay strata can be computed from the following expression -

$$K_v = \frac{\Delta H_1 + \Delta H_2 + \cdots + \Delta H_i}{\Delta H_1 / k_{v1} + \Delta H_2 / k_{v2} + \cdots + \Delta H_i / k_{vi}} \tag{6.7}$$

v. With the equivalent coefficient of volume decrease (m_v) and equivalent coefficient of permeability (k_v) known, the equivalent coefficient of consolidation can be calculated from -

$$C_v = \frac{K_v}{M_v \gamma_w} \tag{6.8}$$

The equivalent parameters for the soft clay strata, for stage 1 and stage 2 construction are displayed in the Table 6.7

Table 6.2 Stage 1 construction (Embankment height = 2m)

Depth (m)	$\Delta\sigma_v + \sigma_v'$ (kN/m^2)	m_v (m^2/MN)	k_v (m/year)	c_v (m^2/year)
1.0	29.4	1.61	0.1051	6.66
2.0	33.8	1.62	0.0803	5.06
3.0	38.0	1.83	0.0080	0.45
4.0	42.1	1.83	0.0046	0.26
5.0	46.2	1.43	0.0078	0.56
6.0	50.4	1.51	0.0076	0.52
7.0	54.7	1.50	0.0070	0.47
8.0	59.2	1.52	0.0064	0.43
9.0	63.9	0.81	0.0071	0.90
10.0	68.9	0.89	0.0067	0.77
11.0	74.3	0.91	0.0056	0.63
12.0	79.9	0.68	0.0157	2.37
13.0	85.7	0.72	0.0189	2.67
14.0	91.7	0.72	0.0210	2.99

Table 6.3 Stage 2 construction (Embankment height = 2.5m)

Depth (m)	$\Delta\sigma_v + \sigma_v'$ (kN/m^2)	m_v (m^2/MN)	k_v (m/year)	c_v (m^2/year)
1.0	34.4	1.70	0.0805	4.84
2.0	38.7	1.79	0.0574	3.27
3.0	42.7	1.87	0.0050	0.27
4.0	46.6	2.04	0.0055	0.27
5.0	50.4	1.51	0.0076	0.52
6.0	54.3	1.51	0.0071	0.48
7.0	58.4	1.51	0.0064	0.44
8.0	62.6	1.47	0.0057	0.39
9.0	67.1	0.86	0.0069	0.82
10.0	71.8	0.90	0.0061	0.69
11.0	77.0	0.96	0.0052	0.56
12.0	82.4	0.70	0.0172	2.50
13.0	88.1	0.75	0.0205	2.80
14.0	94.0	0.74	0.0226	3.11

Table 6.4 Stage 2 construction (Embankment height = 4m)

Depth (m)	$\Delta\sigma_v + \sigma_v'$ (kN/m^2)	m_v (m^2/MN)	k_v (m/year)	c_v (m^2/year)
1.0	49.2	2.00	0.0388	1.98
2.0	52.6	2.01	0.0367	1.86
3.0	55.4	2.04	0.0056	0.28
4.0	57.9	2.09	0.0058	0.28
5.0	60.5	1.49	0.0060	0.41
6.0	63.4	1.51	0.0057	0.39
7.0	66.5	1.53	0.0053	0.35
8.0	70.0	1.57	0.0049	0.32
9.0	73.8	0.91	0.0058	0.64
10.0	77.9	0.99	0.0052	0.53
11.0	82.6	1.01	0.0041	0.41
12.0	87.7	0.75	0.0204	2.78
13.0	93.0	0.75	0.0224	3.06
14.0	98.5	0.74	0.0245	3.35

Table 6.5 Incremental in stress

	Embankment Height (m)		
	2	2.5	4
Depth (m)	$\Delta\sigma_v$ (kN/m^2)	$\Delta\sigma_v$ (kN/m^2)	$\Delta\sigma_v$ (kN/m^2)
1.0	19.98	24.97	39.78
2.0	19.86	24.77	38.72
3.0	19.58	24.32	36.98
4.0	19.12	23.63	34.94
5.0	18.51	22.74	32.82
6.0	17.80	21.74	30.75
7.0	17.03	20.69	28.79
8.0	16.23	19.63	26.96
9.0	15.44	18.60	25.28
10.0	14.68	17.62	23.74
11.0	13.95	16.70	22.34
12.0	13.26	15.83	21.06
13.0	12.61	15.03	19.90
14.0	12.01	14.28	18.84

Table 6.6 Layer settlement for different embankment heights

	Height (m)		
	2	2.5	4
Depth (m)	ρ (mm)	ρ (mm)	ρ (mm)
1.0	16	21	40
2.0	16	22	39
3.0	18	23	38
4.0	18	24	36
5.0	13	17	24
6.0	13	16	23
7.0	13	16	22
8.0	12	14	21
9.0	6	8	12
10.0	7	8	12
11.0	6	8	11
12.0	4	6	8
13.0	5	6	7
14.0	4	5	7

Table 6.7(a) Back calculated in-situ coefficient of consolidation (stage 1 construction; embankment height = 2m; no ground improvement)

	Depth (m)									
	1.40		3.40		5.40		8.40		9.90	
t(day)	u_e(kPa)	c_v (m^2/year)	u_e(kPa)	c_v (m^2/year)	u_e(kPa)	c_v (m^2/year)	u_e(kPa)	c_v (m^2/year)	u_e(kPa)	c_v (m^2/year)
49	28.60	10.44	39.02	12.48	36.44	55.12	32.08	93.37	27.40	94.43
56	18.60	25.33	31.02	38.07	30.44	84.28	24.08	134.47	18.40	153.04
66	14.30	35.30	28.73	38.11	28.15	79.10	20.78	128.77	15.10	150.82
91	14.30	22.89	27.73	27.56	28.15	51.94	20.78	84.10	14.10	105.16
132	12.70	18.73	27.12	18.69	27.54	34.68	22.18	49.57	13.49	69.93
188	9.40	22.48	22.82	18.88	25.25	27.01	18.88	40.11	10.20	58.80
231	8.62	20.70	22.04	16.17	24.46	22.65	17.10	35.41	9.42	49.60

Table 6.7(b) Back calculated in-situ coefficient of consolidation (stage 1 construction; embankment height = 2m; stone columns spacing = 2m)

	Depth (m)							
	1.40		3.40		5.40		8.40	
t(day)	u_e(kPa)	c_v (m^2/year)	u_e(kPa)	c_v (m^2/year)	u_e(kPa)	c_v (m^2/year)	u_e(kPa)	c_v (m^2/year)
49	35.60	4.48	30.02	52.56	31.44	95.27	43.08	-
56	26.60	10.37	24.02	76.94	23.44	136.88	36.08	50.37
66	22.30	12.85	18.73	96.18	20.15	131.14	30.78	67.23
91	21.30	9.33	17.73	68.26	17.15	101.84	27.78	54.82
132	18.70	8.06	16.12	49.64	14.54	75.56	23.18	46.72
188	16.40	7.24	12.82	43.00	12.25	57.93	17.88	42.45

Table 6.7(c) Back calculated in-situ coefficient of consolidation (stage 1 construction; embankment height = 2m; stone columns spacing = 3m)

	Depth (m)									
	1.25		3.25		5.25		8.25		9.75	
T (day)	u_e (kPa)	c_v (m^2/year)	u_e (kPa)	c_v (m^2/year)	u_e (kPa)	c_v (m^2/year)	u_e (kPa)	c_v (m^2/year)	u_e (kPa)	c_v (m^2/year)
49	22.07	16.86	33.49	32.19	43.91	-	51.55	-	34.86	45.63
56	13.07	43.80	24.49	68.07	31.91	72.27	41.55	-	24.86	99.02
66	10.77	51.10	19.20	87.24	26.62	85.78	35.25	45.84	19.57	114.43
91	9.77	40.15	17.20	67.71	22.62	72.64	35.25	30.33	17.57	85.56
132	10.16	23.73	15.59	49.46	21.01	51.17	30.64	29.31	13.96	69.35
188	11.16	13.14	14.29	36.87	16.72	44.06	24.35	29.67	9.67	62.12
231	9.09	15.70	12.51	33.95	12.93	43.91	21.57	27.82	7.88	56.58
273	10.70	9.49	13.12	27.01	14.54	33.36	21.18	23.76	8.49	45.11
314	9.09	11.28	12.51	24.46	13.93	29.78	19.57	22.41	7.88	40.66
485	9.87	6.13	12.29	15.77	12.72	20.29	18.35	15.21	6.67	28.36

6.5.1 Predicted one dimensional settlement

Once the coefficient of consolidation (c_v) is known, conventional design methods can be utilised to predict the settlement of the soft clay layer. Before the settlement can be

calculated, the degree of consolidation (U_{av}) must first be determined. Olson's (1977) mathematical solution was used to determine the degree of consolidation of the soft clay layer.

For $T_v \leq T_c$:

$$U_{av} = \frac{T_v}{T_c}\left\{1 - \frac{2}{T_v}\sum_{m=0}^{m=\infty}\frac{1}{M^4}\left[1 - \exp\left(-M^2 T_v\right)\right]\right\} \tag{6.9}$$

For $T_v > T_c$:

$$U_{av} = 1 - \frac{2}{T_c}\sum_{m=0}^{m=\infty}\frac{1}{M^4}\left[\exp\left(M^2 T_c\right)\right]\exp\left(-M^2 T_v\right) \tag{6.10}$$

When referring to Figure 6.8 the variation of the vertical time factor (T_v) against the average degree of consolidation (U_{av}) for various construction time factor (T_c) values is illustrated. From the knowledge of the Principal Geotechnical Testing Officer at QDMR, it took approximately 35 days to construct each stage of the trial embankment. For a construction time of 35 days, the corresponding T_c value is 0.001 (Figure 6.8). Using this curve and the total soft clay layer settlement (ρ_c), the settlement at any time (ρ_t) can be calculated from the following expression:

$$\rho_t = U_{av}\rho_c \tag{6.11}$$

The predicted settlement time plots for stage 1 and stage 2 construction of the embankment are illustrated in Figure 6.9.

6.5.2 Field instrumentation

During construction of the trial embankment field instrumentation was installed to monitor its performance. The following instrumentation was installed -

i. Settlement gauges

ii. Horizontal profile gauges

iii. Inclinometers

iv. Piezometers

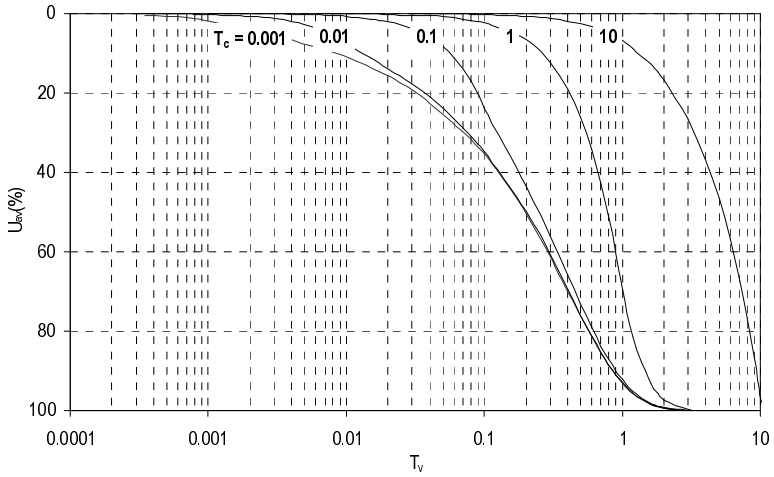

Figure 6.8 Average degree of consolidation against time factor for single ramp load

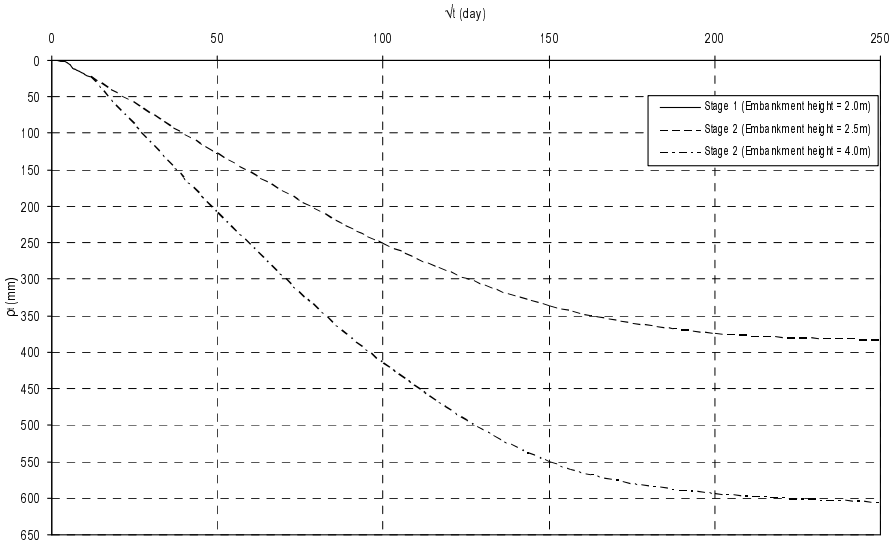

Figure 6.9 Stage 1 and Stage 2 construction one dimensional settlement time plots

Settlement gauges were installed, at the centre line of the embankment, to monitor vertical settlement. The surface and subsurface vertical settlement time plots for the trial embankment with no ground improvement, stone columns at 2m spacing and stone columns at 3m spacing is shown in Figures 6.10(a) (Taylor) and 6.10(b) (Casagrande).

Across the base of the embankment, horizontal profile gauges were installed to record the horizontal settlement profile of the embankment. When referring to Figures 6.11, 6.12 and 6.13 the variation of vertical settlement, at regular intervals, across the embankment is shown. Also obtained from these readings, is the horizontal settlement time profile for all three embankments (as shown in Figures 6.14, 6.15 and 6.16). Polynomial aggression curves (solid lines) were fitted to the data series of these figures. The dotted curves which extend from the aggression curves are the predicted horizontal settlement profile.

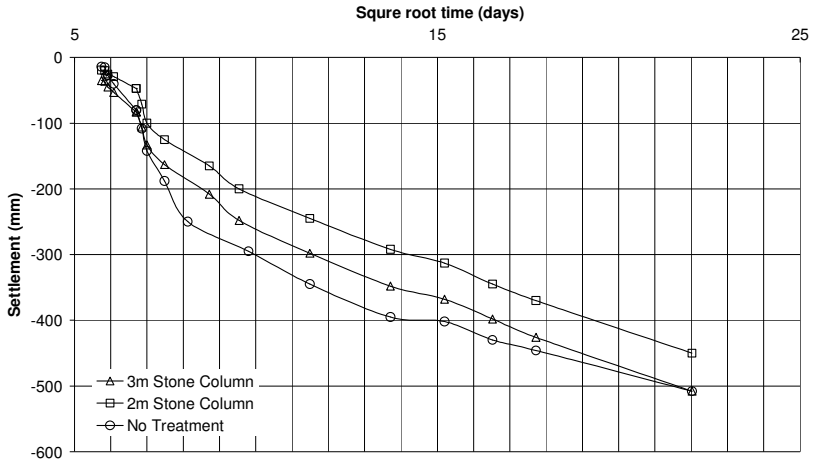

Figure 6.10(a) settlement time plots at the trial embankment centre line (Taylor)

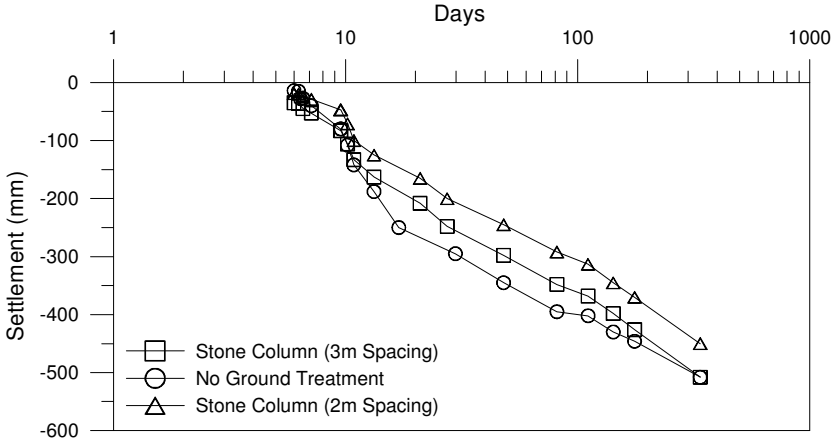

Figure 6.10(b) settlement time plots at the trial embankment centre line (Casagrande)

Inclinometers were installed at the toe of the embankment to monitor lateral displacement. The variation of lateral displacement with depth, for the embankment

with no ground improvement, stone columns at 2m spacing and stone columns at 3m spacing is shown in Figure 6.17.

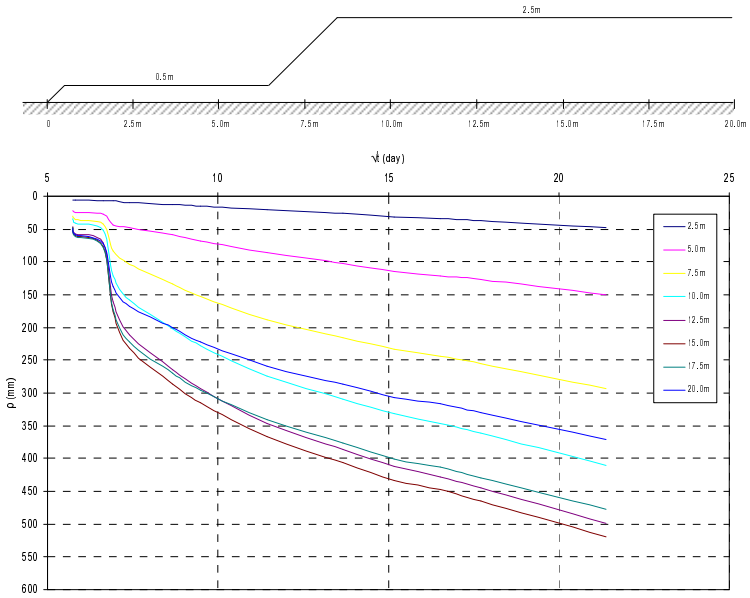

Figure 6.11 In-situ vertical settlement profile at various distances along the embankment with no ground improvement

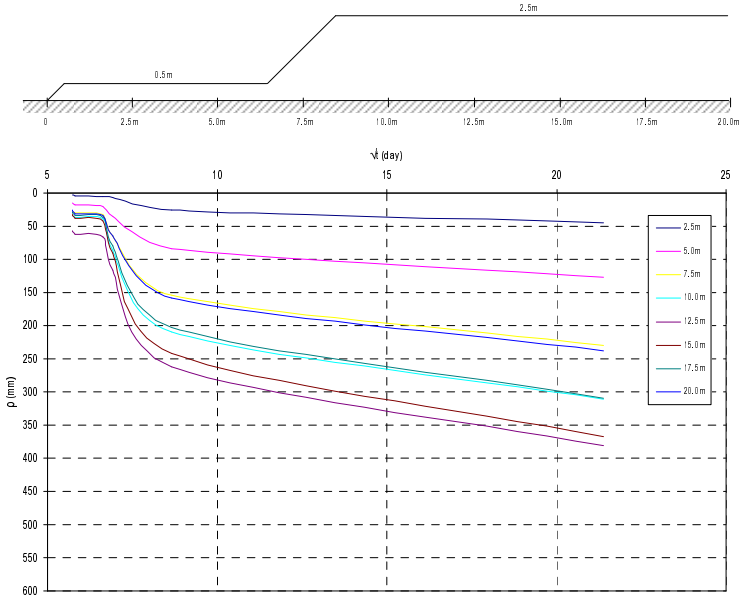

Figure 6.12 In-situ vertical settlement profile at various distances along the embankment with stone columns at 2m spacing

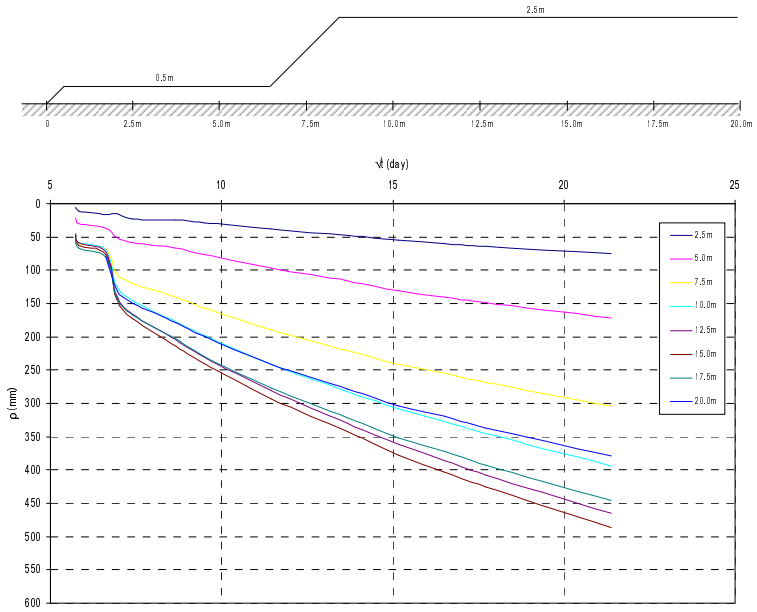

Figure 6.13 In-situ vertical settlement profile at various distances along the embankment with stone columns at 3m spacing

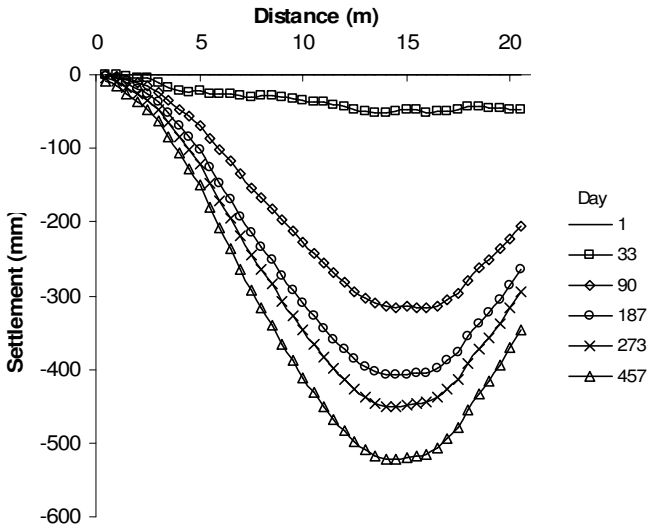

Figure 6.14 In-situ horizontal settlement time profile for the embankment with no ground improvement

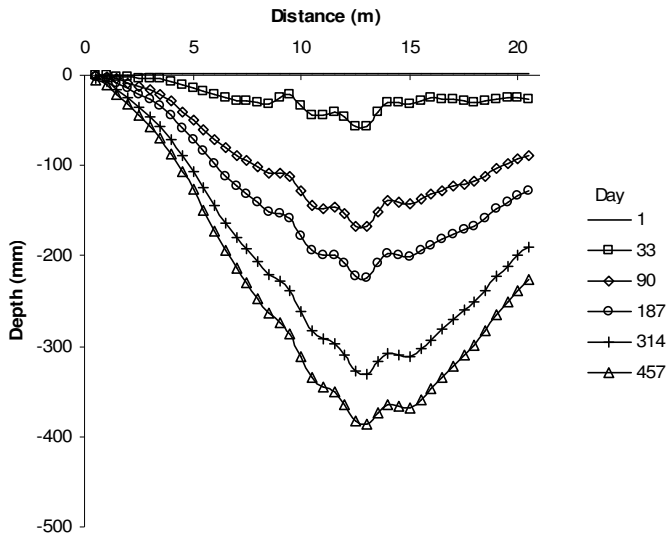

Figure 6.15 In-situ horizontal settlement time profile for the embankment with stone columns at 2m spacing

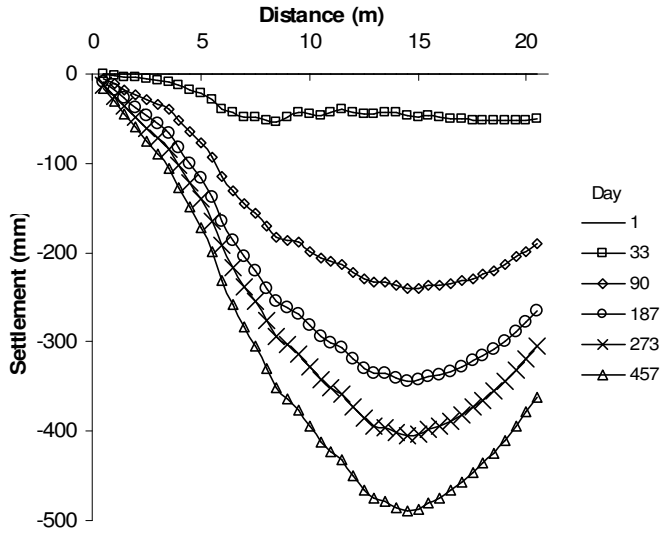

Figure 6.16 In-situ horizontal settlement time profile for the embankment with stone columns at 3m spacing

Piezometers were installed at the centre line of the trial embankment to monitor pore pressure dissipation. The variation of pore pressure with time is shown in Figures 6.18(a), 6.18(b) and 6.18(c) for all three embankments. It should be noted that these plots take into consideration the total excess pore pressure; which includes the static water table and the increase in pore pressure due to the construction of the embankment.

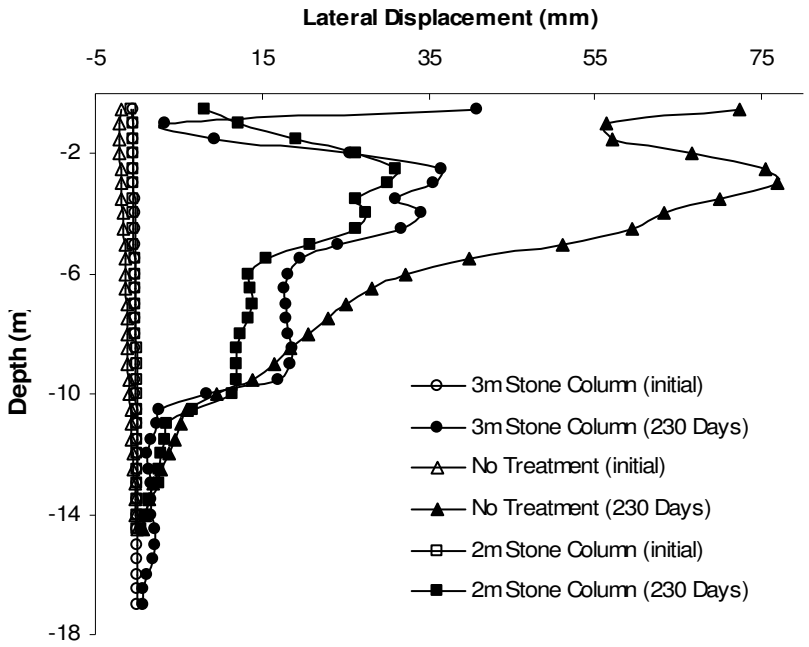

Figure 6.17 In-situ lateral displacements at the toe of the embankment

6.6 Vertical Settlement

6.6.1 Vertical settlement at embankment centre line

From the laboratory results, the settlement of the trial embankment was predicted for each construction stage. The predicted one dimensional settlement time plots are shown in Figure 6.9. The solid line in Figure 6.9 is the settlement after stage 1 construction. The embankment height after stage 1 construction was 2m. Construction of stage 2 began about 100 days after the completion of stage 1. After stage 2 construction, the total embankment height was 2.5m for the embankment with no ground improvement and 6.0m for the embankments with stone columns.

When referring to Figures 6.10(a) and 6.10(b) the in-situ settlement time plots at the centre line of each embankment are shown. These plots illustrate the ground level settlement of the embankment and the subsurface settlement at depths 5.25m and 8.5m. The same settlement time data was used to produce these figures, however, the plotting method is varied. Figure 6.10(a) was plotted using Taylor's square root of time method, whereas, Figure 6.10(b) was plotted using Casagrande's log time method. The ground

level settlement data fits Taylor's method better than Casagrande's method. Both figures illustrate that primary consolidation has not yet been completed.

These figures illustrate that installing closely spaced stone columns reduces the amount of ground level settlement. At square root time 22 days the embankment without ground improvement and the embankment with stone columns at 3m spacing had the same ground level settlement. The subsurface settlement beneath all three embankments decreased with depth. This was expected because the upper weathered crust of the soft clay layer has low strength and is highly compressible. At square root time 22 days the embankment with no ground improvement had the greatest subsurface settlement (Figure 6.10(a)). At the same time interval, the embankment with stone columns at 2m spacing had reduced settlement compared to the embankment with stone columns at 3m spacing. This further illustrates that closely spaced stone columns reduce the amount of subsurface settlement.

The predicted settlement of the trial embankment (Figure 6.9) is under estimated when compared to the measured settlement (Figures 6.10(a) and 6.10(b)). The main reason the settlement was under estimated was due to the large variation in the magnitude of the laboratory and in-situ coefficient of consolidation.

For all three construction heights, the equivalent laboratory coefficient of consolidation (c_v) varied between 0.5 – 0.7m^2/year (Table 6.7). The in-situ coefficient of consolidation was determined for the Coombabah Creek site, to be approximately twenty times greater than the laboratory c_v value. Such a large variation between the laboratory and in-situ coefficient of consolidation has resulted in the under estimation of the settlement. This large variation in the coefficient of consolidation highlights the importance of large scale field tests to determine the actual in-situ soil conditions.

6.6.2 Vertical settlement profile along embankment

The vertical settlement profile at various distances along the three embankments is shown in Figures 6.11, 6.12 and 6.13. This settlement profile was obtained from horizontal profile gauges installed beneath the embankment.

The actual embankment cross-section is also displayed on these figures. Initially, the embankment was constructed to a berm height of 0.5m. After the berm was built, the stage 1 of construction was (height =2m) then built on top of the berm. The stage 1 construction began at 6.5m (horizontally) and extended to 26.5m (horizontally). The centre line of the stage 1 embankment was at 16.5m (horizontally). This construction method is illustrated in the settlement time plots. Initially the settlement was minimal with the berm constructed, however, after stage 1 construction, the amount of settlement increased at distances 7.5m and greater.

The embankment which experienced the greatest amount of vertical settlement was the embankment with no ground improvement (Figure 6.11). Similar vertical settlement was experienced in the embankment with stone columns at 3m spacing (Figure 6.13). Figure 6.12 illustrates that installing stone columns which are closely spaced reduces the amount of settlement. The reduction in vertical settlement is due to the stiffening or reinforcing effect of stone columns. Aboshi (1992) has shown that some of the embankment load is carried by the stiffer stone column, reducing the consolidation load, and hence, lowering the expected settlement.

6.7 Horizontal Settlement Profile along Embankment

Also obtained from the horizontal profile gauge was the horizontal settlement profile of the three embankments shown in Figures 6.14, 6.15 and 6.16. Polynomial aggression equations have been fitted to the known data readings. The dotted curves which extend from these aggression curves, are the predicted settlement profiles.

As stated earlier, the centre line of the stage 1 embankment was at 16.5m. The peak vertical settlement occurred at approximately 15m (horizontally), for the embankments with no ground improvement and stone columns at 3m spacing. The peak vertical

settlement for the embankment with stone columns at 2m spacing occurred at approximately 13m (horizontally). The maximum settlement occurred quite close to the centre line of the embankment. The settlement then decreased either side of the embankment centre line.

The settlement profile for all three embankments cannot be purely classified as consolidation settlement. This settlement is the result of the soft marine clay being unable to support the weight of the embankment. As a result, the embankment sinks in the middle, and causes soil to be heaved at the extreme ends of the embankment. This outward movement of earth from the toe of the embankment is illustrated when referring to the in-situ lateral displacement plots for the embankments.

6.8 Lateral Displacement

When referring to Figure 6.17, the in-situ lateral displacement at the toe of the embankment with no ground improvement, stone columns at 2m spacing and stone columns at 3m spacing is shown, respectively.

These plots illustrate the variation of laterally displacement with depth, for various time increments. Nearly all of these curves move outwards from the vertical axis. This behaviour indicates instability in the trial embankment. When referring to Figure 6.17, the greatest amount of lateral displacement is experienced at depths 0 – 10m, with the lateral displacement peaking between depths 2 – 3m.

The embankment which has the greatest lateral displacement is the embankment with no ground improvement (Figure 6.17 (a)). Installing stone columns at 2m spacing reduces the amount of lateral displacement, approximately by half (Figure 6.17 (b)), when compared to the embankment with no ground improvement. The lateral displacement of the embankment with stone columns at 3m spacing (Figure 6.17 (b)), had slightly higher displacements when compared to the embankment with stone columns at 2m spacing.

Thus installing stone columns beneath the trial embankment reduces lateral displacement.

6.9 Total Excess Pore Pressure

Piezometers were installed in the trial embankment to monitor the dissipation of excess pore pressure. The variation of pore pressure with the square root of time is shown in Figures 6.18(a), 6.18(b), and 6.18(c). This figure illustrates the increase and decrease in pore pressure with the construction of the berm and stage 1 construction. It should be noted that this figure takes into consideration the static water table.

There are two peak total excess pore pressures for each embankment and each corresponding peak value occurs at a similar time (Figures 6.18(a), 6.18(b) and 6.18(c)). The smaller peak value is from the construction of the berm and the larger peak value is from stage 1 construction.

When the berm was being constructed, the pore pressure increased with time. Once the berm was constructed the pore pressure peaked and began to dissipate with time until stage 1 construction began. When stage 1 was being built the pore pressure increased again with time until stage 1 was fully completed. The pore pressure then decreased with time until the static pore pressure was reached.

When comparing Figure 6.18(a) with Figures 6.18(b) and 6.18(c), the embankments with stone columns dissipate the total excess pore pressure at a faster rate than the embankment with no ground improvement. This is because stone columns behave as vertical drains and reduce the drainage length in which the pore water has to travel to be dissipated.

Piezometers are not an accurate means of measuring pore pressure dissipation. For example when considering the embankment without ground improvement at depth 8.40m, the variation of pore pressure, after peaking, fluctuates. There are two reasons

which could explain this behaviour. First the height of the embankment could have been increased, resulting in an increase in pore pressure, or, there are errors with the piezometer.

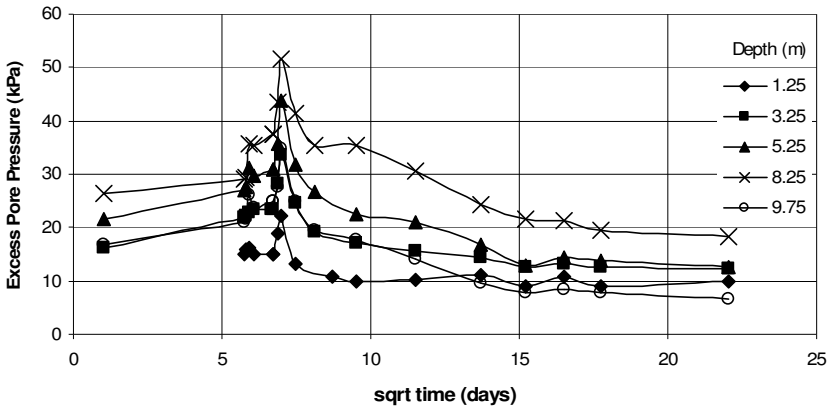

Figure 6.18(a) Total excess pore pressure time plots (3m Stone Column)

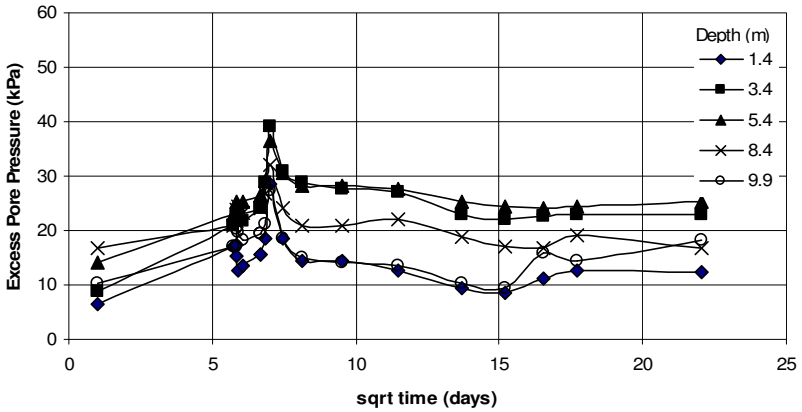

Figure 6.18(b) Total excess pore pressure time plots (No Treatment

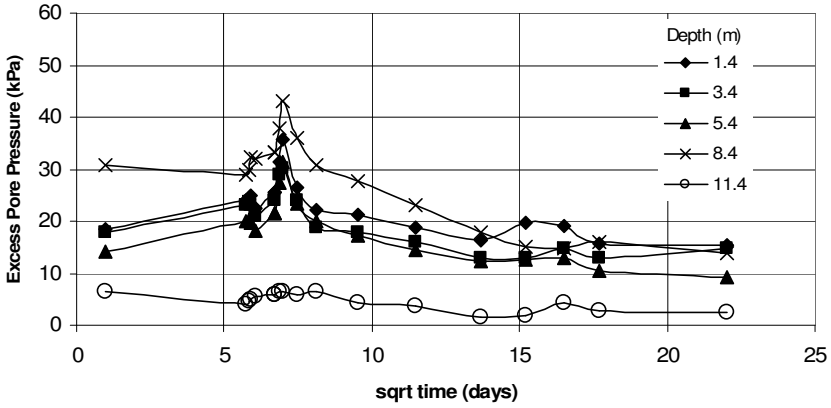

Figure 6.18(c) Total excess pore pressure time plots (2m Stone Column)

6.10 In-situ Coefficient of Consolidation (c_v)

The following two methods were used to back calculate the coefficient of consolidation (c_v) from the large scale field test data.

6.10.1 Olson (1977) Solution

Olson's (1977) mathematical solution to determine the degree of consolidation under a time dependant load was used to determine the in-situ coefficient of consolidation of the soft clay strata. The following two expressions were used –

For $T_v \leq T_c$:

$$U_e = \sum_{m=0}^{m=\infty} \frac{2q_c}{M^3 T_c} \sin\frac{Mz}{H}\left[1 - \exp\left(-M^2 T_v\right)\right] \tag{6.12}$$

For $T_v > T_c$:

$$U_e = \sum_{m=0}^{m=\infty} \frac{2q_c}{M^3 T_c} \left[\exp\left(M^2 T_c\right) - 1\right] \sin\frac{Mz}{H}\left[1 - \exp\left(-M^2 T_v\right)\right] \tag{6.13}$$

The back calculated in-situ c_v values are displayed in Table 6.7. These values were determined from the total excess pore pressure readings after stage 1 had been fully constructed. Also the in-situ coefficient of consolidation was determined for the portion of the curve which didn't contain high increases in pore pressure.

The in-situ coefficient of consolidation was found to be approximately twenty times greater than the laboratory c_v value for some c_v values. For most of c_v values determined using Olson's (1977) solution, the in-situ coefficient of consolidation was found to be much greater.

6.10.2 Asaoka (1978) Solution

In 1978, Asaoka presented a new and practical approach to estimate the final consolidation settlement (ρ_∞) and in-situ coefficient of consolidation (c_v) from

settlement time data for a certain time period. The following steps were completed to determine ρ_∞ and c_v.

i. Using Figure 6.10(a) the ground level settlement (ρ) at 30 day time intervals (Δt) was determined for each embankment.

ii. The settlement values ρ_1, ρ_2,..., ρ_i and ρ_2, ρ_3,..., ρ_{i+1} were then plotted as points in a coordinate system with ρ_i being the x-axis and ρ_{i+1} being the y-axis. A 45° line was also drawn.

iii. A straight line was then drawn through the data points. The location where the 45° line intersects the straight line, gives the final consolidation settlement (ρ_∞). The in-situ coefficient of consolidation (c_v) is given by the following expression –

$$c_v = -\frac{5}{12} H^2 \frac{\ln \beta_1}{\Delta t} \tag{6.14}$$

The plot of the settlement values and fitted straight lines, for the three embankments, is shown in Figures 6.19(a) to 6.19(f). The in-situ coefficient of consolidation (c_v) and final consolidation settlement (ρ_∞) for the embankments is displayed in Tables 6.8 to 6.10.

The same in-situ coefficient of consolidation was obtained for all three embankments. Also the final consolidation settlement predicted by Asaoka's method is inaccurate. The two main functions of stone columns are to accelerate the rate of consolidation and strengthen the soft clay strata. Thus, the embankment with stone column at 3m spacing can not have a higher final consolidation settlement than the embankment without ground improvement.

Table 6.8 Asaoka's graphical method

Embankment	H (m)	Δt (day)	β_1	c_v (m^2/year)	ρ_∞ (mm)
No Ground Improvement	7	30	0.7535	70.3	520
Stone Columns 2m Spacing	7	30	0.7535	70.3	490
Stone Columns 3m Spacing	7	30	0.7535	70.3	560

Table 6.9 Embankment with no ground improvement

Elapsed time (day)	33	56	96	188	314	485
$\sqrt{t}$	5.74	7.48	9.80	13.71	17.72	22.02
FEM vertical settlement (mm)	211	248	296	356	423	484
Measured settlement (mm)	20	190	295	395	446	508

Table 6.10 Embankment with stone columns at 2m spacing

Elapsed time (day)	33	56	96	188	314	485
$\sqrt{t}$	5.74	7.48	9.80	13.71	17.72	22.02
FEM vertical settlement (mm)	291	299	312	329	352	379
Measured settlement (mm)	20	130	200	292	370	450

6.11 Finite Element Embankment Model (PLAXIS Analysis)

The performance of the trial embankment was also evaluated using PLAXIS. PLAXIS is a finite element Geotechnical Engineering computer program. This program was used to determine the consolidation settlement and lateral displacement at the toe of the embankments. Stage 1 construction of the embankment with no ground improvement and the embankment with stone columns at 2m spacing were modelled. The consolidation settlements at various time intervals were determined. The input parameters used in the PLAXIS model are given in Table 6.9. The deformed mesh of the embankment with no ground improvement at 485 days is shown in Figure 6.20.

For day 96 and greater the finite element model (FEM) predicts the vertical settlement (Table 6.10) very close to the actual ground level settlement of the embankment with no ground improvement (Figures 6.10(a) and 6.10(b)). The finite element model for the embankment with stone columns at 2m spacing (Table 6.11), over predicts the settlement for most instances, when compared to Figure 6.10(a) and 6.10(b).

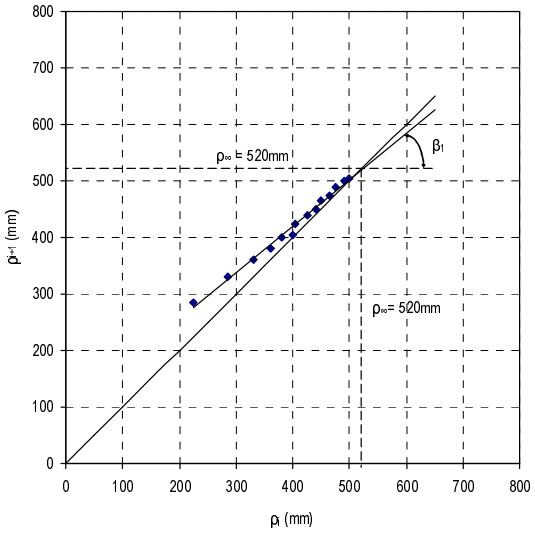

Figure 6.19(a) Asaoka's method for graphical evaluation of settlement records

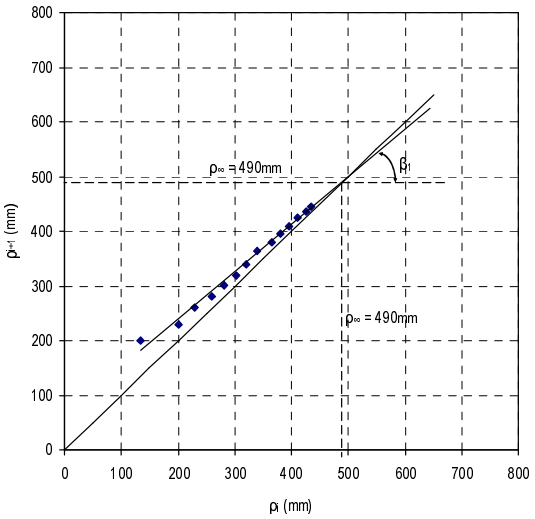

Figure 6.19(b) Asaoka's method for graphical evaluation of settlement records

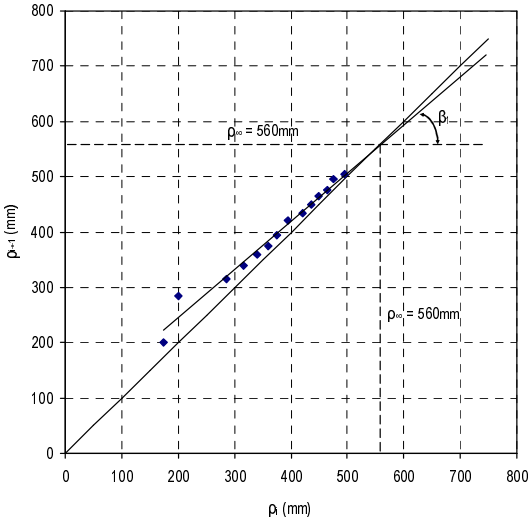

Figure 6.19(c) Asaoka's method for graphical evaluation of settlement records

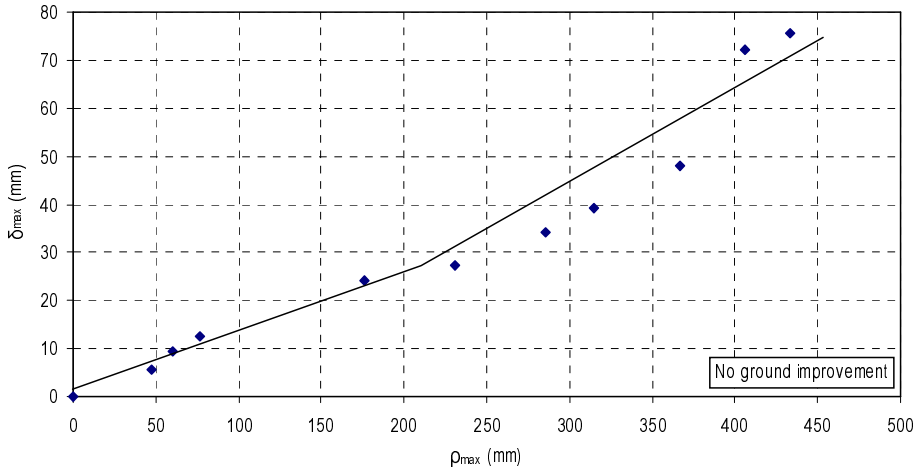

Figure 6.19(d) Maximum settlement against maximum lateral displacement plots

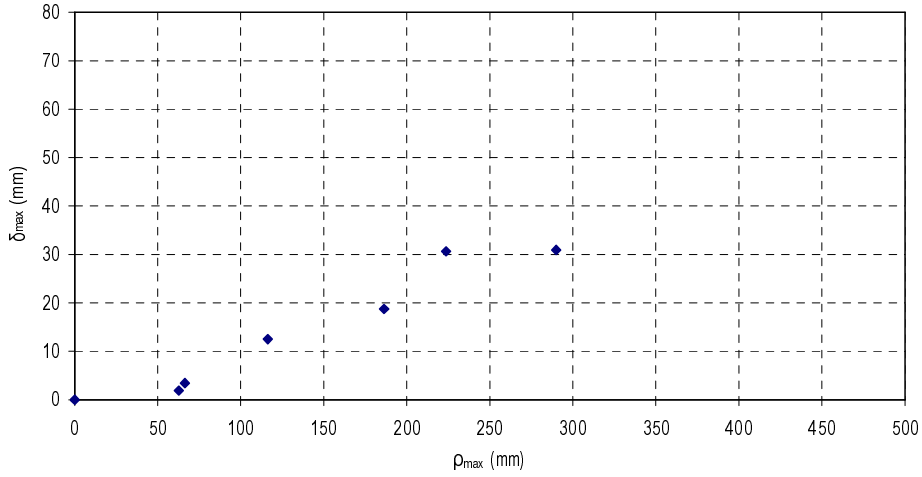

Figure 6.19(e) Maximum settlement against maximum lateral displacement plots

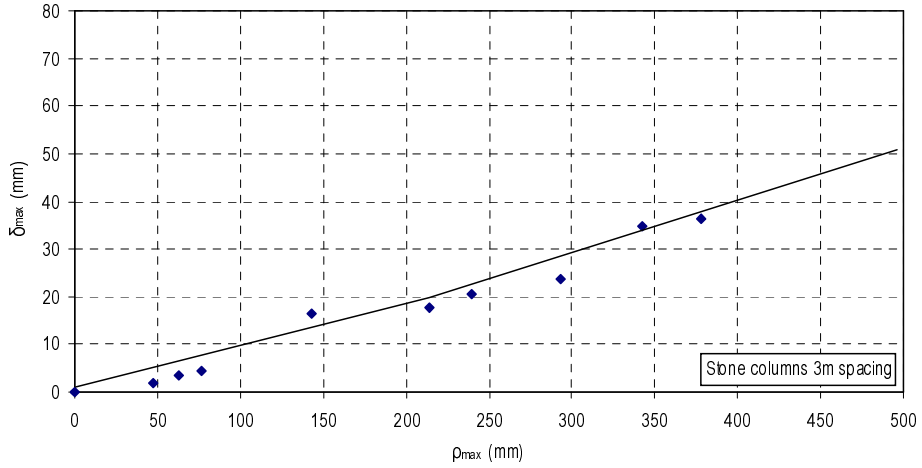

Figure 6.19(f) Maximum settlement against maximum lateral displacement plots

Stage 1 construction for the embankment with no ground improvement and the embankment with stone columns at 3m spacing were modelled. These two embankment

finite element meshes are shown in Figures 6.21 and 6.22 respectively. It was determined that, the lateral displacement at the toe of these embankments (Figure 6.23(a)) and the vertical movement horizontally from the embankment centre line (Figure 6.23(b)).

The lateral displacement was determined immediately after stage 1 construction and 6 months after consolidation began. When comparing the plots in Figures 6.23(a) and 6.23(b), the embankment with stone columns experiences approximately half the lateral displacement as the embankment with no ground improvement; for both time intervals. Thus stone columns reduce the amount of lateral displacement at the embankment toe.

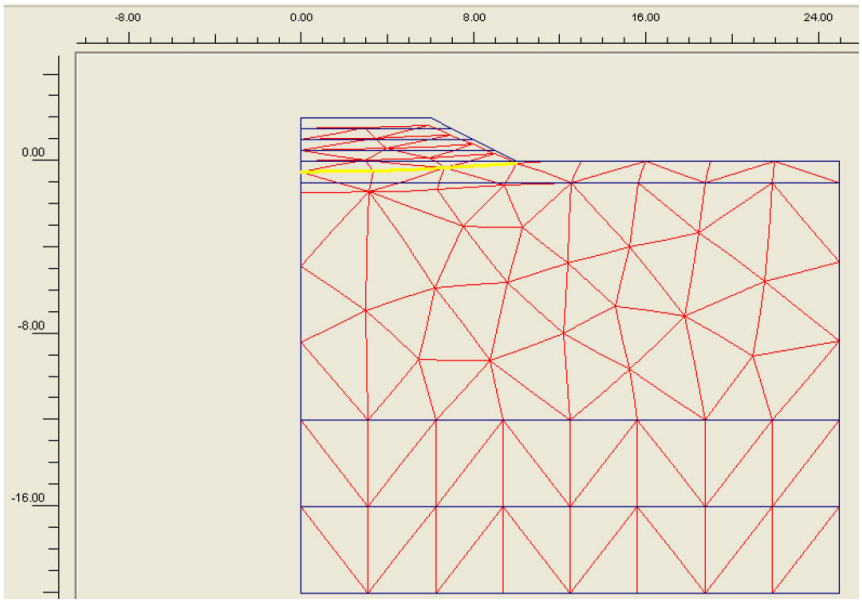

Figure 6.20 Deformed mesh of the embankment with no ground improvement at day 485 (Stage 1 Construction)

The lateral displacement predicted by the finite element models is underestimated when compared to the in-situ lateral displacement (Figure 6.17). This is further illustrated when comparing the FEM vertical movement from the embankment centre line plots (Figure 6.23(b)) with the in-situ horizontal settlement profile (Figures 6.14, 6.15, and 6.16) of the respective embankments.

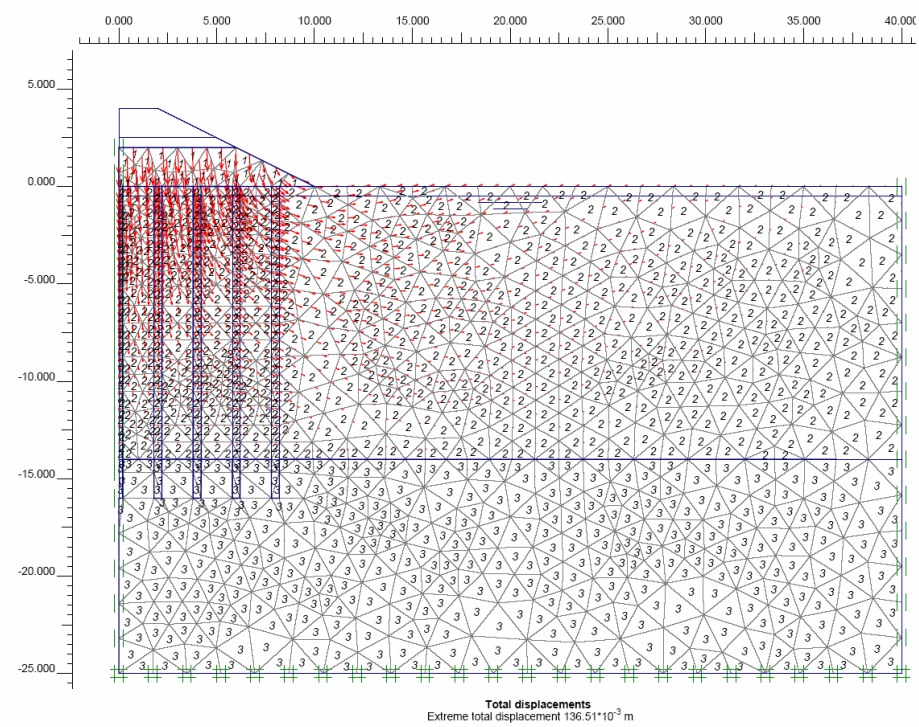

Figure 6.21 Finite element mesh for the embankment with no ground improvement (Stage 1 Construction)

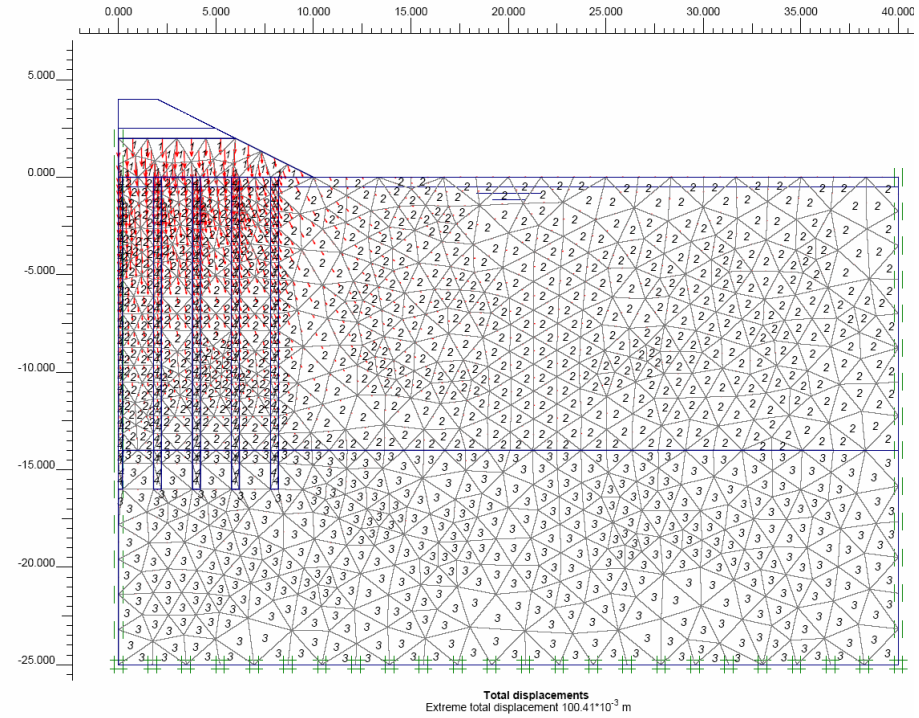

Figure 6.22 Finite element mesh for the embankment with stone columns at 3m spacing (Stage 1 Construction)

6.12 Concluding Remarks

From the extensive research into the performance of the Gold Coast Highway trial embankment, it can be concluded that:

i. Installing stone columns at 2m centres reduces the vertical settlement

ii. Installing stone columns at 3m centres has similar vertical settlement to the embankment without ground improvement

iii. Stone columns reduce lateral displacement at the toe of the embankment by approximately half when compared to the embankment no ground improvement

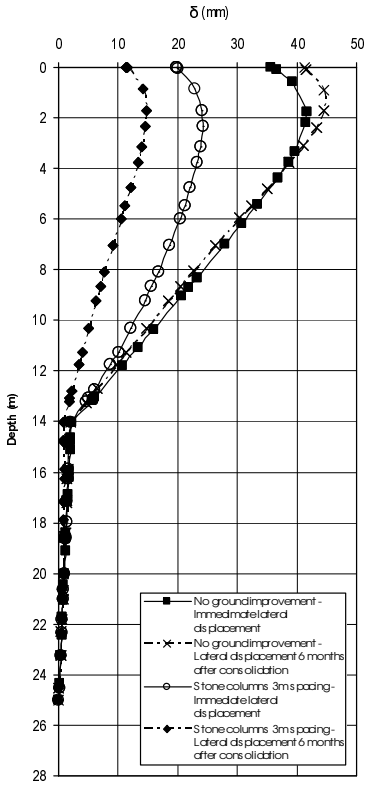

Figure 6.23(a) Predicted lateral displacement at the toe of embankment

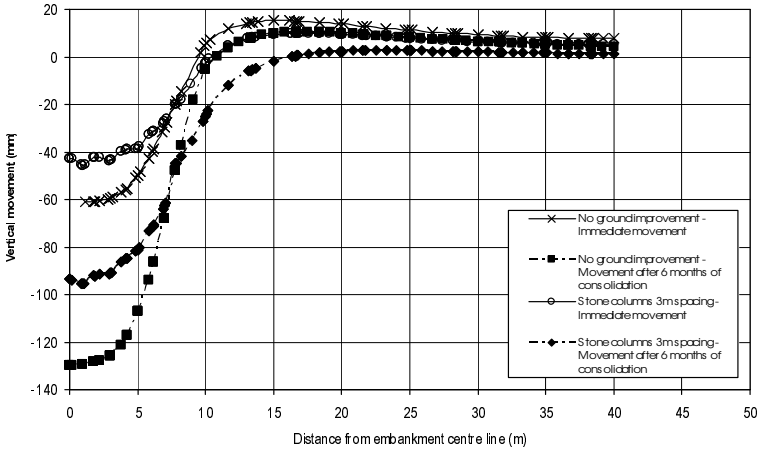

Figure 6.23(b) Predicted vertical movement horizontally from the embankment centre line

CHAPTER 7

BEHAVIOURS OF CHEMICAL TREATED SOIL

7.1 Introduction

A detailed series of laboratory tests were undertaken in order to investigate the unconfined compressive strength of cement and lime treated estuarine clay.

The effects of cement addition to clay are investigated, focusing on components such as compressive strength along with physical characteristics. Unconfined compressive strength tests were undertaken on cement treated samples at varying curing times, and the effects of cement content, curing time and moisture content are examined.

7.2 Untreated Clay and Sample Preparations

7.2.1 Characteristics of Untreated Clay

Characteristics of untreated clay samples are to be defined prior to cement addition by utilising results of laboratory tests such as Atterberg limits, particle size distribution and unconfined compressive strength tests. Physical properties of untreated clay as presented in Table 7.1, show the natural water content for the untreated sample is extremely close the liquid limit of the soil. This signifies that the natural sample is extremely soft and easy to deform.

The particle size distribution of the untreated sample is shown in Figure 7.1. Classification of the sample is determined to be an Organic Clay (OL-M) with 35% passing the No: 200 sieve and PI<50%. Composition of the sample is 25% clay, 65% silt and 10% sand.

7.2.2 Unconfined Compression Strength (UCS) Tests for Untreated Samples

Untreated specimens of Southeast Queensland clay were tested for unconfined compression strength as presented in Figure 7.2. The peak unconfined compressive strengths of 25.5 kPa was obtained at 8% strain. These results show that the natural clay

sample is very soft. After maximum unconfined compressive strength is reached, the residual stress gradient of the sample is extremely low, indicating the ductile failure mechanism for the untreated clay soil.

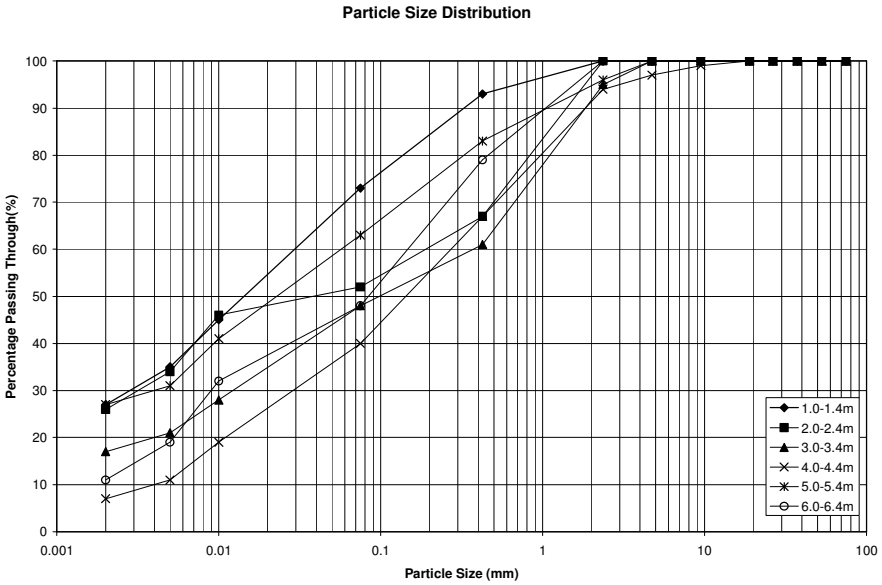

Figure 7.1 Particle Size Distribution for Untreated Clay

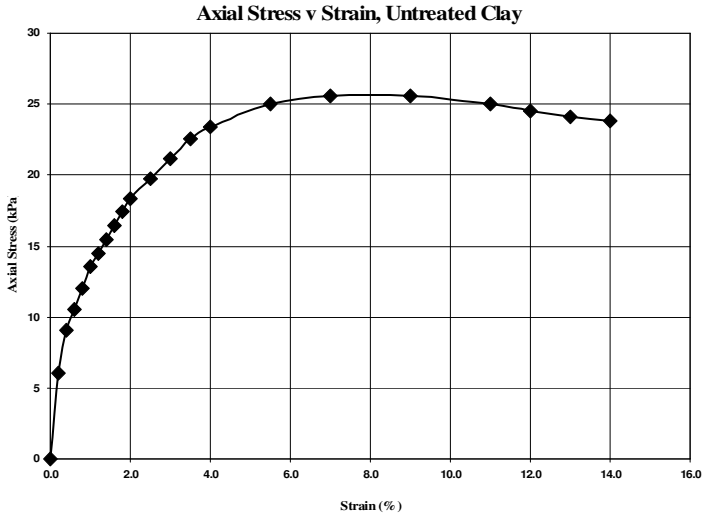

Figure 7.2 UCS for Untreated Clay

Table 7.1 Physical Properties of Untreated Clay

Moisture Content (%)	Liquid Limit (%)	Plastic Limit (%)	Plasticity Index (%)	Linear Shrinkage (%)
67	65	33.25	31.75	18.4

7.2.3 Source of Samples and Preparations Methods

Samples were collected from the estuarine region adjacent to Coombabah Creek and Gold Coast Highway. This low lying area is situated along Brisbane Road in Labrador

on the Gold Coast, Queensland. Soil samples were extracted from depths of l to 6 meters. Samples were kept in a temperature and humidity controlled chamber, before use in testing procedures.

After receiving the sample cylinders, those of appropriate depth were selected for use in the testing program. Initially the selected samples were mixed using a commercial rotary mixer for five minutes. While this was taking place the appropriate amount of cement and lime were carefully weighed, and then mixed into slurry using demineralised water. The slurries of different cement contents added to respective samples were all made using a standard water ratio of 0.25. Percentages of cement and lime addition to each samples was calculated in respect to the dry unit mass of the soil.

The cement slurry and lime slurry were then delicately added to the mixed clay, and then further mixed for a period of ten minutes. During this process, the apparatus was stopped several times to allow clay to be removed from the upper edge of the mixing bowl and placed with the bulk of the specimen. This was to ensure that all clay was able to contact with the cement or lime paste, producing a homogeneous cement-clay or lime-clay blend.

After the fore-mentioned thorough mixing, portions of the respective samples were removed from the mixing vessel and placed in a 100mm long, 50mm inner diameter sample mould. When the mould was filled, slight manual compaction was performed and excess soil was removed using a fine cutting wire. The solid brass cell was then placed in the specially fabricated extrusion apparatus, where a hydraulic jack was used to vertically push the remoulded samples out of the mould. Each sample was covered firmly with a plastic wrap and weighed before being placed in a humidifying chamber until the testing date. All the tests conducted follow the procedures recommended by Standard Australia AS1289 "Method of testing soils for engineering purposes" (AS

1289 3.1.1, 1995; AS 1289 3.2.1, 1995; AS 1289 3.3.1, 1995; AS 1289 3.4.1, 1995; AS 1289 3.5, 1995).

7.3 Cement Treated Clay

7.3.1 Characteristics of Cement Treated Clay

Cement addition to clay samples is undertaken at of 5%, 10%, and 15 % cement and at curing periods of 7, 28 and 56 days. Physical characteristics of clay with cement are examined in Table 7.2. With the increase in cement content we see a direct reduction in moisture content within the sample, primarily due to the initial processes of hydration within the cement. Plasticity index for cement treated samples is considerably higher with cement addition compared to untreated clay as seen in Table 7.2.

Table 7.2 Physical Properties of Cement Treated Clay

Cement Content (%)	Moisture Content (%)	Liquid Limit (%)	Plastic Limit (%)	Plasticity Index (%)
5	66.33	147.26	35.99	111.27
10	63.8	142.91	43.29	99.62
15	59.91	137.11	39.27	97.84

As the samples are cured over time the reduction of water content is present primarily due to the process of hydration in the cement as seen in Figure 7.3. All three samples experience distinct drops in the moisture content for the initial 7 day period and continue to drop throughout the test duration to 56 days.

The initial drop of moisture content at casting date is visible with the addition of cement, whereby moisture content for 15% cement reduces by 10.6% where as 10% and 5% cement contents reduce by only 4.8% and 1% respectively. With the reduction of moisture content in respect to curing time, the 15% cement sample experience a sharp loss of moisture for the initial 7 day period, however this effect on moisture reduced as curing time increases. Comparing this with the 5% cement sample we see a less distinct

reduction of moisture in the first 7 days, but the effect is continued throughout the 56 day curing period.

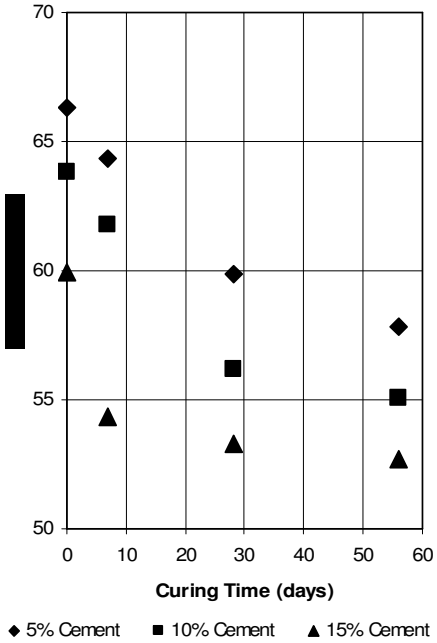

Figure 7.3 Moisture Contents for Cement Treated Clay

7.3.2 UCS Tests for Cement Treated Samples

The addition of varying cement contents of 5, 10 and 15% were added to the clay sample and unconfined compressive strengths tests were undertaken. For each cement composition, curing time of 7, 28 and 56 days was tested. Figure 7.4 – 7.6 overleaf show the results unconfined compressive strength tests the each cement content with varying curing times. As shown in Figures 7.4 to 7.6, the addition of cement to the clay sample causes a distinct increase in the unconfined confined compressive strength in comparison to the untreated sample. For cement contents tested, the increase in maximum stress is present with increase in curing time.

The failure mechanism of cement treated clay changes with the addition of cement. All cement contents attain a more distinct failure pattern compared to the untreated sample. As the cement content increases the failure pattern becomes increasingly brittle, which shown by the sharp decrease in stress with respect to axial strain. For 5% cement the

failure pattern changes with curing time, whereas 10 and 15% cement samples have similar failure patterns irrespective of curing time.

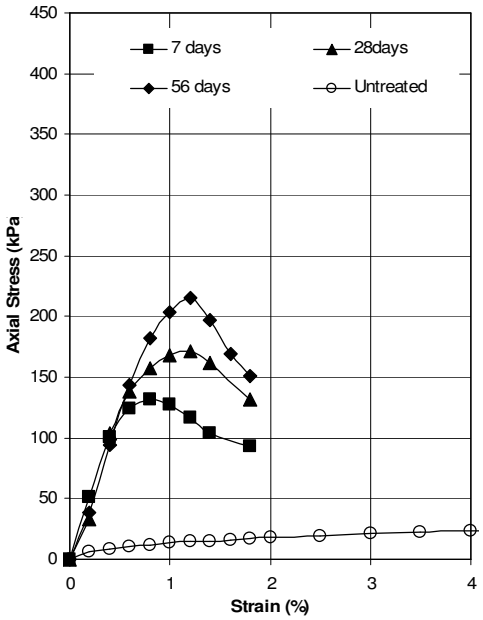

Figure 7.4 UCS for 5% Cement at varying curing times

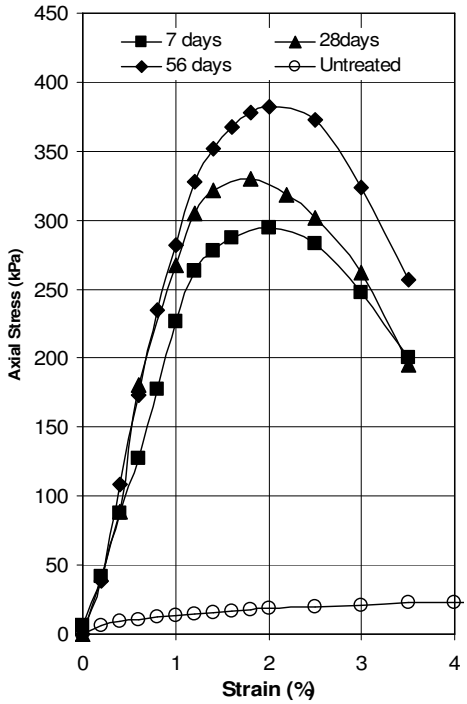

Figure 7.5 UCS for 10% Cement at varying curing times

Maximum unconfined compressive strength increases with the addition of cement independent on curing time as shown by the parallel curves of curing in Figure 7.7. This is due to primary hydration of the cement with pore water, and subsequent cementation strength gain which was completed within 7 days.

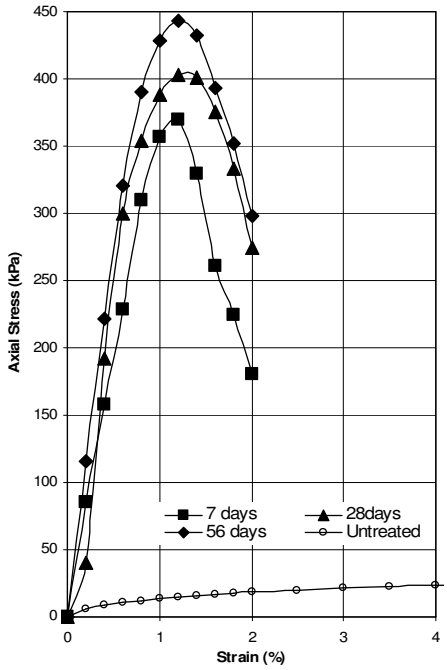

Figure 7.6 UCS for 15% Cement at varying curing times

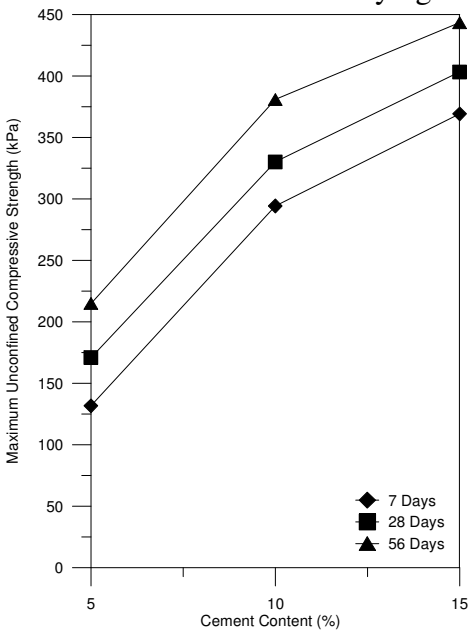

Figure 7.7 Maximum Axial Stress with varying Cement Contents

The increase of cement content from 5% to 10% shows a 94% increase in maximum strength, however with the addition of a further 5% cement, shows an increase of maximum strength of only 22%.

Figure 7.8 overleaf presents the maximum stress found for different cement contents at 7, 28 and 56 days curing. Unconfined compressive strength increases with greater curing time, but at a lesser rate than that observed for the relation with addition cement

content as previously identified. Initial increases in soil strength from 0 to 7 days is due to primary hydration of the cement, where increases in cement content produce higher maximum stresses as previously discussed. After 7 days all three cement contents increase at a similar rate of 1.7 kPa/ day. This increase can be only signified for curing periods of 7 to 56 days and can be denoted by the hardening effect and secondary pozzolanic reactions of minerals within the cement.

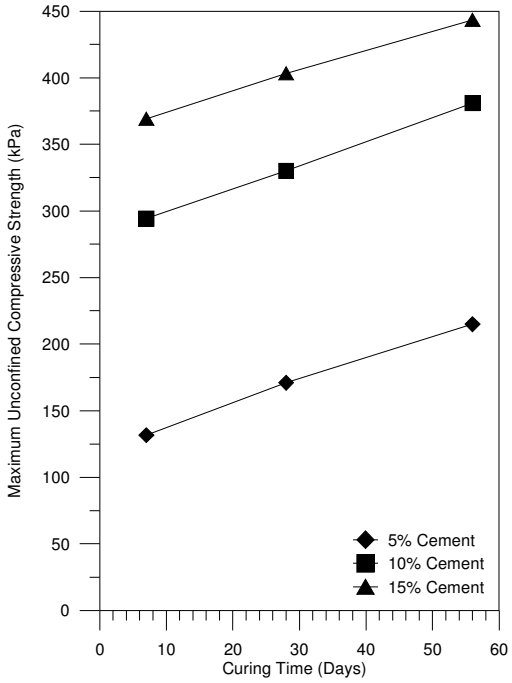

Figure 7.8 Maximum Axial Stress with varying curing times

It can be concluded, that the addition of cement to clay causes considerable increase in the unconfined compressive strength, although cement contents greater than 10% are found to produce less of an increase in strength. The effect of curing time causes an increase in strength gain in all samples, however this can only be stated for curing periods tested in this program. Further testing at longer curing periods will need to be undertaken to provide increased understanding into the effect of curing time on strength gain.

Characteristics of cement addition to south-east Queensland clay can be compared to studies formulated by Uddin (1995) as shown in Figure 7.9. Relationships of unconfined compressive strength and cement content are similar for both types of clay.

Overall the unconfined compressive strength was found to be higher for tested cement contents on south-east Queensland Clay compared to Bangkok Clay. Relationships of cement addition to different clay types show strength gain with cement content to be more distinct than the effect of curing time. Comparisons are restricted to cement contents tested in this program namely 5%, 10% and 15% cement and curing times of 1, 4 and 8 weeks.

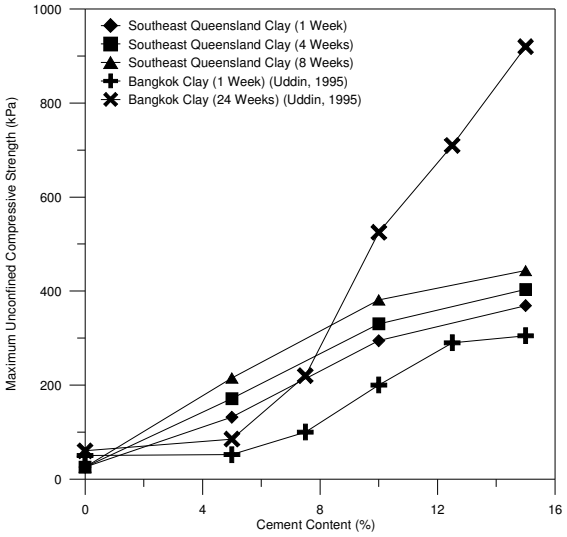

Figure 7.9 Comparison of UCS Tests on Cement Treated Bangkok Clay and SEQ Clay.

7.4 Lime Treated Clay

7.4.1 Characteristics of Lime Treated Clay

Lime addition to the clay sample was undertaken at 2, 5, 7.5, 10, 12.5 and 15% and at curing periods of 7, 14, 28 and 42 days. Changes in the physical characteristic of the clay with these lime additives are presented in Table 7.3. With the increase in lime content a direct reduction in moisture content is seen; primarily due to the initial processes of hydration within lime.

For individual percentage of lime content the moisture content reduction is almost instantaneous throughout the curing period of 42 day. From Table 7.4, the average moisture content is 70% for 2 percent lime content and then decrease continuously to about 62% when the lime content is 15 percent.

7.4.2 UCS Tests for Lime Treated Samples

Figures 7.10 to 7.13, and Table 7.5 show the unconfined compressive strengths with 2, 5, 7.5, 10, 12.5 and 15% lime additive and curing periods of 7, 14, 28 and 42 days. The 7 days sample with 15% lime reached a maximum strength 199 kPa. There is a remarkable increase in strength from 47 kPa to 159 kPa when the lime content increased from 2 percent to 5 percent. Then the strength increased to about 191 kPa with 7.5 percent additive. Further curing period had little effect on the strength increase. With 14 days curing period, substantial strength increase is noted with all percentage of lime additives. Also, the strength increase after 14 days for the 28 days and 42 days curing period were not that substantial as it was for the 14 days curing period. Thus, it can be said that the 2 percent lime additive is not effective.

Table 7.3 Physical Properties of Lime Treated Clay

Lime Content (%)	Moisture Content (%)	Liquid Limit (%)	Plastic Limit (%)	Plasticity Index (%)
0	71	85	47	38
2	69.4	113.4	72.7	40
5	69.3	143.5	81.9	61
7.5	67.6	130.4	72.9	57
10	65.7	122.3	71.2	51
12.5	64.7	111.5	68.7	42
15	63.1	109.6	71.8	37

An additional observation that can be made from Figures 7.10 to 7.13, that is, the failure strains at which the maximum unconfined compressive strengths are reached. As shown in Table 7.6, there is a general tendency for the peak strengths to occur at lower strains with increasing curing time.

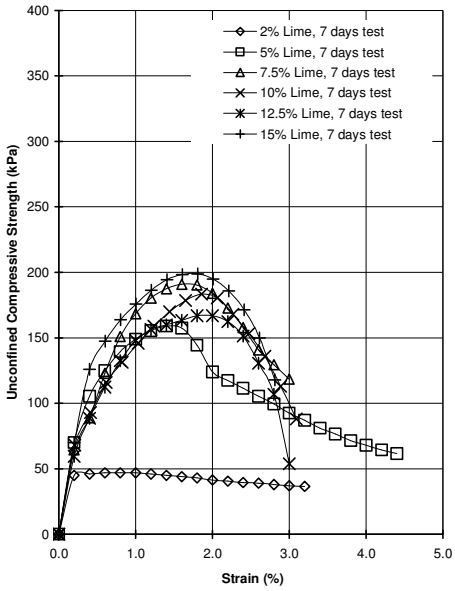

Figure 7.10 UCS for 7 Days with varying Lime contents

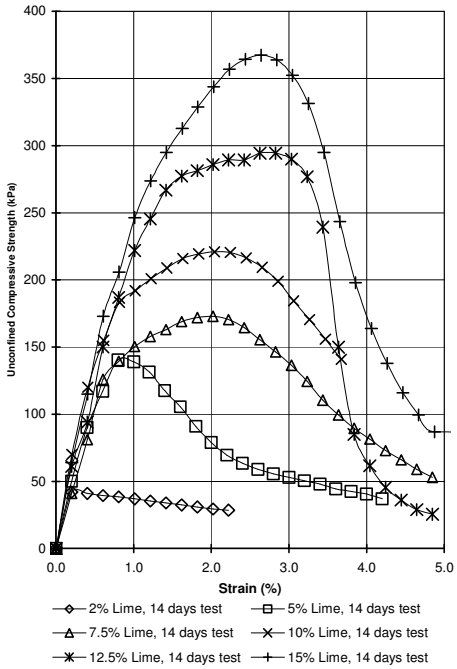

Figure 7.11 UCS for 14 Days with varying Lime contents

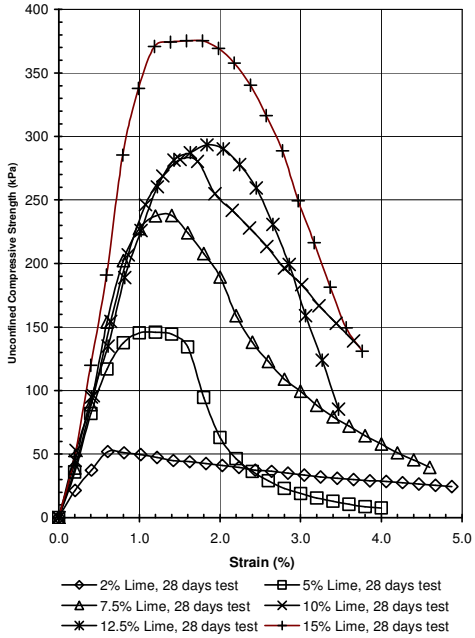

Figure 7.12 UCS for 28 Days with varying Lime contents

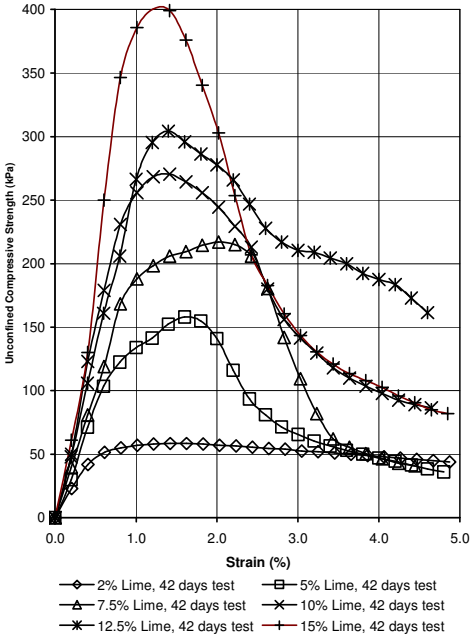

Figure 7.13 UCS for 42 Days with varying Lime contents

Figures 7.14 to 7.19 illustrate the same results now plotted for individual lime content with respect to the various curing time. At low lime content of 2 and 5 percent, the curing time has little effect on the peak unconfined compressive strength. However

when the additive content increased to 7.5 percent, there is substantial strength increase with curing time. At 10 percent lime content, 28 days and 42 days curing periods virtually has the same peak values of strength. Further, at 12.5 percent lime content, a 14 day curing period seems sufficient to reach the maximum value of the unconfined compressive strength. The same trend is noted with the 15 percent lime content. This is quite evident and is shown in Figure 7.20.

Table 7.4 Moisture Content for Varying Curing Times

Lime Content (%)	Moisture Content (%)				
	Curing Time				
	0 Days	7 Days	14 Days	28 Days	42 Days
2	69.4	73.6	72.0	73.0	70.2
5	69.3	68.8	70.6	69.8	68.8
7.5	67.6	67.5	67.4	68.0	67.3
10	65.7	66.6	65.2	66.5	65.7
12.5	64.7	62.5	64.0	64.0	64.6
15	63.1	60.3	61.8	62.6	62.2

Table 7.5 Maximum Unconfined Compressive Strength with Varying Curing Times

Lime Content (%)	Maximum Unconfined Compressive Strength (kPa)			
	Curing Time			
	7 Days	14 Days	28 Days	42 Days
2	47	42	52	58.5
5	159	140.5	146	158
7.5	191	173	238	217
10	184	221	282	270.5
12.5	167	294.5	293.5	304.5
15	199	367.5	375.5	400.5

Table 7.6 Strain with Varying Curing Times

Lime Content (%)	Strain (%)			
	Curing Time			
	7 Days	14 Days	28 Days	42 Days
2	1.0	0.2	0.6	1.4
5	1.4	0.8	1.2	1.6
7.5	1.6	2.0	1.4	2.0
10	1.8	2.0	1.5	1.4
12.5	2.0	2.8	1.8	1.4
15	1.8	2.6	1.7	1.2

Figure 7.21 gives a summary plot of the effect of lime contents for different curing time. These plots indicate that except for the 7 days curing period for all the other cases of 14, 28 and 42 days, the unconfined compressive strength increased in a linear manner with

the percentage of lime additive. The rate of increase with time is higher than the linear value indicated up to 10 percent lime.

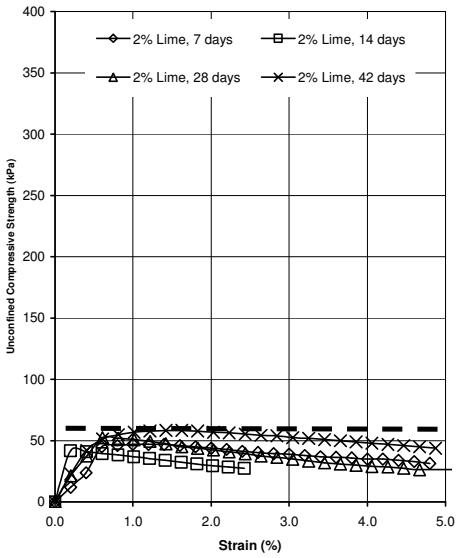

Figure 7.14 UCS for 2% Lime with varying curing times

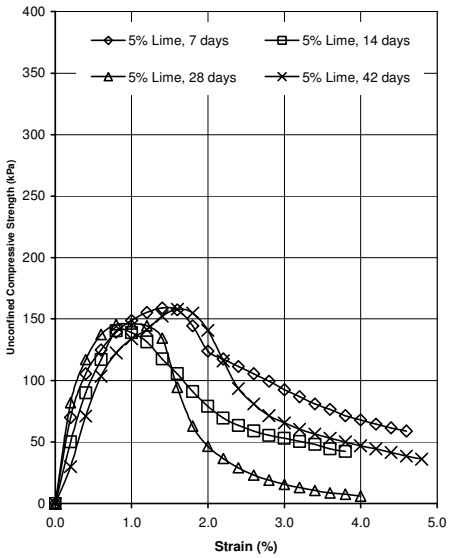

Figure 7.15 UCS for 5% Lime with varying curing times

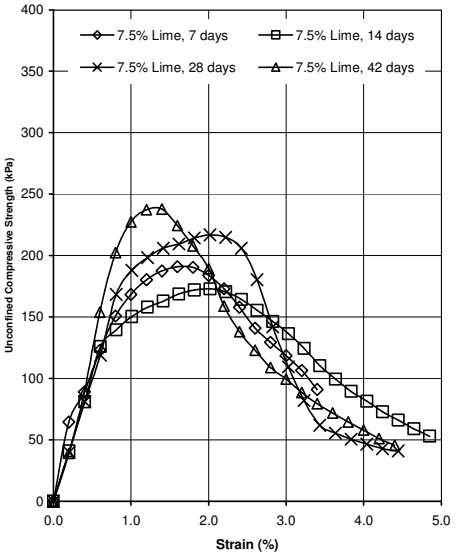

Figure 7.16 UCS for 7.5% Lime with varying curing times

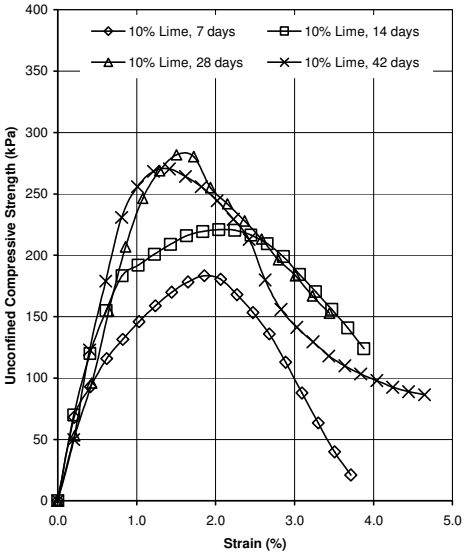

Figure 7.17 UCS for 10% Lime with varying curing times

7.5 Comparison of Lime and Cement Treated Behaviour

In this section, a comparison is made between the lime and cement treated samples for 5%, 10% and 15 % of additive and curing periods of 7 and 28 days. These are the common percentage additive and curing period, where the two types of additives were

compared. When the curing period is 7 days, the cement is found to have greater effect than the lime in the range in which they were tested between 5 percent and 15 percent additive. However, when the curing period is 28 days, the trend in behaviour for lime and cement are the same. Cement is found to be marginally better than lime. The strains at which the peak values of unconfined compressive stress occurred is generally the same for both lime and cement, but in the case of lime, the stress strain curves are more ductile in nature without very sharp peaks (see Tables 7.5, 7.6, 7.7 and 7.8). These comparison results are presented in Figure 7.22 (also in Tables 7.9 and 7.10).

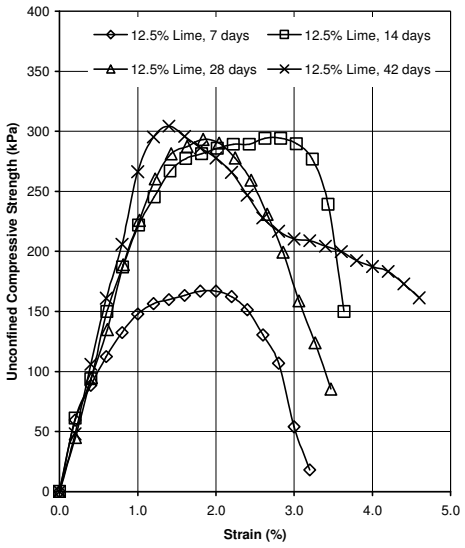

Figure 7.18 UCS for 12.5% Lime with varying curing times

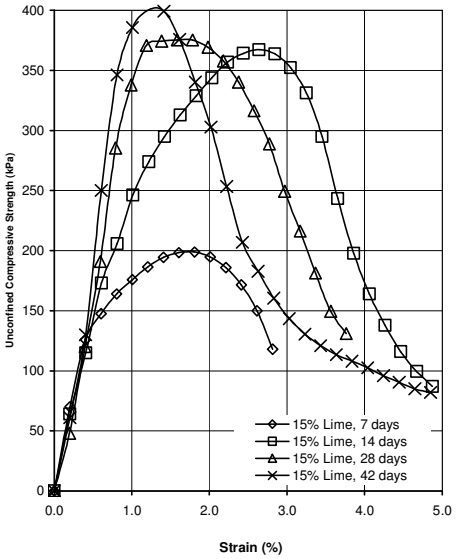

Figure 7.19 UCS for 15% Lime with varying curing times

Table 7.7 Maximum Unconfined Compressive Strength with Varying Curing Times

Cement Content (%)	Maximum Unconfined Compressive Strength (kPa)		
	Curing Time		
	7 Days	28 Days	56 Days
5	132	170	215
10	295	330	380
15	370	405	445

Table 7.8 Strain with Varying Curing Times

Cement Content (%)	Strain (%)		
	Curing Time		
	7 Days	28 Days	56 Days
5	0.8	1.2	1.3
10	2.0	1.8	2.0
15	1.2	1.3	1.2

Table 7.9 Maximum Unconfined Compressive Strength Comparison of Lime and Cement

Additive Content (%)	Maximum Unconfined Compressive Strength (kPa)			
	7 Days		28 Days	
	Lime	Cement	Lime	Cement
5	159	132	146	170
10	184	295	282	330
15	199	370	375.5	405

Table 7.10 Strain Comparison of Lime and Cement

Additive Content (%)	Strain (%)			
	7 Days		28 Days	
	Lime	Cement	Lime	Cement
5	1.4	0.8	1.2	1.2
10	1.8	2.0	1.5	1.8
15	1.8	1.2	1.7	1.3

7.6 Concluding Remarks

A variety of issues were identified whilst completing laboratory tests and analysing test results. These include variations in tests procedures, applicability to in-situ conditions and additional test required to further validate results. The laboratory results presented in this chapter showed the applicability of chemical mixing to the studied soft clay sites in Southeast Queensland (Sunshine Motorway, Port of Brisbane Motorway, and Gold Coast Highway).

There were several conclusions drawn from the laboratory testing program undertaken on samples of Southeast Queensland soft estuarine treated with varying percentages of cement and lime. In general, it was observed that cement and lime addition produced improvements in strength. The specific nature of this improvement has been thoroughly analysed in this chapter.

This improvement in strength and compressibility characteristics suggests that the cement and lime mixing technique of ground improvement is theoretically feasible for the estuarine clay deposits of Southeast Queensland. The in-situ formation of soil cement columns can provide stiffening effects to clay foundations, enabling the safe construction of earth embankment structures and other light civil works. Cement and

lime stabilisation can also be used in shallow applications to produce a stiff layer across large areas, depending on the efficiency of the mixing apparatus. The data presented in this research can be used to aid design of such ground improvement schemes.

7.6.1 Cement Treated Samples

The addition of cement was undertaken with the use of a water/cement ratio of 0.25. This process was undertaken to provide a uniform slurry mix to the clay sample. This intern may have contributed to variations of initial strength gain due to hydration. Immediate interactions of cement with clay were visible at the time of mixing, where samples become increasingly dryer and harder to manipulate. The effect of cement hydration was not thoroughly tested for the initial mixing period other than moisture content and Atterberg limits. Testing of unconfined compression at the time of mixing would further investigate the effect of this ground improvement technique on allowable loading immediately after mixing in the field.

Samples tested in this program were prepared following a thorough procedure where proportions and mixing of additives was carefully maintained, however mixing is not as accurate with proportioning of additives and uniformity in the field. The use of unconfined compression strength tests gives minimal comparisons to in-situ conditions. Closer comparisons may be identified with testing methods such as a triaxial testing apparatus to further investigate shear failure under various confining pressures.

7.6.2 Lime Treated Samples

Several difficulties were encountered during the course of the laboratory study. These issues include variation in tests procedures, the constraint period of tests, and limitation of laboratory apparatus. Therefore, additional test are required in validating the results.

As with most experimental studies, it is not proposed that the results of laboratory testing is directly applicable to the field. The sample tested in this program were

thoroughly mixed and carefully proportioned, a condition not always achieved in practice. However it is intended that the findings of this research be used as a preliminary measure of the effects of lime treatment on South-East Queensland soft estuarine clays.

Immediate interactions of lime with clay were visible at the time of mixing, where samples become increasingly dryer and harder to manipulate. The effect of lime hydration was not thoroughly tested for the initial mixing period other than moisture content and Atterberg limits. Testing of unconfined compressive strength at the time of mixing would further investigate the effect of this lime stabilization technique.

In this laboratory testing program, the maximum curing period for lime treated clay was 42 days but ideally all samples would have also been tested at even more curing periods namely 56 days and 84 days to provide a better indication of the effect of curing period.

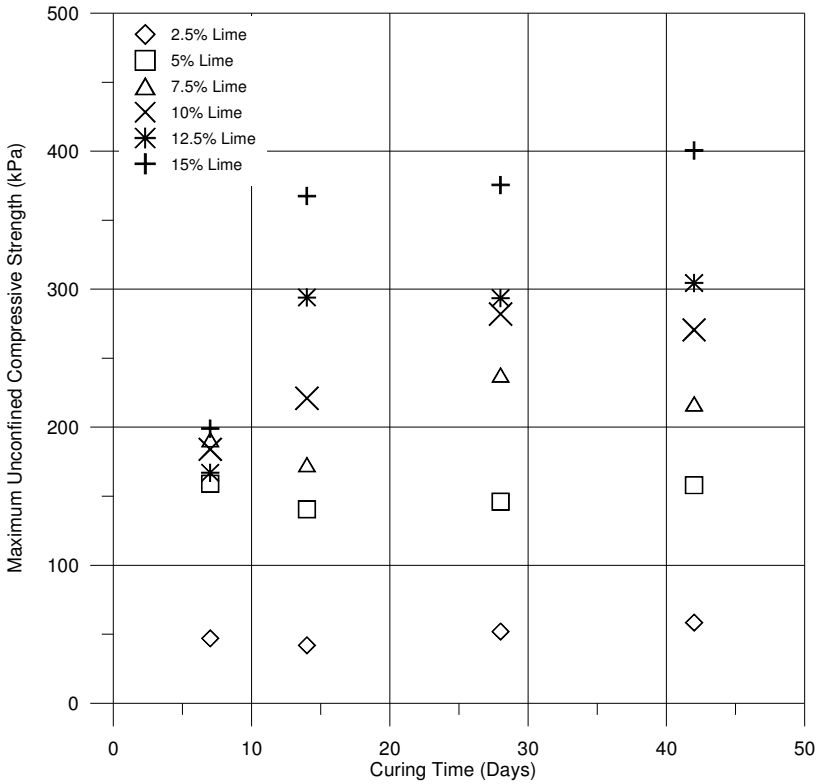

Figure 7.20 Maximum UCS for various Lime contents with varying curing times

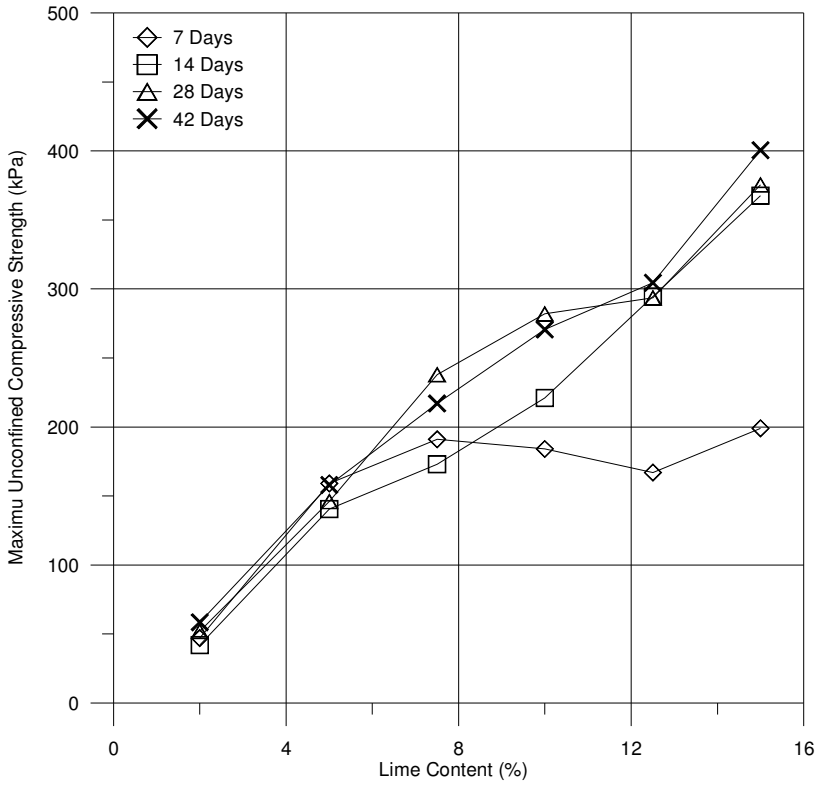

Figure 7.21 Maximum UCS for various curing time with varying Lime contents

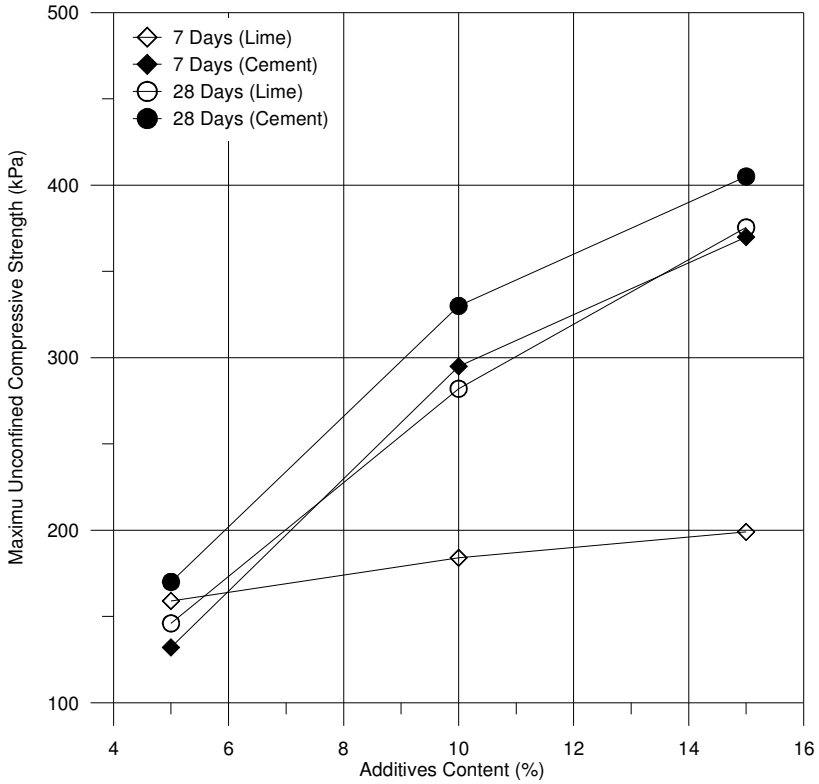

Figure 7.22 Maximum UCS for 7 and 28 days with varying additive contents

CHAPTER 8

CONCLUSIONS AND RECOMMENDATIONS

8.1 Introduction

This thesis is devoted to a better understanding and characterization of the soft clays as encountered in Southeast Queensland. Further, this is the first Geotechnical Engineering doctoral thesis in Griffith University.

Three case studies (Sunshine Motorway, Port of Brisbane Motorway, and Gold Coast Highway) are presented in this thesis, and laboratory tests are conducted to investigate the application of cement and lime columns. The work contained here are in four parts. The first one being on the delineation of the soft clay profile and the analysis of laboratory and field vane data at the three selected sites; the second one on the interpretation of a full scale test embankment at three sites, two of them having vertical installed, and one with stone column installed. The third part is the use of PLAXIS to make predictions of the behaviour of the test embankment. The four part is the laboratory tests conducted on cement and lime treated soil samples.

The major emphasis of this thesis was made on the proper interpretation of the settlement, pore pressures and lateral deformations as measured below the test embankment. In this thesis, field data of trial embankments constructed at three separate sites: Gold Coast Highway, Sunshine Coast Motorway and Port of Brisbane Motorway, was analysed. A summary of this analysis is given in Table 8.1. The following conclusions and recommendations are reached on all aspects of the work.

8.2 Conclusions

1. The following conclusions are reached from the work on Sunshine Coast Motorway embankments (Chapter 4).

    i. The soft clay profiles in estuarine deposits vary in thickness at close

proximities, and are interbedded with sand and silt seams. The deepest soft clay in the Sunshine Motorway is encountered around the area of the test embankment and is about 10.5m thick. The natural water content of the clay is high of the order of 120pc and is higher than the liquid limit; thus the liquidity index is greater than one and the deposit is young and normally consolidated. The undrained shear strength as determined from field vane boring is only 15 kN/m^2 for all the depth range. Thus the clay is highly compressible and of low strength

Table 8.1 Summary of all trial embankments

Trial Embankment	Treatment Type	Installation Details	Maximum Embankment Height (m)	Maximum Settlement (mm)
Sunshine Coast Motorway	Vertical Drain	1 m spacing (square grid)	3	1565
	None	-	3	1197
Port of Brisbane Motorway	Vertical Drain	3.0 m spacing (triangular grid)	5	1087
	Vertical Drain	1.5 m spacing (triangular grid)	6	1049
	Vertical Drain	1.5 m spacing (triangular grid)	6	1036
Gold Coast Highway	Stone Column	1 m Dia. @ 3 m Spacing (square grid)	4	508
	None	-	4	508
	Stone Column	1 m Dia. @ 2 m Spacing (square grid)	4	450

ii. Consolidation tests performed on samples taken from three boreholes in the closer vicinity of the test embankment at depths ranging from 0.8 to 9.0m revealed

(a) Maximum past pressure close to in-situ effective overburden stress

(b) The compression index (C_c) in most cases ranging from 0.5 to 1.0

reaching occasionally a higher value of 1.5.

(c) The coefficient of volume decrease, m_v ranged from 1 to 5 MN/m^2 at low stress range and converged to the range of 1 to 3 MN/m^2 at higher stress levels.

(d) The constraint modulus, D was found to increase linearly with the effective vertical stress.

(e) The coefficient of consolidation, c_v was found to range in most instances between 0.25 to 0.5 m^2/year.

iii. The interpretation of the settlement, lateral movement and excess pore pressures below the full scale test embankment revealed

(a) The surface settlement across Section A (with PVD at 1.0m spacing in triangular pattern) and Section B, with no PVD are found to be maximum at the centre line and gradually reduced towards the left and right hand ends.

(b) Section A and Section B (with PVD at 2m spacing in triangular pattern as well) consistently had higher settlement with time when compared to the Section B with no PVD.

(c) In Section A, the centre line location and all other considered at 5m intervals to the left, indicated in the Casagrande plot where settlement is plotted with respect to log time, which the 100 percent consolidation settlements are achieved. However, for section B with no PVD, the Casagrande settlement-log time plots did not show clear "S" shaped curves to determine the one hundred percent consolidation settlements. For Section B, Asaoka method was used to estimate one hundred percent consolidation settlement. As shown in

Figures 4.18(a) and 4.18(b), both figures gave the settlement-time plot up to 3000 days. The centreline and the locations to the left in Section A gave 100% consolidation. Whereas, the locations to the right of centreline in Section A do not show 100% consolidation.

(d) The field value of m_v as determined from the centre line settlement in Section A is only 2.1 MN/m^2 and can be compared with the laboratory range of values given in ii(c) above.

(e) The back-calculated, coefficient of horizontal consolidation, c_h from Section A was generally less than or equal to 0.5 m^2/year and is of the same order as the lower range of laboratory values quoted in ii(e) above

(f) The lateral deformations of all three sections A, B and C showed similar trend at all times and the maximum lateral deformation is contained in the upper 7m or so indicating that this part of the soft clay is more vulnerable for the propagation of undrained failure surfaces. Thus the consolidation settlement in all Sections is virtually one dimensional in nature.

(g) The pressure development and dissipation from the piezometer data are found to be consistent with the depth and lateral locations. For section A with PVD, back calculated c_h values are presented and compared with the c_h values obtained from, settlement interpretations.

iv. A coupled consolidation analysis using Soft Soil Model in the PLAXIS program was also carried out. The PLAXIS predictions in general follow the same trend as the observations on settlement, lateral movement, and pore pressures. The input parameters for the PLAXIS Program needs further

refinement and various types of soft soil models now available need to be used in the analysis. Also, initially an undrained analysis be conducted to examine the pore pressure development, immediate settlement and lateral deformations. Then a drained analysis is conducted with time effects. These aspects of the work are beyond the scope of the current study

2. Based on the work on Port of Brisbane Motorway embankments (Chapter 5), the following conclusions are reached.

   i. The Port of Brisbane Motorway embankments are installed with vertical drains and consist of three sections. Embankment A had drains at 3 meter spacing, and Embankments B and C had drains at 1.5 meter spacings. Embankment A was 160 meters in length starting at CH790 and finishing at CH950. Embankment B is in between embankment A and embankment C and is 184 meters in length finishing at CH1134. Embankment C is 104 meters in length starting from embankment B and finishing at CH1238. The width of the motorway varies from 32 meters in width to 26 meters in width for the stretches of straight road.

   ii. The maximum settlement obtained after 226 days of monitoring is shown. It can be seen that vertical drain treatment significantly increased final settlement. The increase in “rate of consolidation” varied from 70 to 80%. It can be concluded from the settlement results that vertical drains would have increased rate of consolidation.

   iii. Inclinometer INC1 installed beneath the toe of Embankment A reached a maximum lateral deformation of 134.5 mm at a depth in the soil layer of 2.64 meters 179 days after construction commenced, the deformation reduced after reaching the maximum of 134.5 mm to 128 mm at 210 days

before increasing again to a deflection of 131 mm at 240 days. This increase suggests that an increase in the load was introduced between day 210 and day 240 although no report of the increase was evident in the corresponding construction sequence. Inclinometer INC4 installed at the toe of Embankment B reached a maximum lateral deformation of 286 mm at a depth of 3.27 meters 198 days after construction commenced. As in Embankment A the deformation reduced after reaching a maximum deflection of 286 mm to 266 mm 291 days after construction. Inclinometer INC3 installed at the toe of Embankment C reached a maximum deformation of 28.3 mm at a depth of 1.72 meters 194 days after construction commenced.

iv. The readings of the piezometers in Embankment A show the largest increase of excess porewater pressure of 55.58 kPa in PP3 installed at a depth of 6.79 meters. Embankment B's increase in excess porewater pressure reached a maximum of 45.59 kPa in PP6 installed at a depth of 2.1 meters after the second stage of loading. Embankment C's increase in excess porewater pressure reached a maximum of 39 kPa in PP10 on the second stage of loading installed at a depth of 3.3 meters.

v. From both Embankment B and C the back calculated c_v values can be seen to increase semi-linearly to maximums of around 0.4 to 1 m^2/year at 90% degree of consolidation. The same is similar for Embankment A where by the back calculated c_v values can be seen to decrease semi-linearly to maximum back calculated c_v values at 90% degree of consolidation, however the rate is greatly increased reaching maximums between 0.7 to 2 m^2/year.

3. From the work on Gold Coast Highway embankments with stone columns (Chapter 6), the following findings are concluded.

   i. A trial embankment was constructed along the Gold Coast Highway. This embankment was divided into three sections – section (1) contained no ground improvement, section (2) had stone columns at 2m spacing and section (3) had stone columns at 3m spacing.

   ii. Settlement gauges and horizontal profile gauges were installed in the trial embankment to record the variation of vertical settlement with time. The embankment with stone columns at 2m spacing had the least settlement. The embankment with no ground improvement and stone columns at 3m spacing had comparable settlement.

   iii. The settlements measured are relatively similar in profile and magnitude. It is shown that the settlement rate is initially uniform, but increases around day 48, and again around day 131. The final settlement readings obtained after 485 days of monitoring.

      (a) For embankment A (3m spacing), the maximum Horizontal Profile Gauge Reading was 490 mm.

      (b) For embankment B (no stone column), the maximum Horizontal Profile Gauge Reading was 522 mm.

      (c) For embankment C (2m spacing), the maximum Horizontal Profile Gauge Reading was 386 mm.

   iv. At the Gold Coast Highway trial embankment, lateral displacement was monitored at the trial embankment toe and centreline. The maximum lateral displacement at the toe was 76.84 mm, and 47.95 mm at the centreline.

4. Comprehensive laboratory investigations were carried out to investigate the unconfined compressive strength characteristics of Southeast Queensland soft clay treated with cement and lime. The sample was taken from Coombabah Creek of Gold Coast, at a depth of 1 to 4m. Using the laboratory tests results, the following conclusions can be made for the chemical treated soils (Chapter 7). This improvement in strength and compressibility characteristics suggests that the cement and lime mixing technique of ground improvement is theoretically feasible for the estuarine clay deposits of Southeast Queensland. The data presented in this research can be used to aid design of such ground improvement schemes.

   i. For cement treated soil samples, based on the Unconfined Compression Test results, the following conclusions are reached.

      (a) The increase of cement content from 5% to 10% shows a 94% increase in maximum strength, however with the addition of a further 5% cement, shows an increase of maximum strength of only 22%.

      (b) Unconfined compressive strength increases with greater curing time. Initial increases in soil strength from 0 to 7 days is due to primary hydration of the cement, where increases in cement content produce higher maximum stresses as previously discussed. After 7 days all three cement contents increase at a similar rate of 1.7 kPa/ day.

      (c) For cement treated samples with 5 percent to 15 percent cement content, the maximum unconfined compressive strength increased from 132 kPa to 370 kPa for 7 days curing period; these values for 28days curing increased from 170 kPa to 405 kPa.

   ii. Based on the Unconfined Compression Tests conducted on lime treated

samples, the following conclusions are reached.

(a) For lime treated samples with lime contents from 2 percent to 15 percent, the maximum unconfined compressive strength increases from 47 kPa to 199 kPa (for 7 days curing period). Results indicated that, 2 percent lime has little effect on peak unconfined compressive strength. Similar trend is found for sample at 28 days curing period.

(b) In general the maximum unconfined compressive strength increased with the lime for all percentage of lime additives.

(c) In general with low lime contents of 2 and 5 percent, the curing time did not affect the peak unconfined compressive strength. As the additive content increased to 7.5 percent, there is substantial strength increase with curing time (191 kPa at 7 days curing and 238 kPa at 28 days curing). As for curing period of 14, 28 and 42 days, the unconfined compressive strength generally increased in a linear manner with the percentage of lime. The rate of increase with time was found to be even higher when the lime content increased from 12.5 to 15 percent.

5. Ground improvement techniques developed for roads, expressways and other infra-structure developments are now widely used in particular for embankments on soft clays. This thesis summarises some ground improvement techniques used in Southeast Queensland, and demonstrated the applicable of chemical stabilisation. Overall it was concluded that the addition of cement and lime has favourable effects on the strength characteristics of Southeast Queensland soft clays.

8.3 Recommendations

Soft clay deposits are encountered in Southeast Queensland in most of the Highways and Motorways projects, and as such it is important to characterise their behaviours from laboratory and field observations. Some aspects of the following work can prove to be useful.

1. Continuous sampling of the soft clays and fully log the sand and silt seams encountered
2. To carry out index tests wherever possible in association with Oedometer tests and triaxial tests.
3. To ensure the quality of undisturbed sampling and quantify them.
4. Oedometer tests be conducted on larger samples and to determine the time effects
5. Triaxial undrained and drained tests to be conducted to determine the input parameters for the Soft soil Model. Also undrained and drained creep tests be conducted.
6. Initially attempts are to be made to improve the soft soil model to accommodate aspects such as anisotropy, stress history effects and long-term time effects.
7. Test embankments must be conducted with independent settlement measurements carried out at the surface and at deeper depths using settlement-measuring devices other than the hydraulic profile gauges.
8. Several attempts are to be made with PLAXIS initially in an undrained mode followed by the drained mode.
9. Field Deformation Analysis as described by Loganathan et al. (1993) may prove to be useful in accommodating undrained creep and settlement arising from such creep.
10. Further analyses including smear effects are to be conducted.

11. In this thesis, only limited time was available to conduct unconfined compression tests on cement and lime treated samples. It is recommended that a further detail study be carried out both in the Odometer and Triaxial apparatus. Such a study must have a wide range of additive content and curing period as well

REFERENCES

Aboshi, H. and Monden, H., (1963). Determination of the horizontal coefficient of consolidation of an alluvial clay. Proc. 4th Australian-New Zealand Conf. SMFE, 159-164.

Aboshi, H., (1992). Applied Ground Improvement Techniques, Workshop. Southeast Asian Geotechnical Society (SEAGS), Asian Institute of Technology, Bangkok, Thailand, 40 p.

Aboshi, H., Ichimoto, E., Enoki, M., and Harada, K. (1979). The compozer—a method to improve characteristics of soft clays by inclusionof large diameter sand columns. Proc., Int. Conf. on Soil Reinforcement,E.N.P.C., 1, Paris, 211–216.

Ahnberg, H. and Holm, G. (1999). Stabilization of some Swedish organic soils with different types of binder. In Bredenberg, H., Holm, G. and Broms, B.B. (Eds). Deep Mix Methods for Deep Soil Stabilization. Balkema: Rotterdam, 101-108.

Akagi, T., (1977). Effect of mandrel-driven sand drains on strength. Proc. 9th Int. Conf. Soil Mech. and Found. Eng., Tokyo, Vol. 1, 3-6.

Akagi, T., (1981). Effect of Mandrel-driven sand drains on soft clay. Proc. 10th Int. Conf. Soil Mech. and Found. Eng., Stockholm, 581-584.

Akai, K. (2000). Insidious settlement of super-reclaimed offshore seabed. Coastal Geotechnical Engineering in Practise, 243-248.

Akai, K. and Tanaka, Y., (1999). Settelemtn behaviour of an offshore airport KIA. 12th European Conf. on Soil Mechanics and Geotechnical Engineering, Vol. 2, 8.1-8.6.

American Society of Testing and Materials, (1993). Annual Book of ASTM Standards: Soil and Rock; dimension Stone; Geosynthetics. Vol. 04.08, Philadelphia, USA, 1469 p.

Asaoka, A., (1978). Observation procedure of settlement prediction. Soils and Foundations, Vol. 18, No. 4, 87-101.

Asian Institute of Technology, (1995). The Full Scale Field Test of Prefabricated Vertical Drains for The Second Bangkok International Airport (SBIA), Final Report. Div. of Geotech. and Trans. Eng. AIT, Bangkok, Thailand, 259 p.

Atkinson, M. S. and Eldred, P. J. L. (1981). Consolidation of soil using vertical drains. Geotechnique, Vol. 31, No. 1, 33–43.

Austroads (1998). Guide to Stabilisation in Roadworks. Austroads: Sydney.

Baker, E. (2005). Stability and Settlement Characteristics of Soft Clay Foundations beneath the Port of Brisbane Motorway. Honour Thesis, School of Engineering, Griffith University, Australia.

Balaam, N. P., and Booker, J. R. (1981). Analysis of rigid rafts supported by granular piles. Int. J. Numer. and Analytical Methods in Geomech., 5, 379–403.

Balasubramaniam, A.S., Bergado, D.T., Buensuceso, B. and Yang, C.W. (1988). Ground Improvement Techniques for Approach Road Design and Rehabilitation of Road Embankments. Proceedings Symposium on Roads, Bridges and Highways for the 21st Century, Bangkok, 7.1-7.13.

Balasubramaniam, A.S., Honjo, Y., Law, K.H., Phien-wej, N., Bergado, D.T. (1989). Ground Improvement Techniques in Bangkok Subsoils. Engineering for Coastal Development, Bangkok, 65-104.

Balasubramaniam, A.S., Hwang, Z.M., Waheed U., Chaudhry, A.R. and Li, Y.G. (1978). Critical State Parameters and Peak Stress Envelopes for Bangkok Clays. Quarterly Journal of Engineering Geology, Vol. 11, 219-232.

Balasubramaniam, A. S., Kim S. R., Lin D. G., Acharya S. S. S., Seah T. H. and Bergado D. T. (1999). Selection of Soft Clay Parameters for Bangkok Lowland

Development, Lowland Technology International, Vol. 1, No.1, 85-98.
Balasubramaniam, A. S., Oh, E. Y. N., Bolton., M., Bergado, D. T., and Phienwej, N., and (2005). Deep well pumping in the Bangkok plain and its influence on the ground improvement development with surcharge and vertical drains. Ground Improvement, Vol. 9, No. 4, 149 – 162.
Baligh, M.M., (1985). Strain path method, J. Geotech. Enggr. ASCE, Vol. 111, No. 9, 1108-1136 Barron, R.A., (1948). Consolidation of fine-grained soils by drain wells. Transactions ASCE, Vol 113, paper 2346, 718-724.
Barksdale, R. D., and Bachus, R. C. (1983). Design and construction of stone columns. Federal Highway Administration, FHWA-RD-83/026.
Barron, R. A. (1947). Consolidation of fine-grained soils by drain wells. Transactions ASCE, Vol. 113, Paper No. 2346, pp. 718–742.
Bell, F.G. (1993). Engineering Treatment of Soils. E and FN Spon: London.
Bell, F.G. (1996). Lime stabilization of clay minerals and soils. Engineering Geology, 223-237.
Bergado, D. T., Alfaro, M. C. and Balasubramaniam, A. S. (1993). Improvement of soft Bangkok clay using vertical drains. Geotextiles and Geomembranes, 12, 615–663.
Bergado, D. T., Anderson, L.R., Miura, N. and Balasubramaniam, A.S. (1996). Soft Ground Improvement in Lowland and Other Environments. American Society of Civil Engineers: USA.
Bergado, D. T., Asakami, H., Alfaro, M. C., and Balasubramaniam, A. S., (1991). Smear effects of vertical drains on soft Bangkok clay. J. Geotech. Eng., ASCE, Vol. 117, No. 10, 1509-1530.
Bergado, D. T., Balasubramaniam, A. S., Fannin, R. J., Holtz, R. D. (2002). Prefabricated vertical drains (PVDs) in soft Bangkok clay: a case study of the new Bangkok International Airport project. Canadian Geotechnical Journal, Vol. 39, No. 3, 304-315.
Bergado, D. T., Chai, J.C., Miura, N., and Balasubramaniam, A. S., (1998). PVD improvement of soft Bangkok clay with combined vacuum and reduced sand embankment preloading. J. Geotech. Eng., Southeast Asian Geotch. Soc., Vol. 29, No. 1, 95-122.
Bishop, A. W., (1959). The principle of effective stress- lecture delivered in Oslo in 1955, Teknisk Ukeblad, Vol. 106, No. 2, 859- 863.
Bo, M. W. and Choa, V. (2002). Geotecnical Instrumentation for Land Reclamation Projects. IES Conference on Case Studies in Geotechnical Engineering.
Bo, M. W. and Choa, V. (2004). Reclamation and Ground Improvement. Thomson Press, Singapore.
Bo M. W., Arulrajah, A., and Choa, V. (1997). Assessment of Degree of Consolidation in Soil Improvement Project. International Conference on Ground Improvement Techniques, Macau, 71-80.
Bo, M. W., Arulrajah, A., and Chao, V., (1998). Instrumentation and Monitoring of Soil Improvement Work in Land Reclamation Projects. 8th International IAEU Congress. Balkema: Rotterdam, 385-392.
Bo, M. W., Chu, J., Low, B. K., and Choa, V. (2003). Soil Improvement-Prefabricated Vertical Drain Techniques. Thomson Press, Singapore.
Botha, P. (2005). Identification and Material Composition of A Typical Gold Coast Marine Clay Deposit. Honour Thesis, School of Engineering, Griffith University, Australia.
Brand, E.W. and Premchitt, J. (1989). Moderator's Report for the Predicted Performance of the Muar Test Embankment. International Symposium on Trial Embankments

on Malaysian Marine Clays, Kuala Lumpur, Malaysia.
Brandl, H. (1981). lteration of Soil Parameters by Stabilization with Lime, Proc.10th ICSMFE, Stockholm, 587-594.
Braund, M.W. (2004). Observed and Predicted Performance of the Coombabah Creek Trial Embankment with and without Ground Improvement, Honour Thesis, School of Engineering, Griffith University.
Bredenberg, H. (1999). Equipment for deep soil mixing with the dry jet mix method. In Bredenberg, H., Holm, G. and Broms, B.B. (Eds). Deep Mix Methods for Deep Soil Stabilization. Balkema: Rotterdam, 323-331.
Brenner, R.P. and Prebaharan, N., (1983). Analysis of sandwick performance in soft Bangkok clay. Proc. 8th European Conf. Soil Mech and Foundation Enggr., Helsinki, Vol. 1, 579-586.
Brinkgreve, R. B. J. (2002). PLAXIS finite element code for soil and rock analyses-Version 8: User's Manual. Balkema, Netherlands.
Britto, A.M., and Gunn, M.J., (1987). Critical State Soil Mechanics via Finite Elements. Elis Horwood Limited, England, 488 p.
Broms, B. (1984). The Lime Column Method, Seminar on Soil Improvement and Construction Techniques, Singapore
Broms, B. and Boman, P. (1975). Lime Stabilized Columns, Proceeding 5th Asian Regional Conference on SMFE, Bangalore, Vol.1, pp 227-234.
Broms, B.B. (1986). Stabilization of soft clay with lime and cement columns in Southeast Asia. Applied Research Project RP10/83, Nanyang Technical Institute, Singapore.
Broms, B.B. (1999). Design of lime, lime/cement and cement columns. In Bredenberg, H.,Holm, G. and Broms, B.B. (Eds). Deep Mix Methods for Deep Soil Stabilisation. Balkema: Rottterdam. 125-154.
Bujang, B. K. H. (1996). Obsrevational Method of Predicting the Settlement. 12th Southeast Asian Geotechnical Conference. Vol. 1, 106-110.
Bujang, B. K. H., Khalit, O., Jaafar, A. (1995). Geotechnical Properties of Malaysian Marine Clays. Journal of Institute of Engineers Malaysia. Vol. 56, 31-49.
Carillo, N., (1942). Simple Two and Three Dimensional Cases in the Theory of Consolidation of Soils. J. Math. and Phys, Vol. 21, No. 1, 1-5.
Chai, J. C., and Miura, N., (1997). Method of modeling vertical drain-improved sub-soil. Proc. China-Japan Joint symposium on Recent Developments of Theory and Practice in Geotechnology, Shanghai, China, 1-8.
Chai, J. C., Miura, N. and Sakajo, S. (1997). A theoretical study on smear effect around vertical drain. Proc. 14th Int. Conf. Soil Mech. Found. Eng., Hamburg, Vol. 3, 1581–1584.
Chai, J. C., Miura, N., Sakajo, S., and Bergado, D., (1995). Behavior of vertical drain improved subsoil under embankment loading. J. Soil and Foundations, Japanese Geotechnical Society, Vol. 35, No. 4, 49-61.
Chai, J., Bergado, D. T., Miura, N. and Sakajo, S. (1996). Back calculated field effect of vertical drain. 2nd Int. Conf. on Soft Soil Eng., Nanjing, 270–275.
Cheung, Y. K., Lee, P. K. K., and Xie, K. H., (1991). Some remarks on two and three dimensional consolidation analysis of sand-drained ground. J. Computer and Geotechnics, Elsevier Sci. Publishers Ltd, England (GB), Vol. 12, 73-87.
Choa, V., Karunaratne, G., Ramaswamy, S. D., Vijiaratnam, A. and Lee, S. L. (1981). Drain Performance in Changi Marine Clay. Proceedings of 10th International Conference on Soil Mechanics and Foundation Engineering, Sweden, Vol. 3, 623-626.

Choa, V. (1989). Drains and vacuum preloading pilot test, Proceedings of the Twelfth International Conference on Soil Mechanics and Foundation Engineering, Rio de Janeiro, Brazil, 1347-1350.

Choa, V. (1995). Changi East Reclamation Project. Proceedings of the International Symposium on Compression and Consolidation of Clayey Soils (edited by Yoshikuni and Kusakabe), IS-Hiroshima, Japan, Balkema, Rotterdam, Vol. 2, 1005-1017.

Christopher, B.R. and Holtz, R.D., (1985). Geotextile Engineering Manual. U.S. Federal Highway Administration, Report No. FHWA-TS-86/203, 1044 p.

Chu, J. and Choa, V. (1995). Quality control tests of vertical drains for land reclamation project. Compression and Consolidation of Clayey Soils, Yoshijuni and Kusakabe (eds.), Japan, 43-48.

Chu J., Bo, M. W., Chang M. F., and Choa V. (2002). Consolidation and permeability properties of Singapore marine clay. Journal of Geotechnical and Geoenvironmental Engineering, ASCE, Vol. 128, No. 9, 724-732.

Cognon, J. M., Juran, I and Thevanayagam, S., (1994), Vacuum consolidation technology- principles and field experience, Proceedings of conference on foundations and embankments deformations, Texas, 73-80.

Cooper, M. R. and Rose, A. N. (1999). Stone column support for an embankment on deep alluvial soils. Procedings of Institute of Civil Engineers, Geotechnical Engineering, Vol.137, No.1, 15-25.

Cortlever, N. and Hansbo, S. (2004). Aspects of vertical drain quality and action. EuroGeo 3 Conf., München, B2-01, 335–340

Das, B. M. (1997). Advanced Soil Mechanics. Taylor & Francis.

Du, J., and Zhang, L. (2001). Simplified procedure for estimating ground settlement under embankments, Proceedings of the Third International Conference on Soft Soil Engineering, Hong Kong, 193-198.

Dunnicliff, J. (1993). Geotechnical Istrumentation for Monitoring Field Performance. Wiley, New York.

Eades, J. L. and Grim, R. E. (1966). A Quick Test to Determine Lime Requirements for Lime Stabilization. Highway Research Board, Bullettin No.262, 51-63.

Eddie, B. (2003). Ground Improvement Techniques Adopted in Brisbane and the Gold Coast for the Construction of Roads and Motorways, Honour Thesis, School of Engineering, Griffith University

Eke, A. (2005). The Effects of Bentonite on Shear Strength Properties of Cured Compressible Queensland Clay Soils. Honour Thesis, School of Engineering, Griffith University, Australia.

Esrig, M. I. (1999). Properties of binders and stabilised soils. In Bredenberg, H., Holm, G. and Broms, B.B. (Eds). Deep Mix Methods for Deep Soil Stabilization. Balkema: Rotterdam, 67-72.

Feng, T. W. (1993). Consolidation Properties of a Lacustrine Clay in Taipei. Proceedings of 11th Southeast Asian Geotechnical Conference, Singapore, 117-120.

Fredland, D. G., Rahardjo, H. (1993). Soil mechanics for unsaturated soils. New York: John Wiley & Sons.

Greenwood, D. A. (1975). Vibroflotation: Rotinale for Design and Practice. Methods of Treatment of Unstable Ground (Edited by Bell, F. G.), Newness-Butterworth, London, 189-209.

Greenwood, D. A. and Kirsch, K. (1984). Specialist Ground Treatment by Vibratory and Dynamic Methods. Proceedings of International Conference on Advances in Pilingand Ground Treatment for Foundation, ICE, 17-45.

Han, J., and Ye, S. L. (1991). Field tests of soft clay stabilized by stone columns in coastal areas in China. Proc., 4th Int. Conf. on Piling and Deep Found., Balkema, Rotterdam, The Netherlands, 243–248.

Han, J., and Ye, S. L. (1992). Settlement analysis of buildings on the soft clays stabilized by stone columns. Proc., Int. Conf. on Soil Improvement and Pile Found., 446–451.

Hansbo, S. (1960). Consolidation of clay with special reference to influence of vertical sand drains. Swedish Geotechnical Institute, Proc., No. 18, 160 p.

Hansbo, S. (1979). Conslidation of clay by band-shaped prefabricated drains. Ground Eng., Vol. 12, No. 5, 16-25.

Hansbo, S. (1981). Consolidation of fine-grained soils by prefabricated drains. Proc. 10th Int. Conf. SMFE., Stokholm, Vol. 3, 677-682.

Hansbo, S. (1987). Design aspects of vertical drains and lime column installation. Proc. 9th Southeast Asian Geotechnical Conference, Vol. 2, No. 8, 1-12.

Hansbo, S. (1993). Band Drains, Ground Improvement. Maryland, USA. 40-62.

Hansbo, S. (1997a). Practical aspects of vertical drain design. Proc. 14th Int. Conf. Soil Mech. Found. Eng., Hamburg, Vol. 3, 1749–1752.

Hansbo, S. (1997b). Aspects of vertical drain design: Darcian or non-Darcian flow. Geotechnique, Vol. 47, No. 5, 983-992.

Hansbo, S. (2001). Consolidation equation valid for both Darcian and non-Darcian flow. Géotechnique 51, No. 1, 51–54.

Hansbo, S. (2003). Deviation from Darcy's law observed in one-dimensional consolidation. Géotechnique 53, No. 6, 601–605.

Hansbo, S. (2004). Band drains. In Moseley, M. P. & Kirsch, K., Ground Improvement. (Editors), 2nd edition. Spon Press, Taylor and Francis Group, London and New York.

Hansbo, S. and Massarsch, K. R. (2005). Standardisation of Deep Mixing Methods. Proceedings of International Conference on Deep Mixing - Best Practice and Recent Advances (Deep Mixing 05), Sweden, 3-10.

Hausmann, M. R. (1990). Engineering Principles of Ground Modification. McGraw-Hill, Singapore.

Hilt, G.H. and Davidson, D.T. (1960). Lime Fixation in Clayey Soils. Highway Research Board, No. 262, 20-32.

Hird, C. C. and Moseley, V. J. (2000). Model study of smear around vertical drains in layered soil. Geotechnique Vol. 50, No. 1, 89–97.

Hird, C.C., Pyrah, I.C., and Russell, D., (1992). Finite element modelling of vertical drains beneath embankments on soft ground. Geotechnique, Vol. 42, No. 3, 499--511.

Hird, C.C., Pyrah, I.C., Russell, D., and Cinicioglu, F., (1995). Modeling the effect of vertical drains in two-dimensional finite element analyses of embankments on soft ground. Can. Geotech. J., Vol. 32, 795-807.

Holm, G. (1999). Applications of dry mix methods for deep soil stabilizations. In Bredenberg, H., Holm, G. and Broms, B.B. (Eds). Deep Mix Methods for Deep Soil Stabilization. Balkema: Rotterdam, 3-14.

Holm, G. (2000). Deep Mixing. Soft Ground Technology (edited by Hanson. J. L. and Termaat. R. J.), Netherlands. 105-122.

Holm, G. (2001). Deep Mixing. American Society of Civil Engineers, Geotechnical Special Publication 112, pp. 105-122.

Holtz, R. D. (1989). National Cooperative Highway Research Program: Synthesis of Highway Practice. No. 147, TRP, Washington, D.C.

Holtz, R. D. and Christopher, B.R. (1987). Characteristics of Prefabricated Drains for Accelerating Consolidation. Proceedings 9th European Conference on Soil Mechanics and Foundation Engineering, Dublin, Vol. 2, 903-906.

Holtz, R. D., Jamiolkowski, M., Lancellotta, R., and Pedroni, S., (1988). Behaviour of Pre-prefabricated vertical drains. Proc. 12th ICSMFE, Rio De Janeiro, Vol. 3. 1657-1660.

Holtz, R. D., Jamiolkowski, M., Lancellotta, R., and Pedroni, S., (1991). Prefabricated vertical drains: design and performance, CIRIA ground engineering report: ground improvement. Butterworth-Heinemann Ltd, UK, 131 p.

Horpibulsuk, S. Miura, N. and Berdago, D.T. (2005) Undrained Shear behaviour of Cement Admixed Clay at High Water Content. American Society of Civil Engineers, October edition: USA, 1096-1105.

Houston, S. L., Houston, W. N., Wagner, A. M., (1994) Laboratory Filter paper suction measurements, Geotechnical Testing Journal, ASTM, GTJODJ, **17** (2), 185-194.

Hudson, R.R., (1990). Fill Compaction and Geotechnical Aspects of the North–South Expressway. Projek Lebuhraya Utara-Selatan Berhad, Kuala Lumpur, Malaysia.

Hughes, J. M. O and Withers, N. L. (1974). Reinforcing of Soft Cohesive Soils with Stone Column. Ground Engineering, Vol.7, No.3, 42-49.

Hughes, J. M. O., Withers, N. J. and Greenwood, D. A. (1975). A Field Trial of Reinforcing Effects of Stone Columns in Soils. Geotechnique, Vol.25, No.1, 31-44.

Hunter, G., Fell, R. (2003). Prediction of impending failure of embankments on soft ground, Canadian Geotechnical Journal, 40, 209-220

Iizuka, A., Tachibana, S., Kawai, K., and Ohta, H., (2005). Changes in the Instantaneous Shear Modulus of Normally Consolidated Clay with Shear History. Soils and Foundations, Vol.45, No.2, 135-143.

Iizuka, A., Yamamoto, N., Sueoka, M., Sato, N., Kawaida, M., and Ohta, H., (2003). Deformation Analysis of Soft Subsoil on Sloping Bedrock Loaded by Highway Embankment with Stabilization Methods. Soils and Foundations, Vol.43, No.5, 81-92.

Imai, G. (1995). Analytical examination of the foundation to formulate consolidation phenomena with inherent time-dependence. Compression and Consolidation of Clayey Soils, Balkema, Rotterdam, 891-935.

Jelisic, N. and Leppänen, M. (2003). Mass stabilization of organic soils and soft clay. American Society of Civil Engineers. Geotechnical Special Publication 120, 552-561.

Indraratna, B., and Bamunawita, C. (2002). Soft Clay Stabilization by Mandrel Driven Geosynthetic Vertical Drains. Australian Geomechanics, Vol. 37, No. 5, 57-86.

Indraratna, B., and Redana, I W. (2000). Numerical modeling of vertical drains with smear and well resistance installed in soft clay, Canadian Geotechnical Journal, 37, 132-145

Indraratna, B., and Redana, I W., (1995), large-scale, radial drainage consolidometer with central drain facility. Australian Geomechanics, Vol 29, 103-105.

Indraratna, B., and Redana, I W., (1997), Plane strain modeling of smear effects associated with vertical drains. J. Geotech. Eng., ASCE, Vol. 123, No. 5, 474-478

Indraratna, B., and Redana, I W., (1998), Laboratory determination of smear zone due to vertical drain installation. J. Geotechnical and Geoenvironmental Eng., ASCE, Vol. 124, No. 2, 180-184.

Indraratna, B., and Redana, I W., (1999), Closure: Plane strain modeling of smear effects associated with vertical drains. J. Geotech. Eng., ASCE, Vol. 125, No. 1, 96-99.

Indraratna, B., Balasubramaniam, A. S., and Balachandran, S., (1992). Performance of test embankment constructed to failure on soft marine clay. J. Geotech. Eng., ASCE, No. 118, 12-33.

Indraratna, B., Balasubramaniam, A. S., and Ratnayake, P., (1994). Performance of embankment stabilized with vertical drains on soft clay. J. Geotech. Eng., ASCE, Vol. 120, No. 2, 257-273.

Indraratna, B., Balasubramaniam, A. S., and Sivaneswaran, N., (1997). Analysis of settlement and lateral deformation of soft clay foundation beneath two full-scale embankments. Int. J. for Numerical and Analytical Methods in Geomechanics, Vol. 21, 599-618.

Indraratna, B., Bamunawita, C., Redana, I W., McIntosh, G., (2002). keynote paper: Modelling of prefabricated vertical drains in soft clay and evaluation of their effectiveness in practice, Proc. 4th Int. Conf. on Ground Improvement Techniques. Malaysia, 47-62.

Indraratna, B., Rujikiatkamjorn C., Balasubramaniam, A. S. and Wijeyakulasuriya, V. (2005b). Chapter 7 - Predictions and observations of soft clay foundations stabilized with geosynthetic drains and vacuum surcharge. Ground Improvement-Case Histories (ISBN 0-080-44633-7, edited by Indraratna and Chu), 199-230.

Indraratna, B., Sathananthan, I., Bamunawita, C., and Balasubramaniam, A. S. (2005a). Chapter 2 - Theoretical and numerical perspectives and field observations for the design and performance evaluation of embankments constructed on soft marine clay. Ground Improvement-Case Histories (ISBN 0-080-44633-7, edited by Indraratna and Chu), 51-90.

Jamiolkowski, M., and Lancellotta, R., (1981). Consolidation by vertical drains - uncertaities involved in prediction of settlement rates. Panel Discussion, Proc. 10th Int. Conf. Soil Mech. and Found. Eng., Stockholm, Vol. 1, 345-451.

Jamiolkowski, M., and Lancellotta, R., (1984). Embankment on vertical drains-pore pressure during construction. Proc. Int. Conf. on Case Histories in Geotech. Enggr., St. Louis, Vol. 1, 275-278.

Jamiolkowski, M., Lancellotta, R., and Wolski, W., (1983). Precompression and speeding up consolidation. Proc. 8th Eropean Conf. Soil Mech. And Found. Eng., Helsinki, Vol. 3, Spec. Session No. 6, 1201-1226.

Juran, I., and Guermazi, A. (1988). Settlement response of soft soils reinforced by compacted sand columns. J. Geotech. Engrg., ASCE, 114(8), 930–943.

Kezdi, A. (1979). Stabilization with lime. Development in Geotechnical Engineering, Vol. 19. Elsevier Scientific: Amsterdam. pp 163-174.

Khabbaz, H. (1997). An effective stress based numerical model for flow and deformation in unsaturated soil, PhD thesis, University of New South Wales, Sydney, Australia.

Kim, S. S., Kang, M.S. and Jung, S.Y. (1999). The Geotechnical Characteristics of Marine Deposit Soil and Its Distribution. Characterization of Soft Marine Clays (edited by Tsuchida and Nakase), Balkema, Rotterdam, 83-106.

Kjellman, S. (1948). Accelerating consolidation of fine grain soils by means of cardboard wicks. Proc. 2nd ICSMFE, Vol. 2, 302-305.

Kjellman, (1952). Consolidation of clay soil by means of atmospheric pressure, Proc. of conference on soil stabilization, MIT, Cambridge, 258-263.

Lane, K. S. (1948). Consolidation of fine-grained soils by drain wells —discussion. Proc., ASCE, 74(1), 153–155.

Larsson, S. (1999). The mixing process at the dry jet mixing method. In Bredenberg, H., Holm, G. and Broms, B.B. (Eds). Deep Mix Methods for Deep Soil

Stabilization. Balkema: Rotterdam, 339-346.
Lawton, E. C. (1999). Performance of geopier foundations during simulated seismic tests at South Temple Bridge on Interstate 15, Salt Lake City Utah. UUCVEEN, Report No. 99-06.
Lee, F. H. Lee, Y., Chew, S. H., and Yong, K. Y. (2005). Strength and Modulus of Marine Clay-Cement Mixes. Journal of Geotechnical and Geoenviromental Engineering, ASCE, Vol. 131, No.1, 178-185.
Lee, H. J., Chang, C. T., Lee, C. C., and Fang, J. S. (1993). Geotechnical Characteristics of the Keelung River in the Taipei Basin. Proceeding of 11th Southeast Asian Geotechnical Conference, Singapore, 153-158.
Lee, J. S. and Pande, G. N. (1998). Analysis of stone-column reinforced foundations, International Journal for Numerical and Analytical methods in Geomechanics, Vol. 22, No.1, 1001-1020.
Lo, K.Y. and Stermac, A.G. (1965). Failure of an embankment founded on varved clay, Canadian Geotechnical Journal, Vol. 2, No.3, pp 345-451
Loeng, E.C., Soemitro, R.A.A., and Rahardjo, H. (2000). Soil improvement by surcharge and vacuum preloading, Geotechnique, Vol. 50, No.5, pp 601-605.
Loganathan, N., Balasubramanaim, A. S., and Bergado, D. T. (1993). Deformation analysis of embankments. Journal of Geotechnical Engineering, ASCE, 119(8), 1185-1206.
Magnan, J. P. and Deroy, J. M., 1980. Analyse Graphique Des Tassements Observes Sous Les Ourages. Bull. Liais. Lab. Points Chauss. 109, 45-52.
Mandel, J. (1950). Etude mathematique de la consolidation des sols. Actes Du Colloque International De Mechanique, Ppoitier, France, Vol. 4, pp 9-19
Mandel, J. (1953). Consolidation des sols (etude mathematique), Geotechnique, Vol. 3, pp 287-299.
Massarsch K.R. (2005). Deformation Properties of Stabilized Soil Columns. Proceedings of International Conference on Deep Mixing - Best Practice and Recent Advances (Deep Mixing 05), Sweden, 129-144.
McDowell, C. (1966). Evaluation of Soil-Lime Stabilization Mixtures. Highway Research Board, Highway Research Record No. 139, 15-41.
Mimura, M. and Jang, W. (2003). Long-Term Settlement of Reclaimed Marine Structural Pleistocene Clay Deposits. Proceedings of the 2nd Conference on Advances in Soft Soil Engineering and Technology, Malaysia, 335-351.
Mitchell, J. K. (1981). Soil improvement—State of the art report. Proc., 10th ICSMFE, Balkema, Rotterdam, The Netherlands, 4, 509– 565.
Mohamedelhassan, E. and Shang, J. Q. (2002). Vacuum and surcharge combined one-dimensional consolidation of clay soils, Canadian Geotechnical Journal, 39, 1126-1138
Moseley, M.P and Pribe, H.J. (1993). Vibro Techniques, Ground Improvement. Maryland USA. 1-19.
Munfakh, G. A., Sarkar, S. K., and Castelli, R. J. (1983). Performance of a test embankment founded on stone columns. Proc., Int. Conf. on Adv. in Piling and Ground Treatment for Found., Thomas Telford, London, 259–265.
Nagahara, H., Fujiyama, T., Ishiguro, T., Ohta, H., (2004). FEM analysis of high airport embankment with horizontal drains. Geotextiles and Geomembranes, Vol.22, 49-62.
Ohta, H., Takeyama, T., Mizuta, T., Nabetani, M., and Nishida, Y. (2005). Deformation of embankments on soft ground - Better computer simulation resulted form in-put data closer to the reality. Proceeding of the 16th International Conference on Soil

Mechanics and Geotechnical Engineering, Osaka, Japan, 1099-1102.
Ohtsubo, M., Egashira, K., Tanaka, H., and Mishima, O. (2002). Clay Minerals and Geotechnical Index Properties of Marine Clays in East Asia. Marine Georesources and Geotechnology. Vol. 20, No. 4, 223-235.
Okamura, T. and Terashi, M.(1975). Deep Lime Mixing Method for Stabilization of Marine Clays, Proc. 5th Asian Regional Conference on SMFE, Bangalore, Vol.1, 69-75.
Olson, R. E. (1977). Consolidation Under Time-Dependent Loading. Journal of the Geotechnical Engineering Division, Vol. 103, No. 1, 55-60 .
Onoue, A., (1988). Consolidation by vertical drains taking well resistance and smear into consideration. J. Soils and Foundations, Vol. 28, No. 4, 165-174.
Onoue, A., Ting, N.H., Germaine, J.T. and Whitman, R.V., (1991). Permeability of disturbed zone around vertical drains. Proc. ASCE Geotech. Enggr. Congress, Colorado, 879-890.
Park, C. L., Jeong, H. J., Park, J. B., Lee S. W., Kim Y. S., Kim S. J. (1997), A case study of vacuum preloading with vertical drains, Ground Improvement Geosystems, Thomas Telford, London, 69-74.
Porbaha, A. (2000). State of the Art in Deep Mixing Technology: Part I basic Concepts and Overview. Ground Improvement. Thomas Telford. 81-92.
Potts, D. M., Zdravković, L. (2000), Finite element analysis in Geotechnical Engineering-application, Thomas Telford Publising, London
Poulos, H. G. (1972). Observed and predicted behaviour of two embankments on clay, Geotechnical Engineering Journal, Southeast Asian geotechnical Society, Hong Kong, 3 (1), 1-20.
Pradhan, T.B.S., Imai, G., Murata, T., Kamon, M. and Suwa, S., (1993). Experiment study on the equivalent diameter of a prefabricated band-shaped drain. Proc. 11th Southeast Asian Geotech. Conf., Vol. 1, 391-396.
Priebe, H. J. (1995). The design of vibro replacement. Ground Engrg., December, 31–37.
Pyke, R. (2003). Compressibility Characteristics of Southeast Queensland Soft Clays, Honour Thesis, School of Engineering, Griffith University
Ratnayake, A.M.P., (1991). Performance of test embankments with and without vertical drains at Muar Flats site, Malaysia. MS thesis, Asian Institute of Technology, Bangkok, Thailand.
Richart, F. E. Jr., (1959). A review of the theories for sand drains. J. Soil Mech. and Foundation Enggr. ASCE, Vol. 83, No. SM 3, 1301(1-38).
Rixner, J.J., Kraemer, S.R., and Smith, A.D., (1986), Prefabricated Vertical Drains, Vol. I, II and III: Summary of Research Report-Final Report. Federal Highway Admin., Report No. FHWA-RD-86/169, Washington D.C, 433 p.
Roscoe, K.H., and Burland, J.B., (1968). On the generalized stress strain behavior of wet clay. Engineering plasticity, Cambridge Univ. Press; Cambridge, U.K., 535609.
Russel, D, (1992). Finite element analysis of embankment on soft ground incorporating reinforcement and drains. PhD thesis, University of Sheffield, UK
Saitoh, S., Suzuki, Y., and Shirai, K. (1985). Hardening of soil improvement by deep mixing method. Proc. 11th International Conference on Soil Mechanics and Foundation Engineering, Helsinki, Finland. 947-950.
Sangmala, S. (1997). Efficiency of drainage syatems of vacuum preloading with surcharge on PVD improved soft Bangkok clay, ME Thesis, Asian Institute of Technology, Bangkok, Thailand.

Sathawara , S. (2006). Effects of Lime and Cement Additives in Strength Improvement of Soft Clay in Helensvale, Gold Coast. Master Thesis, School of Engineering, Griffith University, Australia.

Scarr, A. (2005). Effects of Bentonite Addition on Consolidation Properties of Cement Treated South-East Queensland Soft-Clay. Honour Thesis, School of Engineering, Griffith University, Australia.

Schiffman, R. L., Chen, A. T. F., Jordan, J. C. (1969). An analysis of consolidation theories, Journal of Soil Mechanics and Foundations Division, Proc. ASCE, Vol. 95, No. SM1, 285-312

Schofield, A.N. (2005). Disturbed Soil Properties and Geotechnical Design. Thomas Telford, London.

Schofield, A.N. and Wroth, C.P., (1968). Critical State Soil Mechanics. McGraw Hill, London, 310 p.

Scott, A. (2004). Geotechnical Parameters for Embankments and Piled Structures in the Port of Brisbane Motorway, Honour Thesis, School of Engineering, Griffith University

Shang J. Q., Tang, M. and Miao, Z., (1998). Vacuum preloading consolidation of reclaimed land: a case study, Can. Geotech. J., Vol 35, 740-749.

Shibuya, S., and Tamrakar, S. B. (1999). In-situ and laboratory investigations into engineering properties of Bangkok clay. Proceedings of the International Symposium on characterization of Soft Marine Clays - Bothkennar, Drammen, Quebec and Ariake clays. Balkema, Netherlands, 107–132.

Shogaki, T., Moro, H., Masaharu, M., Kaneko, M., Kogure, K, and Sudho, T., (1995). Effect of sample disturbance on consolidation parameters of anisotropic clays. Proc. Int. Sym. on Compression and Consolidation of Clayey Soils, Hiroshima, Japan, A. A. Balkema, Rotterdam, Vol. 1, 561-566.

Shuttlewood, K. (2003) Effect of Cement Addition on Strength and Compressibility Characteristics of South-East Queensland Soft Estuarine Clay. Griffith University. Gold Coast, Australia.

Skempton, A. W. (1969). The Consolidation of Clays by Gravitational Compaction. Quarterly Journal of the Geological Society of London, Vol. 125, 373-411.

Slope Indicator (2004). Guide to Geotechnical Instrumentation. Washington, USA.

Standards Australia. (1995). AS 1289 3.1.1: Method of testing soils for engineering purposes: Soil Classification tests – Determination of the liquid limit of a soil - Four point Casagrande method.

Standards Australia. (1995). AS 1289 3.2.1: Method of testing soils for engineering purposes: Soil classification tests – Determination of the plastic limit of a soil – Standard Method.

Standards Australia. (1995). AS 1289 3.3.1: Method of testing soils for engineering purposes: Soil Classification tests - Calculation of the plasticity index of a soil.

Standards Australia. (1995). AS 1289 3.4.1: Method of testing soils for engineering purposes: Soil Classification tests - Determination of the linear shrinkage of a soil – Standard method.

Standards Australia. (1995). AS 1289 3.5: Method of testing soils for engineering purposes: Soil Classification tests - Determination of the linear shrinkage of a soil – Standard method.

Standards Australia. (1996). AS1141.51:Methods for sampling and testing aggregates – Method 51 – Unconfined compressive strength of compacted materials.

Stermac, A.G., Lo, K.Y. and Barsvary, A. (1967). The performance of an embankment founded on a deep deposit of varved clay, Canadian Geotechnical Journal, Vol. 4,

No. 1., pp 345-451.
Stocker, M. and Seidel, A. (2005). Twenty-seven Years of Soil Mixing in Germany: The Bauer Mixed-in-Place-Technique. Proceedings of International Conference on Deep Mixing - Best Practice and Recent Advances (Deep Mixing 05), Sweden, 11-13.
Surarak, C. (2005). Characterisation of Southeast Queensland Soft Clay Deposits in Sunshine Motorway. Master Thesis, School of Engineering, Griffith University, Australia.
Takagi, S., (1957). Determination of the process of consolidation by sand drains under variable loading. Proc. 4 th Int. Conf. Soil Mech. and Found. Eng., London, Vol. 1, 444-448.
Tanaka, H. (2000). Re-Examination of Established Relations between Index Properties and Soil Parameters. Proceedings of the International Symposium on Coastal Geotechnical Engineering in Practice, Vol. 2, 2-24.
Tanaka, H., and Locat, J. (1999). A microstructural investigation of Osaka Bay clay: the impact of microfossils on its mechanical behaviour. Canadian Geotechnical Journal, Vol. 36, 493–508.
Tanaka, H., and Tanaka, M. (1999). Key factors governing sample quality. Proceedings of the International Symposium on Characterization of Soft Marine Clays - Bothkennar, Drammen, Quebec and Ariake clays. Balkema, Netherlands, 57–82.
Tang, M., and Shang, J.Q., (2000). Vacuum preloading consolidation of Yaoqiang Airport runway, Geotechnique, Vol. 50, No.6, pp 613-623.
Tavenas, F., Jean, P., and Leroueil, S., (1983). The permeability of natural soft clays, Part 2: Permeability characteristics. Can., Geotech., J., Vol. 20, 645-660.
Taylor, W. H. and Arman, A. (1960). Lime Stabilization Using Pre-Conditioned Soil. Highway Research Board, Bulletin No. 262, 1-11.
Terashi, M. (1997). Deep mixing method-Brief state-of-the-art. Proceedings of 14th Int. Conf. Soil Mech. Found. Engng, Hamburg, Vol. 4, 2475–2478.
Terzaghi, K., (1925). Erdbaumechanik auf bodenphysikalischer grundlage. Franz Deuticke, Leipzig und Wein, 399
Ting, N. H., Onoue, A., Germaine, J. T., Whitman, R. V., and Ladd, C. C., (1990). Effects of disturbance on soil consolidation with vertical drains. Research Report R90-11, Dept. Civil Enggr., MIT, MA, USA, 245 p.
Torrance, J. K. (1999). Mineralogy, Chemistry and the Structure and Microstructure of Sediments. Characterization of Soft Marine Clays (edited by Tsuchida and Nakase), Balkema, Rotterdam, 203-214.
Toth, P.S. (1993). In-situ Soil Mixing, Ground Improvement. Maryland USA. 193-204.
Transport Technology, (2000). Geotechnical Investigation: Brisbane Port Road - Stage 2 Investigation, Report No R3197. Queensland Department of Main Roads: Brisbane.
Tsuchida, T. (1999). Unified Model of e-log p Relationship of Clay and the Interpretation of Natural water Content of Marine Deposits. Characterization of Soft Marine Clays (edited by Tsuchida and Nakase), Balkema, Rotterdam, 185-202.
Tsuchida, T., and Mizukami, J. (1991). Advanced method for determining strength of clay. In Proceedings of the International Conference on Geotechnical Engineering for Coastal Development, Yokohama, Vol. 1, 105–110.
Uddin, M. (1995). Strength and deformation characteristics of cement treated Bangkok clay. D. Eng. Dissertation No. GT-94-1, Asian Institute of Technology, Bangkok, Thailand.
Uddin K., Balasubramaniam A. S., and Bergado D. T., (1997). Engineering Behavior of

Cement-Treated Bangkok Soft Clay, Geotechnical Engineering, Vol. 28, No. 1, 89-119.

Van Impe, W.F. (1989). Soil Improvement Techniques and Their Evolution. A.A. Balkema, Rotterdam.

Wang, J. and Xiong, Z. (1992). Improvement of the soft soil foundation in Shenzhen airport, Rail Road Bed Engineering, No. 3, 60-71

Whitaker, W.G. and Green, P.M. (1980). Moreton Geology. Department of Mines, Queensland. [Online]. Available: http://www.ga.gov.au/map/ [26 July 2003]

Whittle, A. J. (1991). MIT-E3: a constitutive model for over consolidated soils, Computational methods and advances geomechanics, Balkema, Rotterdam.

Wijeyakulasuriya, V., Hobbs, G. and Brandon, A. (1999). Some experiences with performance monitoring of embankments on soft clays. Proc. 8th Australia New Zealand Conference on Geomechanics, Institution of Engineers Australia: Hobart. pp 783-788.

Wood, D. M, Hu, W. and Nash, D.F.T (2000). Group effects in stone column foundations: model tests. Geotechnique, Vol.50, No.6, 689-698.

Wood, D. M. (2004). Geotechnical Modelling. Spon Press, London.

Xiao, D. (2000). Consolidation of soft clay using vertical drains. PhD thesis, Nanyang Technological University, Singapore.

Yang, D. S. (1997). Ground Improvement, Ground Reinforcement. GroundTreatment: Developments 1987-1997 (Edited by Schaefer V. R.), Geotechnical Special Publication No.69, 130-150

Yashima, A., Shigematsu, H. and Oka, F. (1999). Microstructure and Geotechnical Property of Osaka Pleistocene Clay. Characterization of Soft Marine Clays (edited by Tsuchida and Nakase), Balkema, Rotterdam, 165-174.

Yasui, S., Yokozawa, K., Yasuoka, N. and Kondo, H. (2005). Recent technical trends in Dry Mixing (DJM) in Japan. Proceedings of International Conference on Deep Mixing - Best Practice and Recent Advances (Deep Mixing 05), Sweden, 15-22.

Yong, K. Y. and Lee, S. L. (1997). Improvement of soft ground by vertical drains, surcharge and high energy impact in highway embankment construction. In Proceedings of International Conference on Ground Improvement Techniques, 13-25.

Yoshikuni, H., and Nakanodo, H., (1974). Consolidation of Fine-Grained Soils by Drain Wells with Finite Permeability. Japan Soc. Soil Mech. and Found. Eng. Vol. 14, No. 2, 35-46.